MONASH University

A PROCESS INTEGRATION APPROACH TO THE SYNTHESIS OF HYBRID POST-COMBUSTION CARBON DIOXIDE CAPTURE PROCESSES

By

JEAN CHRISTOPHE LI YUEN FONG

BEng (Chemical) (Hons), AMIChemE

Submitted in fulfilment of the requirement for the degree of

Doctor of Philosophy

December 2015

Department of Chemical Engineering

Faculty of Engineering

Monash University

Australia

To my beloved family and friends

Copyright notice

Abstract

It is widely acknowledged that man-made CO_2 emissions to the atmosphere must be significantly reduced to mitigate the damaging effects of global climate change. The energy sector contributes to a large portion of the carbon emissions and a wide range of technologies need to be implemented to make the progression towards the low carbon dioxide emission. CO_2 capture and storage (CCS) is seen as a technology that can reduce the carbon emissions in the coal fired power stations. This will help reduce the rate of climate change by removing greenhouse gases that would otherwise be emitted to the atmosphere.

Carbon capture and storage involves the capture of carbon dioxide gas from within the CO_2 generation process, compressing it into a supercritical fluid and finally sequestrating it. Implementing CCS technology for electricity production has an impact on the net power output of the power plant and it also has a high capital and operating cost. Among the different capture technologies, solvent absorption is considered to be the benchmark amongst the post-combustion carbon capture technologies. However, there are other technologies that have potential to be energy and cost competitive such as: adsorption, membranes and low-temperature separation.

The aim of the PhD is to improve the integration of the capture processes with the power plant stations to reduce the energy penalty associated with the addition of CCS by combining current carbon capture technologies to form hybrid post-combustion carbon capture processes and evaluate their performances. A hybrid post-combustion carbon capture process consists of two steps: an initial recovery step would increase the concentration of CO_2 in the flue gas whilst trying to limit the amount of CO_2 lost in the waste gas. The second step would then be a purification step, where the CO_2 gas is purified and pressurised to the sequestration requirement. The research will develop a methodology to assess carbon capture technologies using exergy analysis, in combination with pinch analysis and optimisation methods, such as multi-objective optimisation (MOO).

The hybrid carbon capture technologies is modelled using Aspen HYSYS®. These models provide the information to perform the analysis and optimisation of the power plants to determine the energy and cost targets. The two hybrid processes that were developed are VSA/low-temperature separation hybrid carbon capture processes and membrane/low-temperature separation hybrid carbon capture processes. The processes were then evaluated using MOO and the energetic and economic performance were compared to the MEA solvent absorption carbon capture processes.

Hybrid carbon capture processes using technologies such as VSA, membranes and low-temperature carbon separation have shown potential to be energetically and economically competitive with the established MEA solvent absorption. The VSA/low-temperature hybrid process requires a specific shaft work of 1.46 GJ_e/t (CO_2 captured) when 90.0 % of the CO_2 is being recovered. The

membrane/low-temperature hybrid carbon capture process required a specific shaft work of 1.38 GJ_e/t (CO_2 captured) at 90% CO_2 recovery rate when mixed refrigerant is used to achieve the low temperatures. On an economic perspective, the VSA/low-temperature separation hybrid process had a higher cost of avoidance of \$78/t (CO_2 avoided) compared to the \$67//t (CO_2 avoided) of the membrane/low-temperature separation hybrid process.

Finally, beyond analysing the overall performance of the hybrid processes, the thesis allowed each hybrid process to be analysed in depth through heat integration and MOO; the energy trade-off between the CO_2 recovery stage and CO_2 purification stage was studied. The difference in using mixed ethane/propane refrigerant versus propane only refrigeration was also investigated.

Declaration

This thesis contains no material which has been accepted for the award of any other degree or diploma at any university or equivalent institution and that, to the best of my knowledge and belief, this thesis contains no material previously published or written by another person, except where due reference is made in the text of the thesis.

Candidate: Jean Christophe Li Yuen Fong

December 15

Publications during enrolment

Conference Publications

Li Yuen Fong, J.C., Anderson, C.J., Hoadley, A.F., 2013. Optimisation of a Hybrid CO_2 Purification Process, Chemeca 2013, Brisbane.

Li Yuen Fong, J.C., Anderson, C.J., Hooper, B., Xiao, G., Webley, P.A., Hoadley, A.F., 2014. Multi-Objective Optimisation of Hybrid CO2 Capture Processes using Exergy Analyis, Process Integration, Modelling and Optimisation for Energy Saving and Pollution Reduction. AIDIC, Prague, CZ.

Li Yuen Fong, J.C., Hoadley, A.F., 2015. Optimisation of a hybrid multi-stage membrane and low-temperature carbon dioxide purification process, APCChE 2015 Congress incorporating Chemeca 2015. RMIT Informit Database, Melbourne, Victoria.

Journal Publications

Li Yuen Fong, J.C., Anderson, C.J., Xiao, G., Webley, P.A., Hoadley, A.F.A., 2015. Multi-objective optimisation of a hybrid vacuum swing adsorption and low-temperature post-combustion CO2 capture. Journal of Cleaner Production.

Student signature: *Jean Christophe Li Yuen Fong* **Date: 21/12/15**

The undersigned hereby certify that the above declaration correctly reflects the nature and extent of the student and co-authors' contributions to this work.

Main Supervisor signature: *Andrew Hoadley* **Date: 21/12/15**

Alone we can do so little;

together we can do so much

Helen Keller

Acknowledgements

This thesis is the culmination of a remarkable journey and would not have been possible without the support of several people. Firstly, I would like to express my deepest gratitude to my co-supervisors, Assoc. Professor Andrew Hoadley and Barry Hooper, for giving me the opportunity to do this PhD.

I would like to thank Andrew for his exceptional guidance throughout the past 4 years and providing me with numerous opportunities to improve my research abilities. I will take away a lot from our weekly meetings thanks to his unwavering support, incredible research acumen and willingness to discuss ideas. I would also like to thank Barry for his insight and confidence in my work. This thesis would not have been possible without their support and the multiple reviews of this thesis.

I would like to thank the CO2CRC for the funding of this research and the CO2CRC engineering team for their readiness to provide the technical assistance in my research. The team was a great support network and I would like to especially acknowledge Clare, Trent, James, Paul, Colin, Minh and Tristan for our valued discussions and exchange of ideas. I have learnt greatly from each one of you and for that, I am very grateful.

I am thankful to the Faculty of Engineering of Monash University for the financial support. I would also like to thank the Department of Chemical Engineering for providing me with the tools to perform my research. I would like to thank the Chemical Engineering staff, particularly Lilyanne Price for her support and facilitation of the paperwork since my PhD application. My thanks to the Chemical Engineering department would not be complete without the acknowledgement of the Chemical Engineering Postgraduate Association and the support of my friends within the department. I made many friends throughout the years and I would like particularly thank my office and lunch mates for always supporting and encouraging me. A special thought goes to Yuzhou.

I am also extremely thankful to my friends outside of the university who have kept me sane throughout the years of being immersed in the research. Most importantly, I would like to thank my beloved family: Mum, Dad, Odile, Valerie and Eric. They have been the best support and motivation that a son and brother could hope for. Last but not least, I wish to express my deepest gratitude to Kaitlin, who has been my pillar of strength during this journey. The completion of this thesis would have not been possible without your support and motivation.

Table of Contents

List of Figures

List of Tables

Nomenclature and Abbreviations

CO_2 – Carbon Dioxide

CCS – Carbon Capture and Storage

CAPEX – Total Capital Cost

$C_{Avoidance}$ – Cost of CO_2 avoided (A$ per tonne of CO_2 avoided)

FGD – Flue Gas Desulphurisation

HEN – Heat Exchanger Network

HI – Heat Integration

IEA – International Environmental Agency

IPCC – Intergovernmental Panel on Climate Change

MEA – Mono Ethyl Amine

m_{Energy} – Mass of CO_2 emitted from the energy used for capture

MOO – Multi-Objective Optimisation

NPV – Net Present Value an annual basis (A$)

N_2 – Nitrogen

OPEX – Total Operating Cost

PEC – Process Equipment Cost

LCOE – Levelised Cost of Electricity (A$/MWh)

LNG – Liquefied Natural Gas

$\alpha_{CO2/N2}$ – Selectivity of CO_2 versus N_2

TEC – Total Equipment Cost

USC – Ultra Supercritical

VSA – Vacuum Swing Adsorption

1 Introduction

Since the start of the industrial era in the mid-18th century, the concentration of CO_2 in the atmosphere has increased from 280 ppm to 391 ppm in 2011, as reported in the IPCC fifth assessment report (AR5) by Stocker et al. (2013). The report determined that from the 1960s to 2005, the average increase in CO_2 emissions is 1.4ppm per year. This alarming increase in CO_2 level is one of the primary causes of global warming, which contributes to a series of negative effects. To mitigate these negative effects, in 1992, the United Nations Framework Convention on Climate Change (UNFCCC) was formed to discuss methods for the stabilisation of greenhouse gas concentrations in the atmosphere at a level where anthropogenic emissions would not affect the climate system.

The IPCC AR5 reported that due to the heavy reliance of the energy sector on coal fired power stations, the energy sector is a large contributor of the anthropogenic carbon emissions. Furthermore, 30% of the total anthropogenic carbon emissions in the atmosphere have come from these coal fired power stations. Critically, it was also reported that the reliance on coal will increase over the next decades. In response, the IPCC and IEA (2012) conducted several studies to establish a strategy to mitigate the CO_2 emissions from the energy sector by 2050. From these studies, it was concluded that no single technology will provide all emission reductions to achieve stabilisation by 2050, but a portfolio of technologies will be required. The range of technologies are shown in Figure 1.1, which includes renewable energy such as solar, wind and biomass energy; and more importantly, carbon capture and storage (CCS). CCS is seen as the technology to reduce CO_2 emissions in the short term and provide more time to the energy sector to transition into an array of sustainable energy sources.

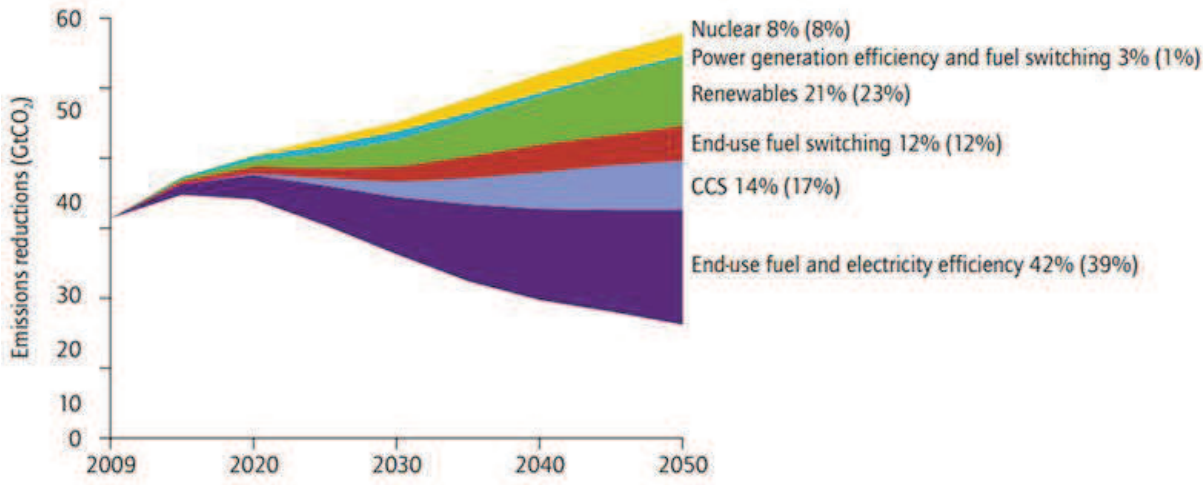

Figure 1.1 Array of technologies that contribute to the reduction of CO_2 emissions by more than half through to the year 2050 (IEA 2012).

1.1 Carbon Capture and Storage

CCS involves the capture of carbon dioxide gas from within a CO_2 generation process, its compression into a supercritical fluid, transport of the CO_2 to a storage site and finally its sequestration at this site. The capture and separation processes were initially studied in order to produce town gas almost 60 years ago by Evans and Siddique (1975). However, when the global warming effect of CO_2 was understood, Horn and Steinberg (1982) started to discuss the prospect of using such carbon capture technology to mitigate the carbon dioxide emissions. Nowadays, CO_2 removal is already being used in industries such as 'enhanced oil recovery' and the production of hydrogen from fossil fuel

The fossil fuel combustion process shown in Figure 1.2 (a) produces the greatest quantity of CO_2 emissions. The capture of CO_2 from a combustion process can be divided into three main categories: post-combustion capture, pre-combustion capture and oxy-fuel combustion. These are defined in more detail below and are represented in Figure 1.2 (b-d).

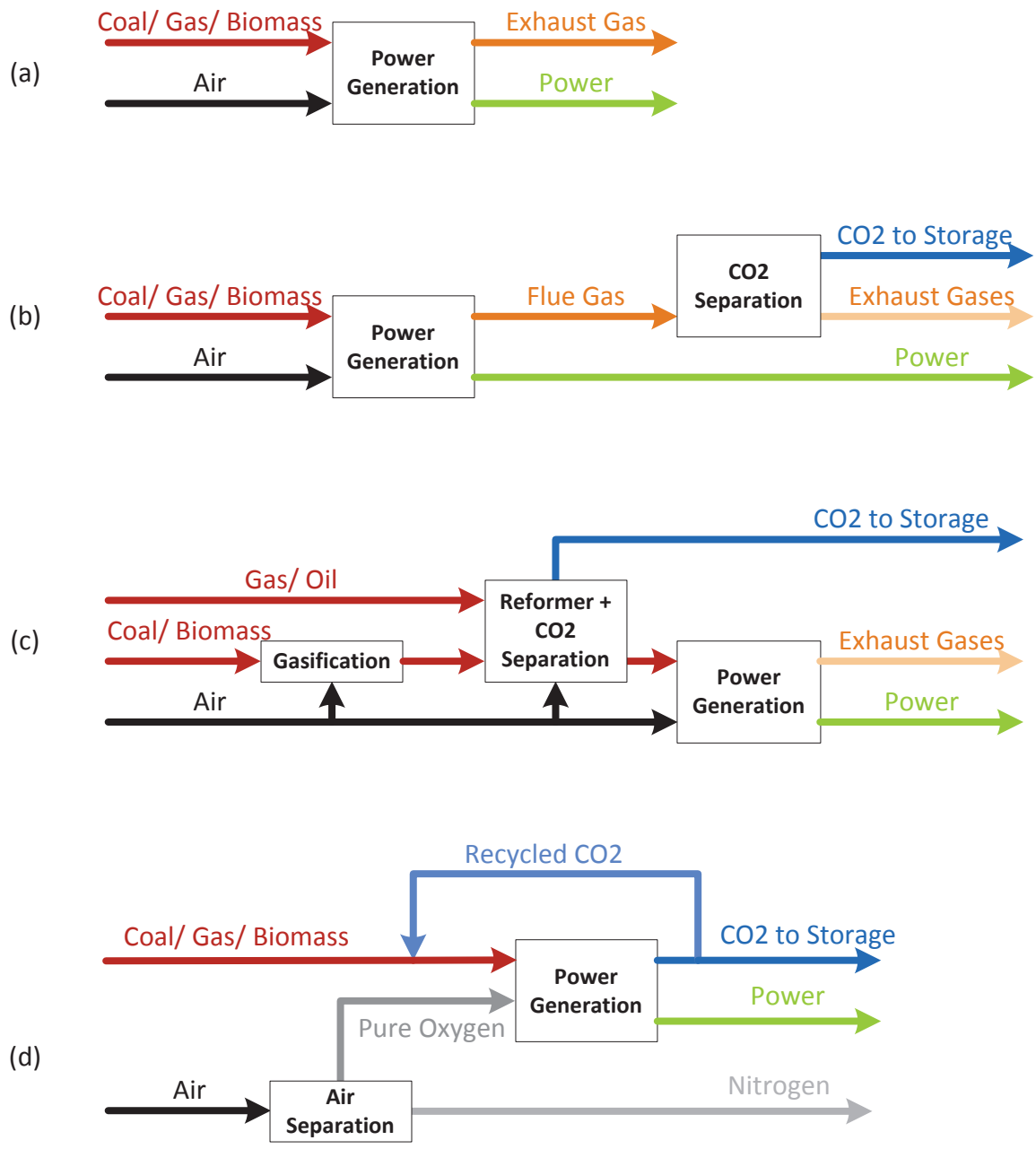

Figure 1.2 (a) Schematic diagram of fossil fuel combustion process for power generation (b) Schematic diagram of post-combustion capture (c) Schematic diagram of pre-combustion capture (d) Oxy-fuel combustion capture

i. Post-combustion Capture

Post-combustion capture (Figure 1.2 (b)) is the process where CO_2 is captured from the flue gas from the combustion of fossil fuel and biomass in air. The pure CO_2 stream is then further processed to be ready for storage. The CO_2-depleted flue gas can then be discharged into the atmosphere since it then contains less greenhouse gases.

ii. Pre-combustion Capture

Pre-combustion capture (Figure 1.2 (c)) is the process where the fuel is reacted with oxygen/ air or steam to form a 'synthetic gas (syngas)' composed of carbon monoxide and hydrogen. This gas is then passed through a catalytic reactor to convert the carbon monoxide into carbon dioxide, which can be separated from the syngas and the resulting hydrogen-rich gas can then be used to generate power.

iii. Oxy-fuel combustion Capture

Oxy-fuel combustion (Figure 1.2 (d)) uses high purity oxygen (~95%) for the combustion of the fuel instead of air. This results in a flue gas that consists mainly of CO_2 and H_2O and therefore facilitates the CO_2 separation due to the relatively high condensation temperature of H_2O compared to CO_2. In this process, the air separation unit is the most energy intensive unit since it requires cryogenic conditions to separate oxygen from air. It should be noted that when combustion occurs in high oxygen content, the temperature exceeds material limits and therefore some of the pure CO_2 is recycled into the combustion chamber to lower the combustion temperature.

Among these three categories, oxy-fuel combustion capture does not require an advanced CO_2 separation unit due to the reasons mentioned. However, both post-combustion and pre-combustion require advanced separation technologies to remove the CO_2 from the flue gas and syngas respectively. The CO_2 capture technologies are discussed in the following sections.

This research will focus on hybrid post-combustion capture technologies (Figure 1.3). In order to determine which technology or combination of technologies is most suited for the process, the carbon capture process needs to be integrated with the power station and then analysed. The process will be simulated using flowsheet modelling tools, with pinch analysis for heat integration and optimised using multi-objective optimisation software. Finally, the cost per tonne of carbon dioxide and the power requirement of the carbon capture process will determine the viability of the process.

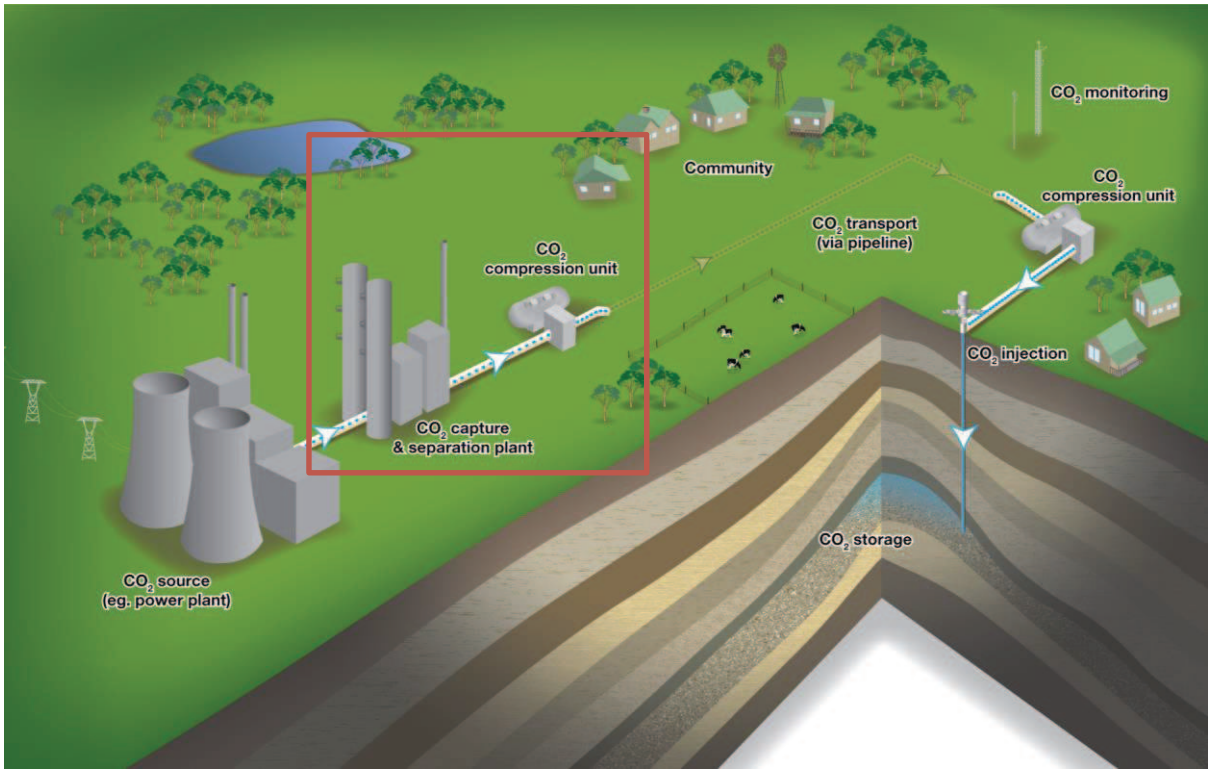

Figure 1.3 Overview of the different elements of a post-combustion CO_2 capture and storage process for a power station (CO2CRC)

1.2 Carbon Capture Processes

Among the different capture technologies, the recent review of the carbon capture technologies by Huisingh et al. (2015) stated that solvent absorption has been considered to be the benchmark among the post-combustion carbon capture technologies and is the only commercially established process. Sreenivasulu et al. (2015) also identified that chemical absorption is the most widely used technology due to the high capture performance at low concentration of CO_2. Furthermore, absorption processes can be easily integrated to any power plant as an end of the pipe technology. However, work from Aaron and Tsouris (2005) and Sreenivasulu et al. (2015) have shown that there are other technologies that have the potential to be energy and cost competitive such as: adsorption, membranes and low-temperature separation (also referred to as "cryogenics" in the literature). Each of those technologies have their respective advantages and disadvantages that are discussed in the next sub-sections.

1.2.1 Solvent Absorption

The review of conventional and emerging carbon capture process technologies from Rufford et al. (2012) states that the solvent absorption is currently the most prominent capture process due to the fact that solvent absorption is the most advanced technology since it has been extensively used for CO_2 removal in the natural gas processing industry. Solvent absorption based carbon capture processes includes amines, alcohols, liquid ammonia and alkalies. Amines are the most used solvents for large industrial applications, but the other solvents are being researched, as summarised by

Sreenivasulu et al. (2015). Solvent absorption has been widely employed due to higher capture efficiencies even at low concentrations of CO_2 and varying selectivities can be achieved depending on the solvent.

A schematic diagram of the absorption process is shown in Figure 1.4 and can be divided in to two main steps: the absorption step, where lean solvent is contacted with the flue gas stream to capture the CO_2 in the absorption column, and the desorption step that occurs in the stripping column, where the solvent is either heated or the pressure is reduced to desorb the CO_2 from the solvent, yielding a high purity stream of CO_2 and regenerating the solvent which is recycled back to the absorption column. Solvents involving chemical reactions are usually regenerated by heating in a reboiler, which utilises a significant proportion of the steam generated by the power station.

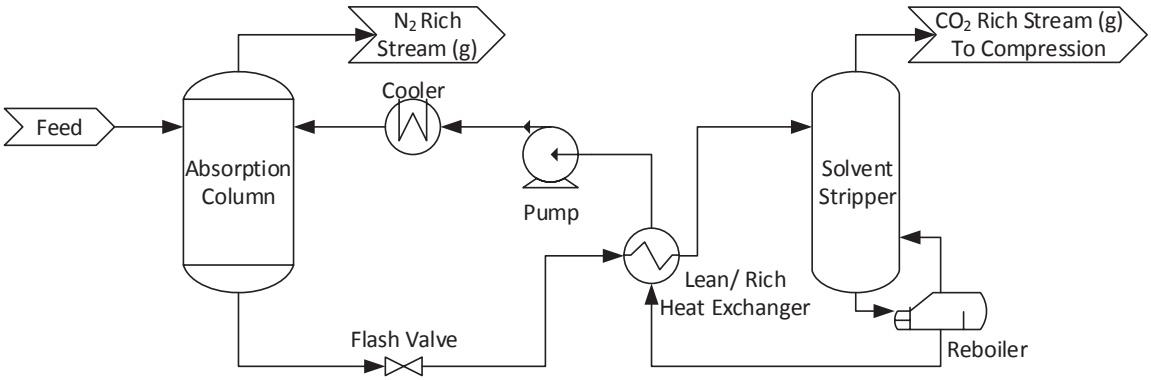

Figure 1.4 Schematic diagram of the solvent absorption process

Chemical absorption is generally used in post-combustion capture but there are still some challenges such as scaling-up issues, solvent degradation and the high reboiler duty. Wang et al. (2015) provided a critical review of research in solvent absorption such as the studies from Le Moullec and Kanniche (2011) on MEA (mono ethanolamine) and Smith, K et al. (2009) on potassium-carbonate based solvents. Furthermore, work from Harkin, Hoadley and Hooper (2010) showed the advantages of performing heat integration on the capture plant and the power plant, which reduced the additional heat requirement for the solvent regeneration process.

1.2.2 Membranes

A membrane process, as the name suggests, consists of a membrane which is a specially developed material that allows the selective permeation of a gas through it (permeate stream). The selectivity of each membrane depends on the nature of the material and the way it has been developed and also the pressure difference driving force that allows the gas to flow through the membrane. Therefore, high pressure streams are preferred when using membrane separation processes. Bernardo, Drioli and Golemme (2009) discuss the different uses of membranes including: air separation, gas dehydration and CO_2 removal from synthesis gas for hydrogen production. There are a wide range of types of

membranes that are specifically developed for different separation processes required such as perfluorodioxole polymer membrane for air separation and polysulfone hollow fiber for the H_2/N_2 separation in hydrogen production. For the post-combustion carbon capture process, again there are numerous types of membranes that are being researched including: polymeric membranes and polyimide membranes.

However, according to Favre (2011), membranes in large scale CO_2 capture such as CCS has not yet been implemented as it is a relatively new technology which has not been tested on a sufficiently large scale, nor does it produce the high purity CO_2 stream that is easily achieved by solvent absorption. Various membrane technologies are being developed to match and exceed the performance of solvent absorption, Luis, Van Gerven and Van der Bruggen (2012) reviewed some of the developments in membrane-based CO_2 capture and demonstrated the potential for membrane technology. The main limitation that they found was the trade-off between membrane stability and cost. It was found that the costs related to membrane manufacture were difficult to estimate, which made it more challenging to compare the cost of membrane processes to other carbon capture processes. Manufacturing efficiencies are expected to bring done membrane costs, but the rate of this occurring depends on rate of installation which makes the estimate imprecise. Furthermore, more research needs to be done on the effect of the impurities and industrial scale gas flow rate on the polymeric membrane. As a result, extensive research is being one on improving the materials, such as carbon hollow fibers and hybrids containing carbon nanotubes to improve the reliability and durability for industrial applications.

Figure 1.5 shows a simple membrane process schematic diagram, where the flue gas needs to be compressed prior to being supplied to the membrane unit to provide the necessary driving force required for the gas separation. However, the pressure difference can also be generated by applying a vacuum pressure to the retentate side of the membrane. Merkel et al. (2010) showed that by using approximately 89% of the total work in the vacuum pump, this configuration can reduce the total work requirement of the membrane unit by approximately 55%.

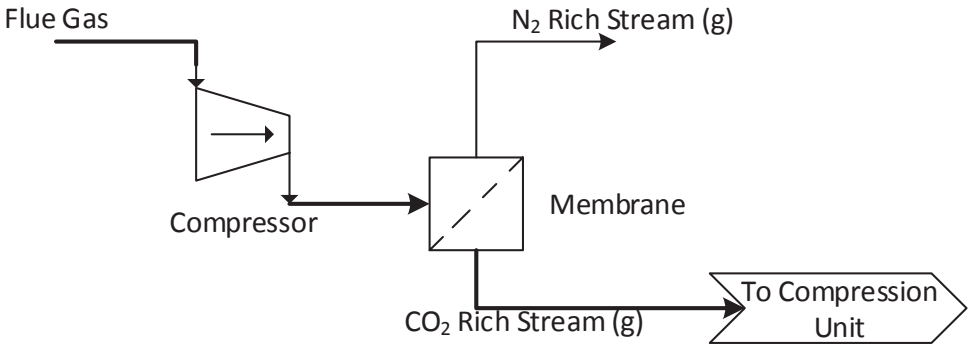

Figure 1.5 Schematic diagram of the membrane process

1.2.3 Adsorption

In adsorption processes, molecules adhere to the porous surface of a solid either by physical and/or chemical forces. The schematic adsorption separation process is shown in Figure 1.6 and typically consists of three steps:

i) The adsorption step, where a film of the adsorbate (CO_2) is formed on the surface of the adsorbent (molecular sieves or activated carbon)

ii) A purging step, where the other gases are purged from the vessel

iii) A desorption step, where the CO_2 is desorbed from the adsorbent by pressure swing operation (PSA) or temperature swing operation (TSA). As stated by Webley (2014), TSA requires longer operating time to heat the adsorbents for regeneration leading to larger sorbent inventory. Therefore, PSA has proved to be a more attractive operation than TSA for the shorter operating time.

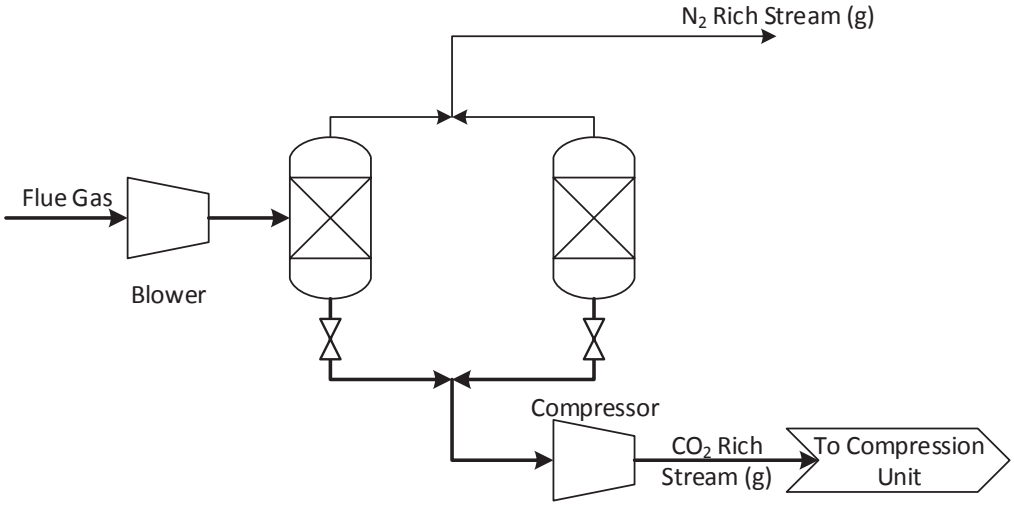

Figure 1.6 Schematic diagram of the adsorption process

Adsorption processes have very similar performance to membranes since they have also been used for air separation, gas dehydration and CO_2 removal from synthesis gas for hydrogen production developed by Sircar (1979). In recent years, there have been extensive research in the materials used for adsorption processes, which resulted in novel materials such as nanostructured carbon, metal organic frameworks (MOFs) and inorganic (oxide) materials. Combined with more conventional materials such as zeolite, alumina and silica gel, there is a wide selection of materials to choose from for adsorption process. However, most of those materials are still in the early research phase and only a few have shown the potential to reach the pilot testing phase. Limitations of materials include availability of materials and operation constraints. Webley (2014) reviewed the different CO_2 selective adsorbent, such as Activated Carbon from Yin et al. (2013) and Zeolite 13X from Xiao, P et al. (2008). Both adsorbents have shown some promising results in carbon dioxide separation due to the small equipment required and the good CO_2 selectivity.

Zhang, J. and Webley (2008) stated that pressure/ vacuum swing adsorption technology has been frequently studied for the carbon capture process due to its relative simplicity and low energy requirements compared to the standard MEA solvents absorption carbon capture. However, one disadvantage of adsorption is that the gaseous feed needs to be treated before going through the adsorber and like the membrane process, the adsorption process does not readily yield a high purity CO_2 stream such as occurs with the solvent absorption regeneration process. According to Webley (2014), adsorption process require extreme conditions such as low vacuum pressures (e.g. 5-10 kPa) in order to simultaneously yield both high CO_2 purity and high CO_2 recovery, which can only be obtained using expensive bespoke high volume vacuum machinery. At those low vacuum pressures, the maximum CO_2 purity is ~90% and recovery is ~70-90%, which does not meet the minimum requirement for CCS.. Further limitations of the process may include the ability of some adsorbent materials (particularly Zeolites) to operate with wet gas and impurities such as NOx and SOx.

1.2.4 Low-Temperature Separation

Low-temperature separation of CO_2 from post-combustion flue gas is achieved by cooling followed by vapour-liquid phase separation. This technology is also commonly known as "cryogenic separation" in the literature. "Low-temperature separation" is used in this work as Berstad, Anantharaman and Nekså (2013) pointed out that cryogenics is defined as temperatures below -153ºC in the International Institute of Refrigeration (2007) dictionary. Since this study does not go to such cold temperatures, the term "cryogenics" was avoided.

A representation of low-temperature separation is shown in Figure 1.7, where the flue gas is compressed to an intermediate pressure. There are two motives for the pre-compression stage; firstly, the CO_2 pressure needs to be above the triple point pressure to avoid crystallisation of CO_2 and secondly, the pre-compression facilitates the liquefaction of CO_2 in the chiller. The liquid CO_2 is separated from the N_2 rich flue gas and the liquid CO_2 can be pumped to the appropriate pressure for transportation and sequestration.

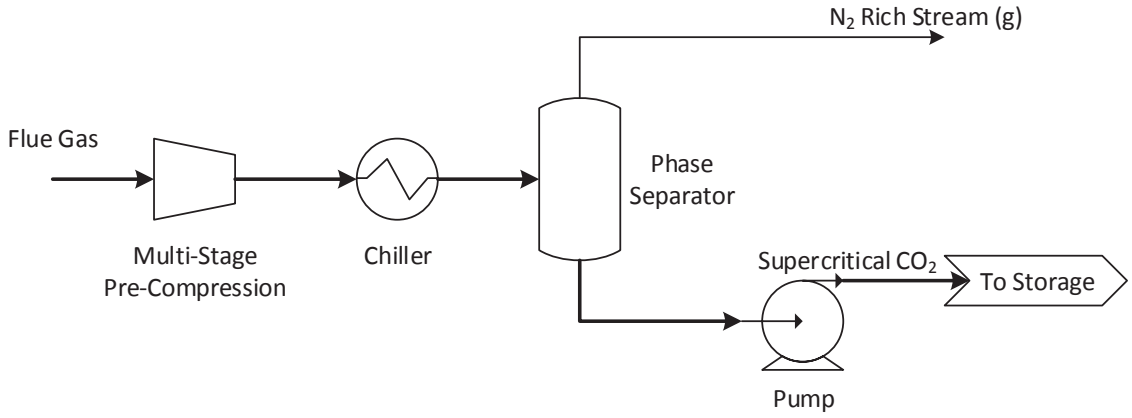

Figure 1.7 Schematic diagram of the low-temperature capture process

The main advantage of low-temperature separation is that it yields liquid CO_2 that is more readily pumped to a supercritical state relative to gaseous CO_2 that would require a separate compression train. Berstad, Anantharaman and Nekså (2013) reported that low-temperature separation shows promising results for feed gas with a high CO_2 composition, such as oxy-fuel combustion. The low-temperature separation and pressurisation process is represented in Figure 1.8, where a typical flue gas (red dot) at 20ºC is compressed to 2 MPa and cooled to approximately -40ºC. At this temperature and pressure, the CO_2 is in a liquid phase and can be pumped to 20 MPa to obtain supercritical CO_2. Figure 1.8 also compares the low-temperature separation and pressurisation to the conventional CO_2 multi-stage compression (orange arrow).

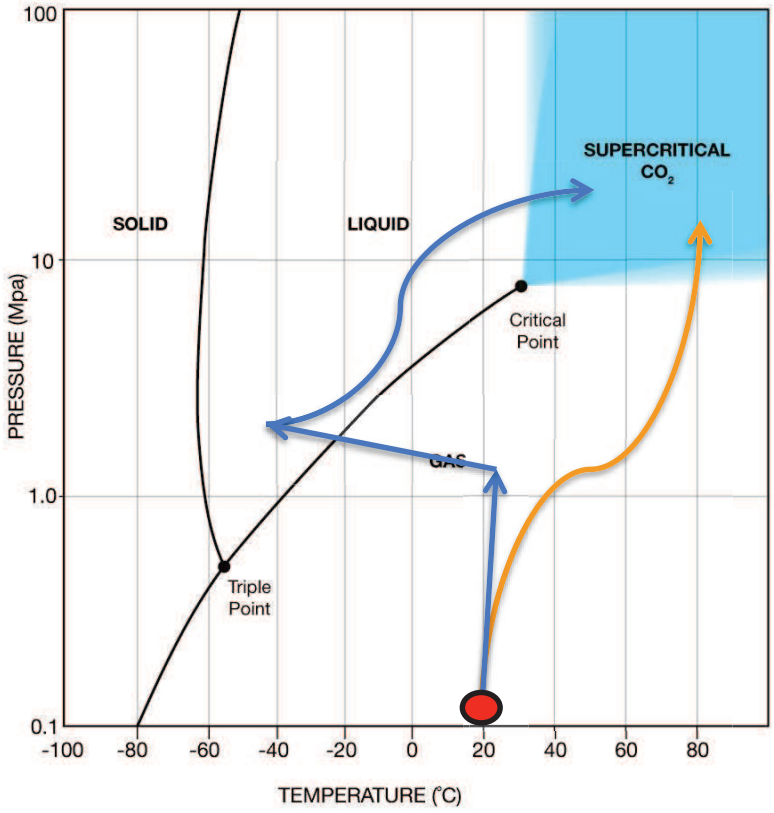

Figure 1.8 Carbon dioxide phase envelope and comparison of conventional carbon dioxide multi-stage compression system (orange) vs low-temperature carbon dioxide liquefaction and pressurisation.

Sreenivasulu et al. (2015) states that there are two main the low-temperature carbon capture process limitations: the compulsory removal of the moisture in the gas to avoid plugging of the system and more importantly, the high capital and operating costs.

1.3 Carbon Capture and Storage Energy Penalty

According to the Global CCS Institute (2014), as of the end of 2014, there were 22 large-scale CCS projects in operation and construction around the world, which represents twice the number of large-scale CCS projects since the beginning of the decade. Leung, Caramanna and Maroto-Valer (2014) states that the major challenge for post-combustion is the energy penalty and associated costs for the capture unit to operate. The energy penalty, ΔE (%) is defined as the ratio of power output lost for implementing CCS over the power output of the power plant without CCS. Eq. 1.1 is the equation used to determine the energy penalty:

$$\Delta \boldsymbol{E} = \frac{\boldsymbol{P_{wo\ cap} - P_{cap}}}{\boldsymbol{P_{wo\ cap}}} \% \qquad \textbf{Eq. 1.1}$$

Where, $P_{wo\ cap}$ is the net power output from the power plant without CCS

P_{cap} is the net power output from the power plant with CCS.

Finally, the specific energy penalty, $\Delta \dot{\boldsymbol{E}}$ (kJ/ t(CO_2 captured)) is defined as the energy required per unit of CO_2 captured by the CCS unit.

$$\Delta \dot{\boldsymbol{E}} = \frac{\boldsymbol{P_{wo\ cap} - P_{cap}}}{\dot{\boldsymbol{m}}_{\boldsymbol{CO_2}}} \qquad \textbf{Eq. 1.2}$$

Where, $\dot{m}_{CO_2}$ is the mass flow rate of the CO_2 captured from the CCS unit.

Both the energy penalty and the specific energy penalty are used throughout this study as they are strong indicators of the reduction in the energy output of the power plant, which is particularly relevant when retrofitting CCS in power stations. The energy penalty of carbon capture processes is highly dependent on the size of the power plant and the flowrate and composition of the flue gas stream. On the other hand, the specific energy penalty is a function of the amount of CO_2 being captured, which allows different carbon capture processes to be compared on a consistent basis. Table 1.1 shows the specific energy penalty of the three main carbon capture technology, including compression of the high purity CO_2, when recovering approximately 90% of the CO_2 from the flue gas. The relationship between CCS energy penalty as % and power plant size is displayed in Eq 1.1, where the denominator represents the power plant size and the numerator represents the power requirement for capture. Assuming that the power plant condition remains the same, mathematically, the energy penalty and size of power plant would have a proportional correlation. However, in practice, smaller power plants tend to be older and therefore have lower efficiency. As a result, due to the lower power plant efficiency of smaller power plants, there would be a higher impact on the energy penalty of implementing CCS on smaller power plants.

Table 1.1 Summary of specific energy penalty for carbon capture processes

Carbon Capture Technology	Power plant	Units	Value
MEA (Xu et al. 2013)	600 MW	$GJ_{th}/t(CO_2$ Captured)	4.00
VSA (Liu et al. 2012)	N/A	$GJ_e/t(CO_2$ Captured)	2.37
Multi-Stage Membrane (Zhang, X, He & Gundersen 2013)	800 MW	$GJ_e/t(CO_2$ Captured)	2.00
Low-temperature Separation (Song, Kitamura & Li 2012)	600 MW	$GJ_e/t(CO_2$ Captured)	3.40

It should be noted that the unit of MEA specific energy is a thermal energy penalty whereas VSA, membrane and Low-temperature separation are electrical energy penalties. That is due to the fact that most of the energy required in MEA capture solvent is the heat required to regenerate the solvent whereas VSA and membrane processes require electrical energy for the vacuum pumps and compressors.

1.4 Motivation and Research Objectives

Researchers worldwide are calling for both short-term and long-term solutions to the reduction of the CO_2 emissions. The heavy global reliance on coal for electricity production, particularly in Australia, indicate that CCS as a mitigation option is important to provide time for the other low CO_2-emission electricity production to be implemented. The Global CCS Institute (2014) reported that while CCS projects are already been deployed on a large scale such as the Gorgon Project in Australia and White Rose Project in the UK, more CCS projects need to be initiated to meet the 2050 carbon emission target. One of the main challenge to increase the rate at which CCS projects are implemented is the energy penalty and cost associated with CCS. Solvent-based carbon capture process with a conventional CO_2 compression train is the most established process and work from Abu-Zahra, Niederer, et al. (2007) show that an energy requirement of up to 4 GJ_{th}/t (CO_2 captured) is required. The report from Irlam (2015) states that the avoided cost of CO_2 (in 2014US$) for implementing CCS in a coal power plant ranges from US$ 48 to US$ 109.

The main objective of this research is to combine current carbon capture technologies to form hybrid post-combustion carbon capture processes and evaluate their performances. In order to do so, process integration techniques are used to integrate the carbon capture processes and multi-objective optimisation is used as the method to determine the optimum operating conditions of each processes. In order to achieve the main objective, the research can be segregated into multiple research objectives as follows:

1. Evaluate the different combinations of hybrid carbon capture process configurations and determine the configuration that shows the potential to outperform the individual carbon capture processes.
2. Determine the optimum structure for each carbon capture process individually prior to being combined to form a hybrid carbon capture process.
3. Determine a methodology and framework which can be used to evaluate hybrid carbon capture processes.
4. Use multi-objective optimisation to obtain a range of optimum operating condition (Pareto Front).
5. Use the Pareto Front to select different optimum scenarios and further analyse them using energy analysis, exergy analysis and techno-economic analysis to understand the limitations of the hybrid carbon capture processes.
6. Perform a sensitivity analysis to identify the improvement in the individual carbon capture technologies to make hybrid carbon capture processes more viable.

1.5 Thesis Outline

The thesis contains 7 chapters, including this introductory chapter.

Chapter 2 provides a brief overview of the hybrid carbon capture processes technologies that have been studied in the literature and identifies hybrid process configurations with the potential to outperform the individual carbon capture processes. This provides the basis of the hybrid process configurations that are studied further in the thesis.

Chapter 3 reviews and establishes the methodology and framework used to integrate and optimise each individual capture processes as well as the hybrid carbon capture processes. It also provides the framework used to simulate the processes on Aspen HYSYS® to allow replication of the work provided. Finally, Chapter 3 includes the post-simulation analyses used to determine the performance of each hybrid carbon capture configuration.

Chapter 4 and Chapter 5 displays the results obtained for the VSA/low-temperature separation hybrid carbon capture process and membrane/low-temperature separation hybrid carbon capture processes respectively. The chapters also discusses and analyses the results to understand the hybrid carbon capture processes in more detail. This includes energy analysis, exergy analysis and comparison to the base MEA solvents carbon capture process performance.

Chapter 6 combines the main results from the previous 2 chapters to compare the performance of the hybrid processes against each other. It also performs a techno-economic analysis on the optimum

cases for each hybrid carbon capture process. The effect of the potential improvements in the membrane capture technologies on the hybrid carbon capture process was also studied.

Chapter 7 concludes the thesis with a summary of the research findings and recommendations on the hybrid carbon capture process for CCS purposes. There are also recommendations on future work where hybrid processes could be used in different research areas.

The appendix provides examples of the methodologies used as well as results of the optimisation used for individual carbon capture processes. The appendix also contains a copy of all the publications published throughout the PhD candidature.

2 Review of Hybrid Carbon Capture Processes for Coal-Fired Power Stations

In this study, hybrid systems involve the combination of two carbon capture technologies that have been integrated to attempt to compliment the advantages and disadvantages of each process in order to reduce the energy penalty and consequently, the cost of carbon capture. As shown in Figure 2.1, the stages in a hybrid carbon capture process are:

i. The CO_2 recovery stage which rejects nitrogen to the atmosphere with as low a CO_2 concentration as possible.
ii. The CO_2 purification stage that would purify the CO_2 stream to the CO_2 purity required for storage.

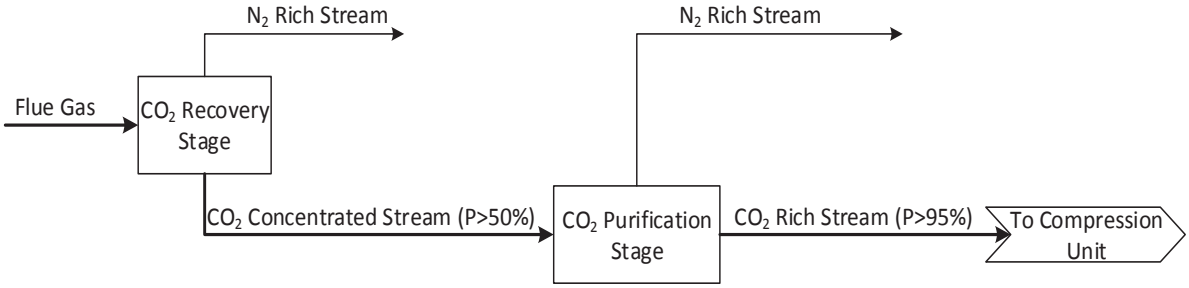

Figure 2.1 Schematic diagram of a hybrid capture process consisting of two capture processes: recovery stage and purification stage.

The different configurations of the two-step hybrid process are shown in Figure 2.1. The potential of each hybrid process has been assessed based on the requirements of high CO_2 recovery rate (horizontal rows) for the initial CO_2 recovery stage and high CO_2 purity (columns) for the secondary stage. The '✗' in the table reflects combinations that do not show potential and '✓' represent options with potential. The justification for those assessments is given in sections 2.1 to 2.4.

CO_2 Recovery \ CO_2 Purity	Absorption	Low-Temp	Adsorption	Membrane
Absorption		✗	✗	✗[1]
Low-Temp	✗		✗	✗
Adsorption	✓[2]	✓		✓
Membrane	✓[3]	✓[4]	✗	

Figure 2.2 Matrix of two-process hybrid systems with assessment of potential for making a hybrid process which gives high CO_2 recovery and purity. Literature references are given in superscript numbers.

2.1 Solvent Absorption

Solvent absorption (Figure 1.4) has been the leading carbon capture technology as a standalone carbon capture process, due in part to the ability to obtain high recovery rates and simultaneously high purity required for carbon sequestration. The main drawback of solvent absorption is the high reboiler duty required to regenerate the solvent in the stripper column when recovering a large amount of CO_2. Hence, when considering the solvent absorption process in a hybrid process, the main aim would be to reduce the reboiler duty. There is active research into new molecules that have a lower specific reboiler duty (i.e. MJ/tonne CO_2), but this is not the subject of this study.

Since the amount of solvent is dependent on the CO_2 concentration, one way to reduce the amount of solvent required for absorption is to increase the concentration of CO_2 in the flue gas as this would improve the absorption kinetics (Rochedo & Szklo 2013). Hence, solvent absorption would be more appropriate as a purification stage, where the feed gas to the solvent absorption process would have been CO_2 enriched from the recovery stage.

Scholes, Anderson, et al. (2013)[3] considered a hybrid system consisting of membrane as a CO_2 recovery stage, followed by a solvent absorption process for both post-combustion and pre-combustion carbon capture. This study showed that the hybrid systems had a higher energy demand for both processes, but would also reduce the solvent absorber height and diameter, which would lead to a reduction in capital cost for this piece of equipment.

It should be noted that some studies have been made by using a hybrid process of solvent absorption and membrane that uses a chemical solvent to increase the performance of the membrane (Zhou et al. 2010)[1]. However, this may be considered as an enhanced membrane process rather than a true integration of two different capture technologies.

2.2 Low-Temperature Carbon Separation

The main energy requirements for low-temperature capture processes (Figure 1.7) comes from the shaft work of the compression of the feed gas prior to the chilling and the compression train required for the refrigeration system. Hence, low-temperature separation would have a high electric power requirement as a recovery stage, as it would have to compress the high flow rate of N_2 in the feed gas compression stage. Furthermore, at low CO_2 concentration and thus low CO_2 partial pressure, a lower temperature would be required to recover the CO_2 resulting in a higher refrigeration duty.

Therefore, a low-temperature capture process performs better as a CO_2 purification stage, when dealing with a smaller feed gas flow rate and higher concentration of CO_2 (Berstad, Anantharaman & Nekså 2013). More importantly, since the low-temperature vapour-liquid separation produces liquid CO_2, it is best for the low-temperature separation process to be used as a purification stage to allow the liquefied CO_2 to be pumped to a supercritical state.

2.3 Adsorption

Adsorption process (Figure 1.6) has shown potential as a stand-alone carbon capture process but has had some challenges meeting the high purity of CO_2 required (>95%) for carbon storage and high CO_2 recovery at the same time (Zhang, Jun, Webley & Xiao 2008). In order to obtain high purity in a Vacuum Swing Adsorption (VSA) process, deep vacuum levels are required to desorb the CO_2 molecules from the adsorbents. This property makes adsorption inefficient as a purification stage but more appropriate for the CO_2 recovery stage, where the VSA process can recover the CO_2 from the flue gas to an intermediate CO_2 concentration that can then go through a CO_2 purification stage.

2.4 Membranes

Finally, membrane separation processes (Figure 1.5) provide more flexibility in a hybrid system, partly due to the balance between permeability and selectivity that usually dictates the performance of a membrane (Favre 2011), as is shown in Figure 2.3. In order to use membranes as a CO_2 recovery step, a high permeability of CO_2 should be prioritised as it will allow more CO_2 through the membrane. On the other hand, when using membranes as a CO_2 purification step, a high selectivity of CO_2/N_2 should be selected to obtain a high purity CO_2 outlet stream.

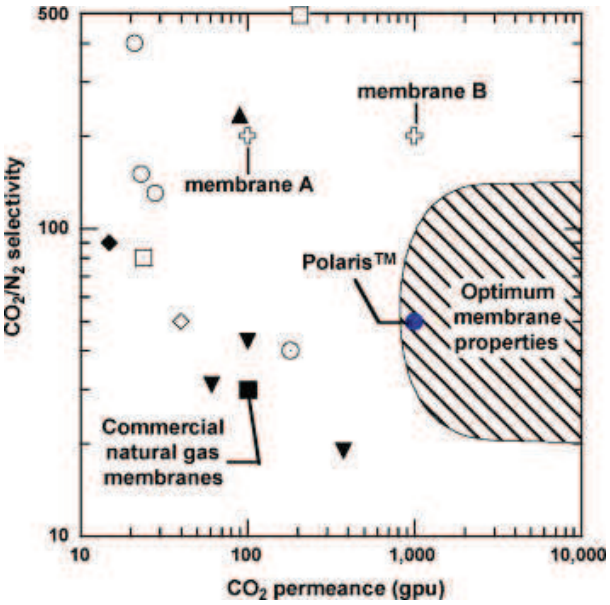

Figure 2.3 CO_2/N_2 selectivity and CO_2 permeance trade-off plot comparing the performance of different membranes reported in the literature. The shaded area represents the region of optimum membrane properties for the separation of CO_2 from flue gas as a single-technology.(Merkel et al. 2010)

Belaissaoui et al. (2012)[4] and Scholes, Ho, et al. (2013)[4] studied the potential application of using membranes as the CO_2 recovery stage with low-temperature separation as the purification stage. Belaissaoui et al. (2012a) reported that this hybrid system showed great potential, especially in the

low-temperature separation and pressurisation of the CO_2, where the power requirement was less than a traditional six-stage intercooled compressor by approximately 10%. Scholes et al. (2013b) reported that the hybrid process were cost competitive with state of the art MEA solvent technology for CO_2 capture from a brown coal power station.

The results obtained by Belaissaoui et al. (2012a) and Scholes et al. (2013b) show that hybrid processes can be competitive with the CCS benchmark process and require further studies to optimise and evaluate other hybrid configurations.

2.5 Concluding Remarks

Low-temperature carbon separation is the ideal CO_2 purification stage since the CO_2 product is in the liquid state. This allows the CO_2 to be pumped to a critical state compared to the conventional method, which requires gaseous CO_2 to be compressed in compression train with intercooling.

For the CO_2 recovery stage, adsorption and membrane separation are the two carbon capture processes that show the most potential since both technologies find it challenging to meet the high CO_2 recovery and CO_2 purity required for CCS. Hence, combining it with low-temperature separation would require the adsorption and membrane separation to focus on the CO_2 recovery while allowing the low-temperature separation to do the final purification required for CCS.

Therefore in this study, two hybrid carbon capture processes will be studied: VSA/ low-temperature hybrid carbon capture system and membrane/ low-temperature hybrid carbon capture system.

3 Process Integration and Optimisation Methodology and Framework

Process integration and optimisation is an important step in the implementation of CCS processes either while retrofitting the process into an existing power plant or when developing a new power plant with CCS. In either case, Process Integration can lead to improved performance and lower costs.

Process integration can be done in two main steps: structural optimisation and parameter optimisation (Smith, R 2005a). Structural optimisation synthesises alternative structures of the process such as selecting the specific capture process. By using the properties of each capture process to determine which process would be best as the recovery and/or purification stage, as represented in the matrix in Figure 2.2. Parameter optimisation changes the operating conditions of the process to improve the performance of the process. Structural optimisation is an important first step as it provides the "skeleton" of the hybrid process, which determine the performance limitation of the process. On the other hand, parameter optimisation is the fine tuning that allows the limitation of the process to be achieved.

Heat integration, also known as pinch analysis, provides a systematic method to maximise the process efficiency through the analysis of heat sources and heat sinks available in the process. Pinch analysis determines the minimum energy target required for the process to run in the ideal situation (Linhoff & Senior 1983). In this study, heat integration was used as part of the structural optimisation to develop a heat exchanger network (HEN), where heat could be exchanged from process stream to process stream.

Therefore, parameter optimisation can be done by systematically varying process operating conditions and monitoring their effects on the performance of the overall process as performed by Belaissaoui, Willson and Favre (2012). Scholes et al., (2013a) also performed a parameter optimisation on a hybrid membrane/solvent absorption carbon capture process by systematically varying parameters such as membrane driving force and the membrane selectivity to study their effects on the CAPEX. Xiao, P et al. (2008) used both structural and parameter optimisation to integrate a VSA carbon capture process with Zeolite 13X as the adsorbent. Structural optimisation was performed by studying a 9-step cycle versus a 12-step cycle and parameter optimisation was performed by varying several key variables whilst monitoring the VSA power performance.

3.1 Chapter Roadmap

Following in this Chapter is a description of the process framework used for the process simulations and the Multi-Objective Optimisation (MOO) methodology utilised to determine the optimum parameters for each case study. The subsequent sub-chapter discusses the flowsheet optimisation, detailing the structural optimisation of each individual carbon capture process to be integrated in a hybrid carbon capture process. The final sub-chapters describe the post-flowsheet optimisation of the carbon capture processes including energy analysis, exergy analysis and techno-economic analysis. A representation of this chapter is shown in Figure 3.2.

3.2 Process Simulation Framework

Throughout the simulations, there was a governing simulation framework, which was required to ensure that all processes were being assessed on a common basis; the power plant used in this study was a standard 300 MW sub-bituminous black coal-fired power plant, as represented in Figure 3.1 The black coal is fed to the furnace where the coal is burnt to heat up the water and the steam is sent to the steam turbine to generate electricity. The flue gas from the furnace is generally exhausted through the stack, as shown in Figure 3.1. The base CO_2 emission of the power plant is considered to be 1.01 t (CO_2)/MWh.

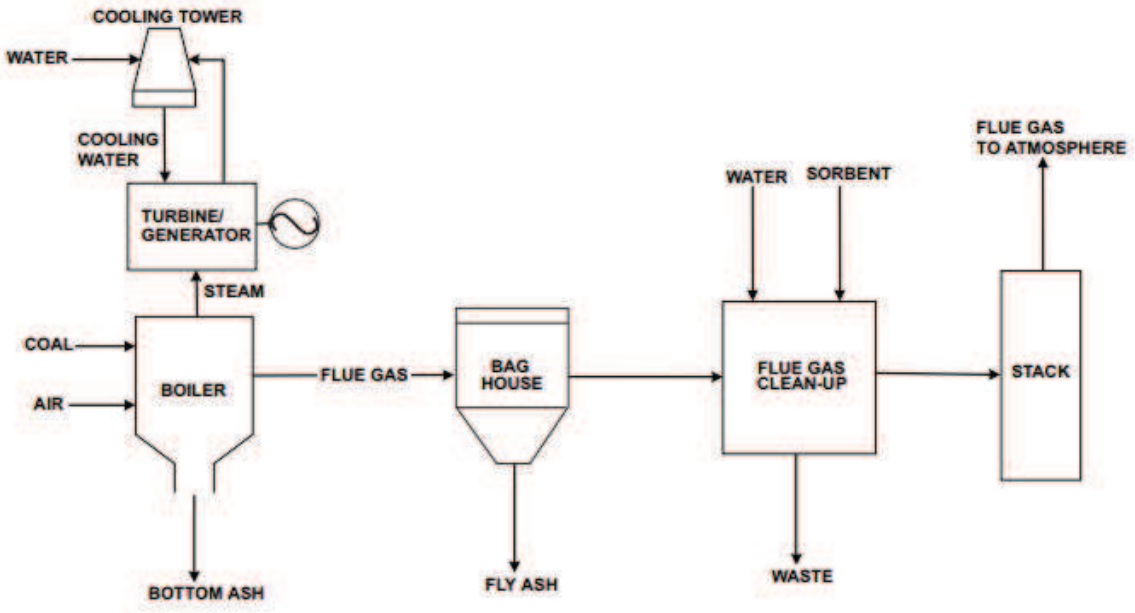

Figure 3.1 Schematic diagram of a coal-fired power station (Spath, Mann & Kerr 1999).

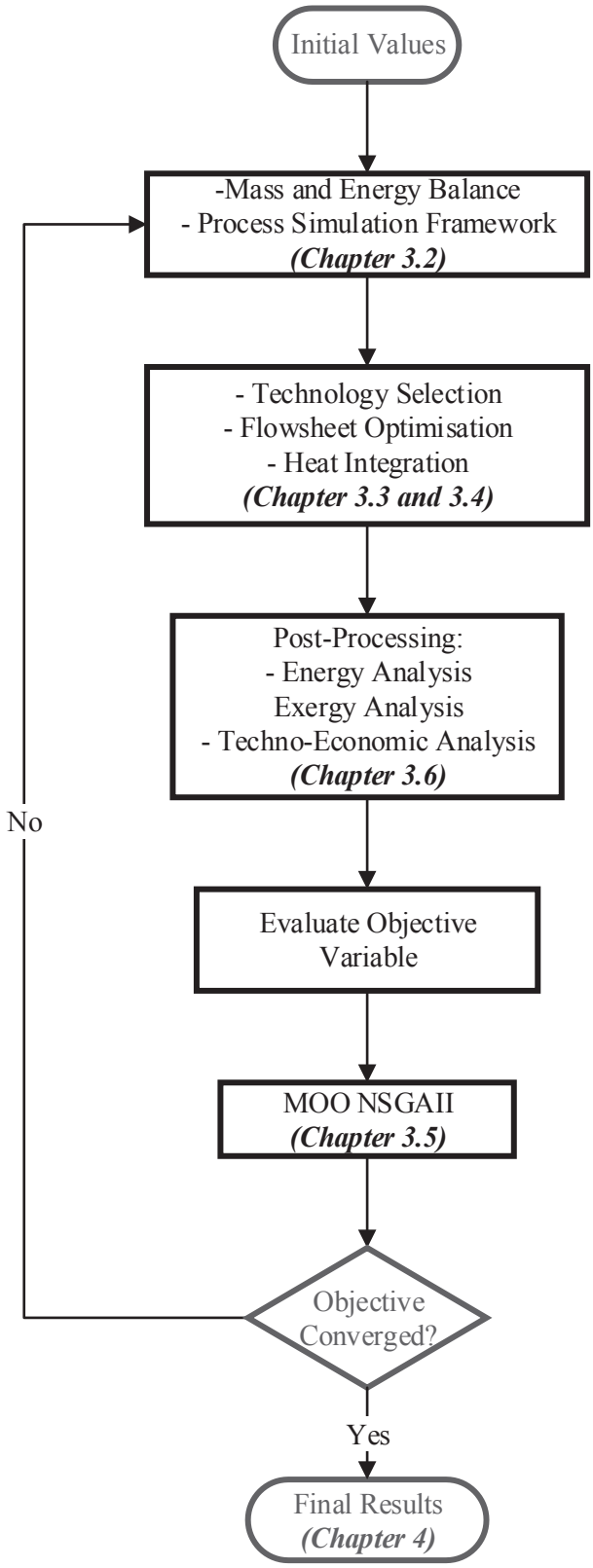

Figure 3.2 Roadmap of Chapter 3, which represents the methodology used to optimise carbon capture processes.

The hybrid carbon capture plant in the power station will be integrated downstream of the flue gas, which may also include flue gas treatment. The flue gas treatment typically contains desulphurisation, denitrification and electrostatic precipitation for dust removal. The flue gas exiting the stack, will generally have temperatures above 100°C and varying levels of impurities depending on the coal feedstock and the environmental regulations of the region. In US and Europe, a flue gas desulphurisation (FGD) unit is installed on most coal power plants to meet their respective EPA regulations (Aaron & Tsouris 2005). In Australia, the coal feedstock has relatively low levels of sulphur and therefore regulations do not necessitate an FGD unit. As a result, a high sulphur content is present in the flue gas (100 ppm-700 ppm), which is higher than US and Europe.

The additional flue gas pre-treatment required prior to the hybrid carbon capture process is dependent on the pre-existing pre-treatment available and the level of contaminants in the flue gas. Therefore, in order to standardise the study, all impurities such as the SO_x and NO_x are removed in the pre-treatment and the flue gas is cooled and pressurised. The water was also removed from the flue gas through a dehydration unit. An example of the additional pre-treatment required for CCS is shown in Figure 3.3.

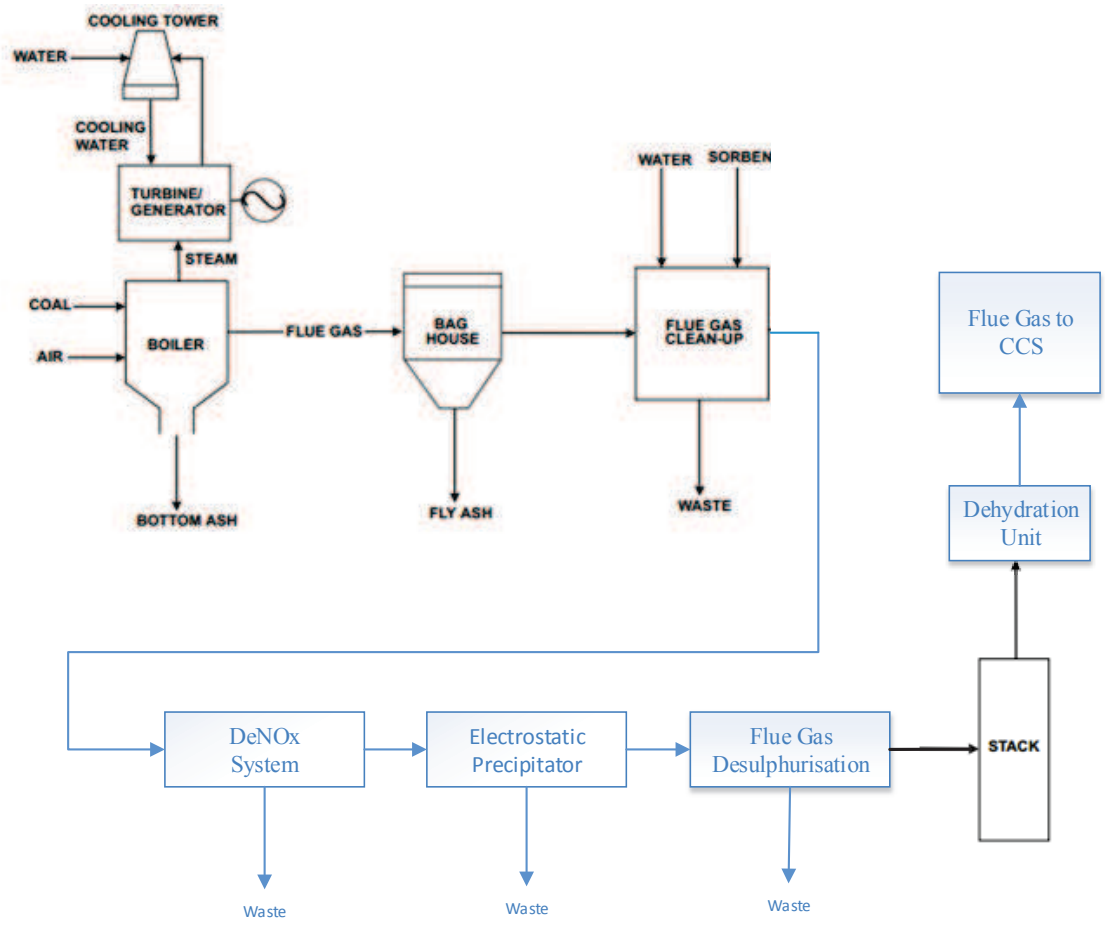

Figure 3.3 Schematic diagram of a coal-fired power station with additional pre-treatment required for CCS.

Following the pre-treatment the flue gas exiting the stack is mainly composed of carbon dioxide, nitrogen and oxygen. The properties of the flue gas are shown in Table 3.1. However, in the simulation cases, the flue gas was assumed to be a binary mixture of CO_2 and N_2 since the VSA and membrane simulation model were based on binary mixtures of CO_2 and N_2.

Table 3.1 Post-combustion flue gas properties based on a 300 MW sub-bituminous coal-fired power station after pre-treatment

Feed Conditions	**Units**	**Value**
Vapour Fraction	-	1.00
Temperature	(°C)	50
Pressure	(kPa)	103
Molar Flow	(kmol/h)	57,800
Mass Flow	(kg/h)	1,670,000
Composition	**(mol frac)**	
CO_2	-	0.1284
N_2	-	0.8135
O_2	-	0.0581

The general modelling process parameters that were used throughout the process simulations are shown in Table 3.2. The compressor and vacuum pump polytropic efficiency were set at 80% (Ho, Allinson & Wiley 2008; Romeo et al. 2009) and the pump adiabatic efficiency was set at 75% (Alabdulkarem, Hwang & Radermacher 2012), respectively. The cooling water temperature was estimated from the highest monthly mean wet-bulb temperature from the Australian Government Bureau of Meteorology for the 1981-2010 year period. The reference power plant is situated in Perth and BOM (2015) reported that the highest monthly mean wet bulb temperature over this period was 20.0°C in the month of February. Using the GPSA (2004) handbook, the cooling water design supply temperature was estimated to be a conservative 25°C. The calculations are shown in Appendix A.4.

The minimum temperature difference in the cooling water heat exchangers were set to 5°C. This controls the process exit temperature. The minimum temperature difference in the plate fin stream-to-stream heat exchangers in the low temperature HEN were set to 5°C and 2°C at the lowest temperatures. A minimum ΔT of 2°C used in the plate-fin heat exchangers at the lowest temperature was to allow the closest possible approach to the CO_2 freeze-out temperature. As discussed in chapter 1, a minimum CO_2 outlet purity of 95% is required for sequestration (Abbas, Mezher & Abu-Zahra 2013) and was used as a constraint in all the simulations.

Table 3.2 Summary of modelling process parameters governing all process simulations

Process Parameters	Units	Value
Compressor Polytropic Efficiency	%	80
Vacuum Pump Polytropic Efficiency	%	80
Pump Adiabatic Efficiency	%	75
Cooling Water Temperature	°C	25
ΔT in cooling water heat exchangers	°C	5
Minimum ΔT in below ambient stream-to-stream heat exchangers	°C	2-5
Minimum CO_2 Purity in CO_2 capture stream	%	95

All the simulations presented in this study were performed using the Aspen HYSYS® software package, version 8.4. The Peng-Robinson (PR) fluid package (Peng & Robinson 1976) was used throughout for determining the thermodynamic properties of each stream. PR package was selected because it is ideal for the combustion and flue gas streams composition (Leng, Abbas & Khalilpour 2010). PR package is also the most enhanced model in Aspen HYSYS and has the largest applicability range in terms of temperature and pressure (AspenTech 2006).

3.3 Individual Capture Systems Optimisation

This subchapter discusses the structural optimisation performed for the individual carbon capture process throughout the study. This will include the adsorption, membrane and low-temperature carbon capture processes considered. Two parameters were generally used in the optimisation of the carbon capture processes: CO_2 overall recovery rates and CO_2 purity. The CO_2 overall recovery rate was defined as the percentage ratio of the molar flow rate of CO_2 being recovered by the carbon capture process to the molar flow rate of CO_2 entering the carbon capture process. The CO_2 purity was defined as the percentage ratio of the molar flow rate of CO_2 exiting the carbon capture process to the total molar flow rate of the stream exiting carbon capture process.

3.3.1 Adsorption

A Vacuum Swing Adsorption (VSA) process with Zeolite 13X as the adsorbent was used as the CO_2 recovery stage. Zeolite 13X was chosen because of its high capacity for CO_2 adsorption, its high CO_2 selectivity and the small footprint of the equipment required (Xiao, P et al. 2008).

The VSA equation used in the MOO simulation was derived from simulation data obtained from a simulation of Zeolite 13X on Aspen Adsorption® simulation with the rigorous dynamic multi-bed approach (Xiao, G & Webley 2013). The VSA simulation was a 3-bed configuration as shown in Figure 3.4. The VSA vessel was divided into two layers: a 0.2m Sorbead layer to remove the water from the flue gas and a 1m Zeolite 13X layer for the CO_2 capture. When using the Aspen simulation software, the mass and energy balances followed the standard Aspen Adsorption® equation. Furthermore, the following assumptions were made:

- The gas was treated as an ideal gas.
- Mass and heat transfer are modelled by linear lumped parameter equations
- The simulation was isothermal.
- No other reactions other than adsorption occurs in the vessels.
- Axial dispersion is negligible.

Finally, the cycle organiser was also set up in the Aspen Adsorption® simulation software and followed the sequence shown in Table 3.3. More details on the data used to simulate the VSA process is shown in Appendix A.1.

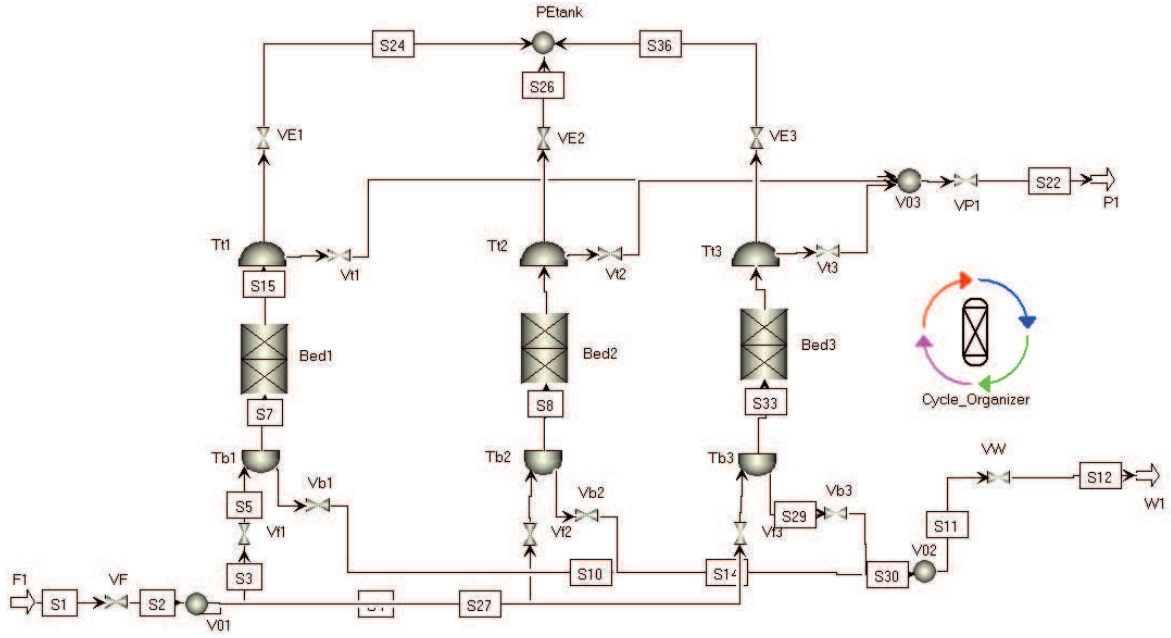

Figure 3.4 Aspen Adsorption® simulation flowsheet & Adsorption bed configuration (Xiao, G & Webley 2013)

Table 3.3 Cycle organiser for three VSA columns: A, B and C. (RP – Re-pressurising; AD – Adsorption; PE↑ - Increase Pressure; PE↓ - Decrease pressurising; IDLE – Idle; EV – Stop Re-pressurisation)

	I	II	III	IV	V	VI	VII	VIII	IX
A	RP	AD	PE ↑	PE ↑	EV	EV	PE ↓	IDLE	PE ↓
B	PE ↓	IDLE	PE ↓	RP	AD	PE ↑	PE ↑	EV	EV
C	PE ↑	EV	EV	PE ↓	IDLE	PE ↓	RP	AD	PE ↑

3.3.1.1 Graphical Residual Modelling

There were 27 different case scenarios obtained from the Aspen Adsorption® simulation, with varying inlet and outlet operating conditions. In order to determine the optimum operating conditions of the VSA carbon capture system, a 3-D graphical residual modelling using data points from 10 optimum case scenarios were used to interpolate the performance of the VSA carbon capture system to yield equation Eq. 3.1. The detailed study is further discussed in the Appendix, Section A.1.

$$f(x,y) = 8.25 - 18.3x - 0.443y + 10.9x^2 + 0.472xy + 0.254y^2 \quad \textbf{Eq. 3.1}$$

Where f is the total specific power required for the VSA

x is the CO_2 recovery rate of the VSA capture process and

y is the product CO_2 concentration.

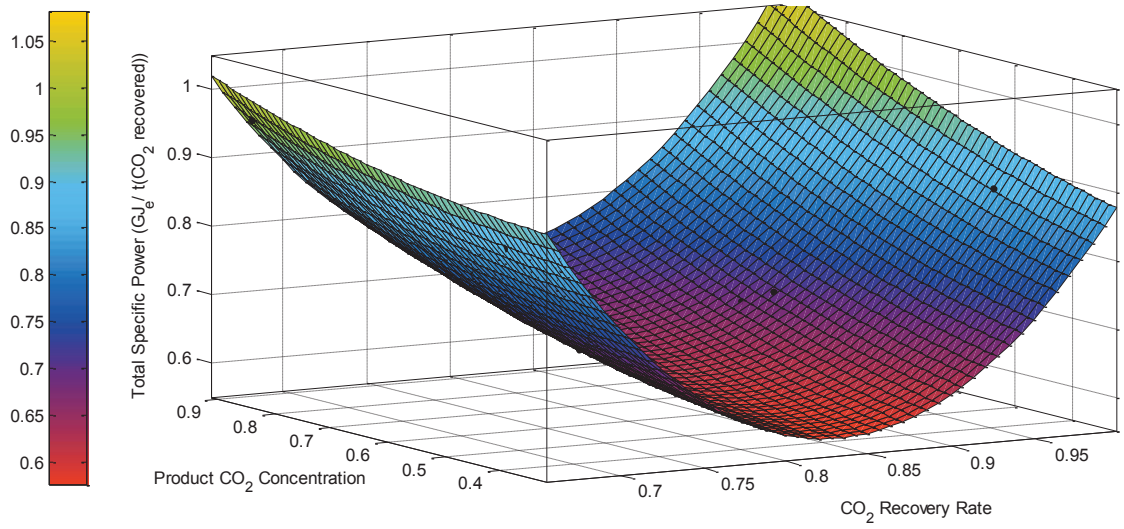

Figure 3.5 Case 3 (10 data points) using MATLAB® software with polynomial order x^2 & y^2 plot of 3-D Surface curve fitting of total specific work required ($GJ_e/t(CO_2)$) vs product CO_2 concentration (%) vs CO_2 recovery rate (%).

The 3-D graphical representation of the equation is shown in Figure 3.5 and the residual error plot is shown in Figure 3.6 (b). Total specific work increases with the product CO_2 concentration because of the duty required by the vacuum pumps, but there is also a parabolic relationship with the CO_2 recovery rate, as there is also a constant component of the work associated with the feed compression, which increases on a specific work basis. The residual error plot shows low errors of Figure 3.6 less than 1% over the range of parameters defined in Table 3.4.

Equation 3.1 provided the operating performance for the VSA carbon capture process within the range given in Table 3.4, which is used in the CO_2 recovery stage of the hybrid carbon capture process.

Table 3.4 Range of VSA performance from interpolated values.

	Units	Minimum	Maximum
VSA CO_2 Recovery Rate	(%)	65	98
VSA CO_2 Outlet Purity	(%)	35	90

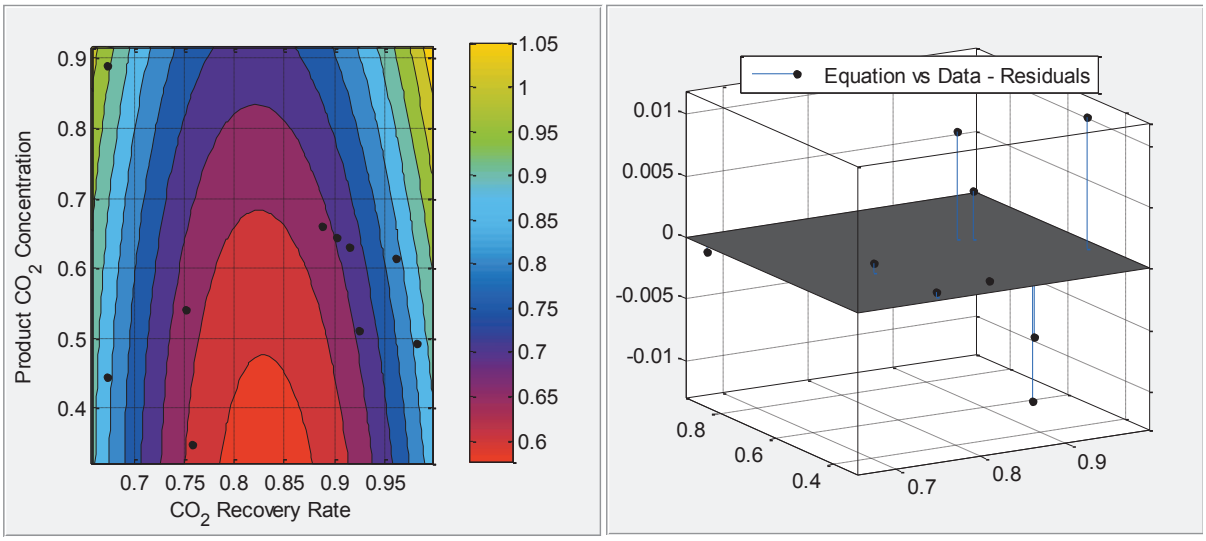

Figure 3.6 Case 3 (10 data points) using MATLAB® software with polynomial order x^2 & y^2(a) Contour plot of total specific work required ($GJ_e/t(CO_2)$) as a function of product CO_2 concentration (%) and CO_2 recovery rate (%). (b) Residual error plot of the total specific work required ($GJ_e/t(CO_2)$).

While Equation 3.1 provided a good fit to the Aspen Adsorption® simulation results, it can be seen from the contour plot in Figure 3.6 that in the high performance zone (CO_2 recovery rate > 0.9 and CO_2 concentration > 0.7), where there were no data points. In order to maintain a conservative performance of the VSA process, a constraint was implemented in the VSA equation when performing the equation in order to maintain the equation within the simulation data. The constraint can be seen in Figure 3.7. The constraint equation is as follows:

$$y_{CO_2} < (-0.949x_{CO_2} + 1.527) \qquad \textbf{Eq. 3.2}$$

Where, y_{CO_2} is the VSA product CO_2 concentration and

x_{CO_2} is the VSA CO_2 recovery rate.

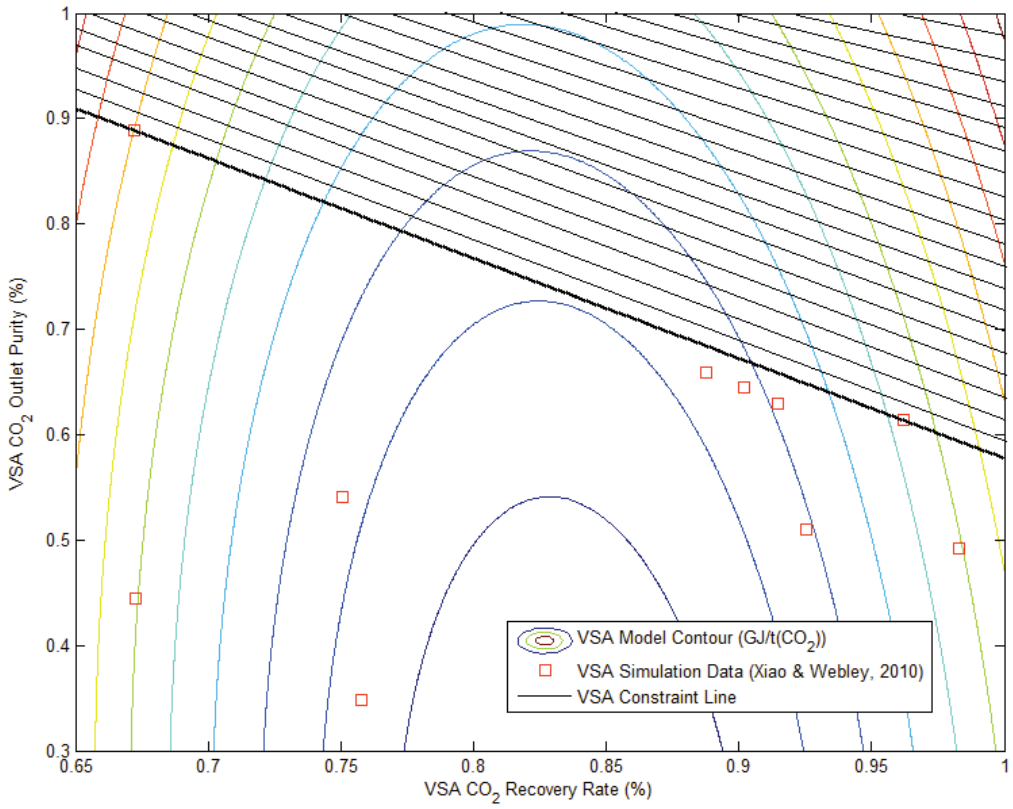

Figure 3.7 VSA Contour plot including the constraint line.

3.3.2 Membrane

The membrane process was an Aspen HYSYS® module based on mass transfer equations, specifically developed for applications in carbon capture simulations (Scholes, Anderson, et al. 2013). There were several assumptions that were made when developing the membrane model:

- Ideal mixing on each stage.
- The gas was treated as an ideal gas; the partial pressure is determined using the molar concentration.
- All components are treated independently; the transfer through the membrane is based only on partial pressure difference and permeability. Therefore, any interaction with other components has been neglected.
- Effects of temperature changes have been neglected.

Using those assumptions, the mathematical model used for the membrane follows the basic ideal gases through a membrane equation (Eq. 3.3).

$$\boldsymbol{Q = \frac{P}{t} A \Delta p} \qquad \textbf{Eq. 3.3}$$

Where Q is the gas permeation rate or flux through the membrane

P is the permeability of the gas through the membrane

A is the surface area of the membrane

t is the thickness of the membrane

Δp is the pressure difference across the membrane

A cross-flow pattern was selected in the simulations as it provides a better performance compared to the other flow patterns(Scholes, Ho, et al. 2013). The detailed mathematical equations used in the membrane module are found in the Appendix, A.2.

The membrane process input parameters used in the simulation are shown in Table 3.5. 100 stages were used to ensure perfect mixing for each flow model. While increasing the number of stages would increase the accuracy, it would also increase the computational time. The input method was "cut"; A membrane cut is defined as the ratio of the molar flowrate of the permeate stream to the feed stream. As discussed in Chapter 2.4, high performance polymer membrane (Merkel et al. 2010; Low et al. 2013) was used with a permeability of CO_2 (P_{CO2}) of 2000 barrer and selectivity of CO_2 versus N_2 ($\alpha_{CO2/N2}$) of 50.

Table 3.5 Membrane Process Input Parameters

Parameter	**Units**	**Value**
No. of Stages	-	100
Method	-	Cross-flow
Input Method	-	Cut
No. of Stages	-	100
Thickness	μm	2.0
CO_2 Permeability	barrer	2000
CO_2 Permeance	gpu	1000
Selectivity, $\alpha_{CO2/N2}$		50

The membrane process was initially analysed individually in order to determine which membrane configuration would be best suited as a recovery stage. Four membrane structures were considered:

I. Single-stage membrane
II. Two-stage membrane with the second membrane on the permeate side
III. Two-stage membrane with the second membrane on the retentate side
IV. Two-stage membrane with an additional membranes on both the permeate side and retentate side of the first membrane.

The membrane process was analysed individually as using the hybrid membrane/low-temperature separation hybrid process in Aspen HYSYS® in combination with the MOO requires significant

computation power and time. For example, running a single generation MOO with a population of 50, using membrane structure IV as the CO_2 recovery stage in combination with the low-temperature separation unit as the CO_2 purification stage, would take approximately 1 day per population calculation. Compared to a VSA/Low-temperature hybrid carbon capture MOO, which would require approximately 1 hour per population calculation. Moreover, it typically requires at least 5-10 generations of MOO to determine whether the hybrid process simulation is performing acceptably and a further 30 generations to obtain converged results.

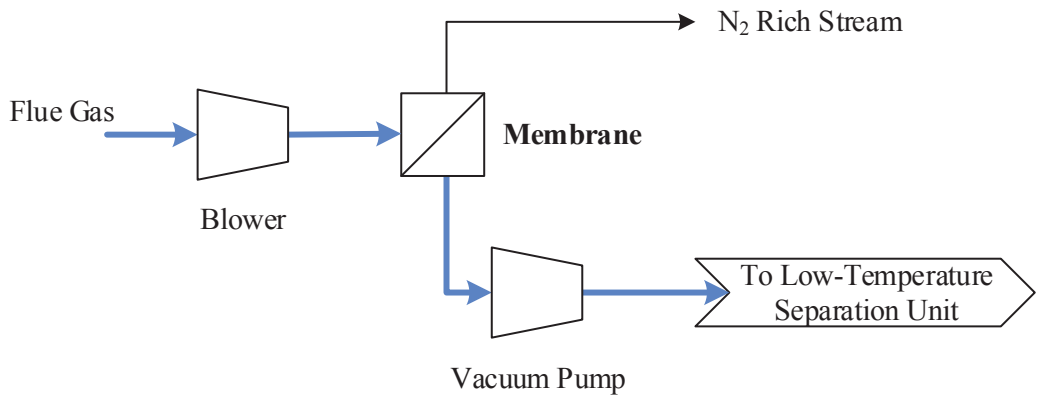

Figure 3.8 Single membrane schematic process flow diagram (Structure I).

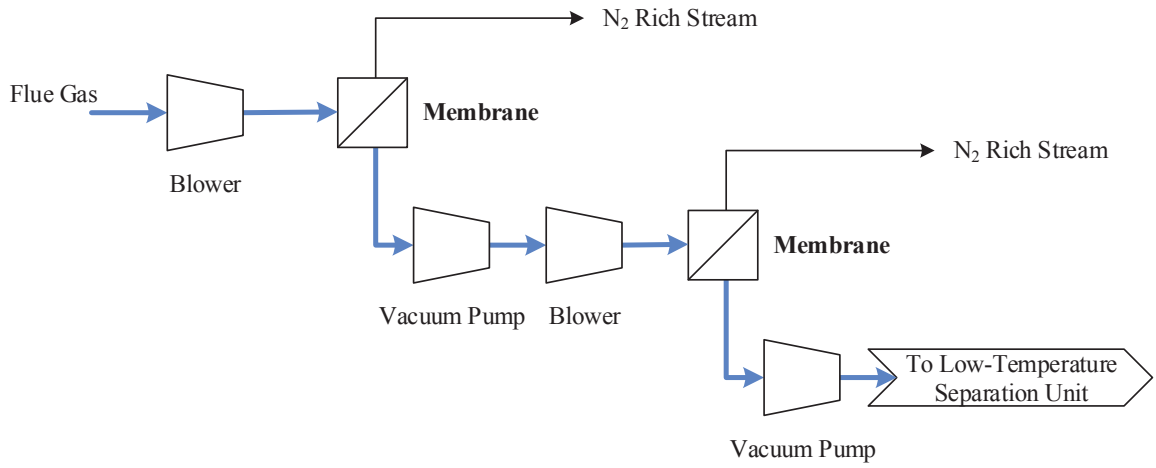

Figure 3.9 Two-stage membrane with the second membrane on the permeate side (Structure II).

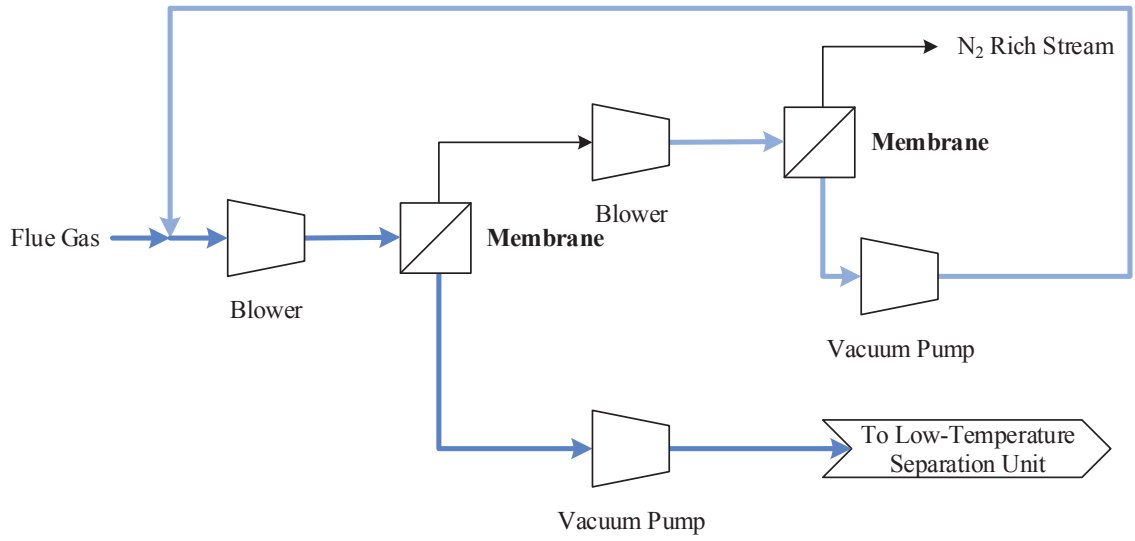

Figure 3.10 Two-stage membrane with the second membrane on the retentate side (Structure III).

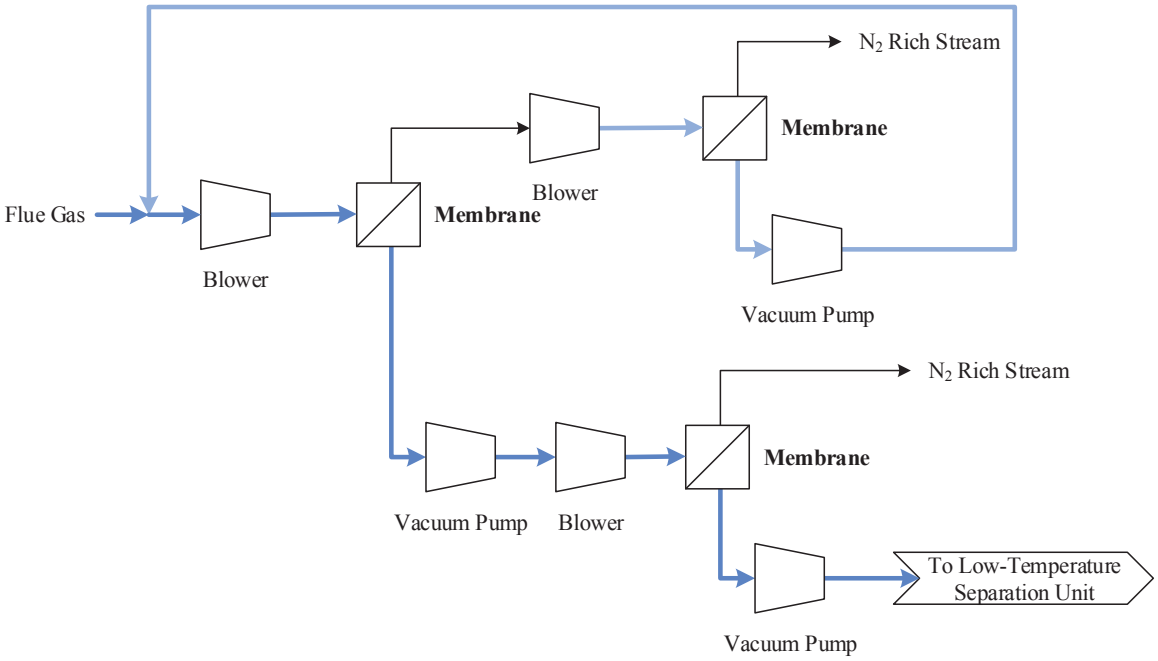

Figure 3.11 Two-stage membrane with an additional membranes on both the permeate side and retentate side of the first membrane (Structure IV).

Among those four structures, single-stage membrane (structure I) and two-stage membrane with an additional two membranes on the permeate side and retentate side of the first membrane respectively (structure IV), were determined to show the most potential as a CO_2 recovery stage in a hybrid carbon capture process. Structure I had the lowest specific work required when lower CO_2 outlet purity was required and Structure IV had better specific work requirement at higher CO_2 outlet purity. Since further purification is performed in the 2nd stage of the hybrid carbon capture process, structure I was

chosen as the CO_2 recovery stage in the membrane/low-temperature hybrid carbon capture process. The detailed results are shown in the Appendix in Section A.2.

The membrane module on Aspen HYSYS® provides a full range of operating performance in terms of the CO_2 recovery rate and the CO_2 outlet purity as shown in Table 3.6. This provides a significant advantage over the VSA carbon capture process as it provides a greater carbon separation and recovery flexibility over the membrane process and the CO_2 purification stage (low-temperature separation).

Table 3.6 Range of membrane performance from Aspen HYSYS® membrane module.

	Units	Minimum	Maximum
Membrane CO_2 Recovery Rate	(%)	0	100
Membrane CO_2 Outlet Purity	(%)	0	100

3.3.3 Low-Temperature Separation

The mixed refrigerants refrigeration systems are primarily used in the LNG process industry (Hatcher, Khalilpour & Abbas 2012). In a mixed refrigerant process, the process stream is cooled in stages, where the refrigerant is separated from its liquid and gaseous phases after each stage. The liquid refrigerant is then cooled and flashed across a valve using the Joule-Thompson effect, causing a temperature drop. (Shukri 2004; Hatcher, Khalilpour & Abbas 2012)

Figure 3.12 shows a hot and cold composite curve, where the hot curve is being cooled down by both mixed refrigerant and pure refrigerant. As it can be seen, the mixed refrigerant has been adjusted so that it can have a better match to the hot composite curve compared to the staggered cooling of the pure refrigerant. This is due to the flexibility the mixed refrigerant can provide by varying the refrigerant composition and the flow rate whereas the pure refrigerant can only vary the number of stages in the refrigeration cycle to match the hot curve.

The other advantage of the mixed refrigeration is that it has fewer stages and therefore has fewer equipment items than the standard cascade refrigeration, thus reducing the equipment capital cost. However, the process is thermodynamically complex and therefore difficult to optimise (Hatcher, Khalilpour & Abbas 2012).

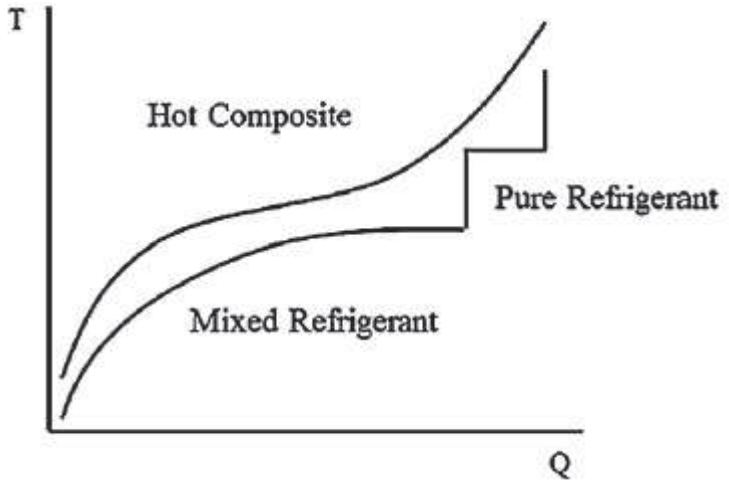

Figure 3.12 Typical hot and cold composite curve for mixed refrigerant versus pure refrigerant (Hatcher, Khalilpour & Abbas 2012)

Three refrigeration systems were initially studied:

i. Propane refrigeration system
ii. Propene refrigeration system
iii. Mixed ethane/propane refrigeration system

The detailed results of the study can be found in the Appendix in Section A.3. It was found that the mixed ethane/propane refrigeration system was the preferred option when lower temperatures were required (approximately -55°C) whereas the propane refrigeration system was preferred at higher temperatures (above -35°C).

An important task in the low-temperature separation is to ensure that the CO_2 is not allowed to form solids at the low-temperature. The temperature at which CO_2 forms solids known as the CO_2 freeze out temperature, which is a property of the CO_2-rich process stream, is determined using Aspen HYSYS®. Therefore, a constraint was embedded in the MOO to reject any process simulation whereby the CO_2-rich process stream temperature is lower than its CO_2 freeze out temperature.

The final structural optimisation was to study the impact of adding a membrane at the nitrogen-rich exit stream of the low temperature separation (Figure 3.13 vs. Figure 3.14). This work was published and presented at the 2013 CHEMECA conference (Li Yuen Fong, Anderson & Hoadley 2013), which is attached in the Appendix Section C.1.

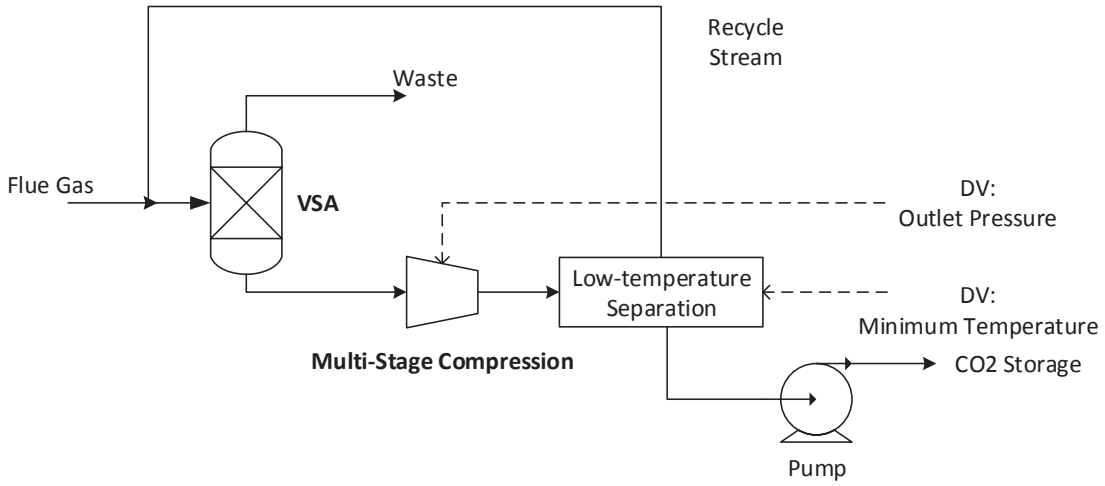

Figure 3.13 Schematic Diagram of VSA & Cryogenic Process without membranes (Case 1)

The low-temperature separation unit shown in Figure 3.13 and Figure 3.14 is shown in further detail in Figure 3.15. The HEN is further discussed in Section 3.6.2.

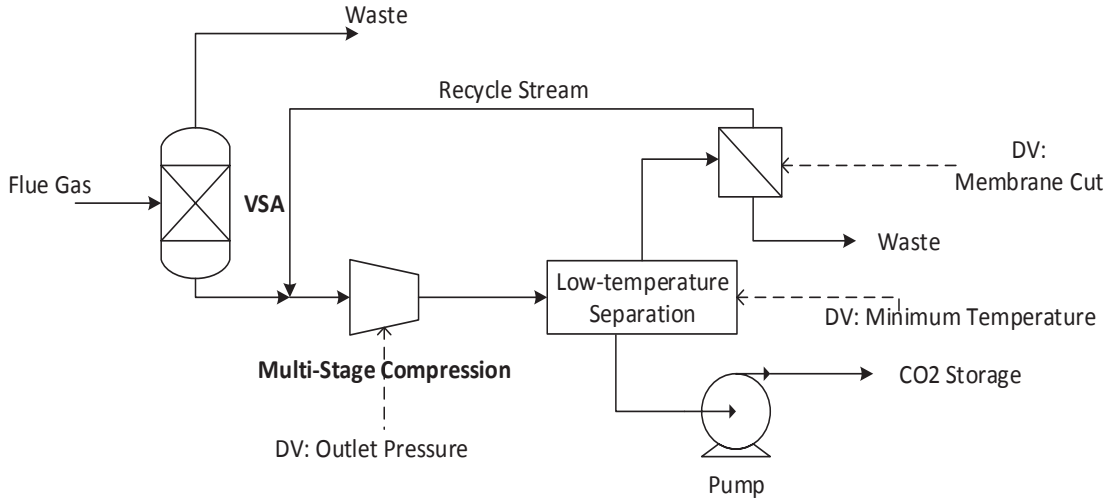

Figure 3.14 Schematic Diagram of VSA & Cryogenic Process with Membranes (Case 2)

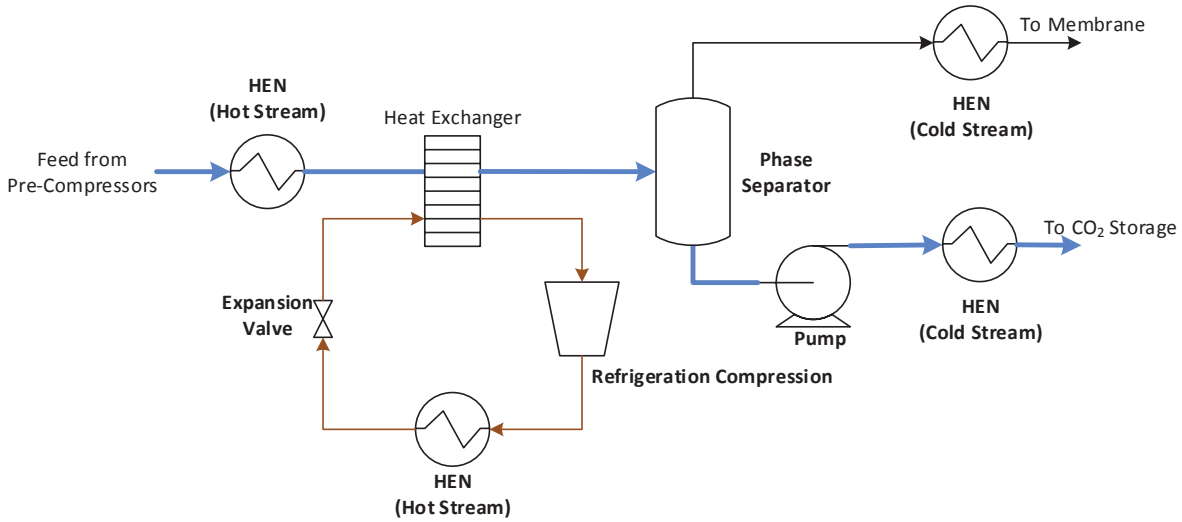

Figure 3.15 Low-Temperature Unit Schematic Diagram (HEN – Heat Exchanger Network)

Finally, the following two subchapters show the final two hybrid structures that were decided to be the optimum structures from the structural optimisation (Figure 3.16 and Figure 3.17). The two hybrid structures (VSA/Low-Temperature Separation and Membrane/Low-Temperature Separation) were further optimised using multi-objective optimisation.

3.4 Hybrid Capture System Parameter Optimisation

3.4.1 VSA/ Low-Temperature Hybrid System

This subchapter will discuss the framework used in order to model the structures on Aspen HYSYS® and the conditions used for the multi-objective optimisation.

In order to determine the optimum operating conditions for each operation in the capture unit, MOO was used to optimise two objective variables:

1. maximising the overall CO_2 recovery rate of the capture process

$$Objective\ 1 = \ Max\left(\frac{Mole\ Flow\ CO_2\ captured}{Mole\ Flow\ CO_2\ in\ Flue\ gas}\right)$$

2. minimising the total shaft work required for the capture process

$$Objective\ 2 = \ Min\sum_{i=1}^{n} Work_i$$

Where n is the total number of equipment requiring work input in the capture process.

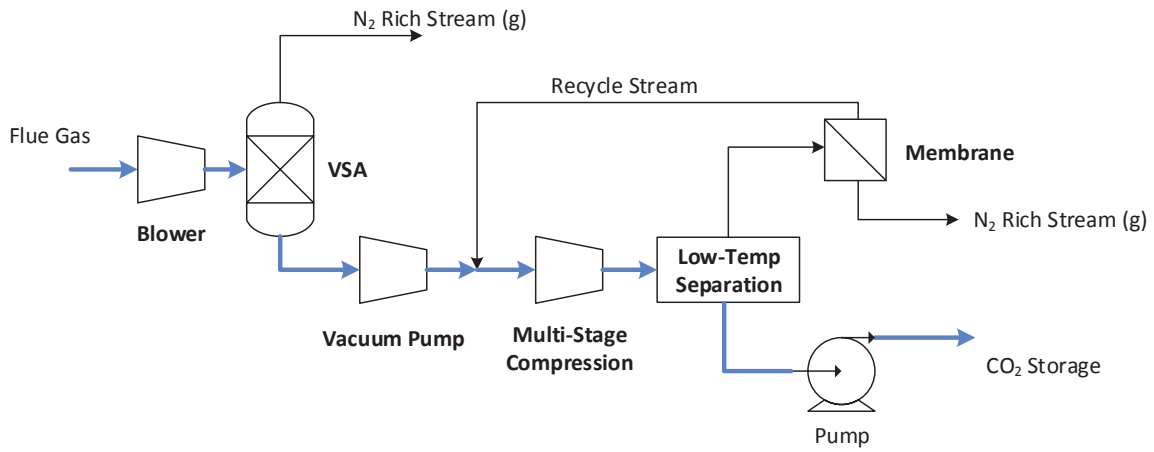

Figure 3.16 Schematic diagram of hybrid carbon capture process using VSA as CO_2 recovery stage and low-temperature separation as CO_2 purification stage.

There were 7 decision variables that were used to optimise the objective variables, which are further discussed in the next section and a table of the decision variables is found in Table 3.7. The decision variables were chosen according to the each capture processes used. The VSA capture process was governed by Eq. 3.1, which determined the two decision variables: *VSA CO_2 recovery rate* and *VSA CO_2 outlet purity*. Following the VSA capture process was the multi-stage compression, which required the output pressure (*multi-stage compression pressure*) as a decision variable. The low-temperature capture process included a refrigeration cycle using a mixed ethane/propane refrigerant. Three decision variables were selected to optimise the performance of the refrigeration cycle: the composition of the refrigerant (*refrigerant ethane molar fraction*), the *refrigerant molar flowrate* and the lowest temperature required from the refrigeration cycle (*Low-Temp Process Stream Outlet Temp.*). Finally the membrane used to purify the recycle stream had only one decision variable: the *membrane cut*.

Table 3.7 Table of decision variable range for MOO of operating conditions for the VSA hybrid process

Decision Variable		Minimum	Maximum
VSA CO_2 Recovery Rate	%	70.0	98.5
VSA CO_2 Outlet Purity	%	50.0	90.0
Multi-Stage Compression Pressure	(kPa)	930	4 000
Refrigerant Ethane Molar Fraction		0.19	0.5
Refrigerant Molar Flow	(mol/s)	1.0	1.65
Low-Temp Process Stream Outlet Temp.	(°C)	-60.5	-40.0
Membrane Cut		0.01	0.76

The results for the MOO are shown in Chapter 4.

3.4.2 Membrane/ Low-Temperature Hybrid System

Similarly to the VSA/Low-Temperature hybrid system, MOO was used to investigate the trade-offs between the two objective functions:

1. maximising the overall CO_2 recovery rate of the capture process

$$Objective\ 1 = \ Max\left(\frac{Mole\ Flow\ CO_2\ captured}{Mole\ Flow\ CO_2\ in\ Flue\ gas}\right)$$

3. minimising the total shaft work required for the capture process

$$Objective\ 2 = \ Min\sum_{i=1}^{n} Work_i$$

Where n is the total number of equipment requiring work input in the capture process.

The schematic diagram of a hybrid membrane/low-temperature carbon capture process is shown in Figure 3.17. Due to the more flexible operating condition of the membrane process as a CO_2 recovery stage (Membrane A) compared to a VSA process, an additional refrigeration system was studied for this hybrid system; a propane refrigerant system was also considered in the low-temperature capture process. Therefore, two cases were optimised using MOO for this hybrid capture process:

Case I – Mixed ethane/propane refrigerant system (minimum temperature of -60°C).

Case II – Propane refrigerant system (minimum temperature of -40°C)

A propane refrigerant system has warmer minimum temperature of -40°C compared to the mixed ethane/propane refrigerant system that was used in the VSA/low-temperature hybrid capture process, which has minimum temperature controlled by the CO_2 freeze out temperature of around -60°C. The warmer temperature from the propane refrigerant system results in a lower degree of CO_2 separation achievable from the low-temperature process. Therefore, in order to meet the CO_2 purity and recovery required for CCS, Membrane A or the multi-stage compression (Compressor C) would need to have a higher performance to compensate for the propane refrigerant system. However, this increase in work from Membrane A or Compressor C, would be a trade-off with the lower work requirement from the propane refrigerant system compared to a mixed refrigerant system.

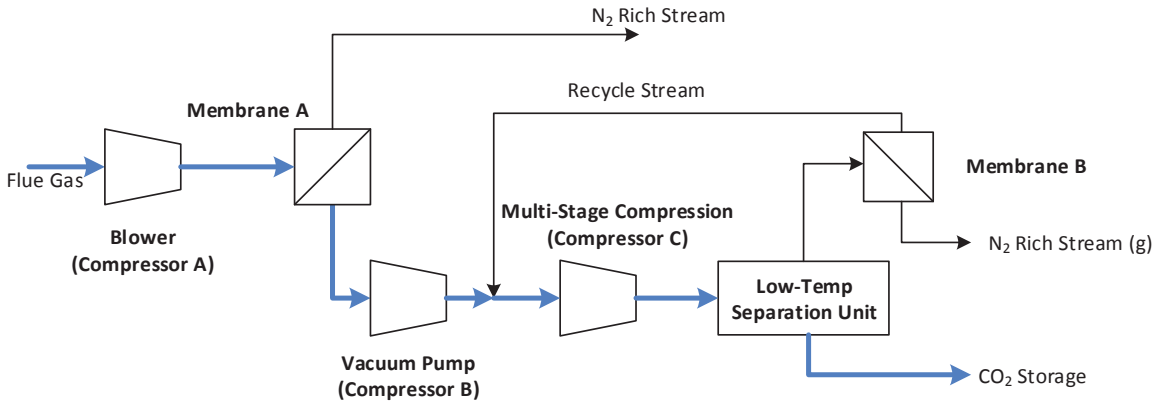

Figure 3.17 Schematic diagram of hybrid carbon capture process using Membrane as CO_2 recovery stage and low-temperature separation as CO_2 purification stage.

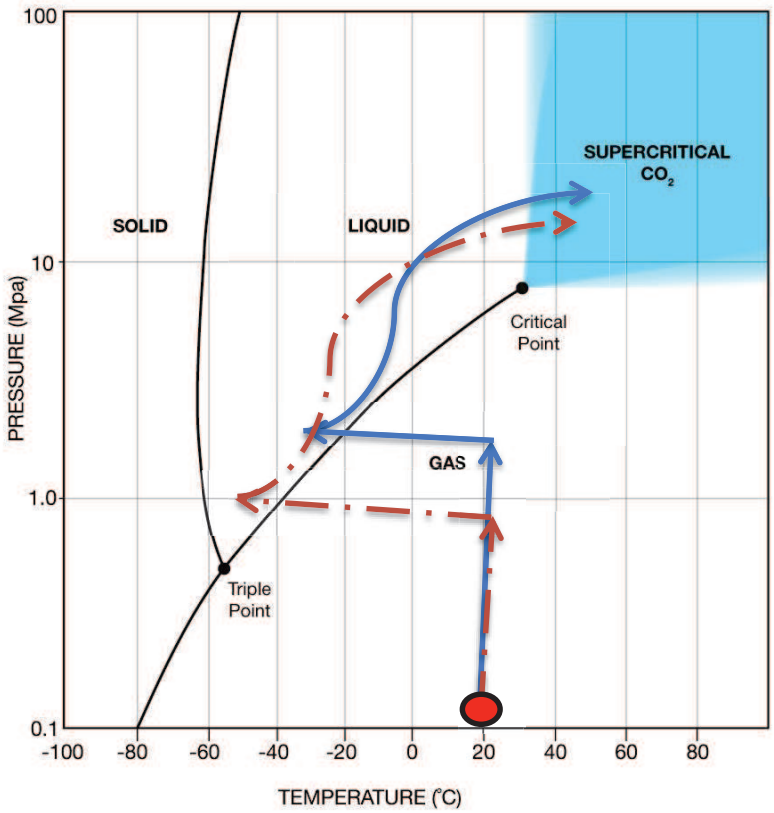

Figure 3.18 Carbon dioxide phase envelope and comparison low-temperature carbon capture system using two refrigeration cycles: mixed ethane/propane refrigerant refrigeration cycle (red dotted line) and propane refrigerant refrigeration cycle (blue full line).

There were 8 and 7 decision variables that were used to optimise the objective variables for Case I and Case II, respectively, as shown in Table 3.8.

The decision variables were chosen according to each capture processes used. The membrane acting as the CO_2 recovery stage, Membrane A, was optimised by varying three decision variables: the *membrane cut*, the *feed pressure* and *permeate pressure*. Following the membrane CO_2 recovery stage was the multi-stage compression, which required the output pressure (*multi-stage compression pressure*) as a decision variable. The low-temperature capture process is where the two cases had different decision variables; Case I had three decision variables that were required to optimise the mixed ethane/propane refrigeration cycle: the composition of the refrigerant (*refrigerant ethane molar fraction*), the *refrigerant molar flowrate* and the lowest temperature required from the refrigeration cycle (*Low-Temp Process Stream Outlet Temp.*). Case II had only two decision variables that were required to optimise the propane refrigeration cycle: the *heat exchanger network intermediate temperature* and the lowest temperature required from the refrigeration cycle (*Low-Temp Process Stream Outlet Temp.*).The difference in decision variables are due to the different heat exchanger network used in each case, which is further discussed in section 3.6.2. Finally the membrane used to purify the recycle stream, membrane B, had only one decision variable: the *membrane cut*.

Table 3.8 Table of decision variable range for MOO of operating conditions for the membrane hybrid process

		Case I - Mixed Refrigerant		**Case II - Propane Refrigerant**	
Decision Variable	**Units**	**Min**	**Max**	**Min**	**Max**
Membrane A Cut	-	0.1	0.8	0.1	0.9
Membrane A Feed Pressure	(kPa)	115	200	115	200
Membrane A Permeate Pressure	(kPa)	20	100	10	100
Multi-Stage Compression Pressure	(kPa)	1250	3000	2000	4500
Refrigerant Molar Flow	(mol/s)	1.2	3	*N/A*	*N/A*
Refrigerant Ethane Molar Fraction	-	0.2	0.8	*N/A*	*N/A*
Heat Exchanger Network Intermediate Temperature	(°C)	*N/A*	*N/A*	-15	5
Low-Temp. Process Stream Outlet Temperature	(°C)	-60	-40	-35	-25
Membrane B Cut	-	0.05	0.8	0.25	0.9

3.5 Multi-Objective Optimisation Methodology

Multi-objective optimisation was used to investigate the trade-offs associated with the two objective functions.

Although a process can be optimised for one objective at a time (single objective optimisation, SOO), there are usually multiple objectives that need to be considered simultaneously. When more than one conflicting objective is involved, the final result will be a set of optimal solution known as Pareto-optimal solutions (Rangaiah 2009).

There are two main MOO methods: generating methods and preference-based methods. As the name would suggest, the main difference between those two categories is that in the latter, the user gets to input their preference while generating the Pareto-optimal solutions whereas generating methods produces Pareto-optimal solutions without any inputs from the user. In this research, a non-dominated sorting genetic algorithm will be used for the generation of the Pareto optimal solutions. A flowchart of the genetic algorithm is shown in Figure 3.19, where a *Random Seed* is used to initiate the first set of data. Each set of data is called a "Population". The initial population is evaluated and checked against the convergence criterion. If the criterion is met, the program will end, otherwise, a new improved population is determined using a combination of crossover probability and mutation probability. The new population is then evaluated and checked for convergence.

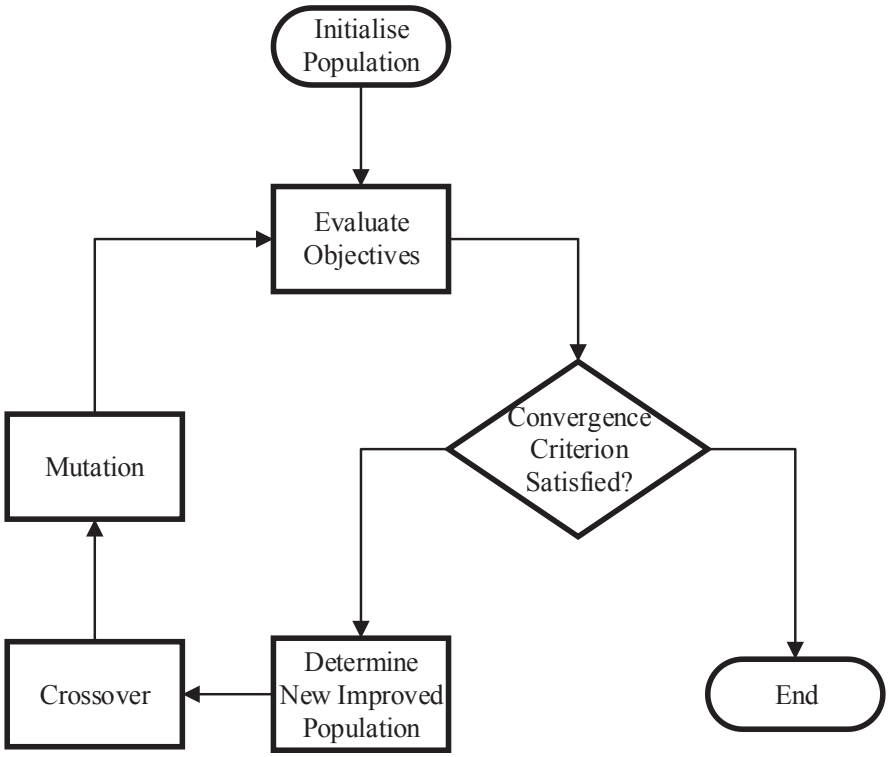

Figure 3.19 Genetic Algorithm Flowchart

This is a well-developed method which produces solutions with a Pareto curve that is well dispersed (Bhutani, Naveen, Ray & Rangaiah 2006). This method has previously been used for the analysis of absorption-based carbon capture systems by Harkin, Hoadley and Hooper (2012). Depending on the results obtained, further optimisation of a specific range of solution using preference-based methods might be applied.

Harkin, Hoadley and Hooper (2012) demonstrated the application of MOO in optimising the solvent absorption process and they also displayed the methodology of MOO using simulation followed by heat integration analysis as depicted in Figure 3.20.

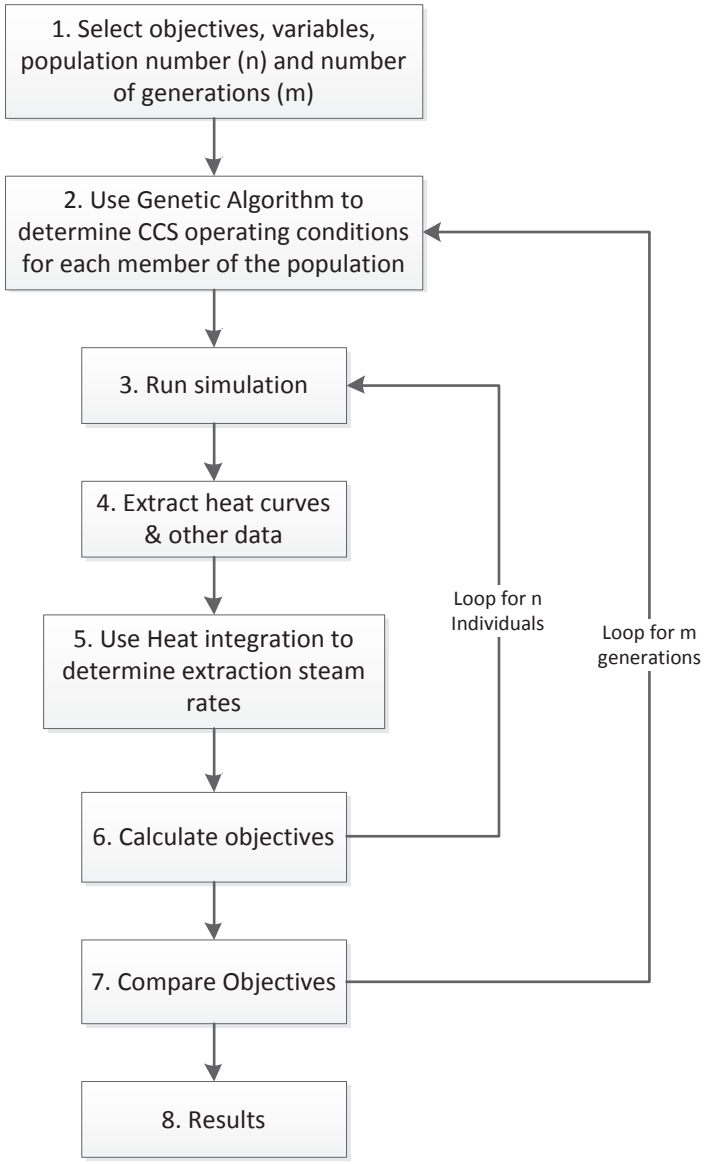

Figure 3.20 Optimisation methodology using combination of MOO and heat integration (Harkin, Hoadley & Hooper 2012)

The methodology has 8 steps:

1) Selecting the input arguments for the optimisation process such as the objectives (e.g. operating cost, capital cost, amount of carbon dioxide captured) and variables (e.g. fraction of carbon dioxide that needs to be captured with respect to the feed stream)
2) Perform the MOO. In this step, the optimisation of the process a genetic algorithm using MS Visual Basic® is performed. This will provide optimised values for the process simulation input for the carbon capture system (CCS).
3) Process simulation. In this step, the carbon capture process along with the flue gas of the power plant is simulated on Aspen HYSYS® and/or Aspen Plus ® using the input data provided in the previous step.
4) Extraction of data. After the simulation of the processes, the necessary data are extracted using MS Visual Basic®.
5) Perform heat integration. Using the data extracted, heat integration can be performed to find the optimum heating and cooling required.
6) Calculate objectives. In this step, the pre-determined objectives can be calculated using all the data obtained from the heat integration and the process simulation. Following this step, step 3 will be repeated if more optimisation is required in the process simulation.
7) Compare objectives. The objectives obtained are then compared using the Pareto-optimal solutions. The procedure is then repeated from step 2 until all the variables have been studied.
8) Finally the results are obtained.

This methodology integrates the MOO and heat integration techniques. When optimising a solvent absorption carbon capture, integrating the heat integration in the MOO is essential since the solvent regeneration heater is a major energy consumer. However, in this research, adsorption and membrane carbon capture are being investigated, therefore the heat integration analysis was performed when designing the process flowsheet prior to the MOO. Further analysis was performed on the MOO results obtained, called "Post-flowsheet optimisation" and is further discussed in section 3.5.

In order to integrate the MOO genetic algorithm to the Aspen HYSYS process simulation, a Visual Basic® Interface (Bhutani, N et al. 2007) was used as shown in Figure 3.21. There were a number of inputs to be selected in the interface:

Objective Variables – Process variables that need to be optimised (minimised or maximised)

Decision Variables – Process variables that are going to be varied over a set range to determine their effect on the carbon capture process, specifically the objective variables.

Constraints – Process variables that need to be monitored in the process simulation that need to be within a specific range to validate the simulation and results. For example, the CO_2 purity in the outlet stream needs to be over 95% to be ready for sequestration, therefore the CO_2 outlet purity would be a constraint

Crossover probability – The method for two parents to be combined to form a child when generating a new population

Mutation probability – The probability that each bit will undergo a change in value in the offspring population

The crossover probability was selected to be in the range of 0.5-0.9 and the mutation probability was selected to be approximately equal to 1/n, where n is the number of decision variables (Deb et al. 2000; Bhutani, Naveen, Ray & Rangaiah 2006).

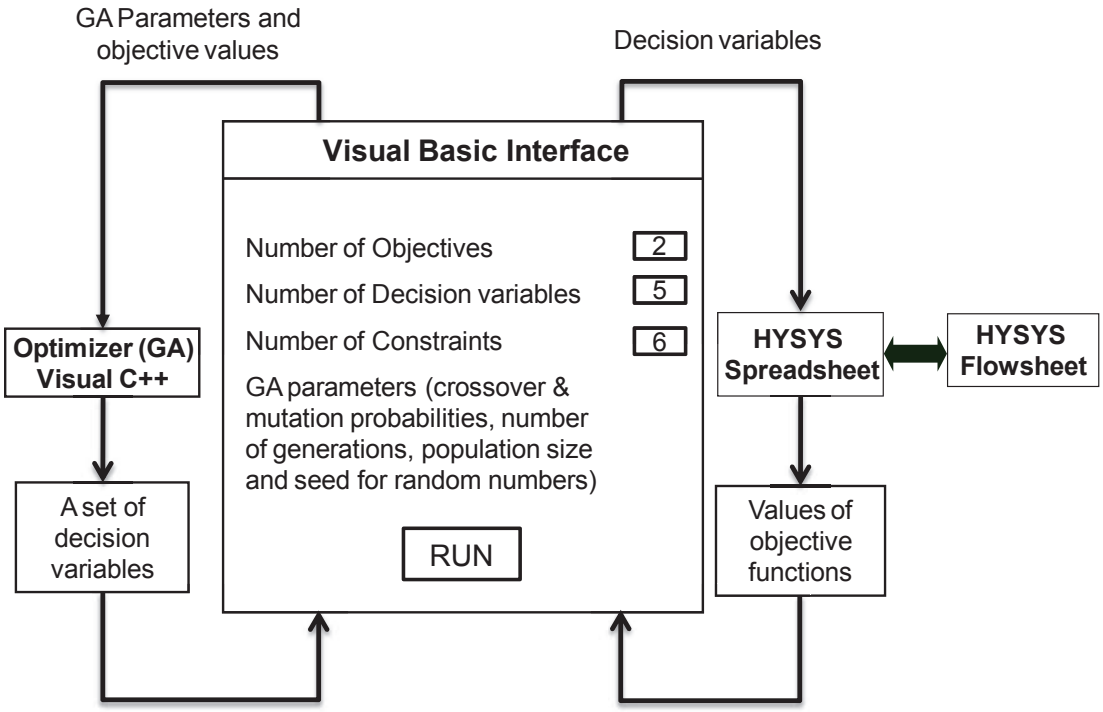

Figure 3.21 MOO Framework with Visual Basic® Interface (Bhutani, N et al. 2007)

3.6 Post-Simulation Analysis

3.6.1 Energy Requirement and Energy Penalty

As discussed in Chapter 1.3, reducing the energy penalty for retro-fitting CCS into coal-fired power plants has been one of the main challenges that CCS faces. Therefore, this study focused on reducing the energy required to implement the hybrid carbon capture technologies.

The energy required for implementing CCS is highly dependent on the technology employed. For solvent absorption, the main energy requirement comes from thermal regeneration of the solvent (Smith, K et al. 2009). On the other hand, VSA and membrane capture technologies are highly dependent on the change in pressure, which is provided by rotating equipment such as compressors and vacuum pumps. Hence, in this study, the energy requirement will be measured in terms of shaft work required (electrical energy) compared to conventional thermal energy required that is used in solvent absorption studies.

$$\boldsymbol{W_{Total} = W_A + W_B + W_C + W_D + W_{Pump}} \qquad \textbf{Eq. 3.4}$$

$$\boldsymbol{\dot{W}_{Total} = W_{Total} \div \dot{m}_{recovered}} \qquad \textbf{Eq. 3.5}$$

Where, W_{Total} is the total shaft work required (MW)

$W_{A,B,C,D}$ is the work required for compressors A,B,C and D respectively (MW)

W_{Pump} is the work required for the CO_2 pump (MW)

$\dot{W}_{Total}$ is the total specific work required (GJ_e/t(CO_2 recovered))

and $\dot{m}_{recovered}$ is the mass flow rate of CO_2 being recovered.

3.6.2 Heat Integration

When integrating the CCS process, pinch analysis provides a systematic method to maximise the process efficiency in terms of heat source and heat sinks available in the process. Heat integration has been used in academia as well as industry since Linhoff and Senior (1983) identified pinch analysis as a systematic way to improve the thermodynamic efficiency of a process. Since then, heat integration has been heavily studied, which can be found in the Handbook of Process Integration (PI) (Klemeš 2013). In this study, heat integration was used in combination with MOO to improve the heat exchange between the process stream and the refrigeration system.

An important aspect of the pinch analysis is that it allows the calculation of the minimum energy target for utilities without the need to design the actual heat exchanger network (Linhoff & Senior 1983). This energy target is then a good indicator to identify whether the simulated process is using the maximum available heat sources (hot streams) and heat sinks (cold streams). Smith, R (2005b) provides a step-by-step overview of the pinch analysis technique.

Processes that require heat sources or sinks, such as solvent absorption and low-temperature separation benefit most from the pinch analysis technique. Harkin, Hoadley and Hooper (2012) performed a heat and process integration analysis of a brown coal-fired power station with a solvent absorption carbon capture process, with a focus on pinch analysis. Their study showed that heat integration was a highly valuable technique as the specific energy penalty was reduced by 0.40 GJ_e/t

(CO_2 captured) with effective heat integration. Capture processes that require mainly electrical power, such as membrane processes would not provide significant improvement through pinch analysis.

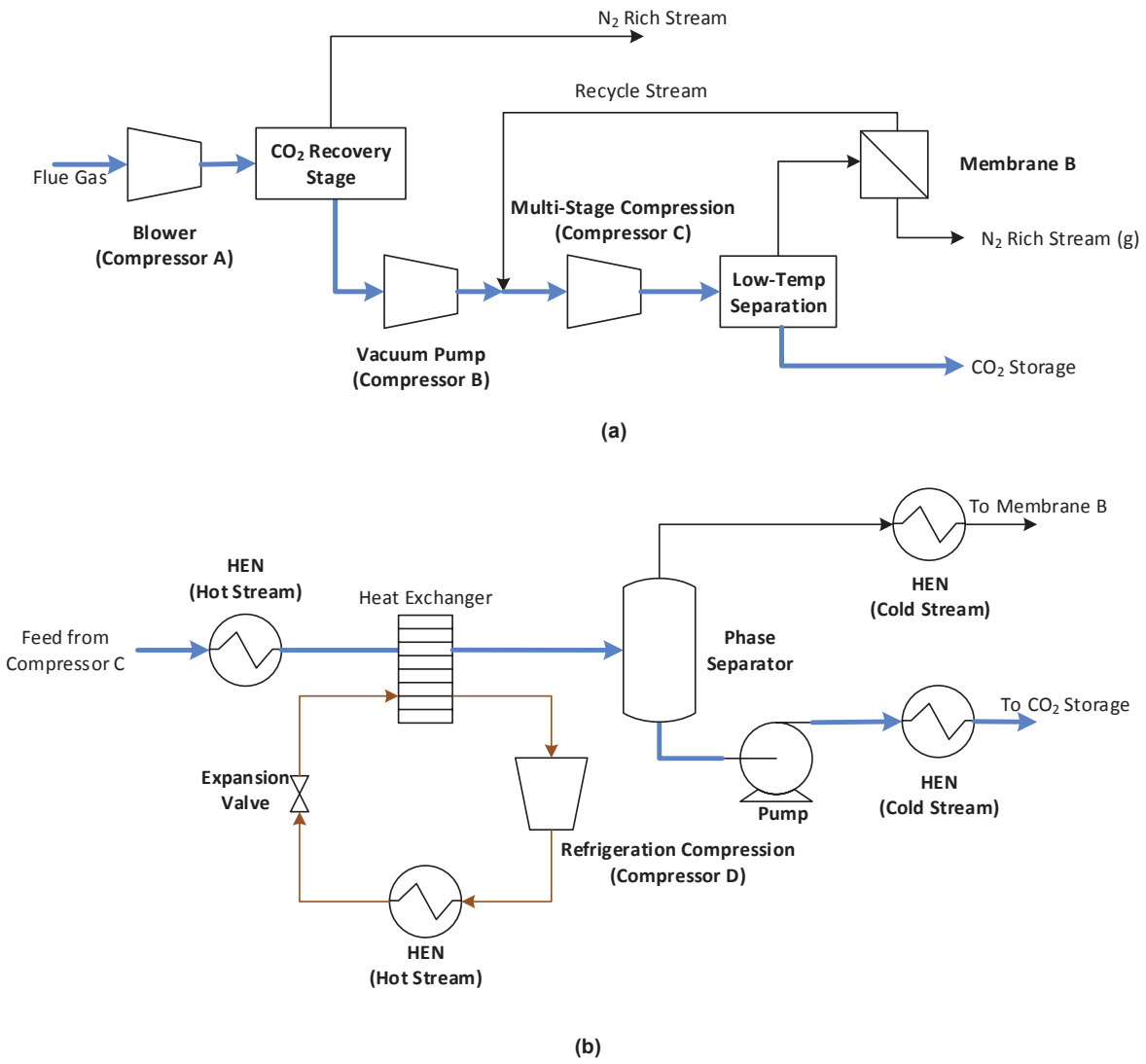

Figure 3.22 (a) Hybrid Carbon Capture Schematic Diagram (b) Low-Temperature Unit Schematic Diagram (HEN – Heat Exchanger Network)

This study focused on the heat integration of the refrigeration system with the cold process stream and develops a heat exchanger network as shown in Figure 3.22.

An example of the heat composite curves for propane refrigerant and mixed refrigerant, when heat integrated in a membrane and low-temperature hybrid carbon capture process is shown in Figure 3.23 and Figure 3.24 respectively. Furthermore, as discussed in Section 3.3.3, the two refrigeration cycles have different heat curves, where the mixed refrigerant has a flexible curve that can match the process

curve. Therefore, the heat exchanger networks for each refrigeration system were different and shown in Figure 3.25 and Figure 3.26.

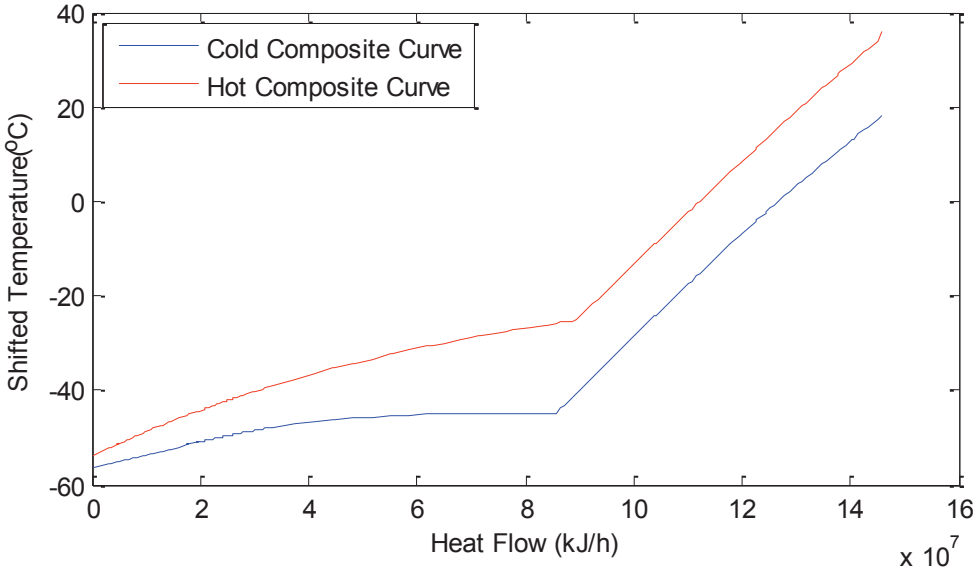

Figure 3.23 Heat composite curve example of heat exchanger network in a low-temperature carbon capture system using a mixed ethane/propane refrigerant refrigeration system.

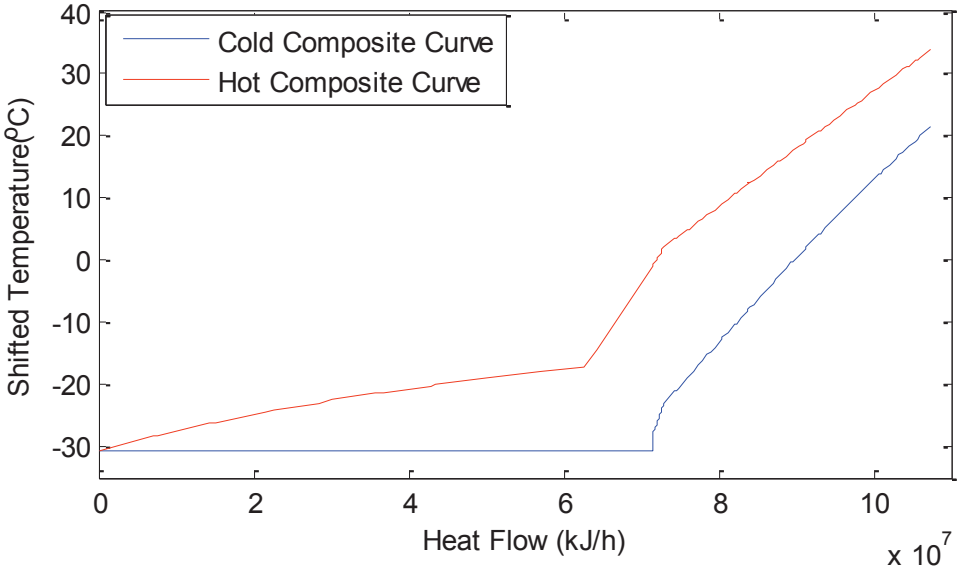

Figure 3.24 Heat composite curve example of heat exchanger network in a low-temperature carbon capture system using a propane refrigerant refrigeration system.

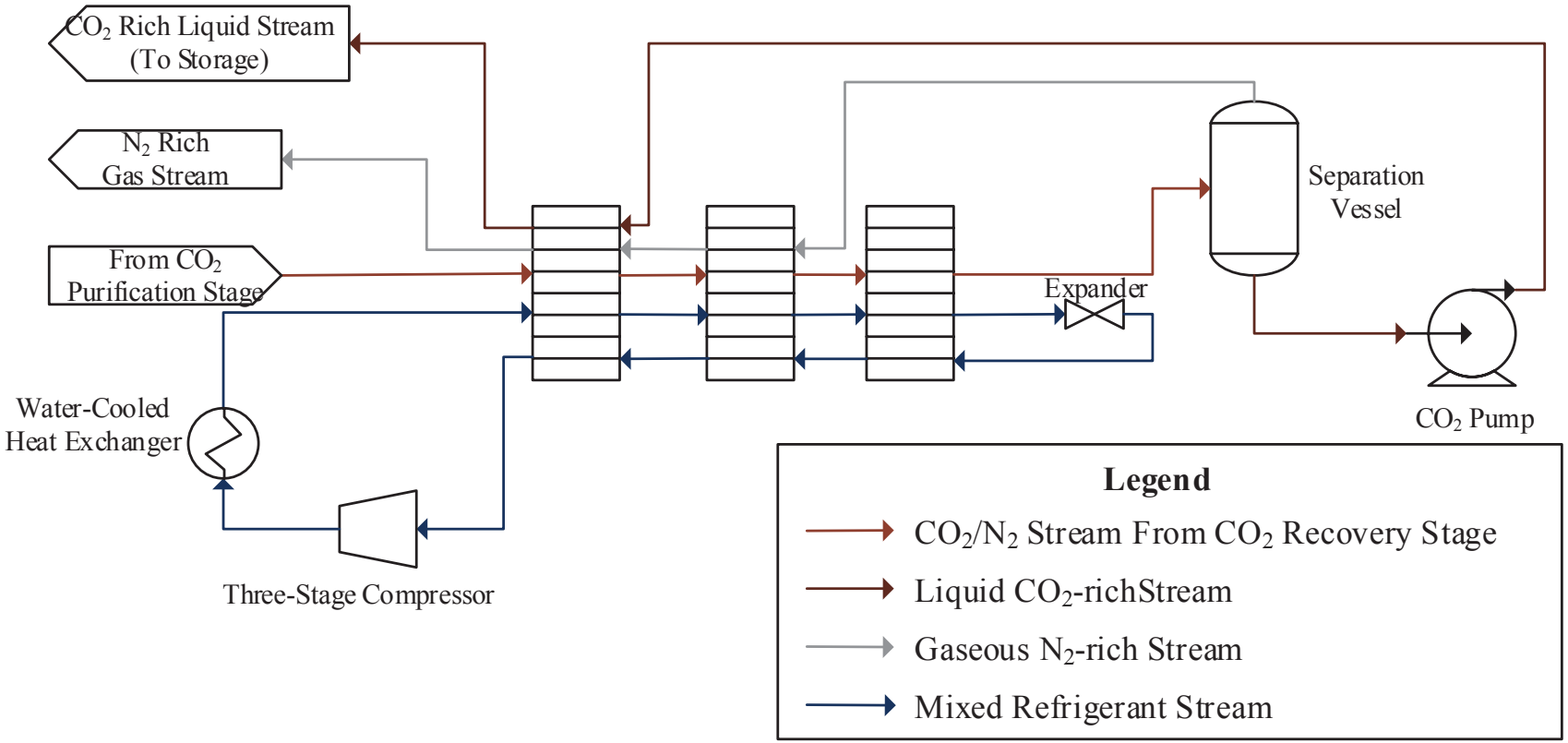

Figure 3.25 Heat Exchanger Network (HEN) mixed refrigerant system.

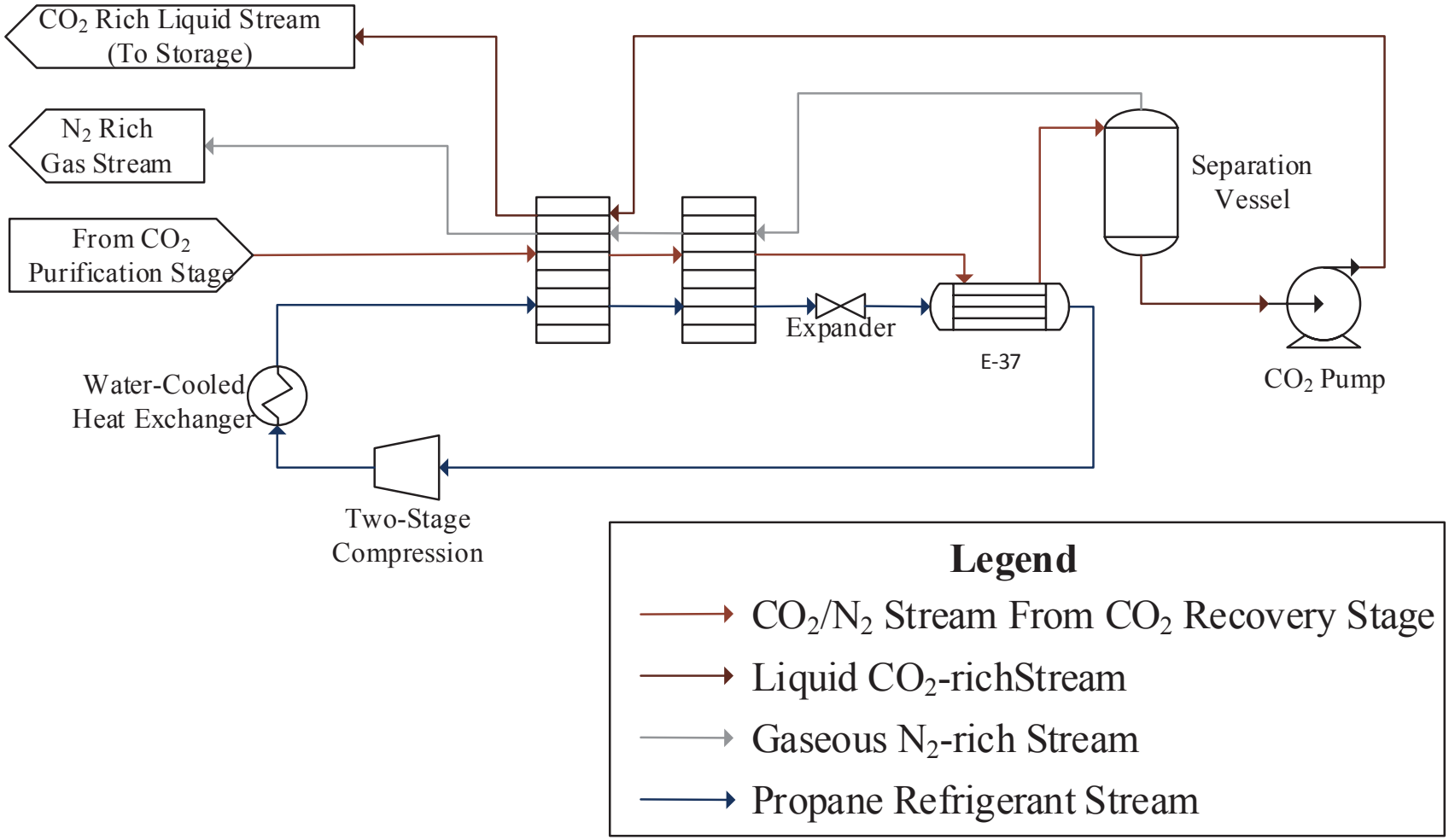

Figure 3.26 Heat Exchanger Network (HEN) propane refrigerant system.

3.6.3 Exergy Analysis

This section explains the concept of exergy analysis and how it can be useful in identifying improvements which reduce the capture penalty.

Energy analysis is used to determine the performance of a process and used to reduce energy costs. It uses the first law of thermodynamics to calculate the quantity of energy going into and out of a system. However, it does not take into account the quality of energy also known as 'loss and gain of thermodynamic efficiency'. In order to take into account both the quantity and the quality of the energy level, both the first and second laws of thermodynamics need to be used simultaneously. This leads to exergy accounting, which allows the calculation of thermodynamic losses of a system coupled with the energy flow in the system.

By taking into account the energy rate balance (First law of thermodynamics) and the entropy changes whilst applying the Second law of thermodynamics, it is possible to derive the exergy rate balance.

This would allow the substitution of energy (Q^+) from the energy balance (Eq 3.6) and to be replaced by exergy (E^+) to form Eq. 3.7 (Borel & Favrat 2010):

$$\sum_k[\dot{E_k^+}] + \sum_i[\int \dot{\delta Q_i^+}] + \dot{Q_a^+} + \sum_n[\dot{Y_n^+}] = 0 \qquad \textbf{Eq. 3.6}$$

$$\sum_k[\dot{E_k^+}] + \sum_i[\dot{E_i^+}] + \sum_n[\dot{E_n^+}] = \dot{L} \geq 0 \qquad \textbf{Eq. 3.7}$$

Where,

$\sum_i[\int \dot{\delta Q_i^+}]$	is the heat received from the reservoir at a temperature T_i
$\dot{Q_a^+}$	is the heat received from the atmosphere at a temperature T_a
$\sum_n[\dot{Y_n^+}]$	is the transformation power received at the level of the network n
$\sum_k[\dot{E_k^+}]$	is the work power received by the system
$\sum_i[\dot{E_i^+}]$	is the heat exergy received from the reservoir at a temperature T_i
$\sum_n[\dot{E_n^+}]$	is the global exergy rate loss (always positive according to the 2nd Law of thermodynamics
$\dot{L}$	is the exergy loss rate

The global exergy rate loss, $\sum_n[\dot{E_n^+}]$, is the exergy rate loss from the streams entering and leaving the process. This exergy can be divided into physical exergy, chemical exergy and mixing exergy.

The physical exergy of a material stream, $\dot{E}_{ph}^{+}$, is the maximum amount of shaft work that can be generated when the stream is changed from the actual conditions (T, P) to thermomechanical equilibrium at reference temperature (T_o, P_o). The physical exergy can be determined using the following equation (Tzanetis, Martavaltzi & Lemonidou 2012):

$$\sum_n \dot{\boldsymbol{E}}_{\boldsymbol{ph}}^{+} = \Delta \boldsymbol{H} + \boldsymbol{T_0}\Delta \boldsymbol{S} \qquad \textbf{Eq. 3.8}$$

Where, ΔH is the difference in enthalpy from the reference stream and the process stream

ΔS is the difference in entropy from the reference stream and the process stream

T_o is the reference temperature

Every material stream has some chemical potential according to the chemical composition of the pure substances; this chemical potential is known as the chemical exergy. The equation of the standard molar exergy, $\dot{\varepsilon}_i^0$, of a compound i can be determined using the following equation:

$$\boldsymbol{\varepsilon_i^o} = \Delta \boldsymbol{G_f^o} + \sum_j \boldsymbol{v_j}\, \boldsymbol{\varepsilon_j^o} \qquad \textbf{Eq. 3.9}$$

Where, ΔG_f^o is the molar free enthalpy for the formation of the compound in the standard state from its constituent elements

ε_i^0 is the standard chemical exergy values of the constituent elements, j, in their stable state at the reference temperature T_o and pressure P_o (Sato 2004; Tzanetis, Martavaltzi & Lemonidou 2012):

After calculating the standard chemical exergy values, the chemical exergy, $\dot{E}_{ch}^{+}$ of the stream can be determined by summing the standard chemical exergy value of all the components in the stream.

$$\dot{\mathbf{E}}_{\mathbf{ch}}^{+} = \sum_{i=1}^{n} \boldsymbol{\varepsilon_i^o} \qquad \textbf{Eq. 3.10}$$

Where n is the number of components in the stream.

Finally, the mixing exergy is due to the isothermal and isobaric mixing of the pure components at the actual temperature (T) and pressure (P). The exergy change of mixing can be calculated by using the following equation:

$$\Delta \dot{\boldsymbol{E}}_{\boldsymbol{mix}} = \boldsymbol{T_0}\Delta \dot{\boldsymbol{S}}_{\boldsymbol{mix}} \qquad \textbf{Eq. 3.11}$$

Where the entropy change of mixing,

$$\Delta \dot{\boldsymbol{S}}_{\boldsymbol{mix}} = \Delta \dot{\boldsymbol{S}} - \sum \boldsymbol{x_i}\Delta \dot{\boldsymbol{S}}_{\boldsymbol{i}} \qquad \textbf{Eq. 3.12}$$

The total global exergy rate loss can then be calculated by adding the three terms.

Feng, Zhu and Zheng (1996), stated that conventional exergy analysis can only provide information about the potential or possibilities of improving performance of processes, but cannot state whether or not the possible improvement is practicable and economic.

3.6.4 Techno-Economic Analysis

This sub-chapter presents the different economic parameter such as correlations, interest rates and equations used throughout this thesis to evaluate the costing of the different components. Detailed calculation examples are found in Appendix section B.4.

In order to evaluate comprehensively the economic performance of the hybrid carbon capture process, a techno-economic analysis was performed on each hybrid carbon capture process. The aim of the analysis was to determine the cost of retrofitting CCS to the reference coal-fired power plant.

The economic assumptions used throughout follow the CO2CRC techno-economic model developed by UNSW (Allinson et al. 2006). This model uses the capital costs to estimate the operating costs and total costs of CO_2 capture and storage. The breakdown of the capital cost components including the equipment and set up costs is summarised in Table 3.9 and the breakdown of the operating cost components are shown in Table 3.10.

Table 3.9 Breakdown of capital cost components for carbon capture.

		Capital cost elements	Nominal value
Equipment costs	A	Process Equipment Cost (PEC)	Sum of all process equipment
	B	General facilities	30 % PEC
		Total Equipment Cost (TEC)	A+B
Set up costs	C	Instrumentation	15 % TEC
	D	Piping	20 % TEC
	E	Electrical	7 % TEC
	F	Total Installed Cost (TIC)	A + B+ C+ D +E
	G	Start-up costs	8 % TIC
	H	Engineering	5 % TIC
	I	Owners costs	7 % (F + G + H)
	J	Engineering, procurement, construction and owner's cost (EPCO)	F + G + H + I
	K	Project Contingency	10 % EPCO
		TOTAL CAPITAL COST (CAPEX)	= J + K

Table 3.10 Breakdown of operating cost components for hybrid carbon capture.

		Operating cost elements	Nominal value
Fixed costs	M	Insurance	2% TCC
	N	Fixed Operating and Maintenance Costs	4% TCC + Ins
	O	Labour Costs	
Variable costs	P	Cooling Costs	
	R	Membrane Replacement Costs	20% Membrane Capital Cost
		TOTAL OPERATING COST (OPEX)	= Variable Costs + Fixed costs

In combination with the CAPEX and OPEX components, Table 3.11 shows the general cost parameters that were used to evaluate the economic lifetime performance of the hybrid carbon capture process. Those parameters followed the standard scoping level process engineering assumptions(Peters, Timmerhaus & West 2002).

Table 3.11 Economic Parameters for techno-economic analysis

Cost Parameters		
Discount Rate	7	%
Years of the project	25	years
Base Year	2011	
Base year CPI	591	
Cost of electricity	40	$/MWh
Load Factor	85	%
Capacity Factor	7446	hrs
Make-up water cost	0.25	$/m3
Individual Labour Cost	82000	$/yr
CO_2 storage cost	6.03	$/t
Cost of Black Coal	1.4	$/$GJ_{th}$ (LHV)
Coal LHV	23.84	MJ/kg
Cost Zeolite 13X	6	$/kg
Cost Membrane	50	$/$m^2$

The techno-economic analysis also took into consideration the costs of energy required for the carbon capture process. The energy required was supplied from the power plant, which represented a loss of revenue as the energy would have otherwise been dispatched to the grid.

There were 2 main parameters that were calculated in techno-economic analysis to determine the performance of the hybrid carbon capture process:

i. Cost of CO_2 avoidance

When implementing CCS, energy is required to operate the process resulting in CO_2 emissions due to CCS. Therefore, the amount of CO_2 avoided takes into account the amount of CO_2 not captured from the power plant as well as the CO_2 emitted due to the energy required from the CCS process. The equation used to determine the CO_2 avoided is shown in Eq. 3.13.

$$\boldsymbol{CO_2\ Avoided = m_{Before} - m_{After} - m_{Energy}} \qquad \textbf{Eq. 3.13}$$

Where, m_{Before} is the mass of CO_2 emitted to atmosphere before capture

m_{After} is the mass of CO_2 emitted to atmosphere after capture

m_{Energy} is the mass of CO_2 emitted from the energy used for capture.

The CO_2 avoided is a better indication of the performance of a carbon capture process over the total CO_2 captured as it provides a net reduction in CO_2 emissions. Furthermore, this allows the cost of CO_2 avoided to be calculated, which represents the carbon price that would make the capture project break even.

The cost of CO_2 avoided (Eq. 3.14) was calculated using the standard CO2CRC methodology developed by Allinson et al. (2006) based on the Net Present Value (NPV).

$$\boldsymbol{C_{Avoidance} = \frac{NPV_{Total\ Costs}}{NPV_{CO_2 avoided}}} \qquad \textbf{Eq. 3.14}$$

Where, $C_{Avoidance}$ (A$ per tonne of CO_2 avoided) is the cost of CO_2 avoided

$NPV_{Total\ Costs}$ (A$) is the Net Present Value of the total costs of the carbon capture on an annual basis (Eq. 3.15)

$NPV_{CO2\ avoided}$ (tonne) is the Net Present Value of the CO_2 avoided on an annual basis (Eq. 3.16).

$$\boldsymbol{NPV_{Total\ Costs} = \sum_{i=1}^{n} \frac{CAPEX_i + OPEX_i}{(1+d)^i}} \qquad \textbf{Eq. 3.15}$$

$$\boldsymbol{NPV_{CO_2 avoided} = \sum_{i=1}^{n} \frac{(CO_2\ avoided)_i}{(1+d)^i}} \qquad \textbf{Eq. 3.16}$$

Where, d (% per annum) is the real discount rate

n (years) is the total project life.

ii. Levelised Cost of Electricity (LCOE)

LCOE represents the final cost of electricity at which the power plant operator provides electricity to the grid. This excludes the costs of electricity transmission and distribution. Using the NPV, the LCOE (A$/MWh) was calculated using the following equation:

$$LCOE_{Capture} = \frac{NPV_{Power\ Plant+Capture}}{NPV_{Net\ Power}}$$

Where, $LCOE_{Capture}$ (A$/MWh) is the Levelised Cost of Electricity after implementing the CCS facility

$NPV_{Powerplant + Capture}$ (A$) is the Net Present Value of the total costs for the power plant and CCS facility

$NPV_{Net\ Power}$ (MWh) is the Net Present Value of the net power output of the power plant.

Finally, in this study, it was estimated that the LCOE for the power plant without capture is A$40/MWh.

4 VSA/Low-Temperature Hybrid Carbon Capture Process Results and Discussion

This chapter presents the main results obtained for the VSA/low-temperature carbon capture process in section 4.1 and discusses those results in more detail in section 4.2.

4.1 VSA/ Low-Temperature Hybrid System Results

The Pareto Optimal Front is the solution obtained from the last generation of the Genetic Algorithm of the non-dominated solution set. The results shown are for a MOO using 75 individuals with a minimum of 50 generations.

The two objective variables (OV) when performing the optimization of the hybrid carbon capture process were:

i. Maximise overall recovery rate of CO_2 from the hybrid carbon capture process (%)
ii. Minimise the total shaft work required for the hybrid carbon capture process (MW_e)

4.1.1 Pareto Optimal Front

Figure 4.1 shows the Pareto Optimal Front of the final generation and the fifth last generation for the two objective variables. The graph shows that not much improvement can be made through the MOO by increasing the number of generations. The table of objective variables and corresponding decision variables for the final generation can be found in the Appendix section B.1.

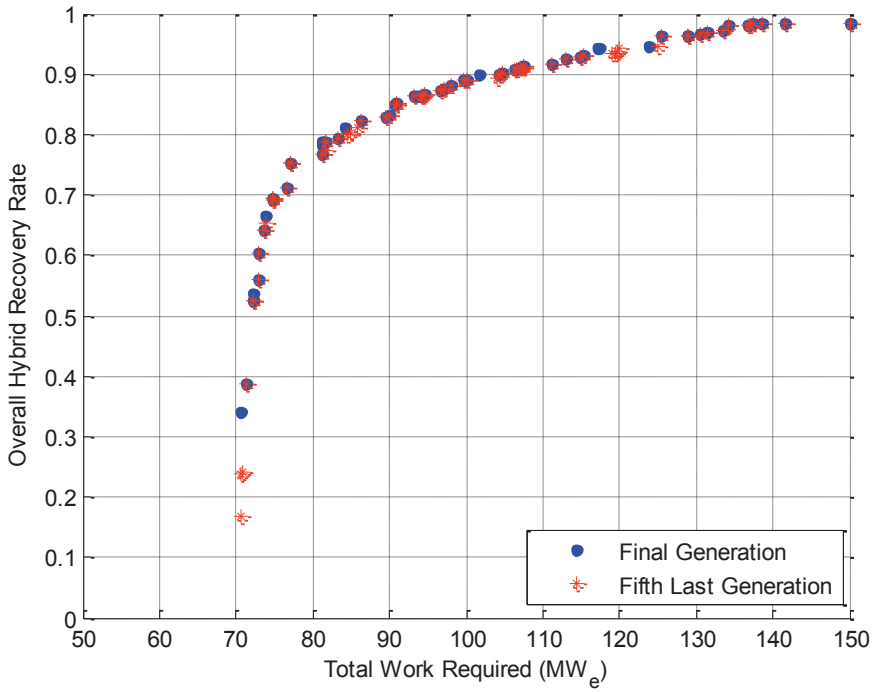

Figure 4.1 Pareto Optimal Front of overall recovery rate as a function of total shaft work required (MW_e)

From the results obtained for the final generation, a second order exponential regression of the data points was performed to obtain a continuous curve representing the total work required as a function of the overall CO_2 recovery rate. The continuous curve is shown in Figure 4.2.

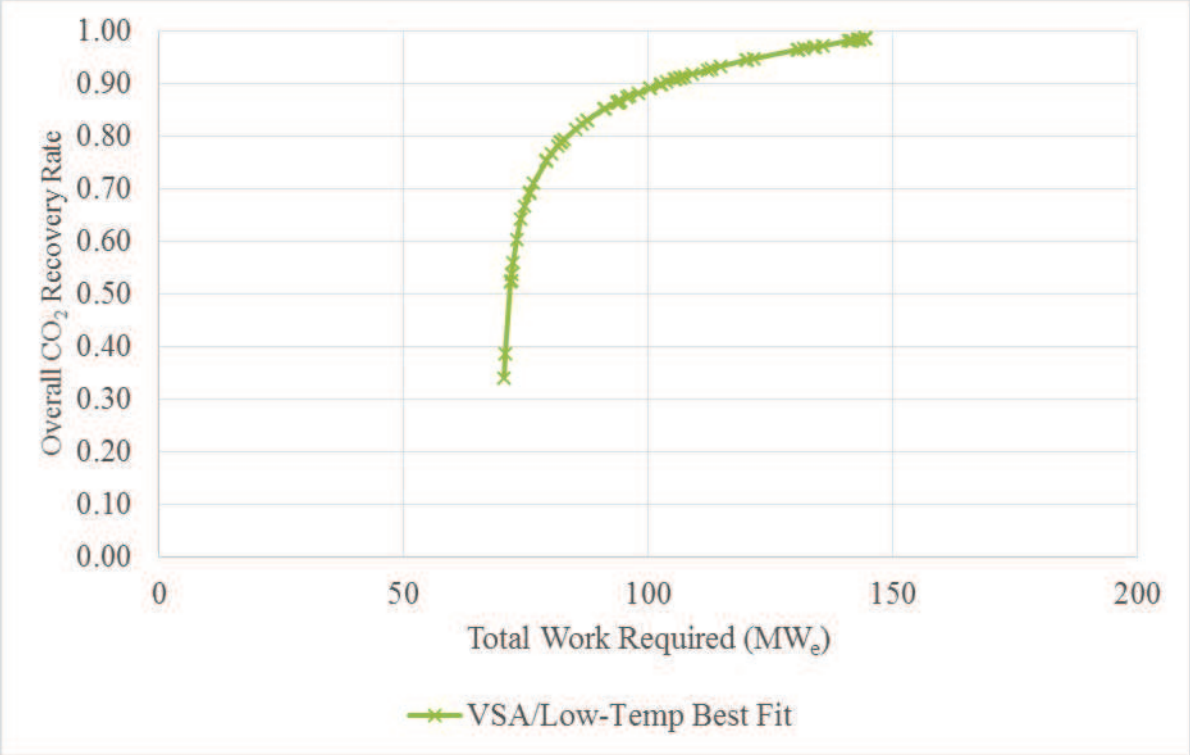

Figure 4.2 Overall recovery rate of hybrid system as a function of total work required (MW_e) for VSA/low-temperature hybrid process fitted to a second order exponential regression.

The equation and the resepective R-squared value for the fitted curve are as follows:

$$W = Ae^{B(1-RR)} + Ce^{D(1-RR)} \qquad \textbf{Eq. 4.1}$$

- VSA/low-temperature separation hybrid process ($R^2 = 0.986$):

A = 82.6; B = -10.2; C = 73.7; D = -0.0713

Where, W is the total work required (MW_e) and

RR is the overall recovery rate of the hybrid carbon capture process.

4.1.2 Decision Variables Pareto Charts

MOO is a very useful tool to also understand how each of the decision variables affects the objective functions. The Pareto charts of the decision variables for the different carbon capture stages are shown in Figure 4.3, Figure 4.4 and Figure 4.5 as a function of objective 1: Maximum overall CO_2 recovery rate of the hybrid carbon capture system. The overall CO_2 recovery rate was chosen as the reference objective variable since CCS systems generally require high capture rate.

Figure 4.3, Figure 4.4 and Figure 4.5 display the Pareto charts of the decision variables affecting the VSA process, low-temperature capture process and membrane process, respectively.

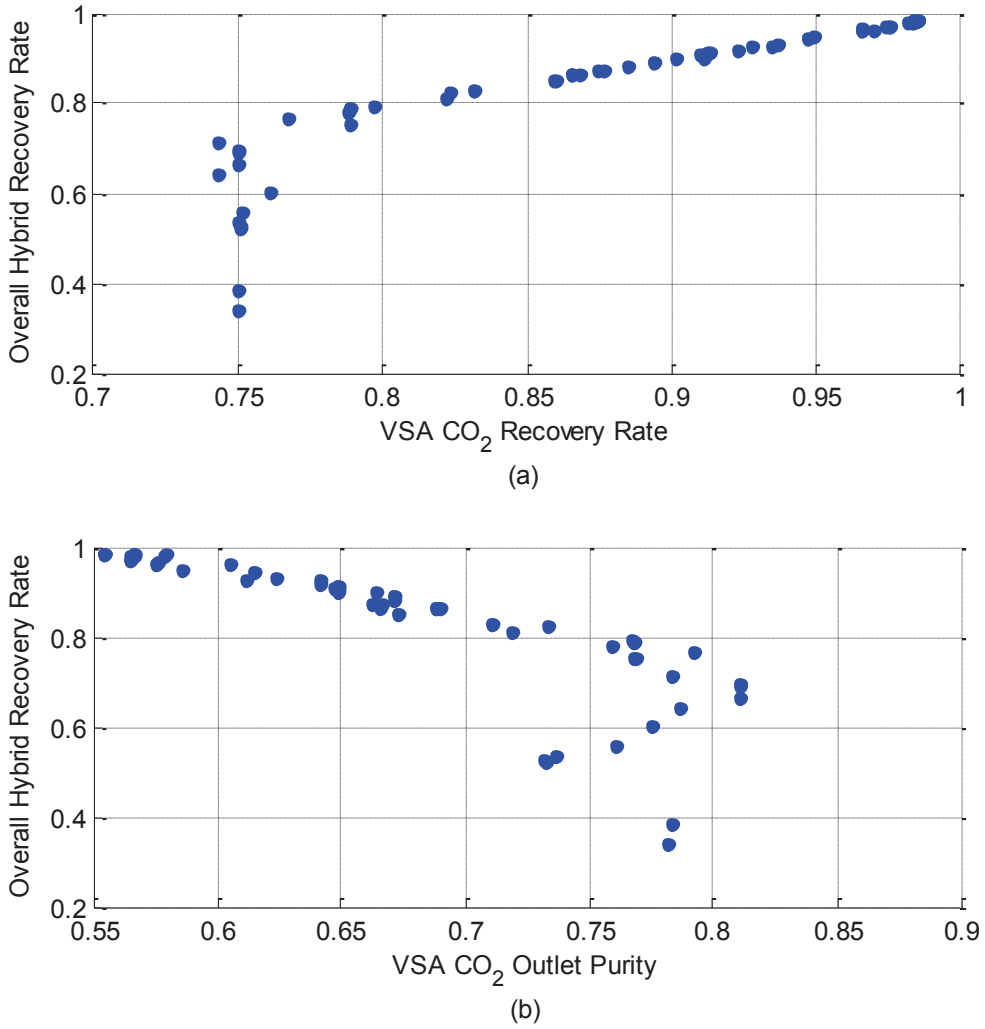

Figure 4.3 Pareto chart of the two decision variables for the VSA capture process versus the overall hybrid process CO_2 recovery rate. (a) CO_2 recovery rate of the VSA process (%); (b) CO_2 outlet purity of the VSA process (%)

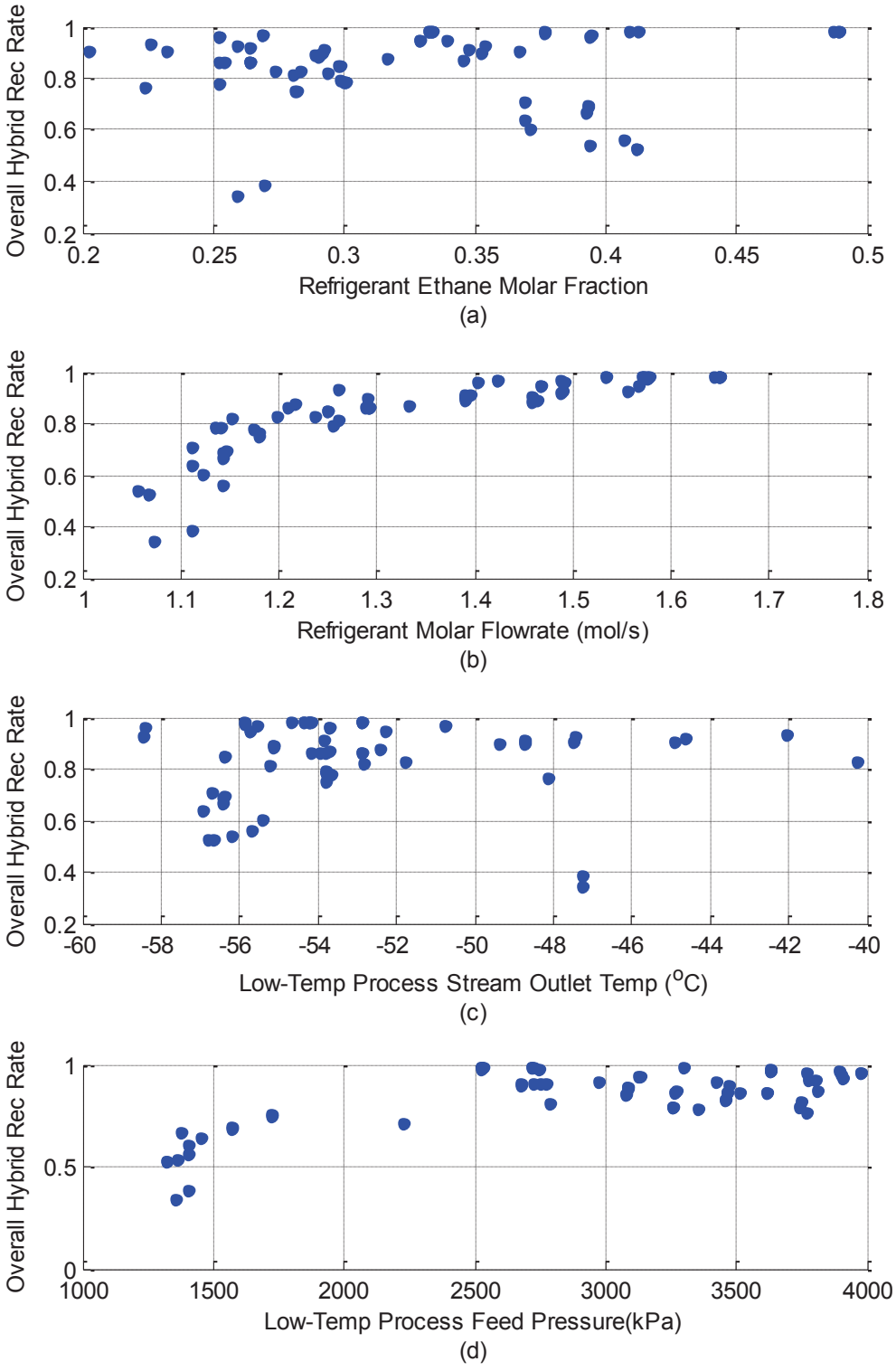

Figure 4.4 Pareto chart of the four decision variables for the low-temperature capture process versus the overall hybrid process CO_2 recovery rate.

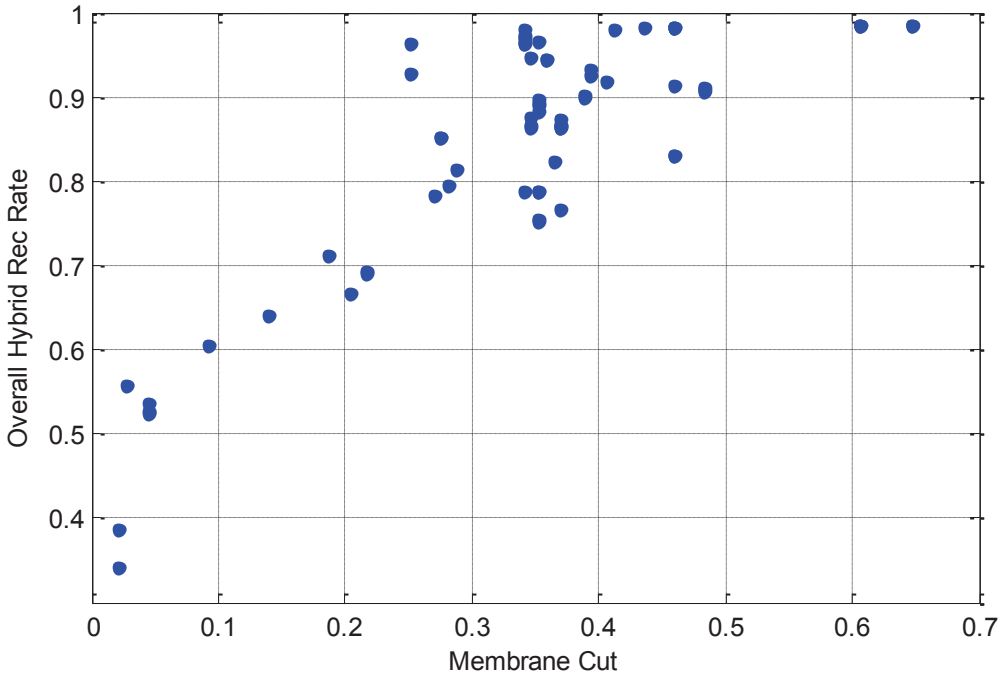

Figure 4.5 Pareto chart of the membrane cut versus the overall hybrid process CO_2 recovery rate.

4.2 VSA/ Low-Temperature Hybrid System Discussion

From the objective variables Pareto Optimal Front (Figure 4.1), it is observed that with increasing recovery rate, there is an increase in the total shaft work required for CO_2 capture. As the slope along the optimum front decreases with increasing recovery, this in turn means that the energy intensity for each additional percentage point of CO_2 capture is increasing. In the next sections the reason for this will be identified, by analysing the decision variables.

4.2.1 Decision Variables

Figure 4.3 shows the two decision variables that were varied to change the power requirement of the VSA process, namely the CO_2 recovery rate and purity. As was expected, the CO_2 recovery rate from the VSA has a direct correlation with the overall CO_2 recovery rate from the hybrid system, where increasing the CO_2 recovery rate of the VSA system increases the overall CO_2 recovery rate of the hybrid carbon capture system. It can also be observed from Figure 4.3 (a) that the VSA CO_2 recovery rate has a linear relationship with the overall CO_2 rate of the hybrid system. This means that the secondary stage of the hybrid carbon capture process is recovering all the CO_2 going through this stage.

Figure 4.3 (b) shows the VSA CO_2 outlet purity which has the mirror effect of the VSA CO_2 recovery rate, where the higher overall recovery rate of the hybrid system selects the lower VSA CO_2 outlet purity and the lower overall recovery rate favours the higher VSA CO_2 purity. There are two components that explain this correlation:

i. The CO_2 in the VSA waste stream is sent straight to the stack, which means that the CO_2 is not being recovered. Hence, in order to obtain a high overall recovery rate, a high VSA CO_2 recovery rate is necessary.

ii. With the first component in consideration, the VSA carbon capture process cannot achieve both high purity and high recovery, which is represented by the constraint discussed in Chapter 3 and displayed in Figure 4.7. Hence, when high overall CO_2 recovery rate is required, a lower CO_2 outlet purity is selected to obtain the higher CO_2 VSA recovery rate. However, when a low overall recovery rate is required, a high VSA CO_2 outlet purity is favoured. Suggesting that the hybrid carbon capture prefers increasing the work load on the VSA capture process to increase the purity, in order to decrease the work required on the CO_2 purification stage (low-temperature carbon capture process). The trade-off between VSA CO_2 outlet purity and low-temperature carbon capture process is seen in Figure 4.6, where the pre-compression work (Figure 4.6 (a)) and the refrigeration work (Figure 4.6 (b)) increases with decreasing VSA CO_2 outlet purity.

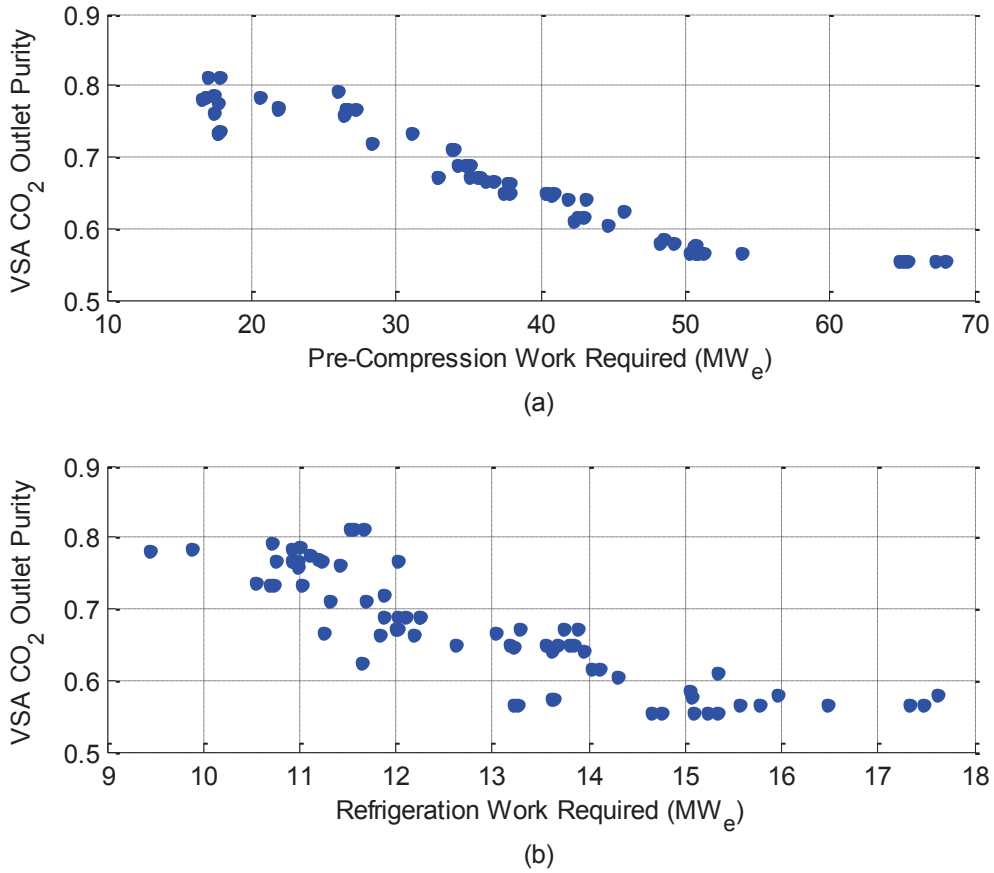

Figure 4.6 Pareto chart representing the correlation between the VSA CO_2 outlet purity vs the refrigeration work required.

The correlation between VSA CO_2 recovery rate and VSA CO_2 outlet purity was further investigated by fitting the VSA performance chosen in the MOO as the optimum conditions in the VSA model contour as shown in Figure 4.7. It can be seen that the VSA performance used in the MOO are all really close to the constraint line, which indicates that the MOO selects to increase the performance of the VSA to the maximum.

This further shows that the hybrid carbon capture process favours increasing the VSA performance at the cost of higher work requirement in order to reduce the work load in the secondary CO_2 purification stage. Figure 4.8 represents this relationship, as the total specific work required for the low-temperature carbon capture system is almost twice the specific work required when the VSA CO_2 outlet purity is 0.55 (Low-temperature specific work ≈ 1.1 GJ_e/t (CO_2 recovered)), compared to when the VSA CO_2 outlet purity is 0.8 (Low-temperature specific work ≈ 0.55 GJ_e/t (CO_2 recovered). Figure 4.7 shows the specific work required for the VSA process has a maximum of 0.9 GJ_e/t (CO_2 recovered), which explains why the hybrid system would select high VSA performance to reduce the work on the low-temperature system.

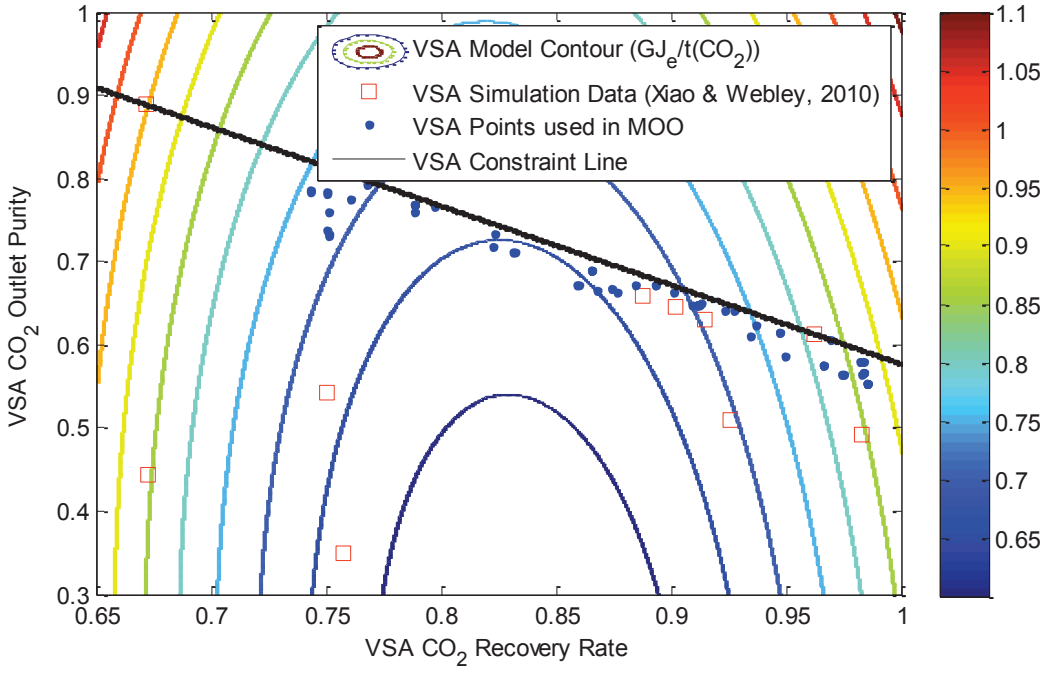

Figure 4.7 VSA model contour representing the VSA performance data selected for the MOO optimum operating conditions.

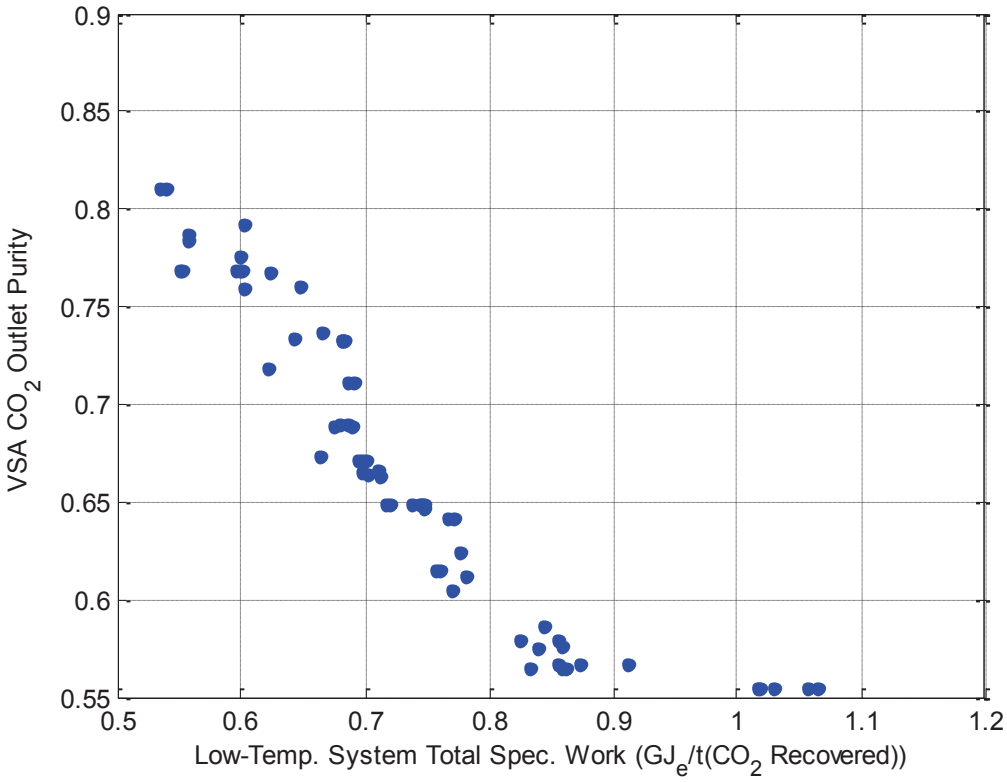

Figure 4.8 Pareto chart of VSA CO_2 outlet purity vs low-temperature carbon capture system total specific work required.

Figure 4.4 displays the four decision variables that determine the performance of the low-temperature separation process. The three parameters: the ethane molar fraction, the refrigerant molar flowrate and the minimum temperature achieved by the process stream shown in Figure 4.4 (a), Figure 4.4 (b) and Figure 4.4 (c) respectively, determined the power requirement of the refrigeration system. It can be seen that the ethane molar fraction and process stream temperature do not seem to have a strong relationship with the overall recovery rate of the hybrid system. This is due to the high correlation that the refrigerant molar flowrate, Figure 4.4 (b), has with the overall hybrid recovery rate since increasing the overall recovery rate increases the duty required to cool this CO_2 as represented in Figure 4.9.

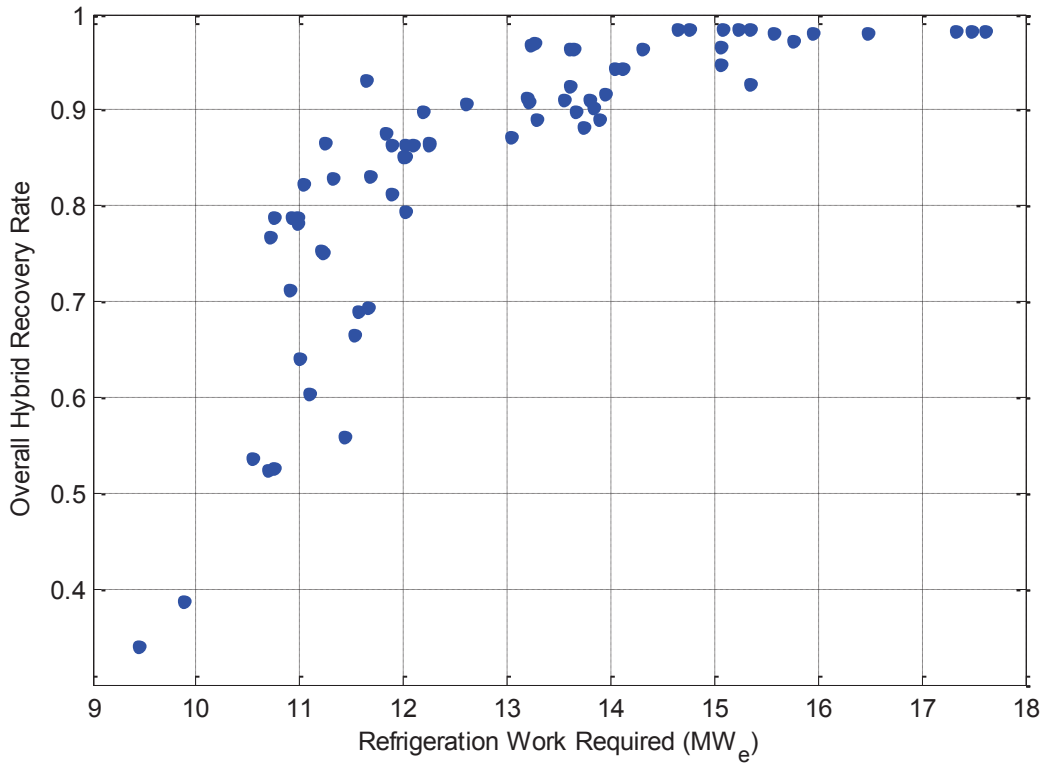

Figure 4.9 Pareto Chart representing the work required for the refrigeration cycle versus the overall CO_2 recovery rate of the VSA/LT hybrid system.

As expected, the pre-compression pressure Pareto chart in Figure 4.4 (d) shows that a higher pressure is required to obtain higher recovery rates since higher compression pressure increases the partial pressure of CO_2 and therefore facilitates the separation of CO_2 from nitrogen. Also important is that higher pressures of this stream lowers the CO_2 freeze out temperature and effectively allows the stream to be cooled to the lowest temperature possible before forming solid CO_2.

The final decision variable, the membrane cut of the membrane process is shown in Figure 4.5. It can be seen that in order to achieve the higher overall CO_2 recovery rate, a higher membrane cut value is required to allow more CO_2 to be recycled back into the system and hence, less CO_2 to be lost in the retentate stream. However, at lower recovery rate, no gas is allowed to permeate through the membrane. This is to reduce the amount of CO_2 being recycled, which leads to a reduced loading in the low-temperature separation. Furthermore, at overall CO_2 recovery rate of greater than 80%, the recovery rate becomes less dependent of the membrane cut as the low-temperature process pre-compression is significantly increased, resulting in higher pressure difference through the membrane. This higher pressure difference allows more CO_2 to be permeated through the membrane.

4.2.2 Objective Variables Pareto Fronts and Optimum Specific Work Required

In order to better understand the total work required with respect to the amount of CO_2 being captured by hybrid capture process, a new graph using the Pareto-Optimal solutions, of total specific shaft work as a function of recovery rate was produced. The total specific shaft work required is the total

shaft work required per mass flowrate of CO_2 being recovered by the process. As discussed in Table 1.1 in Chapter 1, the MEA solvent absorption baseline system with a multi-stage compression system requires approximately 4 GJ_{th}/(t CO_2 recovered) (Belaissaoui et al. 2012). Using a standard 33% thermal efficiency in a coal power plant, the MEA solvent absorption specific energy requirement converts to 1.3 GJ_e/(t CO_2 recovered), which was also added to the graph.

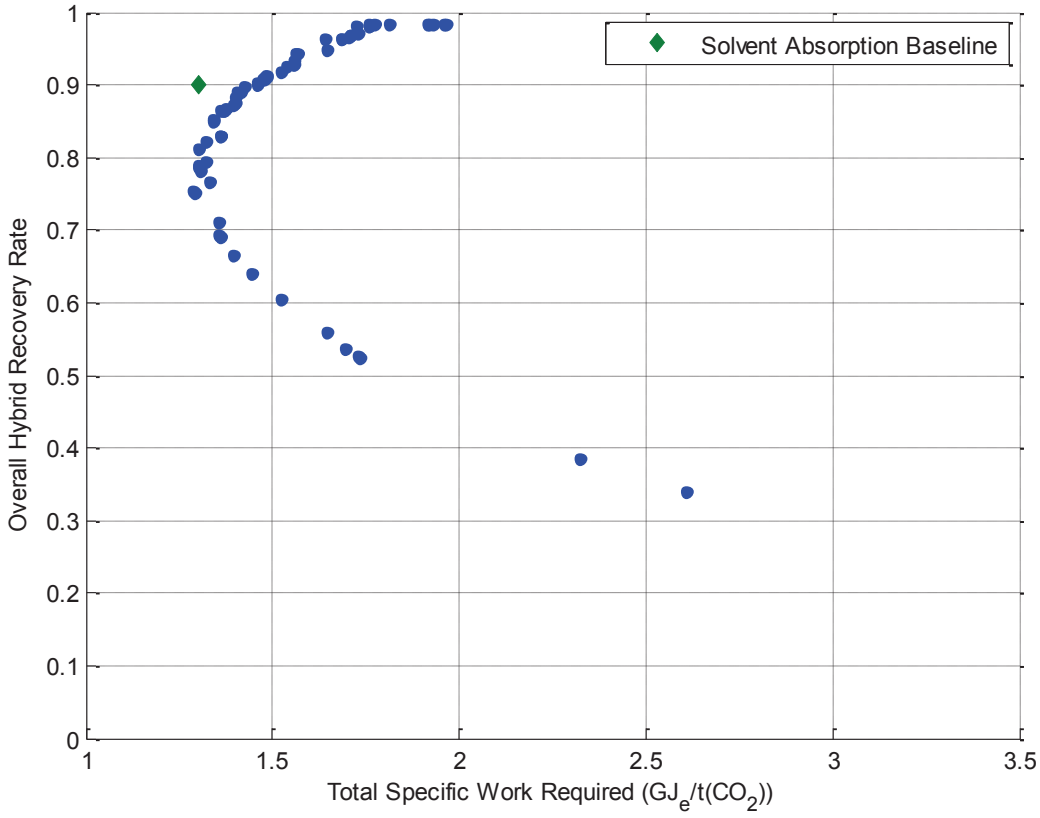

Figure 4.10 Recovery rate as a function of specific shaft work (GJ_e/t(CO_2 recovered))

This optimum operating condition of minimum specific work of 1.29 GJ_e/ (t CO_2 captured) and overall recovery rate of 75.4 % obtained shown in Figure 4.10 can be used to analyse further the performance of the hybrid process. The operating condition of each decision variable to obtain the optimum operating condition is shown in Table 4.1.The heat composite curve of the heat integrated low-temperature separation was generated and shown in Figure 4.11 and the work requirement of each component was analysed and displayed in Figure 4.12.

Table 4.1 Table of decision variable range for MOO and optimum operating conditions of the VSA/low-temperature hybrid capture cases

Decision Variable		Minimum	Maximum	Optimum
VSA CO2 Recovery Rate	%	0.700	0.985	0.789
VSA CO2 Outlet Purity	%	0.500	0.900	0.769
Multi-Stage Compression Pressure	(kPa)	930	4 000	1 723
Refrigerant Ethane Molar Fraction		0.19	0.50	0.28
Refrigerant Molar Flow	(mol/s)	1.00	1.65	1.17
Low-Temp Process Stream Outlet Temp.	(°C)	-60.5	-40.0	-53.8
Membrane Cut		0.01	0.76	0.35

4.2.3 Pinch Analysis

The stream composite curve in Figure 4.11 shows that the pinch point occurs at the lowest temperature since the refrigeration system was included in this composite curve, which indicates that no extra cooling duty is required (Table of heat composite curve data can be found in the Appendix section B.3). The colder section of the cold composite curve represents the mixed refrigeration section. It can be observed that the shape of the mixed refrigerant section matches the hot composite curve closely to allow the pinch point at approximately -35°C, where the CO_2 just starts to condense. Also in Figure 4.11, the total process to process heat exchanged is about 45 MW_{th} or 0.70 GJ_{th}/t (CO_2 recovered).

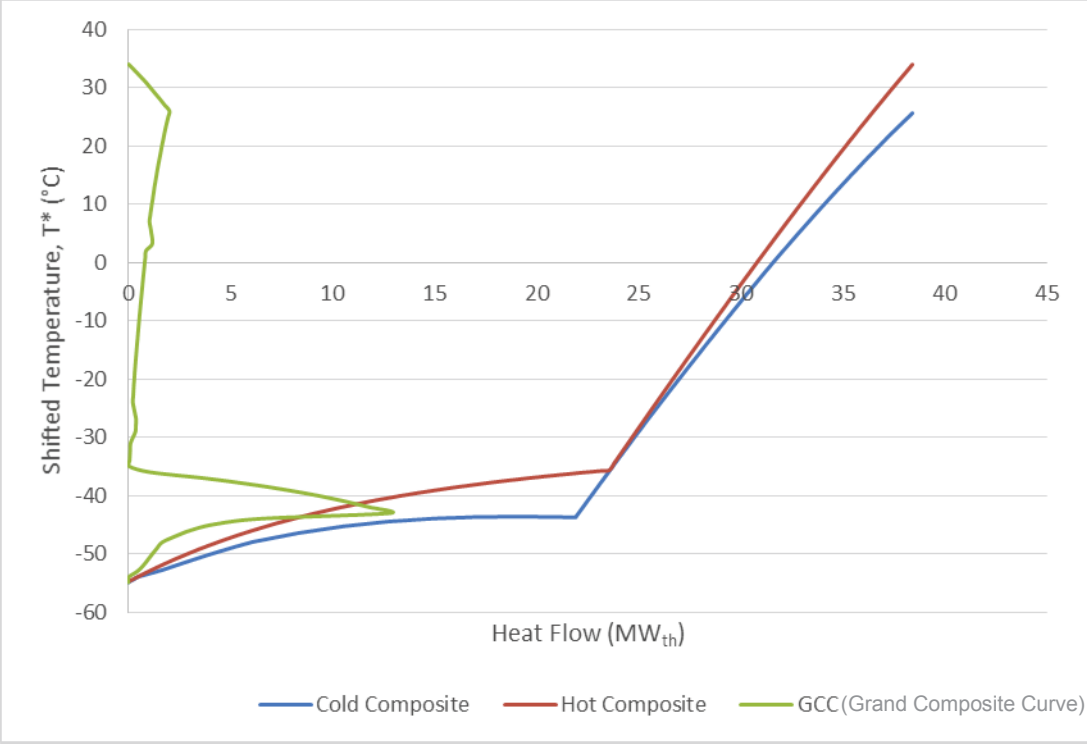

Figure 4.11 Stream composite curve and the grand composite curve shows that the pinch temperature occurs at the cold end of the heat exchangers.

The power requirement of the hybrid carbon capture process was analysed at the optimum operating conditions. There are four consumers of power throughout the process: The VSA process, pre-compression prior to the low-temperature separation, the refrigeration compression train required in the refrigeration system and the pump that pressurises the pure liquid CO_2 to supercritical state. The pump requirement is negligible throughout the process (< 0.1 %). The low-temperature separation unit, which comprises of both the pre-compression and refrigeration cycle compression, requires a total of 43% of the total shaft work requirement, which corresponds to 65 MW_e. The VSA process, which consists of the blower to compress the flue gas prior to entering the VSA and the vacuum pump required to go to vacuum pressure for the desorption stage, requires 56% of the total shaft work.

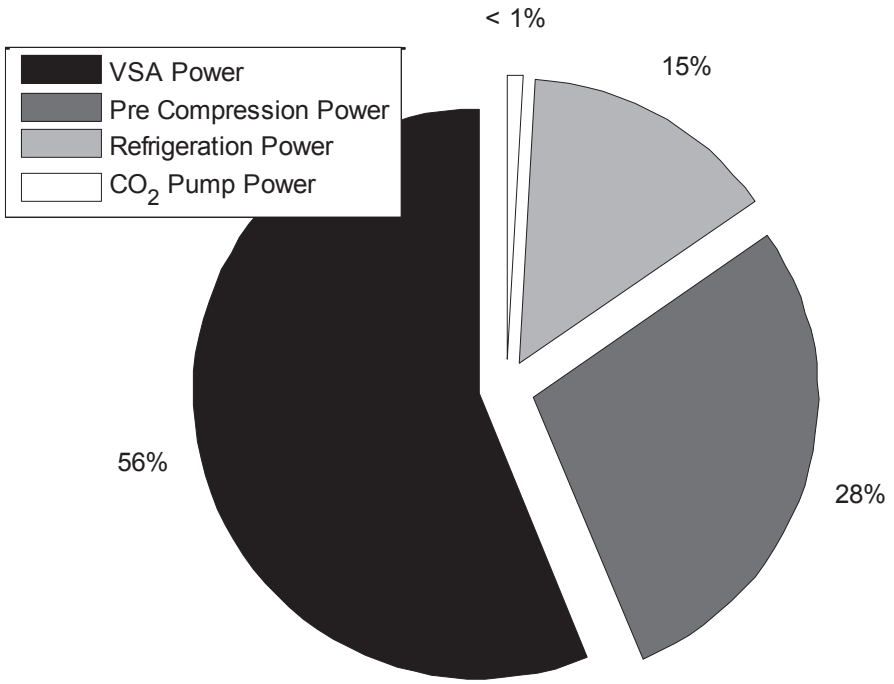

Figure 4.12 Pie chart of total shaft work required for the hybrid capture process. The low-temperature separation process comprises of the pre-compression and refrigeration power requirement. The VSA total power requirement consists of both the blower prior to entering the VSA and the vacuum pump required to go to vacuum pressures.

The two main power consumers are the pre-compression train and the VSA power requirement. The pre-compression train cannot be further optimised other than the decision variables that have been allocated. The second main power consumer is the VSA process and in order to improve the power requirement, further improvement to the VSA process would be required such as better adsorbents or different VSA configurations.

4.2.4 Exergy Analysis

This sub-section displays and discusses the results obtained for the exergy analysis of the VSA/low-temperature separation hybrid carbon capture process. MOO was used to perform the exergy analysis and the two objective variables (OV) when performing the optimization were:

i. Maximise overall recovery rate of hybrid carbon capture process (%)
ii. Minimise the exergy loss rate for the hybrid carbon capture process (kW)

The Pareto Optimal Front is the solution obtained from the last generation of the Genetic Algorithm of the non-dominated solution set. The results shown are for a MOO using 100 individuals with a minimum of 50 generations[1].

The Pareto Optimal Front of the objective variables are shown in Figure 4.13 and the decision variables Pareto charts are shown in Figure 4.14.

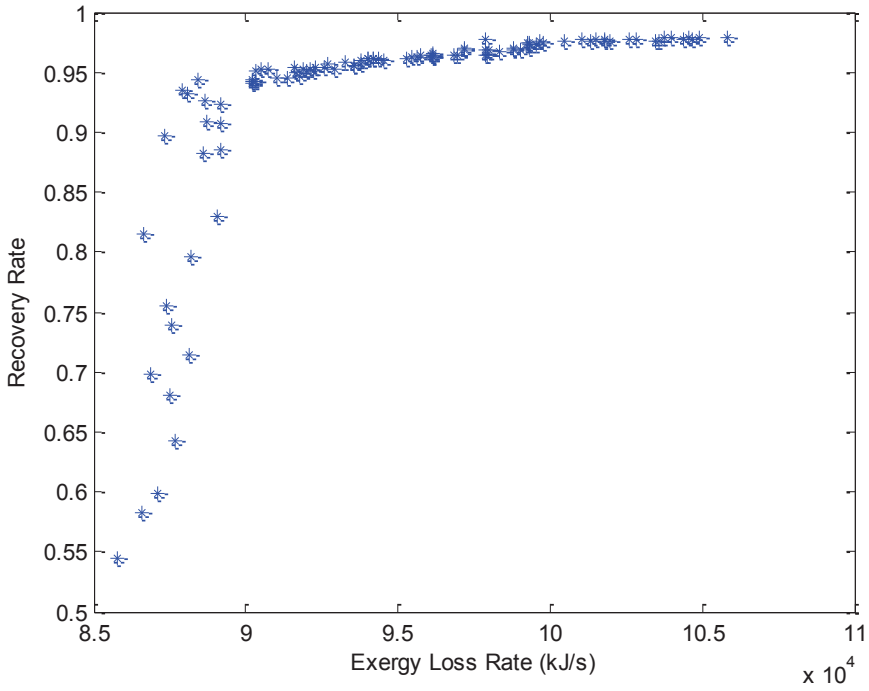

Figure 4.13 Graph of objective variables exergy loss rate (kJ/s) versus recovery rate

[1] The results presented in this chapter were presented at the Process Integration, Modelling and Optimisation for Energy Saving and Pollution Reduction Conference in Prague and published in the Chemical Engineering Transactions (Li Yuen Fong et al. 2014)

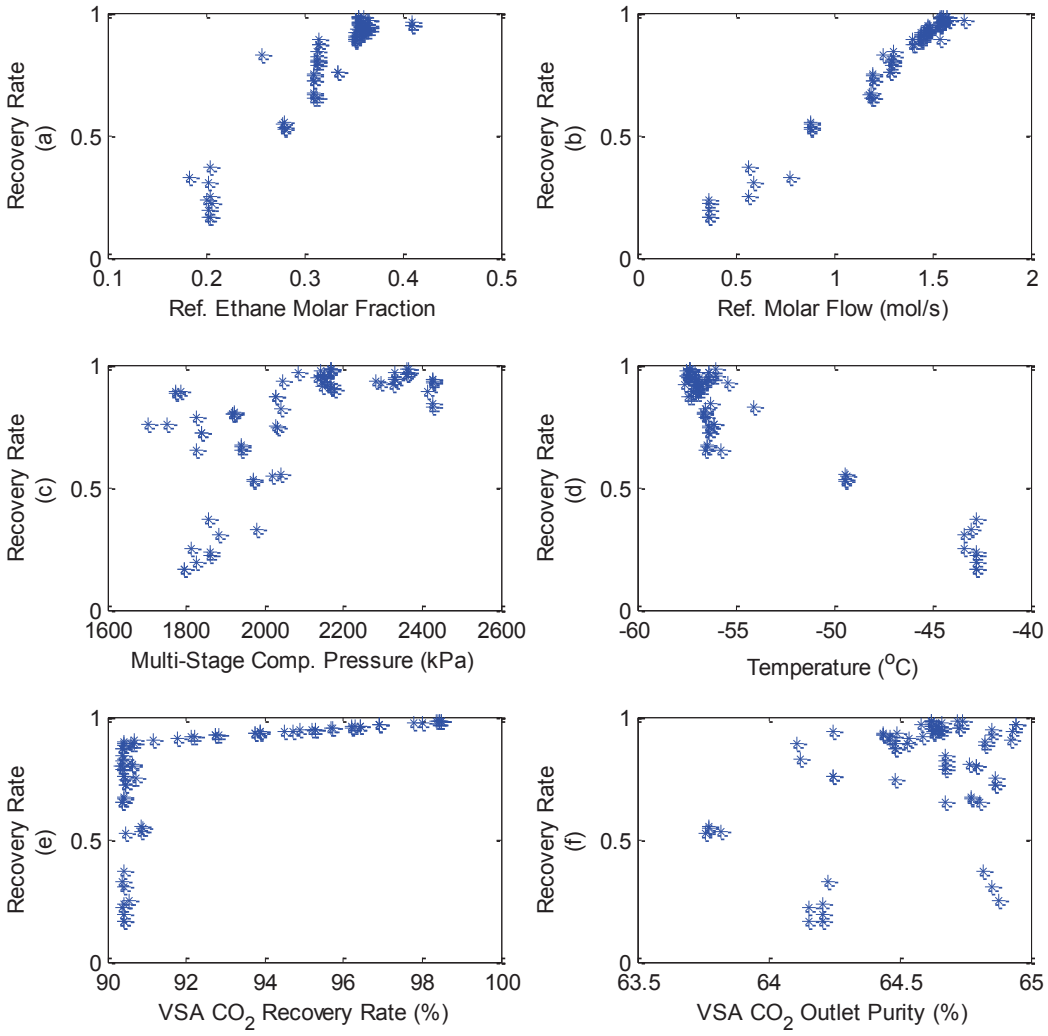

Figure 4.14 Pareto chart of the six decision variables versus the CO_2 recovery rate (a) Ethane molar fraction (b) Refrigerant molar flow (mol/s) ; (c)Multi-stage compression pressure (kPa); (d) Process stream minimum temperature (°C); (e) VSA CO_2 Recovery Rate (f) VSA CO_2 outlet purity (%)

The Pareto charts of the first six decision variables are shown in Figure 4.13 plotted against the objective 1: Maximum CO_2 Recovery. It can be seen from Figure 4.14 that most decision variables seem to have a scattered effect over the recovery rate except for two main decision variables; multi-stage compression pressure and the VSA CO_2 recovery rate. The higher compression pressure increases the partial pressure of CO_2 and therefore facilitates the separation of CO_2 from nitrogen. As discussed in the previous sub-sections, the pressure of the stream lowers the CO_2 freeze out temperature, which effectively allows the stream to be cooled to the lowest temperature possible before forming solid CO_2. Finally, the VSA CO_2 recovery rate dictates the overall recovery rate since the CO_2 lost in the waste stream from the VSA cannot be recovered.

From the objective variable Pareto Optimal Front (Figure 4.13) could be observed that with increasing recovery rate, there was an increase in exergy loss rate. A new graph, using the Pareto-Optimal solutions, of specific exergy loss rate versus recovery rate was also generated (Figure 4.15), where specific exergy loss rate is the exergy loss rate per mass of CO_2 being recovered by the process.

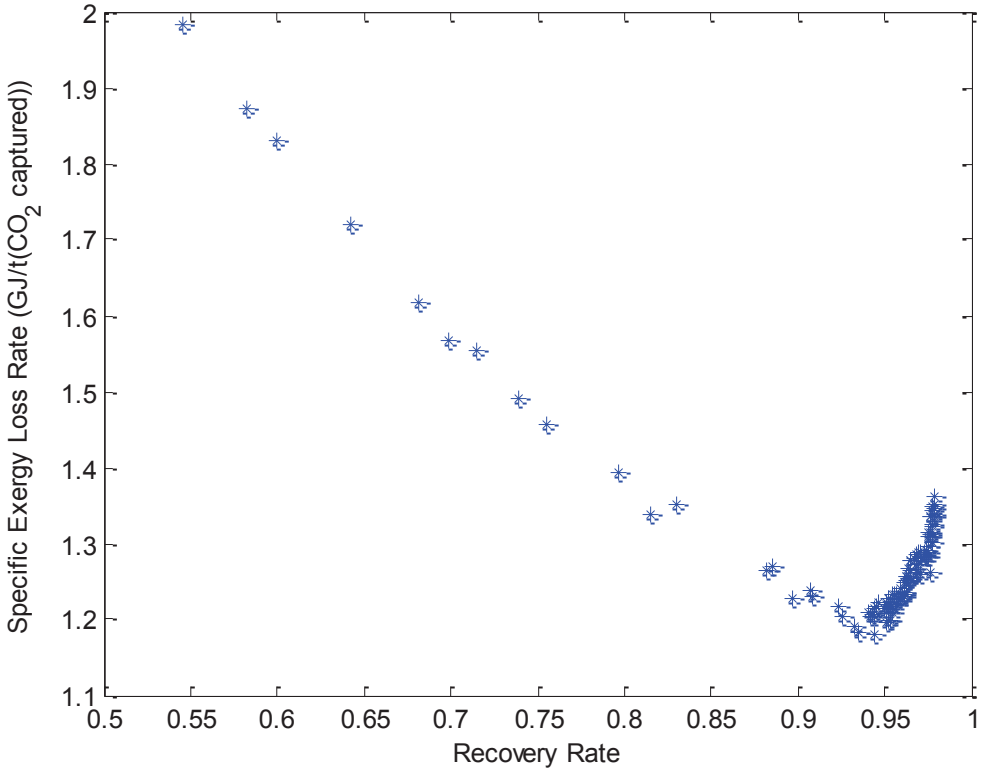

Figure 4.15 Graph of specific exergy required (GJ/t (CO_2)) versus recovery rate

The increase in exergy loss rate with increasing recovery rate from Figure 4.13 can be explained by the increase in exergy required in the compressors in the multi-stage compression of the process stream. Figure 4.15 shows that the rate of change of exergy loss is lower than the rate of change of CO_2 being captured and thus the specific exergy loss rate decreases with increasing CO_2 being captured up until a capture rate of 95 %. Figure 4.15 shows that the specific exergy loss rate has a minimum point at a recovery rate of approximately 95 % and total specific exergy loss rate of around 1.16 GJ/t (CO_2 recovered).

In addition to the decision variables and objective variables, other key process performance variable were also recorded while performing the MOO. Two of those variables can be seen in Figure 4.16 (a) and Figure 4.16 (b), which were the 'total shaft work required' and the 'total specific shaft work required'. This enabled a relationship between the exergy loss rate and total shaft work required to be examined as in Figure 4.17.

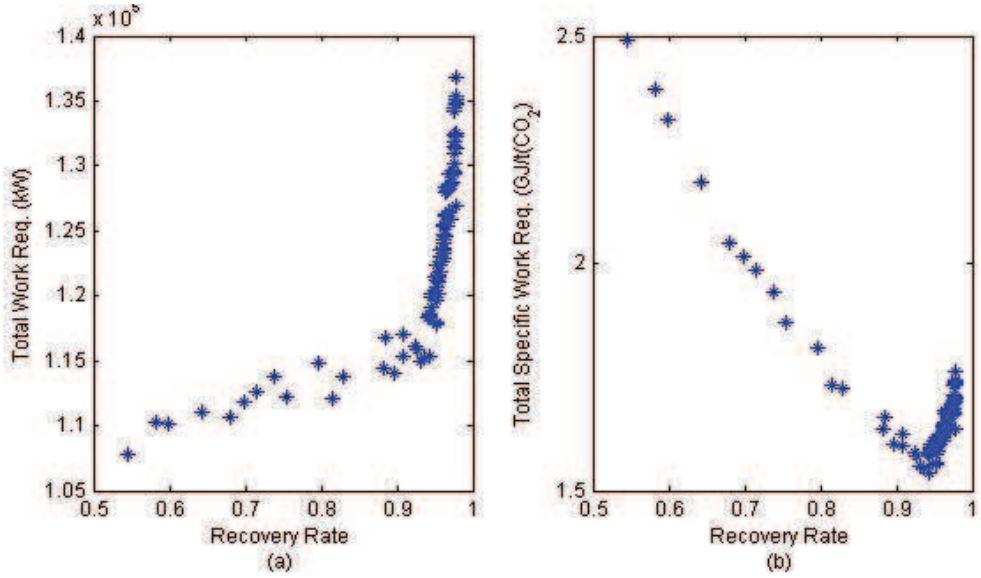

Figure 4.16 (a): Graph of total shaft work required (kW) versus recovery rate. (b): Graph of specific shaft work required (GJ/t (CO_2)) versus recovery rate.

Figure 4.16 (a) and Figure 4.16 (b) yielded results that were similar to Figure 4.13 and Figure 4.15, which means that the total shaft work required and exergy loss rate have a linear relationship. This was further proven in Figure 4.17, where the total specific exergy loss rate and total specific shaft work required showed a linear graph. This relationship can be explained by the fact that approximately 99% of the exergy input is from the shaft work in the compressors.

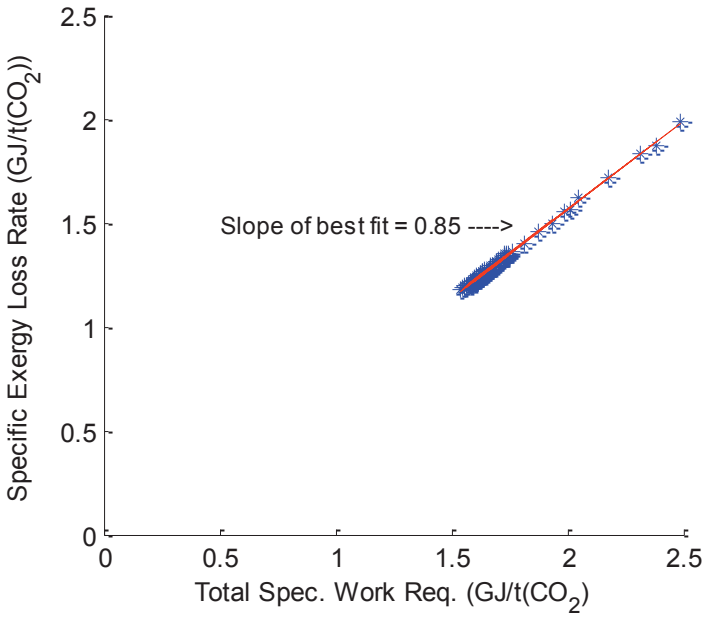

Figure 4.17 Graph of total specific shaft work required (GJ_e/t (CO_2)) versus specific exergy loss rate (GJ/t (CO_2))

Since the compressors account for the majority of the exergy going into the system as well as the total shaft work, exergy analysis does not provide more insight into the process compared to a standard

energy analysis. This is mainly due to the fact that exergy analysis is best used when thermal and chemical energy is involved, such as a solvent absorption process. Therefore, exergy analysis was not used in the future hybrid processes studied in this project.

5 Membrane/Low-Temperature Hybrid Carbon Capture Process Results and Discussion

This chapter follows a similar structure to Chapter 4 and presents the main results obtained for the Membrane/low-temperature carbon capture process in section 5.1 and discusses those results in more detail in section 5.2.

5.1 Membrane/ Low-Temperature Hybrid System Results

The results shown for each membrane/low-temperature hybrid carbon capture case are for a MOO using 50 individuals with a minimum of 100 generations.

Similar to the VSA/low-temperature hybrid carbon capture system, the two objective variables (OV) when performing the optimization of the membrane/low-temperature hybrid carbon capture process were:

i. Maximise overall recovery rate of hybrid carbon capture process (%)
ii. Minimise the total shaft work required for the hybrid carbon capture process (MW_e)

As discussed in Chapter 3, due to the higher flexibility of the membrane performance compared to the VSA process, two refrigeration cycles using two different refrigerants were investigated: mixed ethane/propane refrigerant (Case I) and propane only refrigerant (Case II).

5.1.1 Pareto Optimal Front

The Pareto Optimal Front for Case I and Case II are shown in Figure 5.1 and Figure 5.2, respectively. In order to show convergence of the MOO, each figure show the Pareto Optimal Front for the final generation, Gen_{Final} and the fifth last generation, ($Gen_{Final} - 5$). The table of objective variables and corresponding decision variables can be found in the Appendix section B.2.

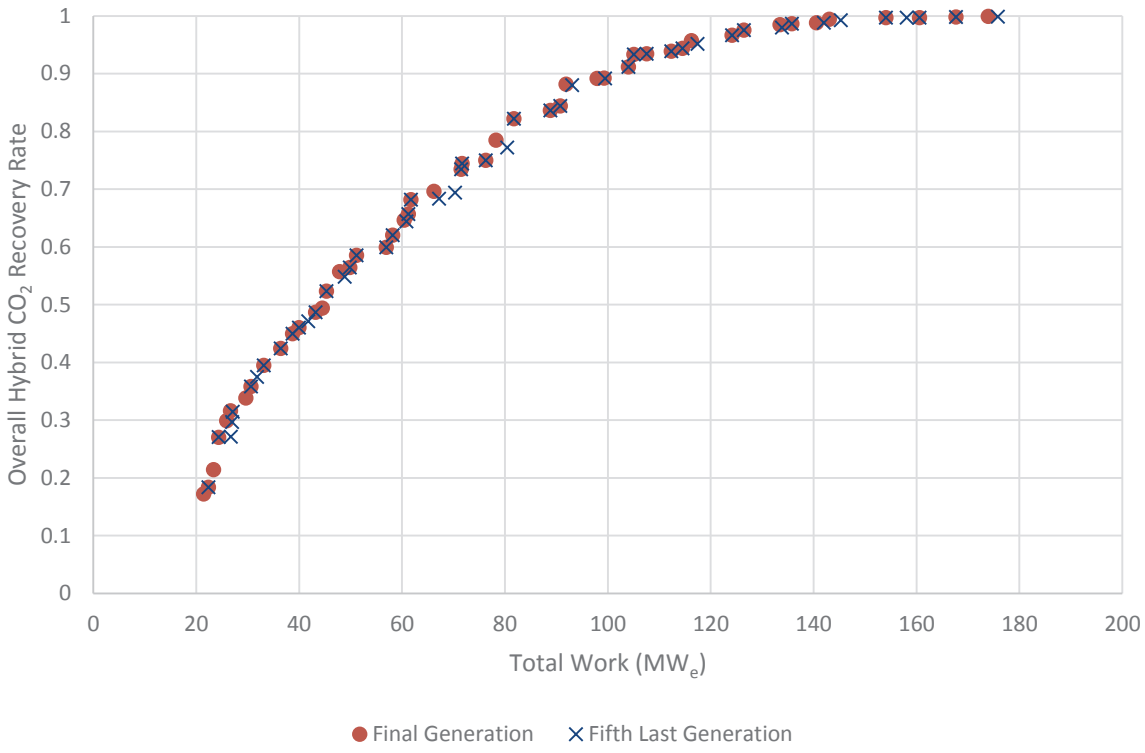

Figure 5.1 Pareto Optimal Front of overall CO_2 recovery rate as a function of total shaft work required (MW_e) for Case I (Mixed Refrigerant)

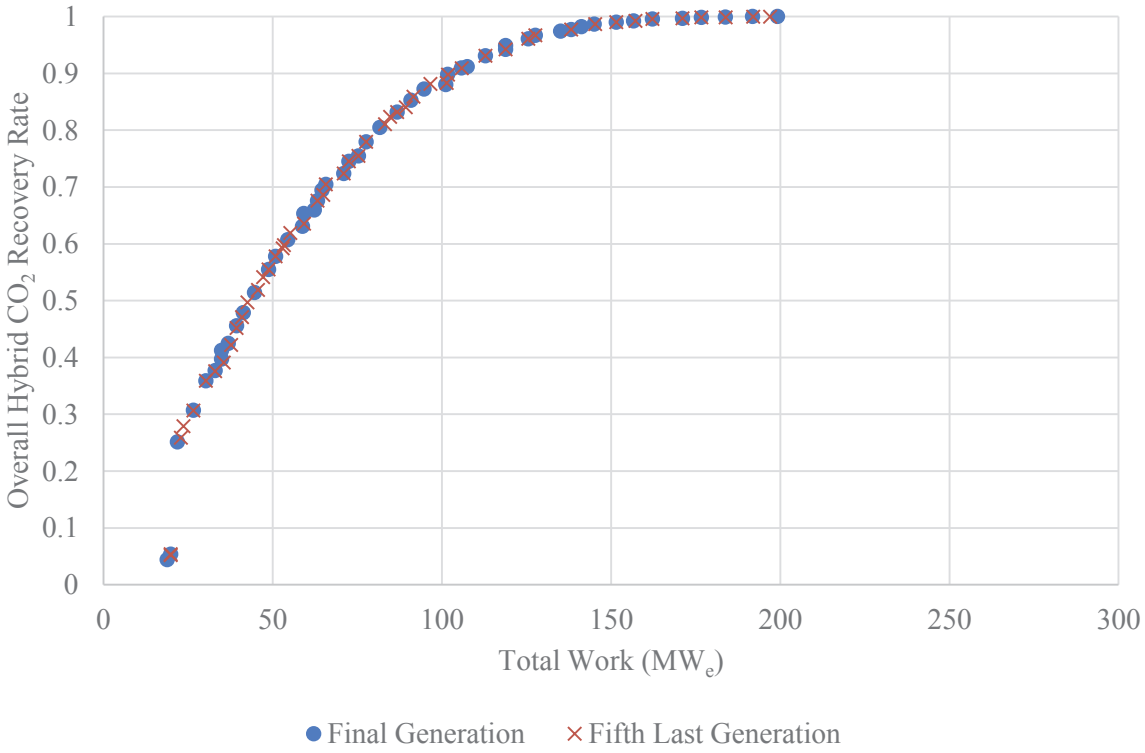

Figure 5.2 Pareto Optimal Front of overall CO_2 recovery rate as a function of total shaft work required (MW_e) for Case II (Propane Refrigerant)

The two cases are compared by combining the Pareto Optimal Front for the final generation on one graph (Figure 5.3). Figure shows a fitted 3rd order polynomial for each case to have a clearer representation of the performance of the hybrid processes.

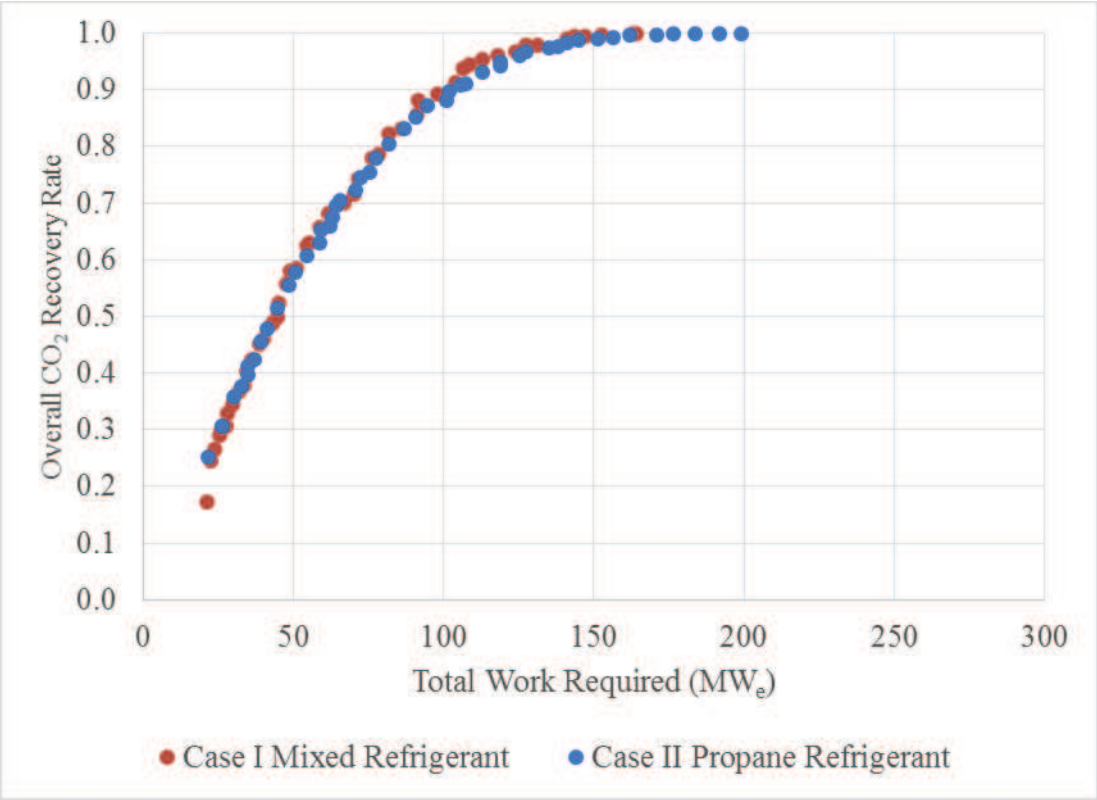

Figure 5.3 Overall recovery rate of hybrid system as a function of total work required (MW_e) for two hybrid processes

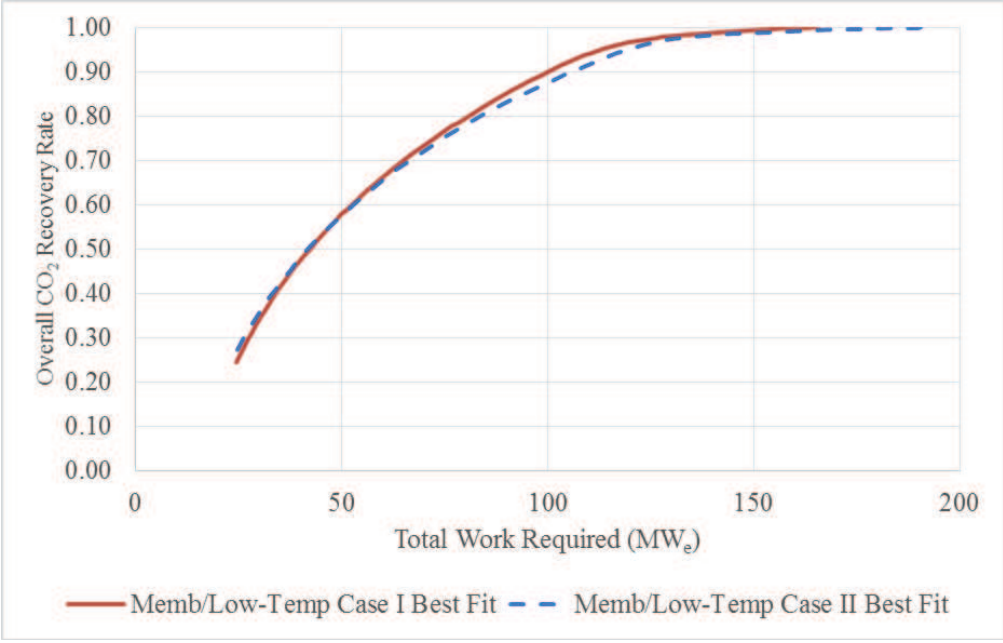

Figure 5.4 Best fit curves of Overall recovery rate of hybrid system as a function of total work required (MW_e) for two hybrid processes

The equation and R-squared values for each fitted curves are as follows:

$$W = Ae^{B(1-RR)} + Ce^{D(1-RR)} \quad \textbf{Eq. 5.1}$$

Where, W is the total work required (MW_e) and

RR is the overall recovery rate of the hybrid carbon capture process.

The coefficients used for each set of data and the respective R-squared values are as follows:

- Membrane/low-temperature separation hybrid process – Case I ($R^2 = 0.998$):

  A = 41.0; B = -71.1; C = 124; D = -2.15

- Membrane/low-temperature separation hybrid process – Case II ($R^2 = 0.997$):

  A = 57.9; B = -98.3; C = 133; D = -2.32

5.1.2 Decision Variables Pareto charts

Similar to Chapter 4, the decision variables are studied to understand their effect on the objective functions. The Pareto charts of the decision variables were separated into three sections, one for each carbon capture stages and are shown in Figure 5.5, Figure 5.6 and Figure 5.7. The overall CO_2 recovery rate was chosen as the reference objective variable for the same reason as chapter 4 and to maintain consistency throughout project.

Figure 5.5, Figure 5.6 and Figure 5.7 display the Pareto charts of the decision variables affecting the membrane process, low-temperature capture process and recycling membrane process, respectively. It should be noted that in Figure 5.6 (c), the Pareto chart for the refrigerant flowrate includes values for both Case I and Case II. However, as specified in Chapter 3, Case II does not use the refrigerant flowrate as a decision variable. The refrigerant values for Case II are simply obtained post-simulation to better understand the correlation between the two cases.

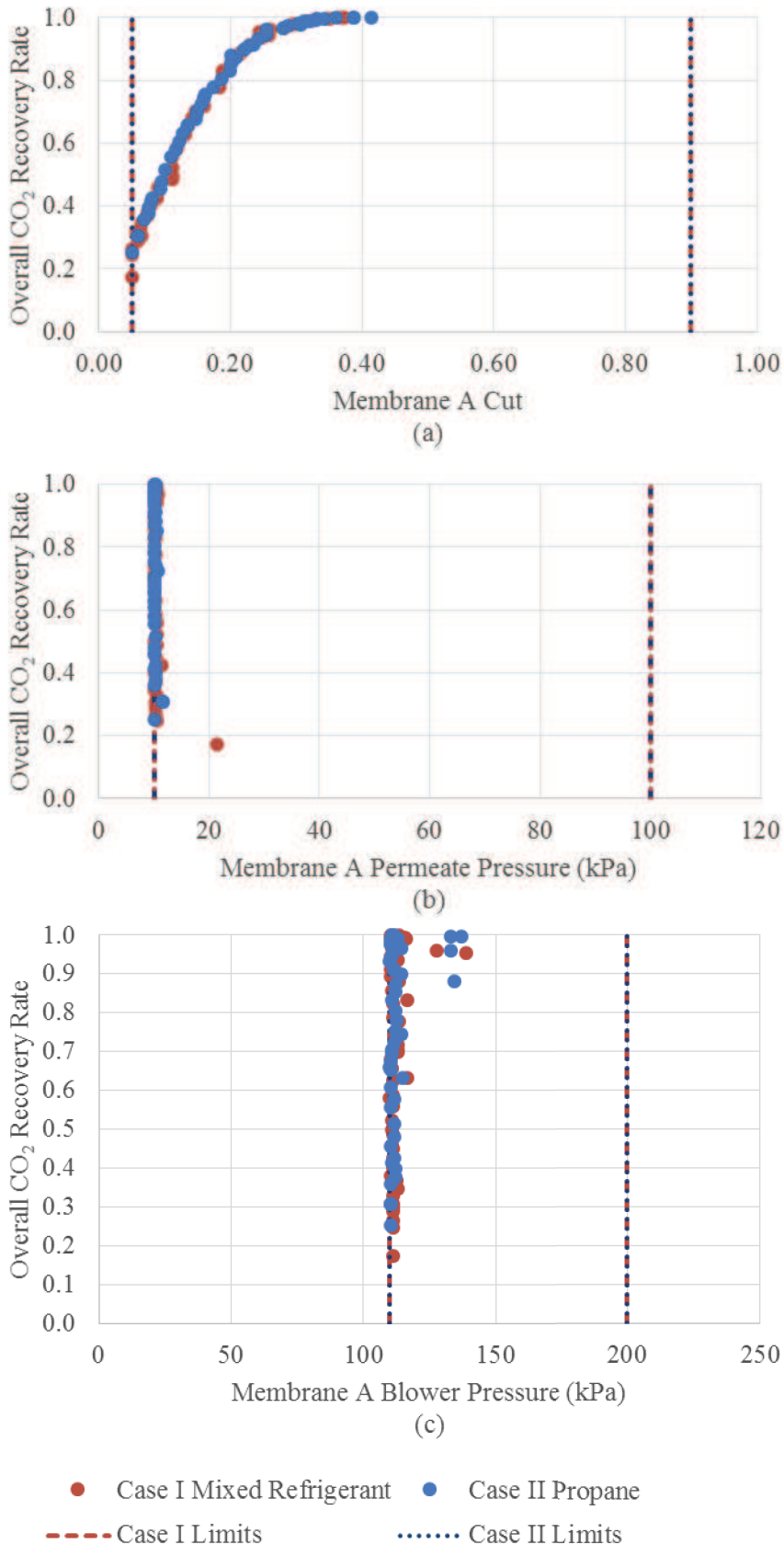

Figure 5.5 Pareto chart of the three decision variables governing Membrane A versus the CO_2 recovery rate (a) Membrane A Cut (b) Membrane A Feed Pressure; (c) Membrane A Permeate Pressure (kPa).

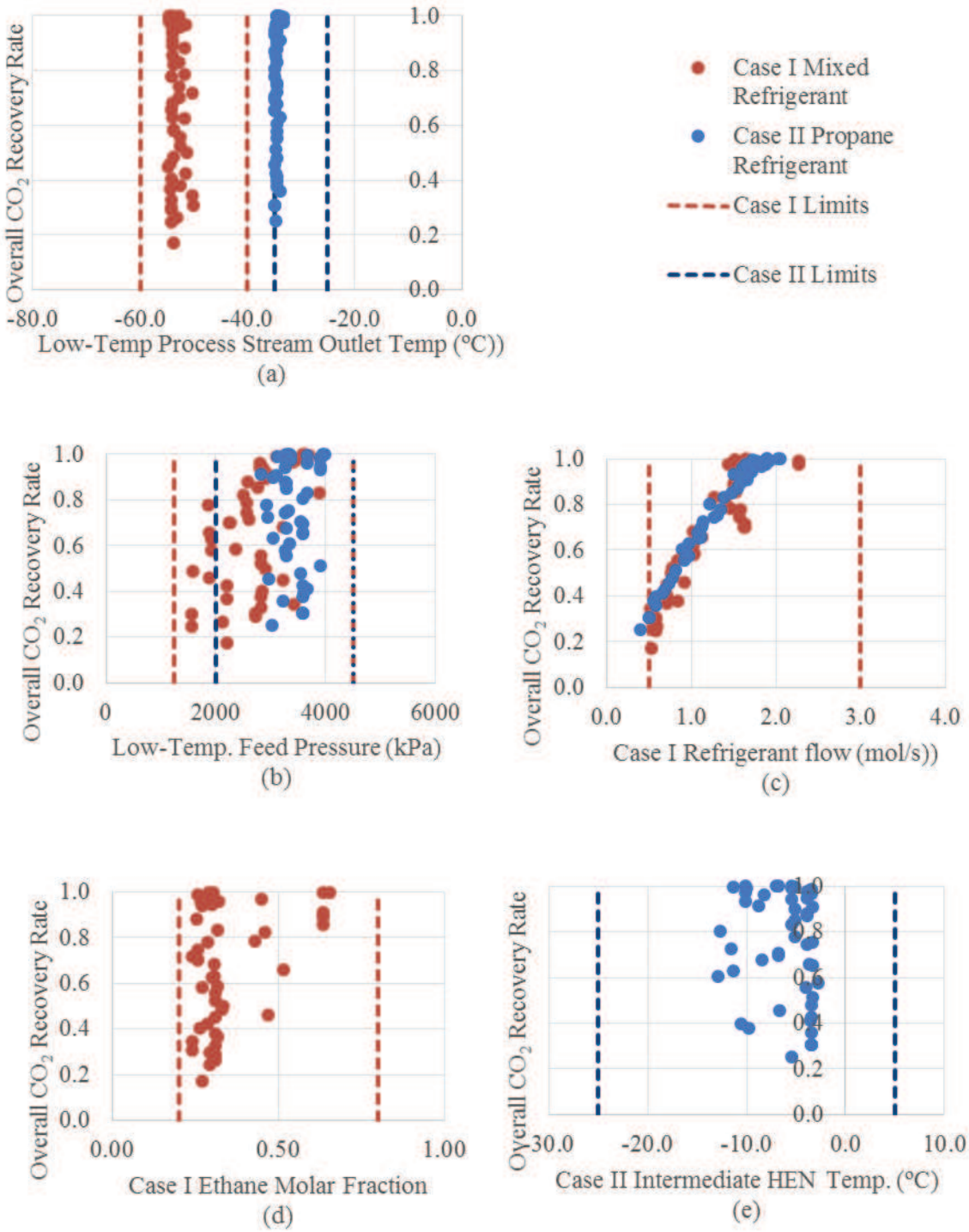

Figure 5.6 Pareto chart of the four decision variables for the low-temperature capture process versus the overall hybrid process CO_2 recovery rate.

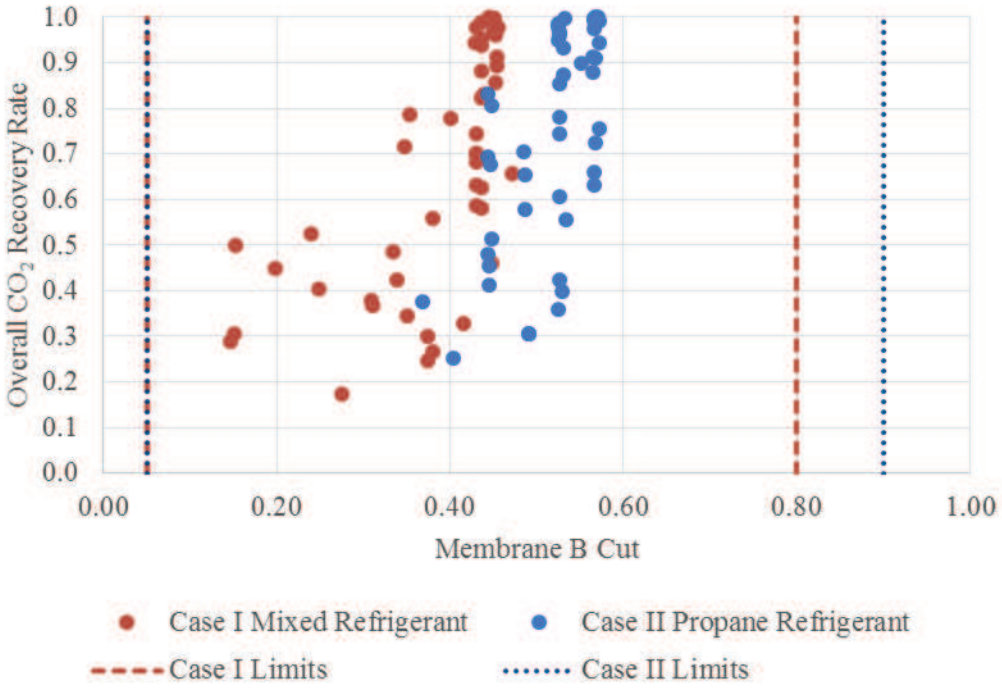

Figure 5.7 Pareto chart of the membrane B cut versus the overall hybrid process CO_2 recovery rate.

5.2 Membrane/ Low-Temperature Hybrid System Discussion

From the objective variables Pareto Optimal Front (Figure 5.3), it is observed that the relationship of the two objective variables for the membrane/low-temperature hybrid carbon capture cases are similar to the VSA/low-temperature hybrid carbon capture process in chapter 4, where the recovery rate increases with the increase in total shaft work required for CO_2 capture.

5.2.1 Decision Variables

Figure 5.5 shows that both cases have an almost identical correlation for the decision variables for the initial membrane process (Membrane A). This shows that in both cases, Membrane A has identical performance for the membrane CO_2 recovery rate and membrane CO_2 outlet purity, which is represented in Figure 5.8 and Figure 5.9, respectively, as a function of the overall CO_2 recovery rate of the hybrid system.

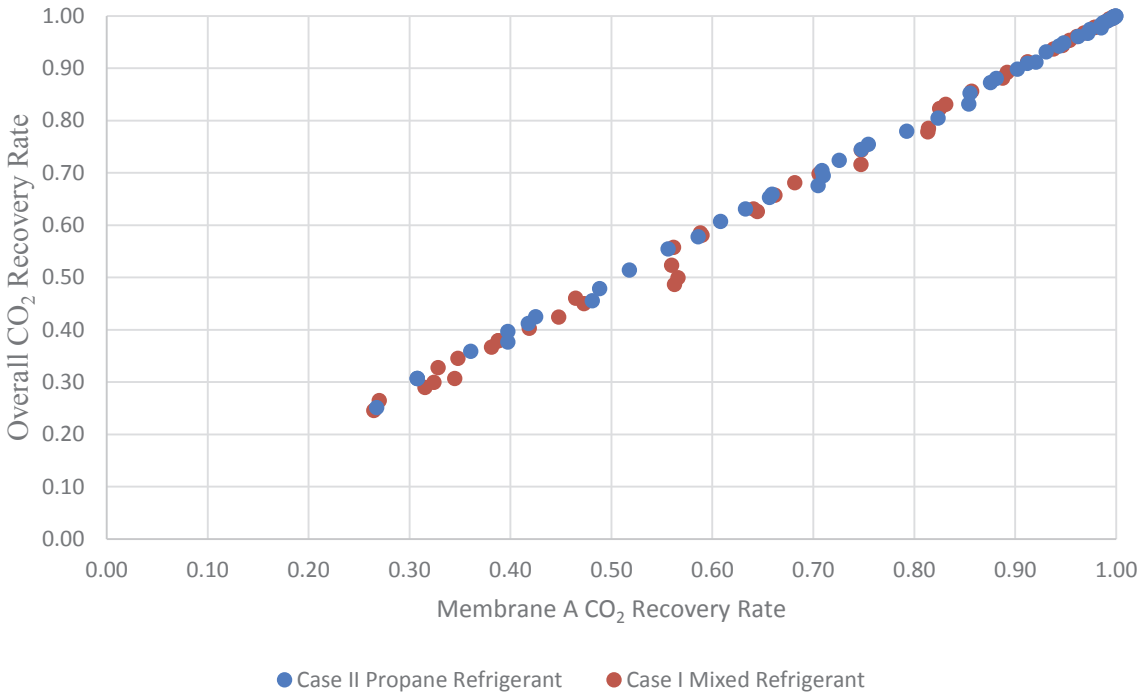

Figure 5.8 Pareto chart representing Membrane A CO_2 recovery rate as a function of the overall CO_2 recovery rate of the hybrid carbon capture system.

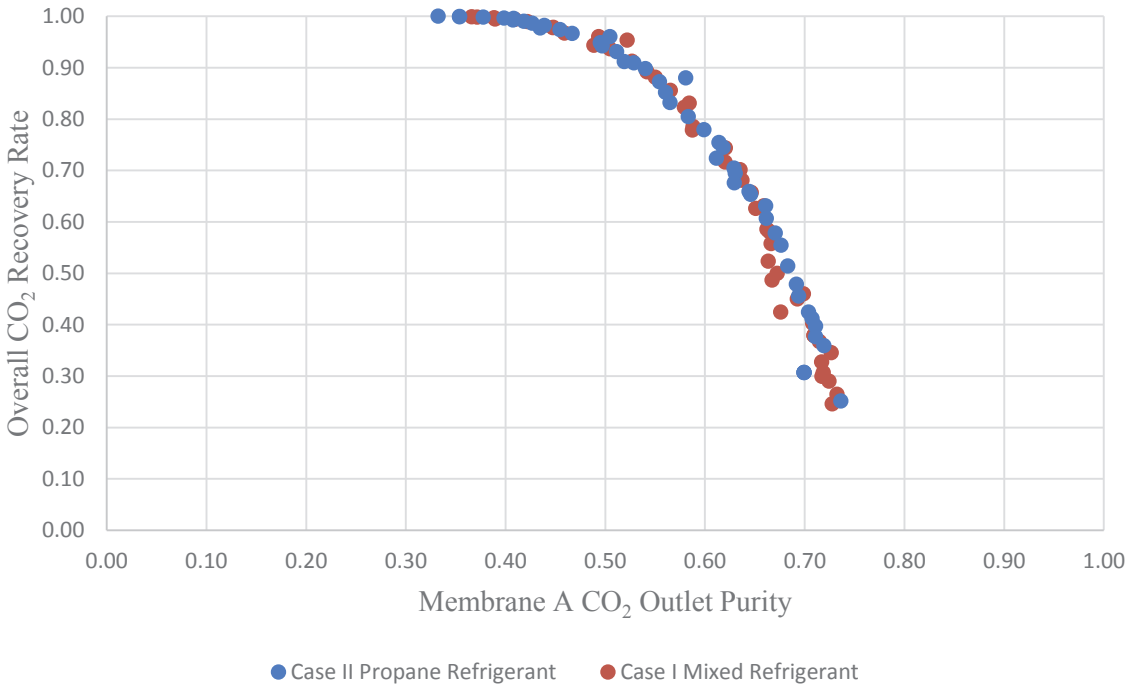

Figure 5.9 Pareto chart representing Membrane A CO_2 outlet purity as a function of the overall CO_2 recovery rate of the hybrid carbon capture system.

As it can be seen in Figure 5.8 and Figure 5.9, the membrane CO_2 recovery rate has a linear relationship with the overall CO_2 recovery rate and the membrane CO_2 outlet purity has an inverse

relationship with the overall recovery rate. This is a similar correlation to the VSA/low-temperature hybrid process and has a similar explanation as discussed in sub-chapter 4.2.1; the overall CO_2 recovery rate is governed by the recovery rate of Membrane A since the retentate stream is sent straight to the stack. At high Membrane A CO_2 recovery rate, Membrane A cannot achieve a high CO_2 outlet purity. This is represented in Figure 5.10, where the Membrane A CO_2 outlet purity is shown as a function of Membrane A specific work.

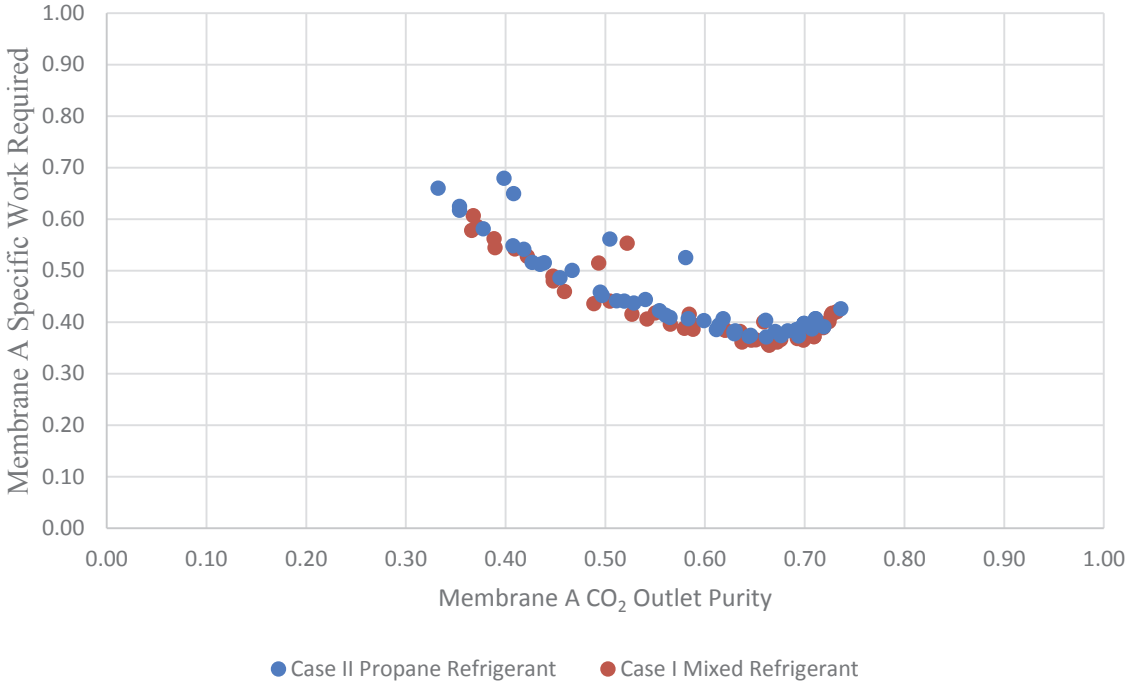

Figure 5.10 Pareto chart representing Membrane A CO_2 outlet purity as a function of the membrane A specific work required.

Furthermore, the identical performance of Membrane A in both cases indicates that the membrane/low-temperature hybrid system prefers increasing the work load of the initial CO_2 recovery stage, Membrane A, instead of the CO_2 purification stage (low-temperature carbon capture system). This is shown in Figure 5.11, where the membrane specific work and the low-temperature specific work is shown as function of overall CO_2 recovered; The low-temperature specific work includes the pre-compression work required and the refrigeration compression work required. It can be observed that both Case I and Case II have the same specific work requirements.

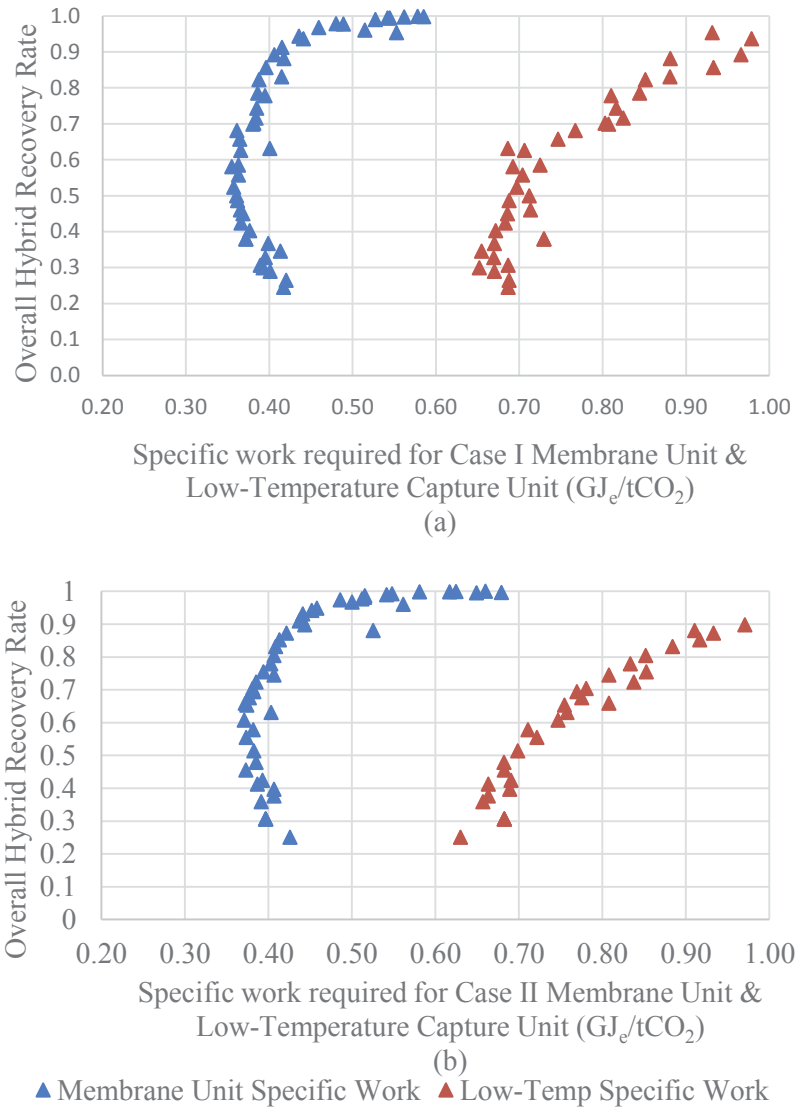

Figure 5.11 Pareto chart representing specific work required for membrane unit (blue) and the low-temperature carbon capture unit (red) for (a) Case I; (b) Case II.

Figure 5.6 (c) shows the refrigerant flowrate increases with overall recovery rate required in order to compensate for the decrease in CO_2 outlet purity of Membrane A. The main difference in all the figures in Figure 5.6 is the temperature of the process stream exiting the refrigeration heat exchanger (Figure 5.6 (a)). As expected, the mixed ethane/propane refrigeration system selected the low-temperatures of approximately -55ºC and the propane only refrigeration system selected higher temperatures of approximately -35ºC. The lower temperatures achieved by the mixed refrigerant (Case I) allowed lower feed pressures to be selected, whereas Case II always required pressures of 3000 kPa or higher.

Figure 5.7 shows that Membrane B, the membrane following the low-temperature process, requires a higher membrane cut in Case II than Case I. This is because Case II, achieves a higher temperature

resulting in the waste stream of the low-temperature CO_2 process has more CO_2 to be recovered from Membrane B. Hence, a higher cut would be required for Membrane B.

5.2.2 Objective Variables Pareto charts and Optimum Specific Work Required

In order to compare the performance of the membrane/low-temperature hybrid carbon capture process on the same basis as the VSA/low-temperature hybrid capture process, the Pareto chart of the total specific shaft work as a function of recovery rate was produced in Figure 5.12. The total specific shaft work required is the total shaft work required per mass flowrate of CO_2 being recovered by the process.

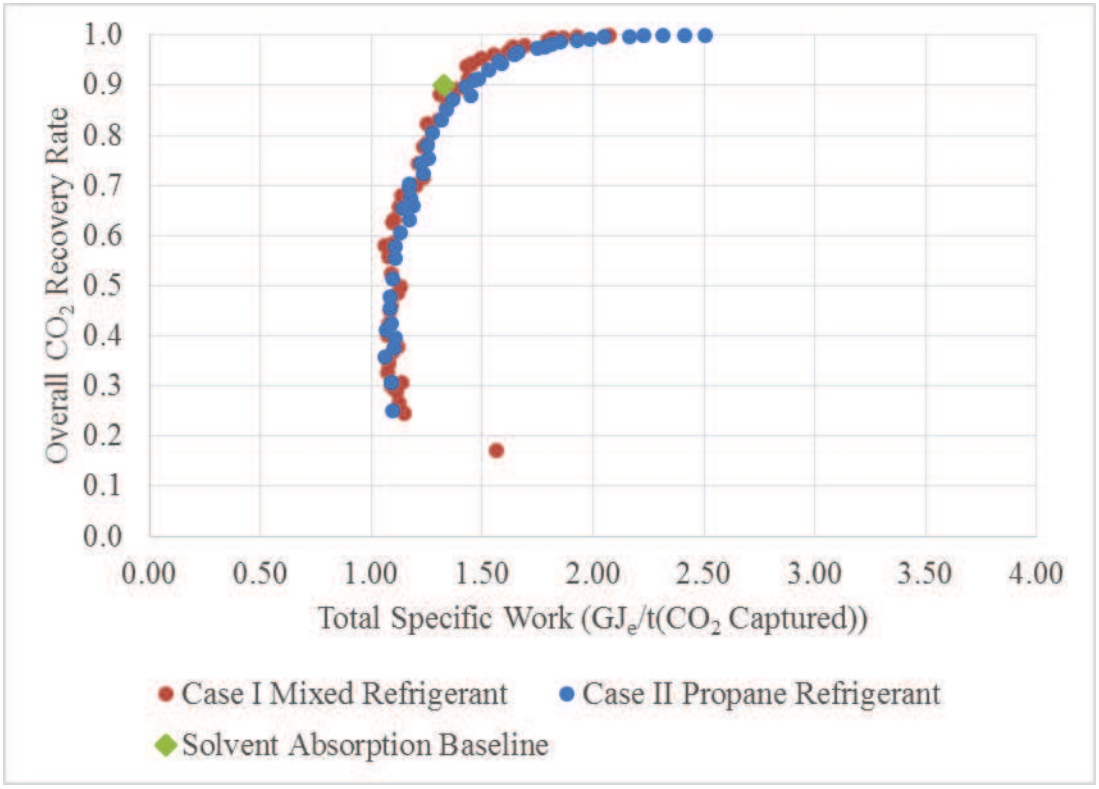

Figure 5.12 Overall recovery rate of hybrid system as a function of total specific work required ($GJ_e/t(CO_2)$) for two hybrid processes

As it can be seen in Figure 5.12, the total specific work required plateaus at overall recovery rate lower than 60% and increases as the overall recovery rate increases to 100%. It can also be observed that the membrane/low-temperature hybrid process for both cases are very competitive with the solvent absorption baseline. Hence, in order to perform further analysis on the hybrid processes, a set of operating conditions need to be selected as the optimum point for each case. An overall CO_2 recovery rate of approximately 90% is selected as the optimum points for each case to allow comparison with the solvent absorption baseline.

The summary of the operating conditions for the optimum minimum specific work and corresponding recovery rate for each hybrid carbon capture case is shown in Table 5.1. These optimum conditions were used to further analyse the performance of the hybrid process in the next sub-chapters.

Table 5.1 Table of decision variable range for MOO and optimum operating conditions of the two membrane/low-temperature hybrid capture cases

		Case I - Mixed Refrigerant			**Case II - Propane Refrigerant**		
Decision Variable	**Units**	**Min**	**Max**	**Optimum**	**Min**	**Max**	**Optimum**
Membrane A Cut	-	0.05	0.90	0.22	0.05	0.90	0.22
Membrane A Feed Pressure	(kPa)	110	200	110	110	200	114
Membrane A Permeate Pressure	(kPa)	10	100	10.0	10	100	10.1
Multi-Stage Compression Pressure	(kPa)	1250	4500	2898	2000	4500	3040
Refrigerant Molar Flow	(mol/s)	1.2	3	1.50	*N/A*	*N/A*	*N/A*
Refrigerant Ethane Molar Fraction	-	0.5	0.8	0.64	*N/A*	*N/A*	*N/A*
Heat Exchanger Network Intermediate Temperature	(°C)	*N/A*	*N/A*	*N/A*	-25	5	-23.0
Low-Temp. Process Stream Outlet Temperature	(°C)	-60	-40	-53.9	-35	-25	-34.4
Membrane B Cut	-	0.05	0.8	0.45	0.05	0.9	0.55
Optimum Overall CO_2 Recovery Rate	-	-	-	0.892	-	-	0.898
Optimum total specific shaft work	(kJ/t(CO_2 captured)	-	-	1.38	-	-	1.43

The difference in optimum performance between the two cases can be further analysed through the Pareto Charts of the three main components that require work which are shown in Figure 5.13. Figure 5.13 (a) shows that the work requirements for Membrane A in both cases are similar. This mirrors the results obtained in Figure 5.5 (b) and Figure 5.5 (c), where the feed pressure and permeate pressure of Membrane A for both cases are comparable.

Figure 5.13 (b) represents the total work required in the compression train of the refrigeration cycles for each case. As expected, the propane refrigerant refrigeration cycle (Case II), requires less work than the mixed refrigerant refrigeration cycle (Case I). As explained in sub-chapter 3.4.2 and Figure 3.14, this is due to the higher temperatures obtained by the propane refrigerant, which require lower pressure ratios in comparison to the mixed refrigerant, where higher pressure ratios are required to achieve the colder temperatures.

Figure 5.13 (c) shows the total work required for the pre-compression of the feed stream entering the low-temperature separation. It can be observed that Case I requires less work than Case II. This further confirms Figure 3.14, whereby the mixed refrigerant hybrid system has lower temperatures in the low-temperature unit. The lower temperature allows the CO_2 to be liquefied at lower pressure, therefore requiring less work in the pre-compression train.

The similar values obtained for the overall work required for both cases mean that the trade-off in work requirement for the refrigeration unit and pre-compression unit is almost equal. Furthermore, it shows the flexibility of the hybrid carbon capture system when using a low-temperature process as using different refrigeration system show almost exact final results.

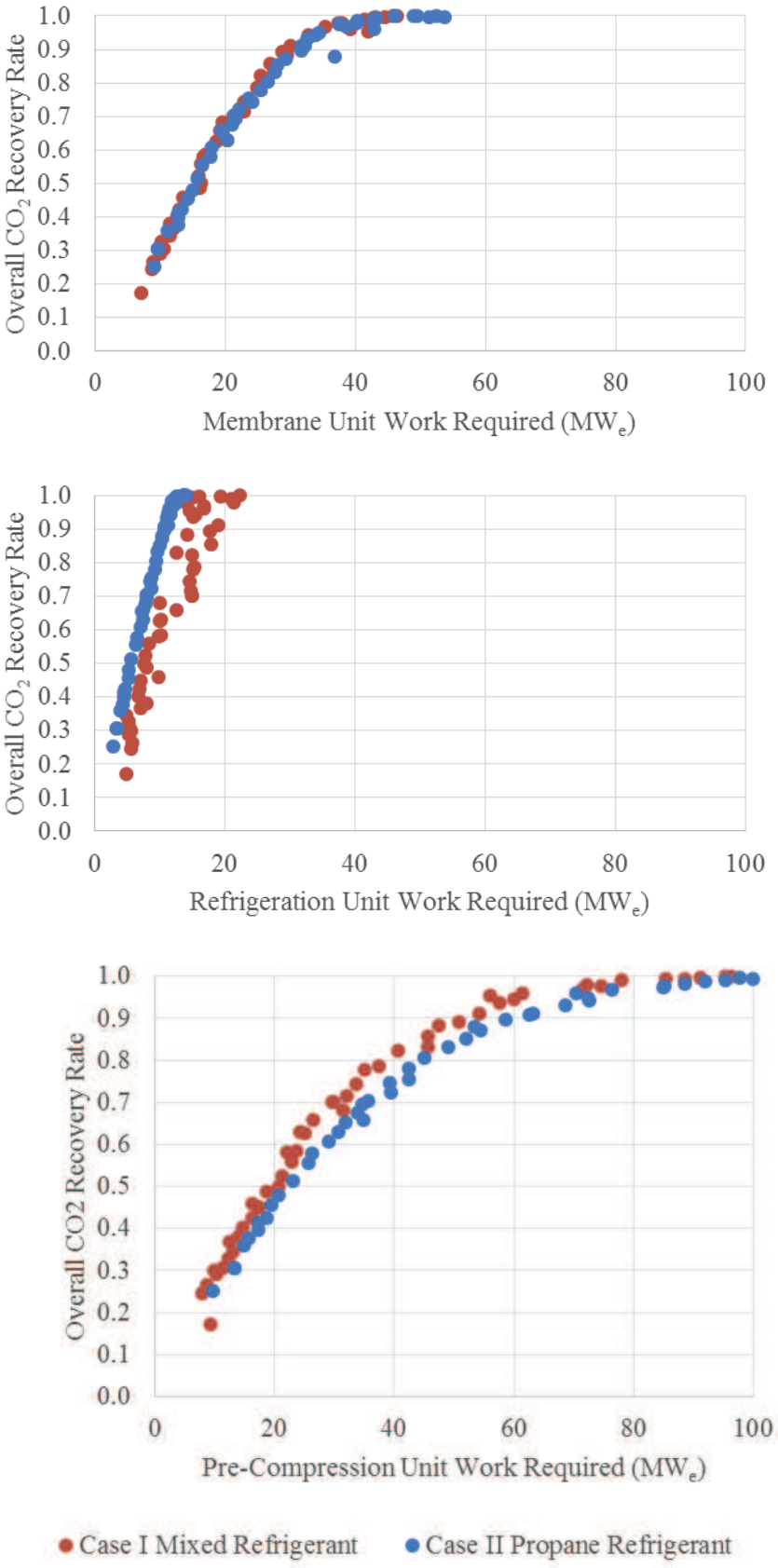

Figure 5.13 Pareto chart of the three main components requiring work versus the CO_2 recovery rate (a) Total Work Required for Membrane A unit (Compressor A + B); (b) Refrigeration Cycle Compressors (Compressor D); (c) Low-Temperature Pre-Compression (Compressor C)

5.2.3 Pinch Analysis

The heat integration of the hybrid carbon capture process was further studied. The heat composite curves of the heat integrated low-temperature separation for each optimum case were generated and shown in Figure 5.14 and Figure 5.15. The table of heat composite curve data are shown in the Appendix section B.4.

The difference in the two refrigeration units can be further observed in the stream composite curve in Figure 5.14 and Figure 5.15**.** More specifically, in the cold composite curve at the low temperatures, which represent the refrigerant streams being heated up from the hot composite curve. The main difference reflects Figure 3.8, where the mixed ethane/propane refrigerant system shows its flexibility in heat exchanging through the curved composite curve, whereas the propane refrigeration system is matched as a straight line. Furthermore, the pinch points at approximately -30°C and 20°C for Case I and Case II, respectively, show that the heat integration was effective.

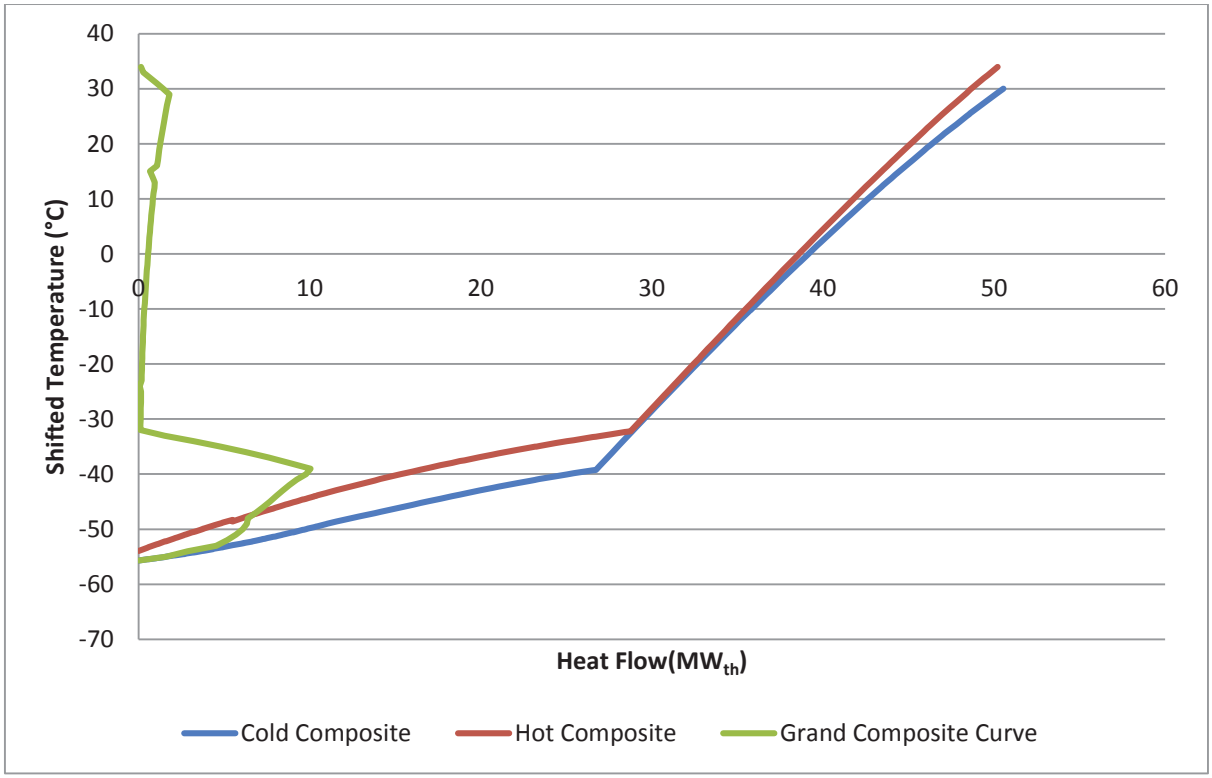

Figure 5.14 Stream composite curve and the grand composite curve for Membrane/Low-Temperature hybrid carbon capture for Case I – Mixed Refrigerant.

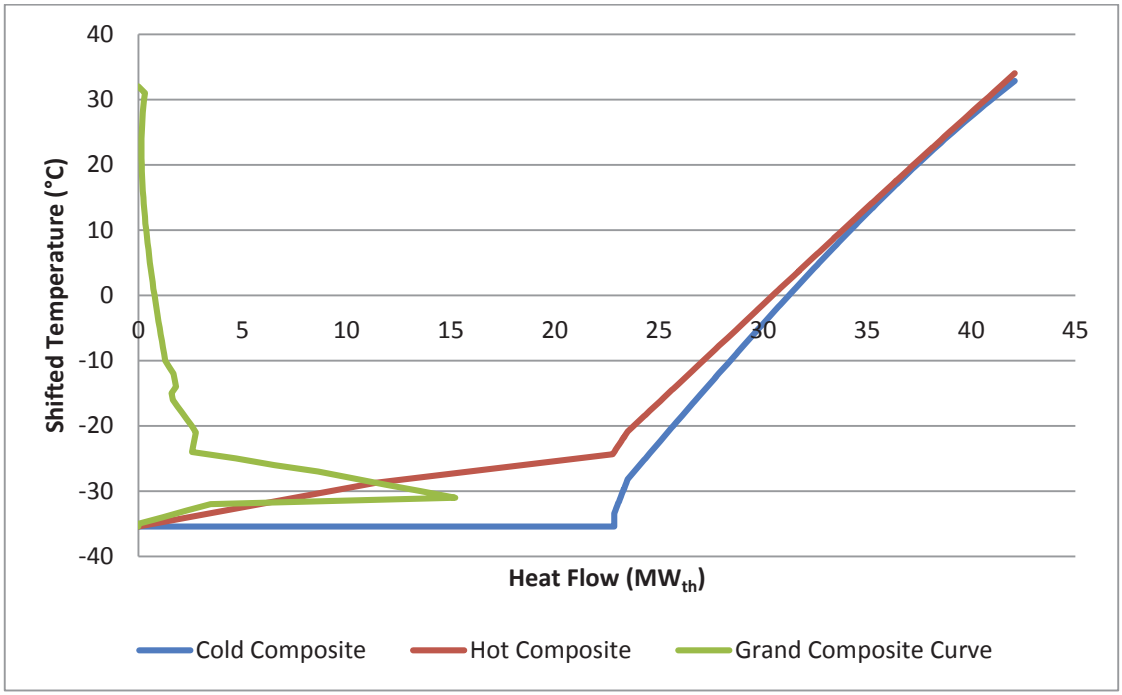

Figure 5.15 Stream composite curve and the grand composite curve for Membrane/Low-Temperature hybrid carbon capture for Case II – Propane Refrigerant.

5.2.4 Sensitivity Analysis

A sensitivity analysis was performed on the membrane/low-temperature hybrid carbon capture process to forecast the performance of the hybrid process when new and better membranes are developed. Using Figure 5.16, 2 different membranes with better performance than the Polaris™ membrane (blue dot) were selected:

i. Red Dot: CO_2 Permeance = 2000 GPU and CO_2/N_2 Selectivity = 50
ii. Green Dot: CO_2 Permeance = 1000 GPU and CO_2/N_2 Selectivity = 100.

Those membrane parameters were inserted in the Aspen HYSYS® simulation using the Case II membrane/low-temperature hybrid process. Since both Case I and Case II performed almost equally competitive with the Polaris™ membrane, Case II with propane only refrigerant was selected for two main reasons:

1. Propane only refrigerant would provide easier process operation due to higher operating temperatures.
2. The simulation of the propane only refrigerant was almost three times faster when running the MOO.

The Pareto Front for the three membranes are shown in Figure 5.17 and the total specific work Pareto chart are shown in Figure 5.18.

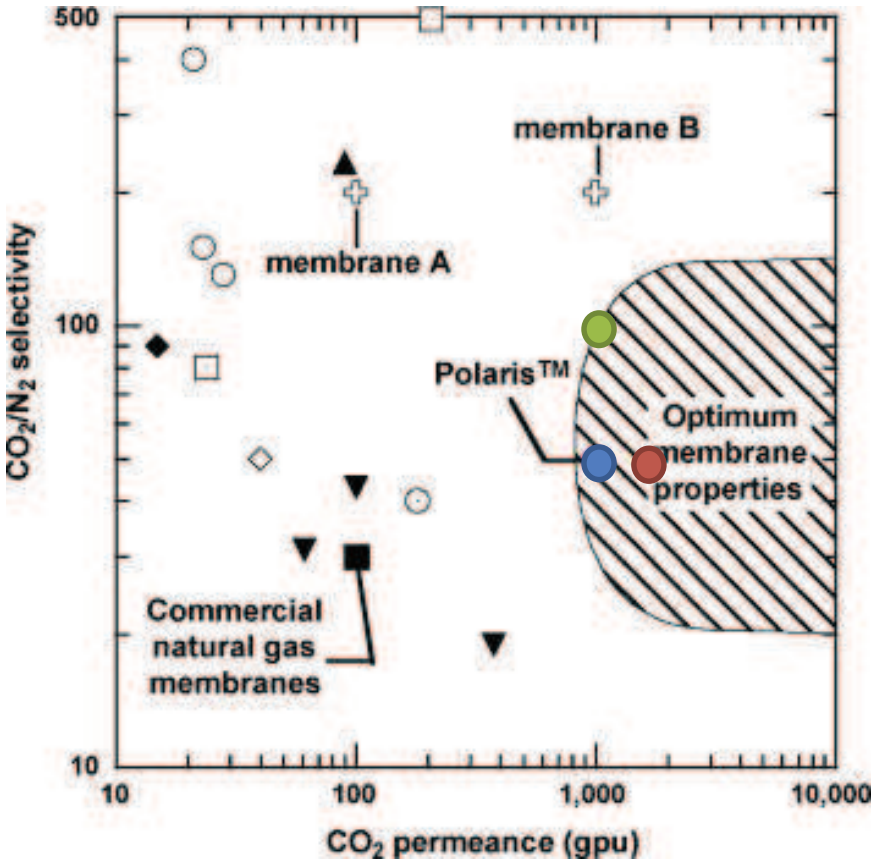

Figure 5.16 CO_2/N_2 selectivity and CO_2 permeance trade-off plot comparing the performance of different membranes reported in the literature. The blue dot represents the Polaris™ membrane and the green and red dot represent the membrane chosen in the sensitivity analysis.

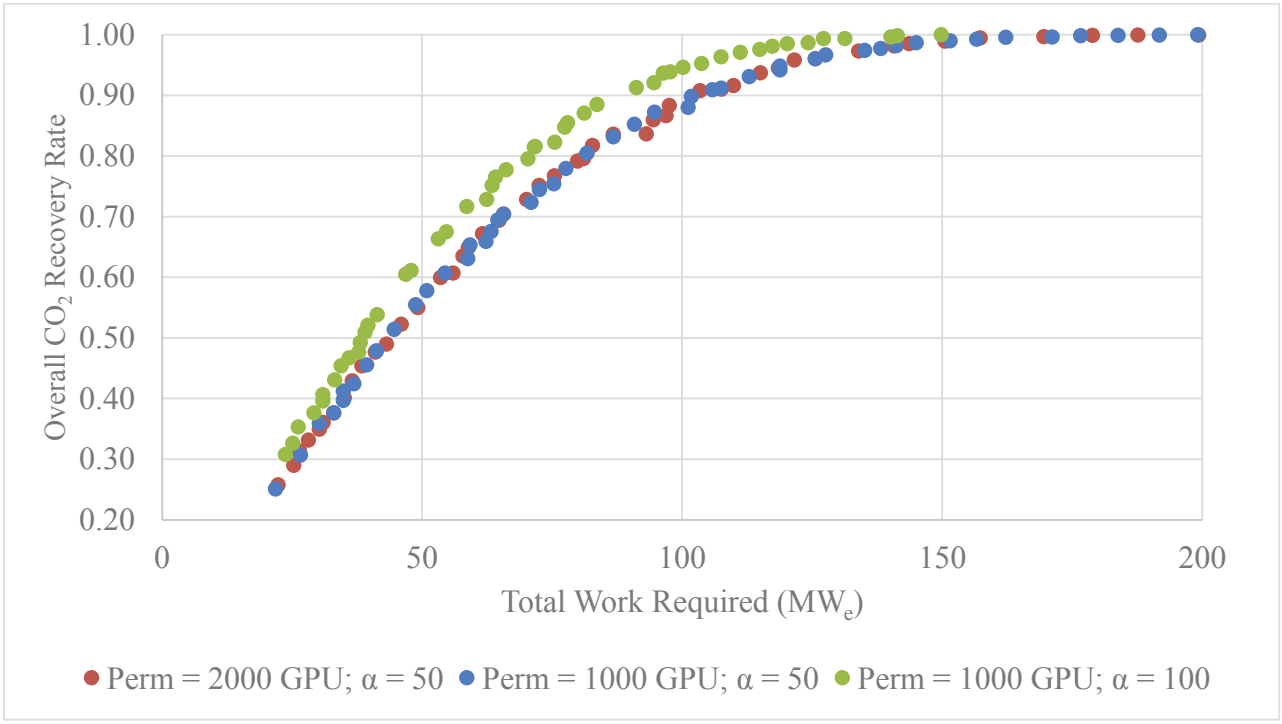

Figure 5.17 Pareto Front representing the results obtained for the three membranes in the sensitivity analysis.

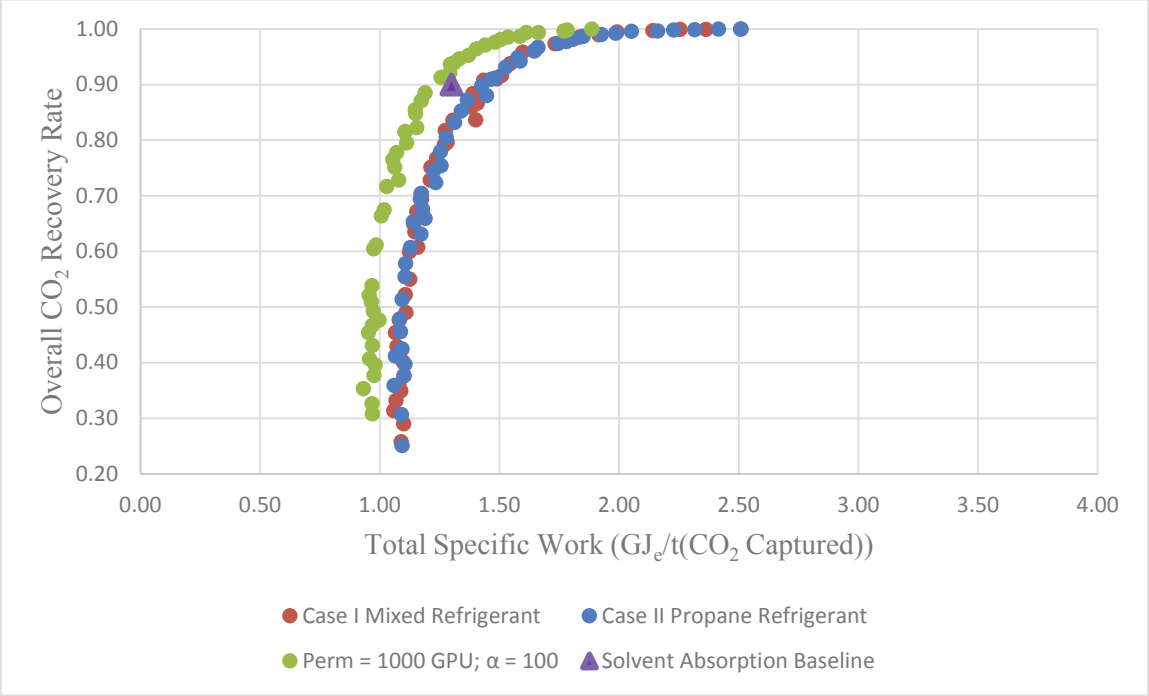

Figure 5.18 Pareto Front representing the results obtained for the three membranes in the sensitivity analysis.

From Figure 5.18, it can be observed that all three membranes have the same trend. However, only doubling the selectivity of the membrane improves on the performance of the Polaris™ membrane. On the other hand, doubling the permeance of the membrane does not significantly improve the performance of the membrane. This is because improving the selectivity of the membrane improves the CO_2 outlet purity at no extra work required. This is shown in Figure 5.19, where a higher CO_2 outlet purity is obtained at lower work requirement for the membrane with higher CO_2 selectivity. Finally, it is important to note that this membrane has a better performance than the solvent absorption baseline.

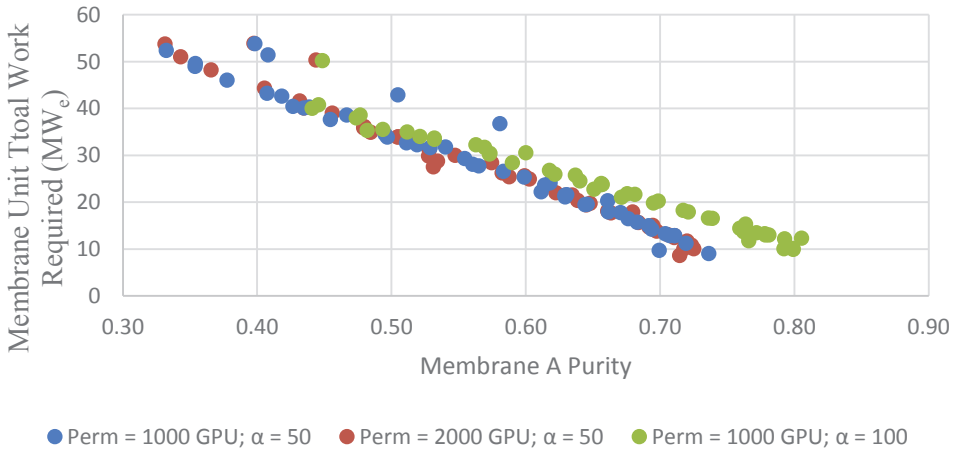

Figure 5.19 Pareto chart representing Membrane A CO_2 outlet purity as a function of the total work required to operate Membrane A unit.

6 Techno-Economic Analysis of VSA/Low-Temperature and Membrane/Low-Temperature Hybrid Carbon Capture Processes

This chapter aims to compare the techno-economic performance of each hybrid carbon capture processes analysed in Chapter 4 and Chapter 5. It starts by comparing the optimum operating conditions of each hybrid system, followed by the techno-economic analysis results of the individual hybrid processes. Finally, the techno-economic performance is discussed for both processes.

6.1 Comparison of VSA/Low-Temperature and Membrane/Low-Temperature Hybrid Carbon Capture Processes

Figure 6.1 was obtained by combining the results obtained in the previous two chapters. It shows the final Pareto Front of both the VSA/low-temperature hybrid carbon capture process and the membrane/low-temperature hybrid carbon capture process.

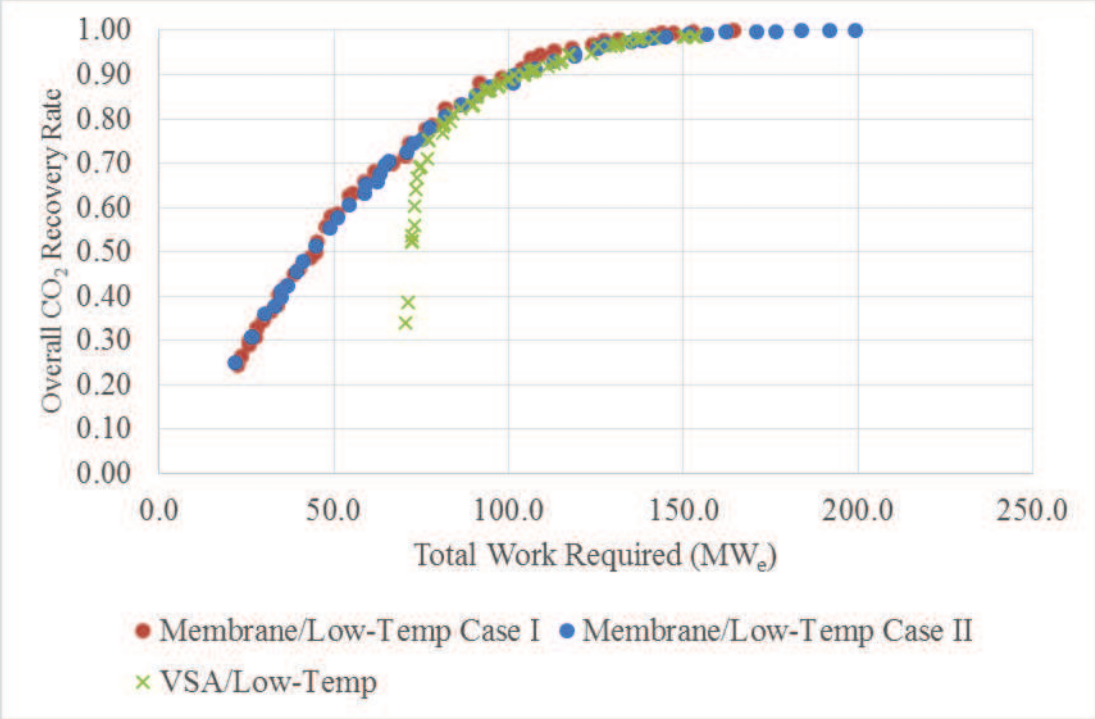

Figure 6.1 Pareto Front of total work required as a function of overall CO_2 recovery rate for three hybrid carbon capture processes: VSA/low-temperature hybrid system, membrane/low-temperature hybrid system using mixed refrigerant (Case I) and membrane/low-temp hybrid system using propane refrigerant (Case II).

Using the Pareto Fronts, a second order exponential regression of the data points was performed to obtain continuous curves representing the total work required as a function of the overall CO_2 recovery rate for each hybrid carbon capture process. These continuous curves are shown in Figure 6.2. The general equation used for the second order exponential regressions was:

$$W = Ae^{B(1-RR)} + Ce^{D(1-RR)} \qquad \textbf{Eq. 6.1}$$

Where, W is the total work required (MW_e) and

RR is the overall recovery rate of the hybrid carbon capture process.

The coefficients used for each set of data and the respective R-squared values are as follows:

- VSA/low-temperature separation hybrid process ($R^2 = 0.986$):

  A = 82.6; B = -10.2; C = 73.7; D = -0.0713

- Membrane/low-temperature separation hybrid process – Case I ($R^2 = 0.998$):

  A = 41.0; B = -71.1; C = 124; D = -2.15

- Membrane/low-temperature separation hybrid process – Case II ($R^2 = 0.997$):

  A = 57.9; B = -98.3; C = 133; D = -2.32

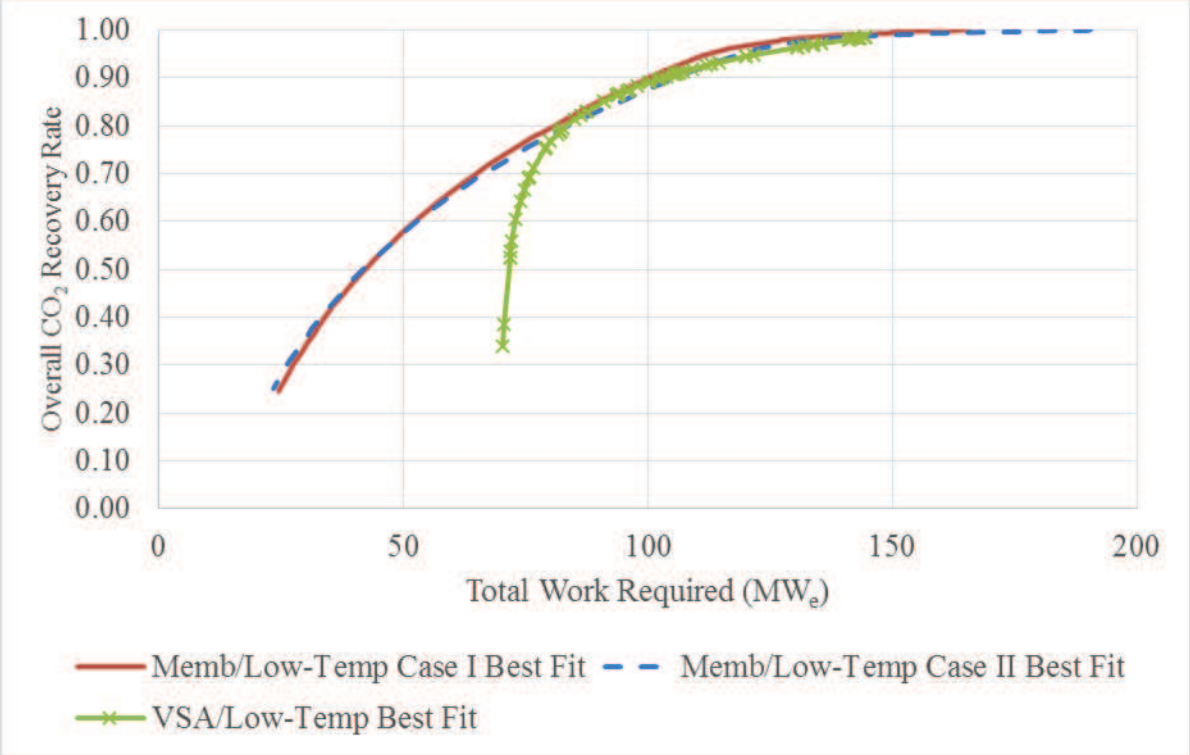

Figure 6.2 Pareto Front of total work required as a function of overall CO_2 recovery rate using 2nd order exponential equations ($a*exp^{by} + c*exp^{dy}$) to fit lines of three hybrid carbon capture processes.

As observed in Figure 6.2, all three hybrid processes increase in total work requirement as the overall recovery rate increases. Finally, in order to compare the performance of the carbon capture processes on the same basis, the total specific work requirement as a function of overall recovery rate was

produced in Figure 6.3. The total specific work requirement was derived from the total work requirement equation (Eq. 6.1) using the following steps:

- Total specific work required (W_{spec}) is the total work required (W) per mass flowrate of CO_2 captured ($\dot{m}_{CO_2 Captured}$).

$$\boldsymbol{W_{Spec} = \frac{W}{\dot{m}_{CO_2 Captured}}} \qquad \textbf{Eq. 6.2}$$

- The overall recovery rate of the hybrid process is the ratio of the CO_2 mass flowrate entering the carbon capture process from the flue gas ($\dot{m}_{CO_2 flue}$) vs the mass flowrate of CO_2 captured ($\dot{m}_{CO_2 Captured}$).

$$\boldsymbol{RR = \frac{\dot{m}_{CO_2 Captured}}{\dot{m}_{CO_2 flue}}} \qquad \textbf{Eq. 6.3}$$

- Making the mass flowrate of CO_2 captured ($\dot{m}_{CO_2 Captured}$) and substituting the parameter into Eq. 6.2 yields Eq. 6.4.

$$\boldsymbol{W_{Spec} = \frac{W}{\dot{m}_{CO_2 flue}} \times \frac{1}{RR}} \qquad \textbf{Eq. 6.4}$$

- Finally, substituting Eq. 6.1 in Eq. 6.4 produces the total specific work required as a function of the overall recovery rate of the hybrid process:

$$\boldsymbol{W_{Spec} = \frac{Ae^{B(1-RR)} + Ce^{D(1-RR)}}{\dot{m}_{CO_2 flue}} \times \frac{1}{RR}} \qquad \textbf{Eq. 6.5}$$

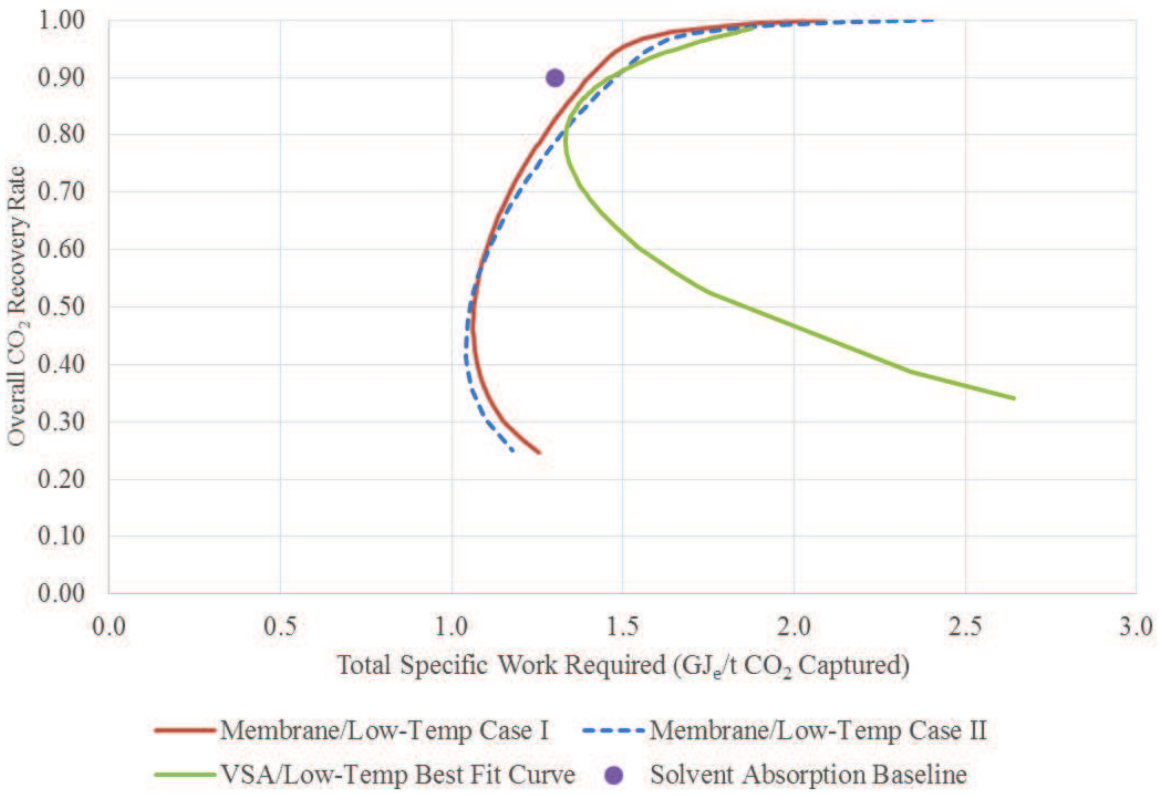

Figure 6.3 Pareto Front of total specific work required as a function of overall CO_2 recovery rate using best fit lines of three hybrid carbon capture processes.

Figure 6.3 shows that at 90% recovery rate, which is the recovery rate for the solvent absorption baseline, Case I of the membrane/low-temperature hybrid carbon capture process performs slightly better than the other two hybrid process. Furthermore, while at overall recovery rates of higher than 80%, all three hybrid processes have similar performance, at lower recovery rates, both membrane/low-temperature hybrid carbon capture cases have much lower total specific work requirement. This is due to the higher flexibility obtained from the membrane process, allowing the hybrid process to perform better over a higher range.

6.2 Techno-Economic Analysis Results

In order to determine the techno-economic performance of each hybrid system, a set of optimum operating conditions were selected and the techno-economic analysis was performed at those conditions. The optimum conditions were determined using the total shaft specific work required for each system, which was further discussed in Chapter 4 and Chapter 5 for the different hybrid carbon capture systems.

A detailed techno-economic result for the membrane/low-temperature separation hybrid carbon capture with an overall CO_2 recovery rate of 90% is shown in the Appendix in section B.4.

6.2.1 VSA/ Low-Temperature Hybrid System

The operating conditions and performance for each case are represented in Table 6.1.

Table 6.1 Operating conditions and performance for the four VSA/Low-Temperature hybrid carbon capture systems used for the techno-economic analysis.

Overall Process Performance					
Overall Recovery Rate of Hybrid System	%	79.4%	85.1%	90.0%	94.7%
Total Shaft Work Required	MW_e	83	91	105	124
Specific Shaft Work Required	$GJ_e/t(CO_2)$	1.40	1.35	1.46	1.65
Decision Variables					
Ethane Fraction	(-)	0.45	0.30	0.37	0.46
Refrigerant Molar Flow	mol/s	1.20	1.25	1.39	1.34
Min Process Temp	C	-53.5	-56.4	-48.7	-51.8
Membrane Cut	(-)	0.16	0.28	0.39	0.31
Pre-LT Pressure	kPa	2026	3079	2770	3871
VSA Purity	%	79.8	67.3	64.9	64.5
VSA Recovery Rate	%	75.4	85.9	91.1	91.8

The techno-economic parameters and methodology discussed in sub-chapter 3.4.4 was applied to each set of optimum conditions to obtain the capital costs for the equipment shown in Table 6.2. This table shows that the compressors are the most expensive equipment, which mirrors the energy requirement of the hybrid carbon capture system.

Table 6.2 Techno-economic summary of four VSA/Low-Temperature hybrid carbon capture systems.

Overall Recovery Rate of Hybrid System	**79.4%**	**85.1%**	**90.0%**	**94.7%**
Low-Temperature Feed Compressors Capital Cost (A$ million)	44	46	53	60
Vacuum Pump Capital Cost (A$ million)	28	33	38	49
Refrigeration Compressors Capital Cost (A$ million)	12	12	14	15
Blower Capital Cost (A$ million)	1	4	3	2
VSA Vessel Capital Cost (A$ million)	2	2	2	2
Other Capital Cost (A$ million)	3	4	4	5
Total Equipment Capital Cost (A$ million)	91	101	114	133

The total equipment cost was used to determine total capital cost and the operating cost from the factors displayed in Table 3.9 and Table 3.10. The loss in revenue was calculated from the energy penalty and the storage cost was a factor of the amount of CO_2 captured from hybrid carbon capture system. Finally, the levelised cost of electricity (LCOE) and the cost of CO_2 avoidance was determined by evaluating all the economic parameters over the 25 years of the project. Figure 6.4 is a graphical representation of the costs breakdown in present value (PV) as well as the LCOE and cost of CO_2 avoidance.

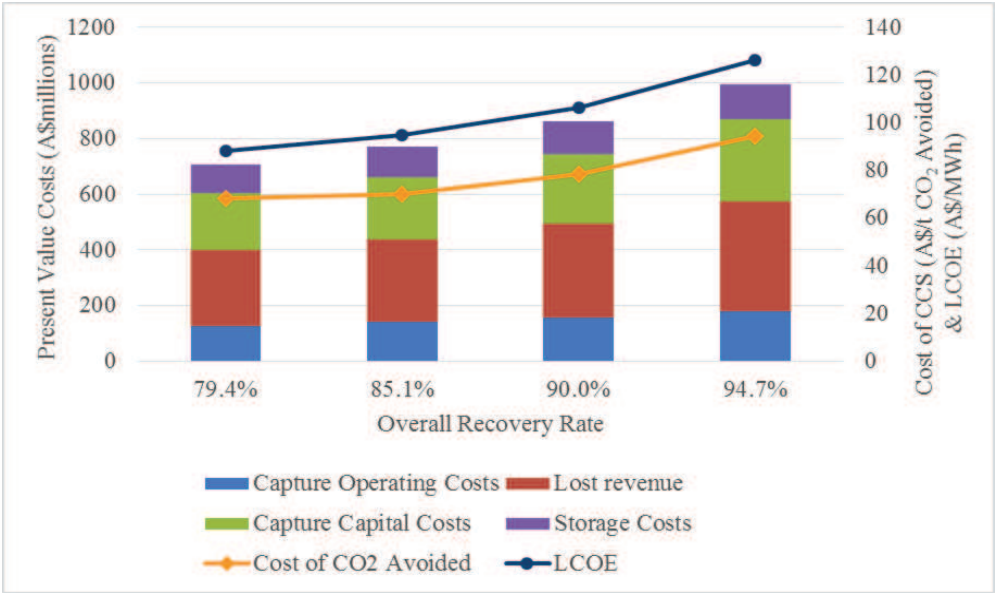

Figure 6.4 Costs breakdown in present value (PV), LCOE and cost of CO_2 avoidance for four VSA/Low-Temperature hybrid carbon capture systems.

6.2.2 Membrane/ Low-Temperature Hybrid System

Three points on the Pareto Optimal front from the MOO results were chosen as possible operating points for each of the two cases for Membrane/low-temperature hybrid carbon capture processes obtained in Chapter 5. The operating performance and the corresponding decision variables for Case I are shown in Table 6.3.

Table 6.3 Operating conditions and performance for the three Case I membrane/low-temperature hybrid carbon capture systems used for the techno-economic analysis.

Overall Process Performance				
Overall Recovery Rate of Hybrid System	%	Case I - 85.6%	Case I - 89.2%	Case I - 95.1%
Total Shaft Work Required	MW_e	91	98	113
Specific Shaft Work Required	$GJ_e/t(CO_2)$	1.34	1.38	1.50
Decision Variables				
Membrane A Cut	-	0.200	0.218	0.244
Membrane A Feed Pressure	(kPa)	111	110	139
Membrane A Permeate Pressure	(kPa)	10.0	10.0	10.1
Multi-Stage Compression Pressure	(kPa)	2769	2898	2828
Refrigerant Molar Flow	(mol/s)	1.530	1.501	1.522
Refrigerant Ethane Molar Fraction	-	0.636	0.636	0.268
Low-Temp. Process Stream Outlet Temperature	(°C)	-54.0	-53.9	-54.0
Membrane B Cut	-	0.452	0.454	0.436

Table 6.4 represents the summary of techno-economic analysis for Case I, where the total capital cost as well as the four main contributors of capital cost is shown. Similar to the VSA/low-temperature hybrid carbon capture process, Figure 6.5 is the graphical representation of the costs breakdown in present value (PV) as well as the LCOE and cost of CO_2 avoidance for Case I.

Table 6.4 Techno-economic summary of Membrane/Low-Temperature hybrid carbon capture systems for Case I.

Overall Recovery Rate of Hybrid System	**Case I - 85.6%**	**Case I - 89.2%**	**Case I - 95.1%**
Compressors Capital Cost (A$ million)	46	51	56
Vacuum Pump Capital Cost (A$ million)	24	26	29
Ref Comp Capital Cost (A$ million)	18	13	15
Blower Capital Cost (A$ million)	4.0	3.7	16.8
Other Capital Cost (A$ million)	6.5	11.5	8.6
Total Capital Cost (A$ million)	99	106	126

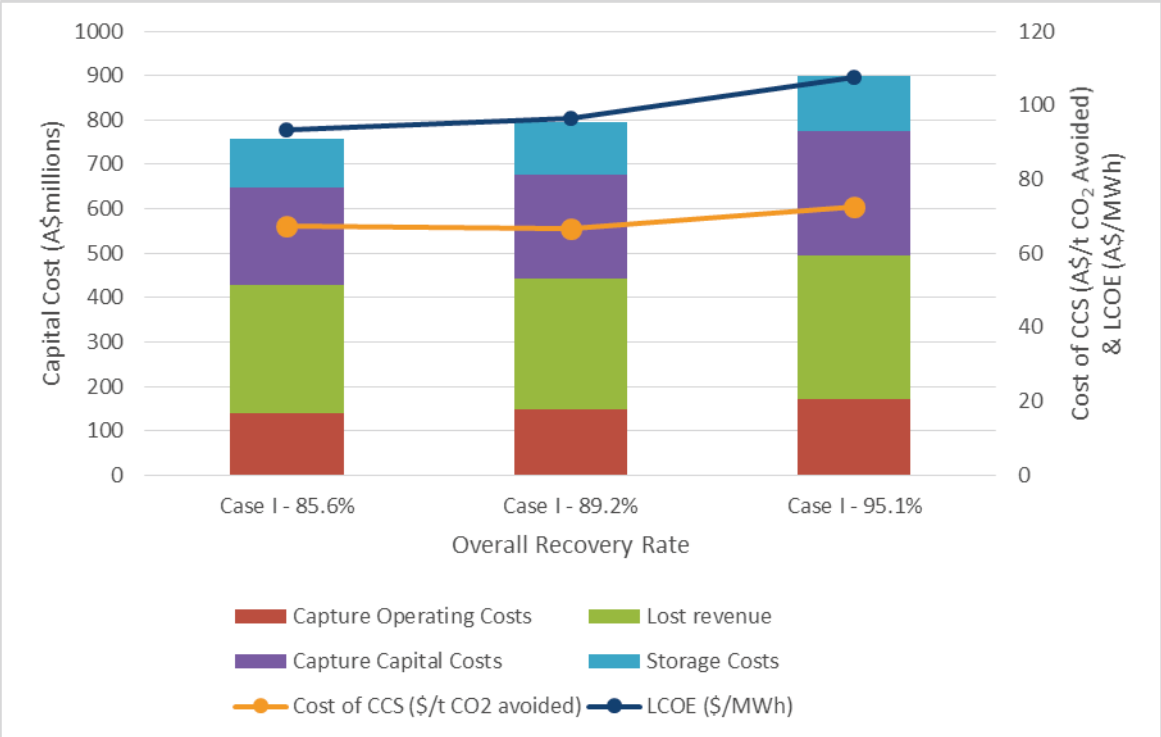

Figure 6.5 Costs breakdown in present value (PV), LCOE and cost of CO_2 avoidance for three operating conditions for Case I (Mixed Refrigerant) Membrane/Low-Temperature hybrid carbon capture systems.

A techno-economic analysis was also performed for the membrane/low-temperature hybrid carbon capture system using propane (Case II). The operating conditions used in the analysis and the corresponding decision variables are shown in Table 6.5.

Table 6.5 Operating conditions and performance for the three Case II membrane/low-temperature hybrid carbon capture systems used for the techno-economic analysis.

Overall Process Performance				
Overall Recovery Rate of Hybrid System	%	Case II - 84.9%	Case II - 89.8%	Case II - 95.3%
Total Shaft Work Required	MW_e	90	102	121
Specific Shaft Work Required	$GJ_e/t(CO_2)$	1.34	1.43	1.58
Decision Variables				
Membrane A Cut	-	0.201	0.221	0.203
Membrane A Feed Pressure	(kPa)	112	114	114
Membrane A Permeate Pressure	(kPa)	10.4	10.1	11.8
Multi-Stage Compression Pressure	(kPa)	3274	3040	4053
Heat Exchanger Network Intermediate Temperature	(°C)	-5.054	-5.054	4.844
Low-Temp. Process Stream Outlet Temperature	(°C)	-34.7	-34.4	-29.0
Membrane B Cut	-	0.526	0.552	0.498

Table 6.6 represents the summary of the equipment capital cost breakdown and Figure 6.6 is the graphical representations of the summary and Case II.

Table 6.6 Techno-economic summary of Membrane/Low-Temperature hybrid carbon capture systems for Case II.

Overall Recovery Rate of Hybrid System	Case II - 84.9%	Case II - 89.8%	Case II - 95.3%
Compressors Capital Cost (A$ million)	52	59	75
Vacuum Pump Capital Cost (A$ million)	24	27	32
Ref Comp Capital Cost (A$ million)	11	12	13
Blower Capital Cost (A$ million)	3.8	4.8	3.3
Other Capital Cost (A$ million)	4.7	5.0	5.5
Total Capital Cost (A$ million)	97	108	129

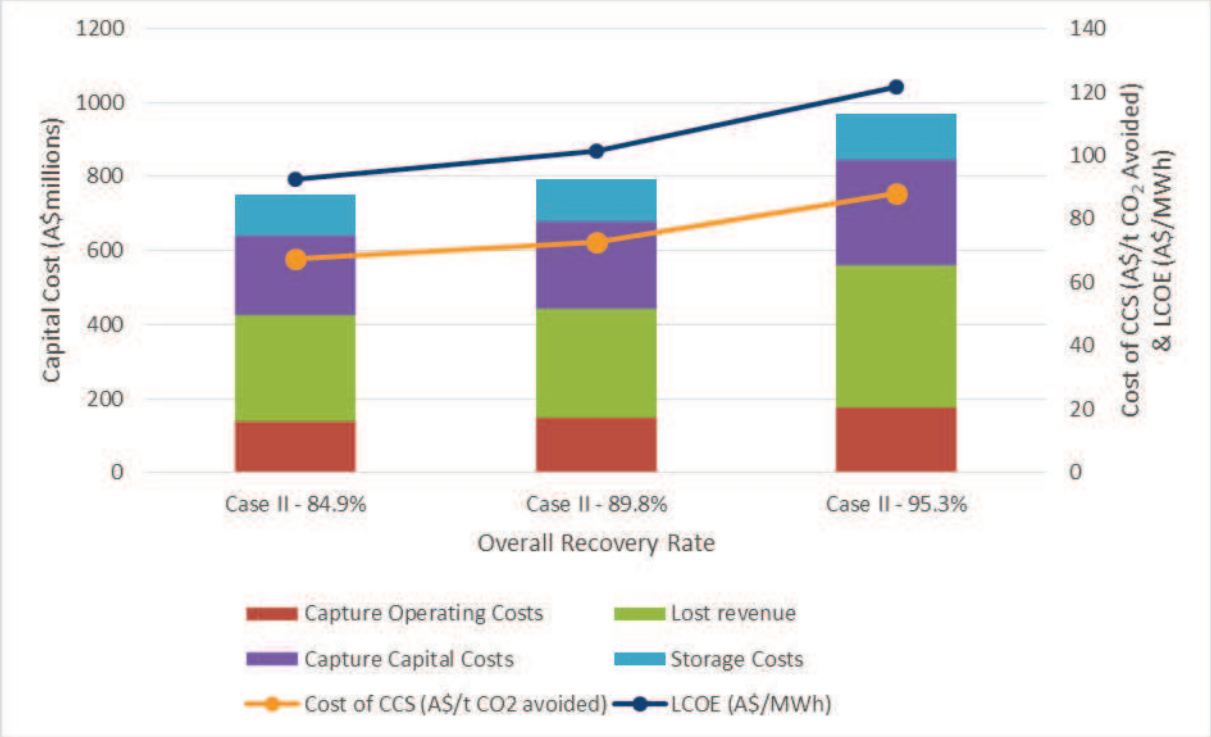

Figure 6.6 Costs breakdown in present value (PV), LCOE and cost of CO_2 avoidance for three operating conditions for Case II (Propane Refrigerant) Membrane/Low-Temperature hybrid carbon capture systems.

6.3 Techno-Economic Analysis Discussion

From the results obtained for the techno-economic analysis, it can be seen that the LCOE and cost of avoidance follows the same trend of the total specific work requirement. The techno-economic results

for each of the hybrid carbon capture processes at 90% overall CO_2 recovery rate is shown in Figure 6.7.

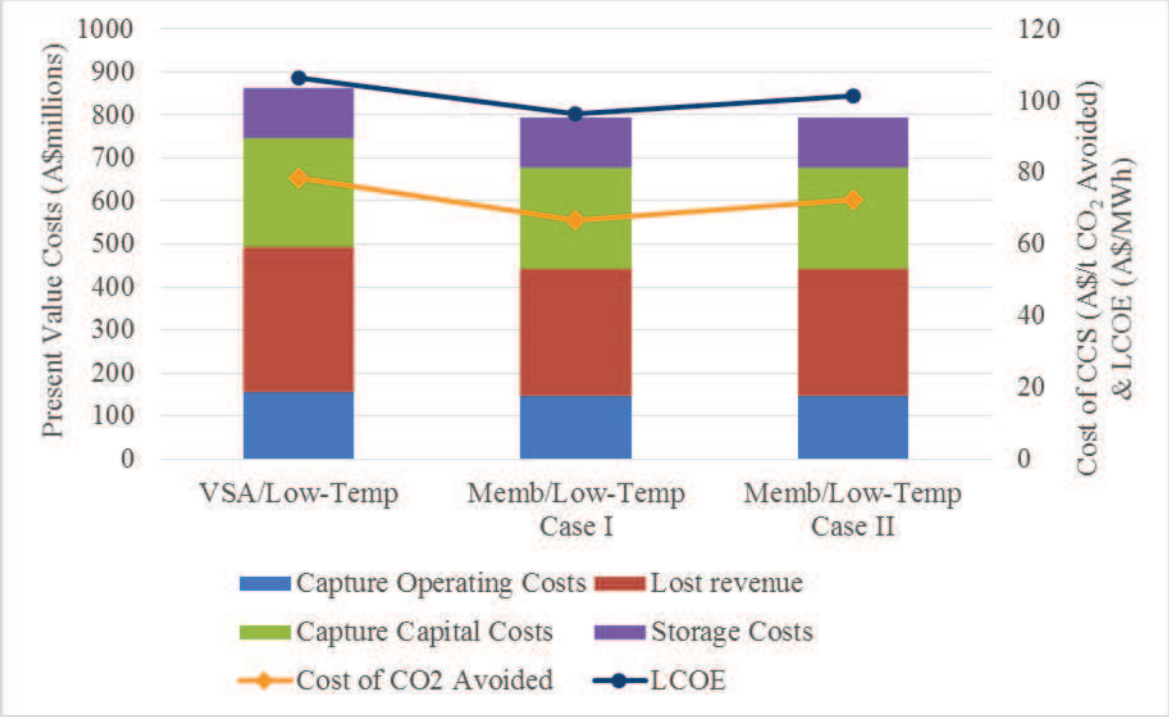

Figure 6.7 Comparison of techno-economic performance for three hybrid carbon capture processes at 90% overall CO_2 recovery rate.

At 90% overall recovery rate, the Case I membrane/low-temperature hybrid carbon capture system has the lowest LCOE of 96 A$/MWh, followed by Case II membrane/low-temperature hybrid carbon capture system (101 A$/MWh) and finally the VSA/low-temperature hybrid carbon capture system has the highest LCOE at 106 A$/MWh. However, even at 96 A$/MWh, this is an increase in cost of electricity of 56 A$/MWh, or more than double the current electricity price.

However, with an LCOE of 96 A$/MWh, the corresponding cost of CO_2 avoidance is 67 A$/t ($CO_2$ avoided), which is competitive with the MEA solvent absorption retrofitted cost of CO_2 avoidance in the literature. Xu et al. (2013) studied an MEA solvent absorption retrofitted to a supercritical power generation power plant and determined a cost of avoidance of 57 $/t ($CO_2$ avoided). Converting the U$ (2013) to the base case of A$(2011), the cost of avoidance from Xu et al. (2013) is approximately 74 A$/t ($CO_2$ avoided).

The economic performance of the hybrid processes follow the work requirement performance due to the heavy reliance of the hybrid process on the compressors. It can be seen from the results that for the three hybrid processes, around 85-95% of the capital costs are distributed in the compressors costs (vacuum pumps, refrigeration compressor train, pre-compression train and blowers). Hence, reducing the work requirement is paramount when aiming to reduce the cost of CCS for the hybrid carbon

capture processes. This is further shown in Figure 6.8, where a techno-economic analysis was performed on the improved membrane (Case IIS) used in the sensitivity analysis in section 5.2.4.

As discussed in section 5.2.4, the higher performing membrane (CO_2 Permeance = 1000 GPU and CO_2/N_2 Selectivity = 100) reduced the total work requirement and total specific work requirement of Case II membrane/low-temperature hybrid process. As it can be seen in Figure 6.8, this resulted in a reduction in LCOE (90 A$/MWh) with an overall recovery rate of 91.1%. On the other hand, improving the CO_2 Permeance to 2000 GPU increased the LCOE to 106 A$/MWh for an overall recovery rate of 91.2%. The increase in LCOE over the base case can be explained by the increase in overall CO_2 recovery rate from 89.2% to 91.2%.

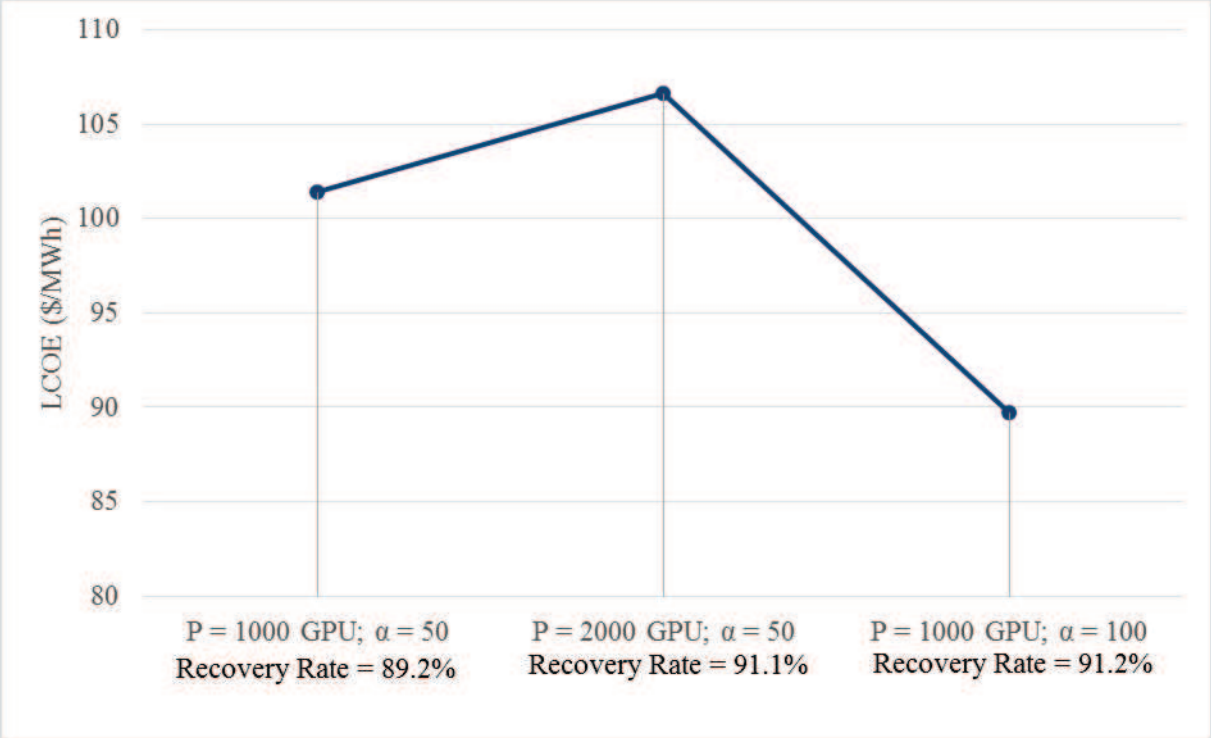

Figure 6.8 LCOE for three operating conditions for Case II (Propane Refrigerant) Membrane/Low-Temperature hybrid carbon capture systems using three different membranes.

7 Research Findings and Recommendations

According to the IPCC report (Metz 2005), the energy sector contributes to a large portion of the carbon emissions and a wide range of technologies need to be implemented to make the progression towards the low carbon dioxide emission; Carbon capture and storage is one of the technologies that needs to be employed (Stocker et al. 2013). CCS projects are being implemented globally on a large scale but more projects need to be initiated to meet the 2050 carbon emission target (Global CCS Institute 2014). One of the major challenge in increasing the rate of projects being initiated is the energetic and economic cost of implementing CCS in power stations. This research developed two hybrid carbon capture processes with the aim to reduce the energetic and economic cost of the current CCS processes.

The two hybrid processes that were developed are VSA/low-temperature separation hybrid carbon capture processes and membrane/low-temperature separation hybrid carbon capture processes. The processes were then evaluated using MOO and the energetic and economic performance were compared to the MEA solvent absorption carbon capture processes. Finally, the effect of potential improvement in membrane technology on the overall performance of the membrane/low-temperature hybrid carbon capture processes were also studied.

7.1 Research Findings

Both the VSA/low-temperature separation hybrid carbon capture process and membrane/low-temperature separation hybrid carbon capture processes show that they can achieve a high CO_2 recovery rate and high CO_2 purity required for carbon sequestration, while also performing well in terms of the energy consumption.

The MOO technique was used to obtain a range of overall CO_2 recovery rates and the matching minimum total shaft work required to operate the hybrid capture processes along with the corresponding operating decision variables. As expected, it was found that the minimum work requirement increased when the overall CO_2 recovery rate was increased, which results in a range of optimum operating conditions for the hybrid carbon capture processes.

In order to compare the hybrid carbon capture processes on the same baseline as other capture processes, the total shaft work required was converted to the total specific shaft work required and compared to an overall CO_2 recovery rate of 90%. The total specific shaft work required by the hybrid capture process (GJ_e/t (CO_2 captured)) was obtained by dividing the total shaft work required (MW_e) by the corresponding amount of CO_2 being recovered for capture (kg/s).

This resulted in an optimum specific shaft work of 1.46 GJ_e/t (CO_2 captured) when 90.0 % of the CO_2 is being recovered by the VSA/low-temperature hybrid process. Both Case I (mixed refrigerant) and

Case II (propane refrigerant) for the membrane/low-temperature hybrid processes considered have an optimum minimum specific work required of 1.38 GJ_e/t (CO_2 recovered) and 1.43 GJ_e/t (CO_2 recovered) with an overall CO_2 recovery rate of 89.2% and 89.8% respectively.

It is to be noted that a comparable established MEA solvent absorption separation system with a multi-stage compression system requires 4 GJ_{th}/t (CO_2 recovered), which converts to approximately 1.3 GJ_e/t (CO_2 recovered). Therefore, both hybrid processes provide a highly competitive option to the commercial MEA solvent absorption separation system on an energy requirement basis. Furthermore, as shown in Table 7.1 the hybrid carbon capture processes always perform better than the individual carbon capture processes in terms of the specific work required.

Table 7.1 Summary of specific work required results for hybrid processes compared with individual carbon capture processes at 90% CO_2 recovery rate.

Individual Carbon Capture Processes		
Carbon Capture Technology	**Units**	**Value**
MEA (Xu et al. 2013)	$GJ_e/t(CO_2$ Captured)	1.32
VSA (Liu et al. 2012)	$GJ_e/t(CO_2$ Captured)	2.37
Multi-Stage Membrane (Zhang, X, He & Gundersen 2013)	$GJ_e/t(CO_2$ Captured)	2.00
Hybrid Carbon Capture Processes		
VSA/Low-Temp	$GJ_e/t(CO_2$ Captured)	1.46
Memb/Low-Temp (Case I)	$GJ_e/t(CO_2$ Captured)	1.38
Memb/Low-Temp (Case II)	$GJ_e/t(CO_2$ Captured)	1.43

An overall exergy analysis of the VSA/low-temperature separation hybrid carbon capture system was also performed while optimising the process using MOO. This allowed different key decision variables to be varied to understand the effect that they have on the overall recovery rate and exergy loss rate. It was determined that the multi-stage compression and the VSA recovery rate had the biggest impact on the overall recovery rate. A minimum specific exergy loss of 1.6 GJ_e per tonne of CO_2 was found at a recovery rate of 95 % which is produced with a multi-stage compressor outlet pressure of 1700 kPa to 2500 kPa and with a VSA recovery rate of between 95% and 96%.

It was observed that the total specific shaft work had a linear relationship with the specific exergy loss rate. This is due to the fact that the compressors account for the majority of the exergy going into the system as well as the total shaft work. It is recommended that an exergy analysis should be performed on a solvent absorption capture process, where the exergetic requirement would come from both compressors and thermal energy, and the results could then be compared to this hybrid process.

A techno-economic analysis was also performed on the hybrid carbon capture processes operating at 85%, 90% and 95% overall CO_2 recovery rate operating an optimum conditions obtained from the

MOO. Table 7.2 represents the summary of results obtained for 90% overall recovery rate; Case I membrane/low-temperature hybrid carbon capture system had the lowest LCOE of 96 A$/MWh, followed by Case II membrane/low-temperature hybrid carbon capture system (101 A$/MWh) and finally the VSA/low-temperature hybrid carbon capture system had the highest LCOE at 106 A$/MWh. This results in doubling the price of electricity to implement CCS. However, it was found that the cost of CO_2 avoidance is still lower than the cost of CO_2 avoidance when implementing MEA solvent absorption. Finally, similar to energetic performance, the economic performance of the membrane/low-temperature hybrid process was significantly improved by improving the CO_2/N_2 Selectivity from 50 to 100 resulting in an LCOE of 90 A$/MWh and cost of CO_2 avoidance of 64 A$/t ($CO_2$ avoided).

Table 7.2 Summary of techno-economic results for hybrid processes compared with singular carbon capture processes at 90% CO_2 recovery rate.

	Cost of Avoidance ($/t($CO_2$ Avoided))
MEA (Xu et al. 2013)	74
VSA/Low-Temp	78
Memb/Low-Temp (Case I)	67
Memb/Low-Temp (Case II)	72

7.2 Concluding Remarks

Hybrid carbon capture processes using technologies such as VSA, membranes and low-temperature carbon separation have shown potential to be energetically and economically competitive with the established MEA solvent absorption. The main advantages of the VSA processes, membrane processes and low-temperature separation are that they require smaller equipment and simpler process operating conditions compared to solvent absorption. The choice of which of the two systems should be employed would probably be based on other factors, such as relative ease of operation or capital cost.

VSA and membranes are still relatively new technologies compared to solvent absorption. Therefore, the improvement in those technologies will be beneficial to the overall performance of the hybrid technologies as was demonstrated in the results obtained in this study.

Finally, the process integration methodology used to assess and optimise the hybrid carbon capture process demonstrated that hybrid carbon capture processes can operate over a wide range of parameters. With the increase in decision variables, this systematic approach combined with MOO allowed all the decision variables to be analysed individually and understand their effect on the overall process. Hence, this methodology is not restricted to the carbon capture and storage field as it

could also be used to assess and optimise other hybrid processes in other fields such as cryogenic distillation.

8 Bibliography

Aaron, D & Tsouris, C 2005, 'Separation of CO2 from flue gas: A review', *Separation Science and Technology*, vol. 40, no. 1-3, pp. 321-48.

Abbas, Z, Mezher, T & Abu-Zahra, MRM 2013, 'CO2 purification. Part I: Purification requirement review and the selection of impurities deep removal technologies', *International Journal of Greenhouse Gas Control*, vol. 16, no. 0, pp. 324-34.

Abu-Zahra, MRM, Niederer, JPM, Feron, PHM & Versteeg, GF 2007, 'CO2 capture from power plants: Part II. A parametric study of the economical performance based on mono-ethanolamine', *International Journal of Greenhouse Gas Control*, vol. 1, no. 2, pp. 135-42.

Alabdulkarem, A, Hwang, Y & Radermacher, R 2012, 'Development of CO2 liquefaction cycles for CO2 sequestration', *Applied Thermal Engineering*, vol. 33–34, no. 0, pp. 144-56.

Allinson, GW, Neal, PR, Ho, M, Wiley, D & McKee, GA 2006, 'CCS Economic Methodology Assumptions', in *CO2CRC Symposium 2006*.

AspenTech 2006, *Overview and Best Practices for Optimum Simulations*, 27/08/2015, Webinar, <http://sites.poli.usp.br/d/pqi2408/bestpracticesoptimumsimulationshysyspropertypackages.pdf>.

Belaissaoui, B, Le Moullec, Y, Willson, D & Favre, E 2012, 'Hybrid membrane cryogenic process for post-combustion CO2 capture', *Journal of Membrane Science*, vol. 415-416, pp. 424-34.

Belaissaoui, B, Willson, D & Favre, E 2012, 'Membrane gas separations and post-combustion carbon dioxide capture: Parametric sensitivity and process integration strategies', *Chemical Engineering Journal*, vol. 211–212, no. 0, pp. 122-32.

Bernardo, P, Drioli, E & Golemme, G 2009, 'Membrane Gas Separation: A Review/State of the Art', *Industrial & Engineering Chemistry Research*, vol. 48, no. 10, pp. 4638-63.

Berstad, D, Anantharaman, R & Nekså, P 2013, 'Low-temperature CO2 capture technologies – Applications and potential', *International Journal of Refrigeration*, vol. 36, no. 5, pp. 1403-16.

Bhutani, N, Ray, AK & Rangaiah, G 2006, 'Modeling, simulation, and multi-objective optimization of an industrial hydrocracking unit', *Industrial & Engineering Chemistry Research*, vol. 45, no. 4, pp. 1354-72.

Bhutani, N, Tarafder, A, Rangaiah, G & Ray, AK 2007, 'A multi-platform, multi-language environment for process modelling, simulation and optimisation', *International Journal of Computer Applications in Technology*, vol. 30, no. 3, pp. 197-214.

BOM, BoM 2015, *Monthly Climate Statistics*, viewed 18/06 2015, <http://www.bom.gov.au/jsp/ncc/cdio/cvg/av?p_stn_num=009034&p_prim_element_index=0&p_comp_element_index=0&redraw=null&p_display_type=full_statistics_table&normals_years=1981-2010&tablesizebutt=normal>.

Borel, L & Favrat, D 2010, *Thermodynamic and Energy Systems Analysis from Energy to Exergy*, CRC Press.

Deb, K, Agrawal, S, Pratap, A & Meyarivan, T 2000, 'A Fast Elitist Non-dominated Sorting Genetic Algorithm for Multi-objective Optimization: NSGA-II', in M Schoenauer, K Deb, G Rudolph, X Yao, E Lutton, J Merelo & H-P Schwefel (eds), *Parallel Problem Solving from Nature PPSN VI*, Springer Berlin Heidelberg, vol. 1917, pp. 849-58.

Evans, LJP & Siddique, QM 1975, 'CO2 removal studies and their application to sng plant conversions'.

Favre, E 2011, 'Membrane processes and postcombustion carbon dioxide capture: Challenges and prospects', *Chemical Engineering Journal*, vol. 171, no. 3, pp. 782-93.

Feng, X, Zhu, XX & Zheng, JP 1996, 'Practical exergy method for system analysis', in *Energy Conversion Engineering Conference*, Washington, DC, vol. 3, pp. 2068-71.

Global CCS Institute 2014, *The Global Status of CCS: 2014*, Melbourne, Australia.

GPSA, S 2004, 'Engineering data book', *Gas Processors Suppliers Association*, pp. 16-24.

Harkin, T, Hoadley, A & Hooper, B 2010, 'Reducing the energy penalty of CO2 capture and compression using pinch analysis', *Journal of Cleaner Production*, vol. 18, no. 9, pp. 857-66.

—— 2012, 'Using multi-objective optimisation in the design of CO2 capture systems for retrofit to coal power stations', *Energy*, vol. 41, no. 1, pp. 228-35.

Hatcher, P, Khalilpour, R & Abbas, A 2012, 'Optimisation of LNG mixed-refrigerant processes considering operation and design objectives', *Computers and Chemical Engineering*, vol. 41, no. 0, pp. 123-33.

Ho, MT, Allinson, GW & Wiley, DE 2008, 'Reducing the Cost of CO2 Capture from Flue Gases Using Membrane Technology', *Industrial & Engineering Chemistry Research*, vol. 47, no. 5, pp. 1562-8.

Horn, FL & Steinberg, M 1982, *Carbon dioxide power plant for total emission control and enhanced oil recovery*, Brookhaven National Laboratory, Upton, N.Y., <http://www.scopus.com/inward/record.url?eid=2-s2.0-0020264626&partnerID=40&md5=aee666e6a96ee0432c8f880220ae5397>.

Huisingh, D, Zhang, Z, Moore, JC, Qiao, Q & Li, Q 2015, 'Recent advances in carbon emissions reduction: policies, technologies, monitoring, assessment and modeling', *Journal of Cleaner Production*, vol. 103, pp. 1-12.

IEA 2012, *Energy Technology Perspective 2014*, IEA Publications, Paris, France.

International Institute of Refrigeration 2007, *International Dictionary of Refrigeration*, Peeters Publishers, Leuven.

Irlam, L 2015, *The Costs of CCS and Other Low-Carbon Technologies in the United States*, Global CCS Institution.

Klemeš, JJ 2013, *Handbook of Process Integration (PI): Minimisation of Energy and Water Use, Waste and Emissions*, Elsevier Science.

Le Moullec, Y & Kanniche, M 2011, 'Screening of flowsheet modifications for an efficient monoethanolamine (MEA) based post-combustion CO2 capture', *International Journal of Greenhouse Gas Control*, vol. 5, no. 4, pp. 727-40.

Leng, W, Abbas, A & Khalilpour, R 2010, 'Pinch analysis for integration of coal-fired power plants with carbon capture', in *20th European Symposium on Computer Aided Process Engineering-ESCAPE20*.

Leung, DYC, Caramanna, G & Maroto-Valer, MM 2014, 'An overview of current status of carbon dioxide capture and storage technologies', *Renewable and Sustainable Energy Reviews*, vol. 39, no. 0, pp. 426-43.

Li Yuen Fong, JC, Anderson, CJ & Hoadley, AF 2013, 'Optimisation of a Hybrid CO_2 Purification Process', paper presented to Chemeca 2013, Brisbane.

Li Yuen Fong, JC, Anderson, CJ, Hooper, B, Xiao, G, Webley, PA & Hoadley, AF 2014, 'Multi-Objective Optimisation of Hybrid CO2 Capture Processes using Exergy Analyis', in *Process Integration, Modelling and Optimisation for Energy Saving and Pollution Reduction*, Prague, CZ, vol. 39.

Linhoff, B & Senior, PR 1983, 'Energy targets clarify Scope for better heat integration', *Process Engineering (London)*, vol. 64, no. 3.

Liu, Z, Wang, L, Kong, X, Li, P, Yu, J & Rodrigues, AE 2012, 'Onsite CO2 Capture from Flue Gas by an Adsorption Process in a Coal-Fired Power Plant', *Industrial & Engineering Chemistry Research*, vol. 51, no. 21, pp. 7355-63.

Low, BT, Zhao, L, Merkel, TC, Weber, M & Stolten, D 2013, 'A parametric study of the impact of membrane materials and process operating conditions on carbon capture from humidified flue gas', *Journal of Membrane Science*, vol. 431, no. 0, pp. 139-55.

Luis, P, Van Gerven, T & Van der Bruggen, B 2012, 'Recent developments in membrane-based technologies for CO2 capture', *Progress in Energy and Combustion Science*, vol. 38, no. 3, pp. 419-48.

Merkel, TC, Lin, H, Wei, X & Baker, R 2010, 'Power plant post-combustion carbon dioxide capture: An opportunity for membranes', *Journal of Membrane Science*, vol. 359, no. 1–2, pp. 126-39.

Metz, B 2005, *IPCC Special Report on Carbon Dioxide Capture and Storage*, Cambridge University Press for the Intergovernmental Panel on Climate Change.

Peng, D-Y & Robinson, DB 1976, 'A new two-constant equation of state', *Industrial & Engineering Chemistry Fundamentals*, vol. 15, no. 1, pp. 59-64.

Peters, MS, Timmerhaus, KD & West, RE 2002, *Plant Design and Economics for Chemical Engineers*.

Rangaiah, GP 2009, *Multi-Ojective Optimization. Techniques and Applications in Chemical Engineering*, vol. 1, Advances in Process Systems Engineering, World Scientific Publishing Co. Pte. Ltd., Singapore.

Rochedo, PRR & Szklo, A 2013, 'Designing learning curves for carbon capture based on chemical absorption according to the minimum work of separation', *Applied Energy*, vol. 108, pp. 383-91.

Romeo, LM, Bolea, I, Lara, Y & Escosa, JM 2009, 'Optimization of intercooling compression in CO2 capture systems', *Applied Thermal Engineering*, vol. 29, no. 8–9, pp. 1744-51.

Rufford, TE, Smart, S, Watson, GCY, Graham, BF, Boxall, J, Diniz da Costa, JC & May, EF 2012, 'The removal of CO2 and N2 from natural gas: A review of conventional and emerging process technologies', *Journal of Petroleum Science and Engineering*, vol. 94–95, no. 0, pp. 123-54.

Sato, N 2004, 'Chapter 10 - Exergy', in *Chemical Energy and Exergy*, Elsevier Science B.V., Amsterdam, pp. 97-114.

Scholes, CA, Anderson, CJ, Cuthbertson, R, Stevens, GW & Kentish, SE 2013, 'Simulations of Membrane Gas Separation: Chemical Solvent Absorption Hybrid Plants for Pre- and Post-Combustion Carbon Capture', *Separation Science and Technology (Philadelphia)*, vol. 48, no. 13, pp. 1954-62.

Scholes, CA, Ho, MT, Wiley, DE, Stevens, GW & Kentish, SE 2013, 'Cost competitive membrane—cryogenic post-combustion carbon capture', *International Journal of Greenhouse Gas Control*, vol. 17, no. 0, pp. 341-8.

Shukri, T 2004, 'LNG technology selection', *Hydrocarbon Engineering*, vol. 9, no. 2, pp. 71-6.

Sircar, S 1979, *Separation of Multicomponent Gas Mixtures*, Air Products and Chemicals, Inc., Allentown, Pa, patent, 935435.

Smith, K, Ghosh, U, Khan, A, Simioni, M, Endo, K, Zhao, X, Kentish, S, Qader, A, Hooper, B & Stevens, G 2009, 'Recent developments in solvent absorption technologies at the CO2CRC in Australia', *Energy Procedia*, vol. 1, no. 1, pp. 1549-55.

Smith, R 2005a, 'Chemical process design and integration', in Hoboken, NJ : John Wiley & Sons, Hoboken, NJ, pp. 5-9.

—— 2005b, *Chemical process design and integration*, Hoboken, NJ : John Wiley & Sons, Hoboken, NJ.

Song, CF, Kitamura, Y & Li, SH 2012, 'Evaluation of Stirling cooler system for cryogenic CO2 capture', *Applied Energy*, vol. 98, pp. 491-501.

Spath, PL, Mann, MK & Kerr, DR 1999, *Life cycle assessment of coal-fired power production*, National Renewable Energy Lab., Golden, CO.

Sreenivasulu, B, Gayatri, DV, Sreedhar, I & Raghavan, KV 2015, 'A journey into the process and engineering aspects of carbon capture technologies', *Renewable and Sustainable Energy Reviews*, vol. 41, no. 0, pp. 1324-50.

Stocker, T, Qin, D, Plattner, G, Tignor, M, Allen, S, Boschung, J, Nauels, A, Xia, Y, Bex, V & Midgley, P 2013, *IPCC, 2013: Climate Change 2013: The Physical Science Basis. Contribution of Working Group I to the Fifth Assessment Report of the Intergovernmental Panel on Climate Change*, Cambridge: Cambridge University Press.

Tzanetis, KF, Martavaltzi, CS & Lemonidou, AA 2012, 'Comparative exergy analysis of sorption enhanced and conventional methane steam reforming', *International Journal of Hydrogen Energy*, vol. 37, no. 21, pp. 16308-20.

Wang, M, Joel, AS, Ramshaw, C, Eimer, D & Musa, NM 2015, 'Process intensification for post-combustion CO2 capture with chemical absorption: A critical review', *Applied Energy*, vol. 158, pp. 275-91.

Webley, PA 2014, 'Adsorption technology for CO2 separation and capture: a perspective', *Adsorption*, vol. 20, no. 2-3, pp. 225-31.

Xiao, G & Webley, P 2013, *VSA Zeolite 13X Experimental Results*.

Xiao, P, Zhang, J, Webley, P, Li, G, Singh, R & Todd, R 2008, 'Capture of CO2 from flue gas streams with zeolite 13X by vacuum-pressure swing adsorption', *Adsorption*, vol. 14, no. 4-5, pp. 575-82.

Xu, G, Yang, Y-p, Ding, J, Li, S, Liu, W & Zhang, K 2013, 'Analysis and optimization of CO2 capture in an existing coal-fired power plant in China', *Energy*, vol. 58, pp. 117-27.

Yin, G, Liu, Z, Liu, Q & Wu, W 2013, 'The role of different properties of activated carbon in CO2 adsorption', *Chemical Engineering Journal*, vol. 230, no. 0, pp. 133-40.

Zhang, J & Webley, PA 2008, 'Cycle development and design for CO2 capture from flue gas by vacuum swing adsorption', *Environmental Science & Technology*, vol. 42, no. 2, pp. 563-9.

Zhang, J, Webley, PA & Xiao, P 2008, 'Effect of process parameters on power requirements of vacuum swing adsorption technology for CO2 capture from flue gas', *Energy Conversion and Management*, vol. 49, no. 2, pp. 346-56.

Zhang, X, He, X & Gundersen, T 2013, 'Post-combustion carbon capture with a gas separation membrane: Parametric study, capture cost, and exergy analysis', *Energy and Fuels*, vol. 27, no. 8, pp. 4137-49.

Zhou, SJ, Meyer, H, Bikson, B & Ding, Y 2010, 'Hybrid membrane absorption process for post combustion CO 2 capture', in *AIECHE Spring Meeting and 6th Global Congress on Process Safety*, San Antonio, TX.

Appendix Table of Contents

List of Figures

List of Tables

A. Carbon Capture Processes Framework

Table A.0. Flue gas composition following pre-treatment

Feed Conditions	**Units**	**Value**
Vapour Fraction	-	1.00
Temperature	(°C)	38
Pressure	(kPa)	100
Molar Flow	(kmol/h)	10,922
Mass Flow	(kg/h)	405,818
Composition	**(mol frac)**	
CO_2	-	0.5716
N_2	-	0.4284

A.1 Vacuum Swing Adsorption (VSA) Process Simulation

The VSA equation used in the MOO simulation was derived from a set of simulation data obtained by using a simulation of Zeolite 13X on Aspen Adsorption® simulation (Xiao & Webley 2013). The VSA simulated was a 3-bed configuration is shown in Figure A.1 using the cycle organiser shown in Table A.1. The VSA vessel was divided into two layers: a 0.2m Sorbead layer to remove the water from the flue gas and 1m Zeolite 13X layer for the CO_2 capture.

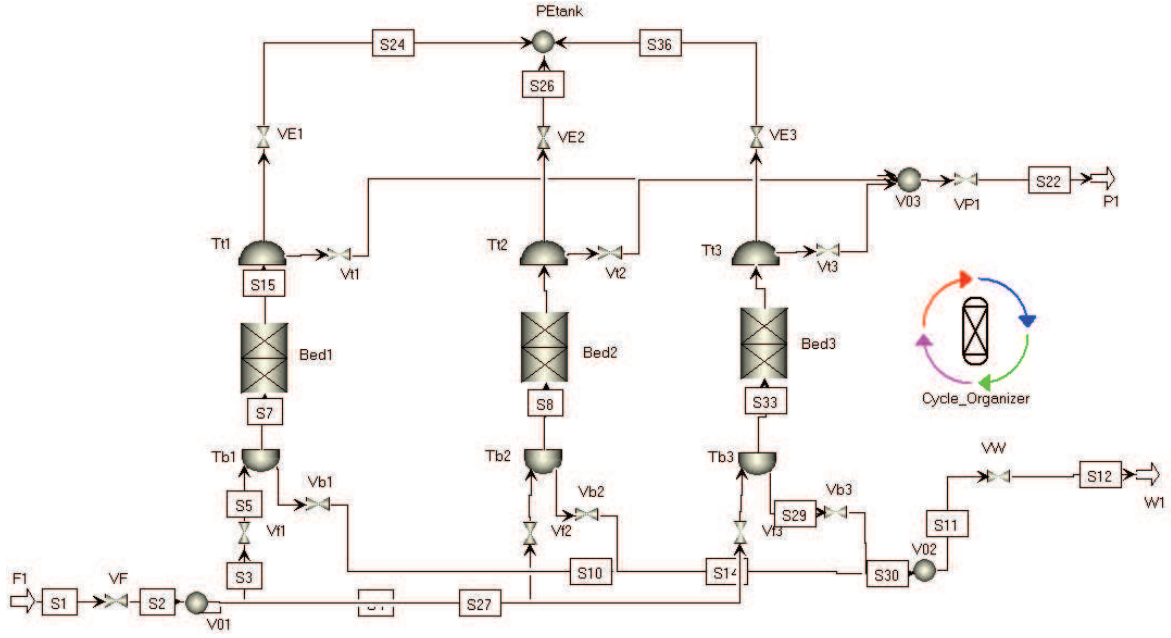

Figure A.1 Aspen Adsorption® simulation flowsheet & Adsorption bed configuration

Table A.1 Cycle organiser for three VSA columns: A, B and C. (RP – Re-pressurising; AD – Adsorption; PE↑ - Increase Pressure; PE↓ - Decrease pressurising; IDLE – Idle; EV – Stop Re-pressurisation)

	I	II	III	IV	V	VI	VII	VIII	IX

A	RP	AD	PE ↑	PE ↑	EV	EV	PE ↓	IDLE	PE ↓
B	PE ↓	IDLE	PE ↓	RP	AD	PE ↑	PE ↑	EV	EV
C	PE ↑	EV	EV	PE ↓	IDLE	PE ↓	RP	AD	PE ↑

The model involves three input process conditions being varied (waste stream CO_2 concentration, feed pressure and vacuum pressure) to determine the performance of the VSA according to three output variables: product stream CO_2 concentration, VSA CO_2 recovery rate and the vacuum specific power required. There were 27 different data points obtained; a sample of the data is shown in Table A.2.

Table A.2. VSA Aspen Adsim® simulation sample data points.

VSA Feed Pressure (kPa)	Vacuum Pressure (kPa)	Waste CO_2 conc. (wet)	Product CO_2 conc. (dry)	CO_2 Recovery Rate (%)	Vacuum Specific power (MJ/kg CO_2)	Productivity (mole CO_2/hr/kg ads)	Productivity (kg CO_2/hr/kg ads)
110	5	0.68%	54.53%	98.64%	0.787	2.84	0.125
	10	0.76%	33.92%	96.12%	0.789	3.05	0.134
	20	0.98%	24.52%	96.25%	0.856	3.37	0.148

The total specific power required for the VSA process was determined in two steps:

1) Calculate the blower specific power required to increase the pressure of the flue gas to the required VSA inlet pressure.
2) Add the blower specific power to the vacuum specific power to obtain the total specific power.

An equation representing the total specific power required as function of the product stream CO_2 concentration and CO_2 recovery rate was obtained. This was achieved by selecting 6-10 data points that gave the best total specific power, while having a high product stream CO_2 concentration or CO_2 recovery rate and fitting a 3D surface curve to the points. This method discards the values that have sub-par operating conditions to generate an equation for the best operating conditions of the VSA. In order to fit the 3D surface curve, the *Curve Fitting* application on MATLAB® software was used. This application allows the user to choose the polynomial order for each parameter (x and y), determines the r-square value and also provides the coefficients to the equation.

Three cases with three set of data points were used to determine the VSA performance equation:

Case 1:

Number of data points: 6

Polynomial order: $f(x^2, y^1)$

Initially, six data points, as shown in Table A.3 were used to determine the performance of the VSA over a small range of CO_2 recovery rate (x) and product CO_2 concentration (y). Those initial points were chosen since it had high recovery rate and low specific power requirement.

Table A.3 Case 1 six data points used to determine the performance of VSA.

Product CO2 Conc. (%)	CO2 Recovered (%)	Vacuum + Blower Specific Power (GJ/t CO2)
49.21	98.27	0.874
62.96	91.48	0.719
64.50	90.21	0.708
65.93	88.75	0.695
61.34	96.22	0.826
51.06	92.56	0.699

Two polynomial orders were possible with six data points: $f(x^2, y^1)$ and $f(x^1, y^2)$. The polynomial order with the highest r-square value was chosen; in this case it was $f(x^2, y^1)$. The plots of the curve fitting results are shown in Figure A.2 and Figure A.3 and the equation obtained is:

$$f(x,y) = 6.61 - 0.175x + 0.0374y + 0.00118x^2 - 0.000366xy \qquad \textbf{Eq. A.1}$$

Where f is the total specific power required for the VSA

x is the CO_2 recovery rate and

y is the product CO_2 concentration.

As it can be seen from Figure A.2 and Figure A.3(b), the total specific shaft work increases with increasing product CO_2 concentration and increasing CO_2 recovery rate. The residual errors are also negligible, which corresponds to the high r-square value of 0.999. Therefore, this shows that equation A.1 can be used to accurately simulate the specific power requirement of the VSA within that product CO_2 concentration and CO_2 recovery rate range.

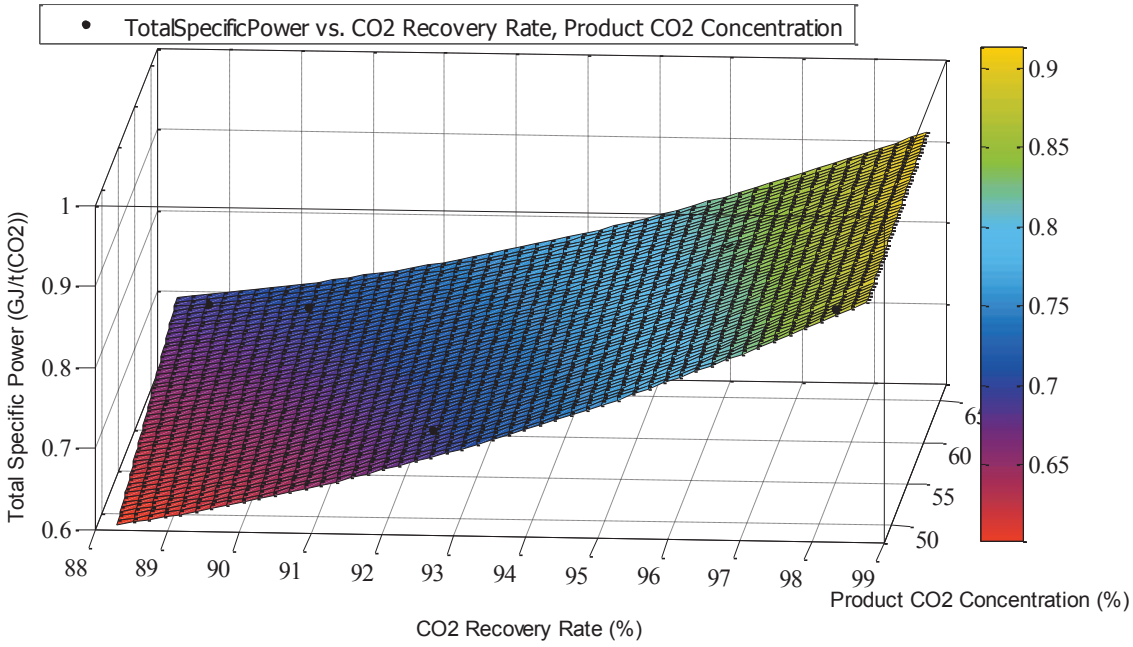

Figure A.2. Plot of 3-D Surface curve fitting of total specific work required (GJ/t(CO_2)) vs product CO_2 concentration (%) vs CO_2 recovery rate (%) for Case 1 (6 data points) using MATLAB® software with polynomial order x^2 & y^1.

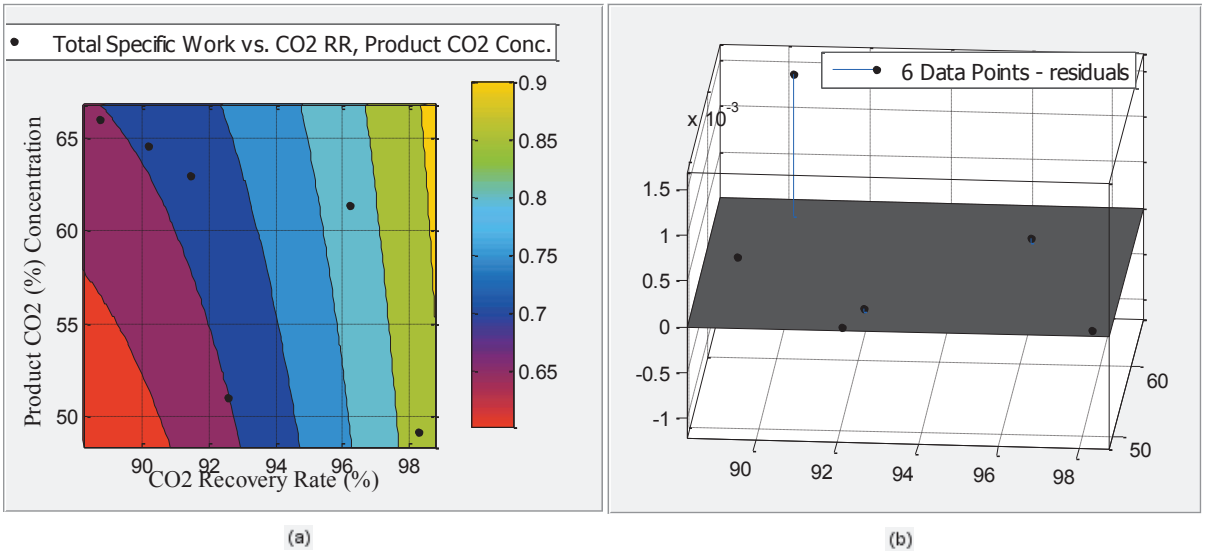

Figure A.3. (a) Contour plot of total specific work required (GJ/t(CO_2)) as a function of product CO_2 concentration (%) and CO_2 recovery rate (%) for Case 1 (6 data points) using MATLAB® software with polynomial order x^2 & y^1. (b) Residual error plot of the total specific work required (GJ/t(CO_2)) with polynomial order x^2 & y^1 and the Aspen Adsim® data for Case 1 (6 data points) using MATLAB® software.

Case 2:

Number of data points: 8

Polynomial order: f(x^2, y^2) and f(x^3, y^1)

In order to increase the range of the equation, two more points were added to the 6 points from case 1, as shown in Table A.4. Since the number of points was increased for case 2, a higher polynomial order of $f(x^3, y^1)$ or $f(x^2, y^2)$ could be used. However, as it can be seen from Figure A.4 and Figure A.5, both polynomials provided an unexpected surface plot as the total specific work would decrease with increasing product CO_2 concentration. This relationship would not be accurate for a VSA process as increasing the product CO_2 concentration would require an increase in power requirement. This inaccuracy can be due to two main reasons: there are not enough data points over the increased range of x and y to predict the correct function or one or two experimental data points that was added were outliers. Hence, more data points were added in **case 3** to improve the function.

Table A.4 Case 2 eight data points used to determine the performance of VSA.

Product CO2 Conc. (%)	CO2 Recovered (%)	Vacuum + Blower Specific Power (GJ/t CO2)
49.21	98.27	0.874
62.96	91.48	0.719
64.50	90.21	0.708
65.93	88.75	0.695
61.34	96.22	0.826
51.06	92.56	0.699
73.60	81.59	0.666
79.55	64.26	0.623

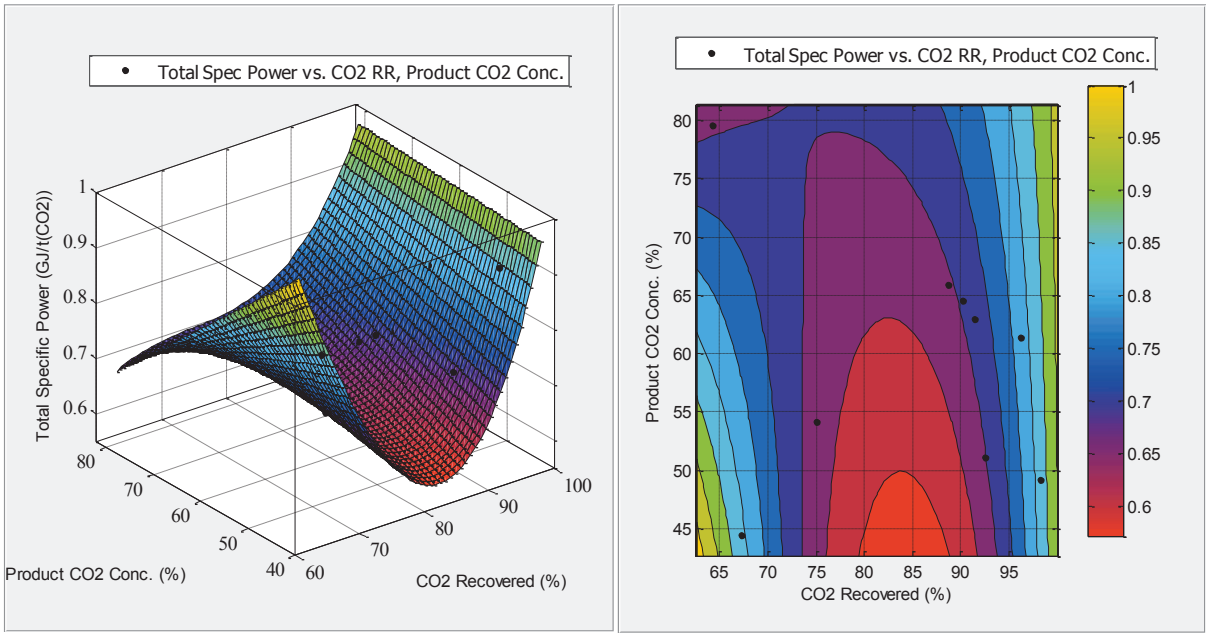

Figure A.4. Case 2 (8 data points) using MATLAB® software with polynomial order x^3 & y^1 (a) Plot of 3-D Surface curve fitting of total specific work required ($GJ/t(CO_2)$) vs product CO_2 concentration (%) vs CO_2 recovery rate (%). (b) Contour plot of total specific work required ($GJ/t(CO_2)$) as a function of product CO_2 concentration (%) and CO_2 recovery rate (%).

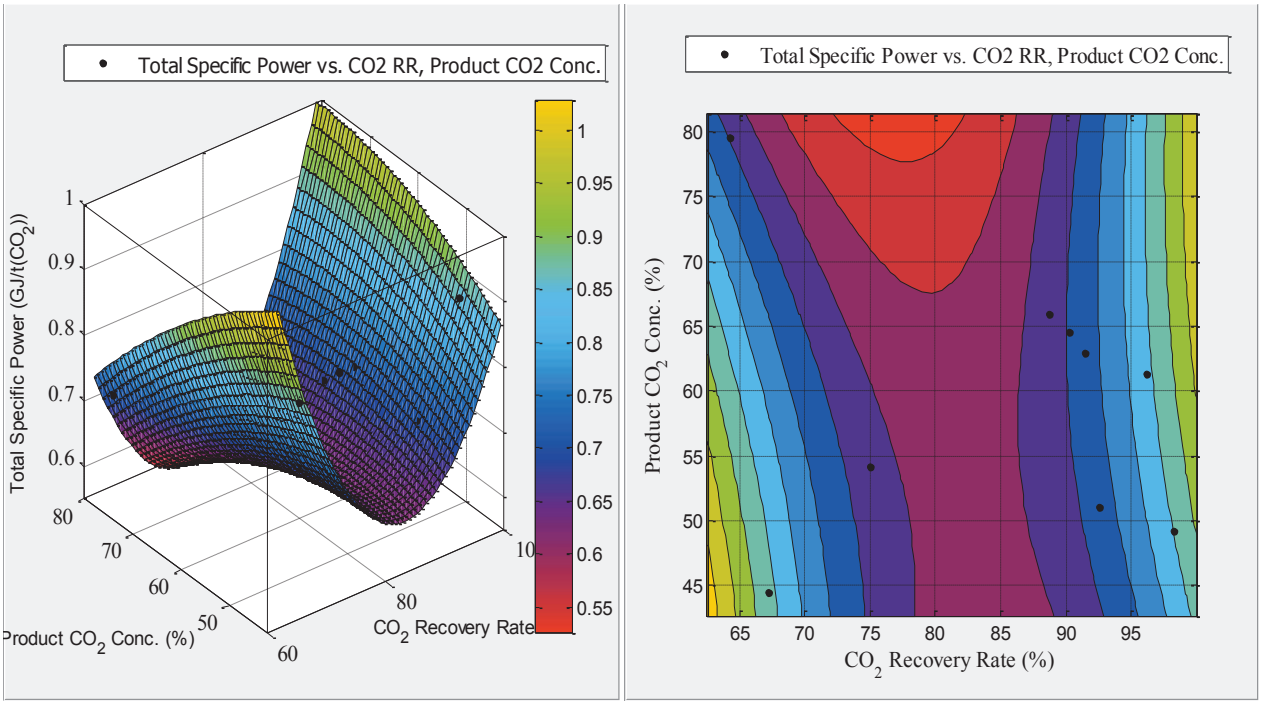

Figure A.5. Case 2 (8 data points) using MATLAB® software with polynomial order x^2 & y^2 (a) Plot of 3-D Surface curve fitting of total specific work required (GJ/t(CO_2)) vs product CO_2 concentration (%) vs CO_2 recovery rate (%). (b) Contour plot of total specific work required (GJ/t(CO_2)) as a function of product CO_2 concentration (%) and CO_2 recovery rate (%).

Case 3:

Number of data points: 10

Polynomial order: $f(x^2, y^2)$ and $f(x^3, y^1)$

In order to increase the range of the equation, two more points were added to the 6 points from case 1, as shown in Table A.5**.**

Table A.5 Case 3 ten data points used to determine the performance of VSA.

Product CO2 Conc. (%)	CO2 Recovered (%)	Vacuum + Blower Specific Power (GJ/t CO2)
49.21	98.27	0.874
62.96	91.48	0.719
64.50	90.21	0.708
65.93	88.75	0.695
61.34	96.22	0.826
51.06	92.56	0.699
44.42	67.25	0.862
88.87	67.22	0.957
54.14	75.06	0.678
34.88	75.77	0.639

Similar to case 2, higher number of points allowed a high polynomial order of $f(x^3, y^1)$ or $f(x^2, y^2)$ to be used. It should be noted that while a higher polynomial order of $f(x^3, y^2)$ could be used, higher polynomial order increase the complexity of the equation, which increases the computational time when doing the simulation in Aspen HYSYS®. Furthermore, $f(x^3, y^2)$ polynomial order produced a steep curve and had very small coefficients (approximately 10^{-6}), which indicates that this polynomial order is not adequate for the VSA equation.

Figure A.6 and Figure A.7 shows the results for the $f(x^2, y^2)$ polynomial fit and the equation obtained is:

$$\boldsymbol{f(x,y) = 8.25 - 0.183x - 0.00443y + 0.00109x^2 + 0.0000472xy + 0.0000254y^2} \quad \textbf{Eq. A.2}$$

Where f is the total specific power required for the VSA

x is the CO_2 recovery rate and

y is the product CO_2 concentration.

Figure A.8 and Figure A.9Figure A.7 shows the results for the $f(x^3, y^1)$ polynomial fit and the equation obtained is:

$$\boldsymbol{f(x,y) = 6.407 - 0.116x - 0.00600y + 0.000231x^2 - 0.000187xy + 3.68 \times 10^{-6}x^3 - 9.90 \times 10^{-7}x^2y} \quad \textbf{Eq. A.3}$$

Where f is the total specific power required for the VSA

x is the CO_2 recovery rate and

y is the product CO_2 concentration.

Both polynomial orders provide a good representation of a VSA process, with total specific work increasing with increasing product CO_2 concentration, while the CO_2 recovery rate has an optimum minimum. However, $f(x^3, y^1)$ has very low co-efficient, which confirms that the higher order x^3 is not necessary. Therefore, $f(x^2, y^2)$ is the preferred equation for any further VSA process simulations.

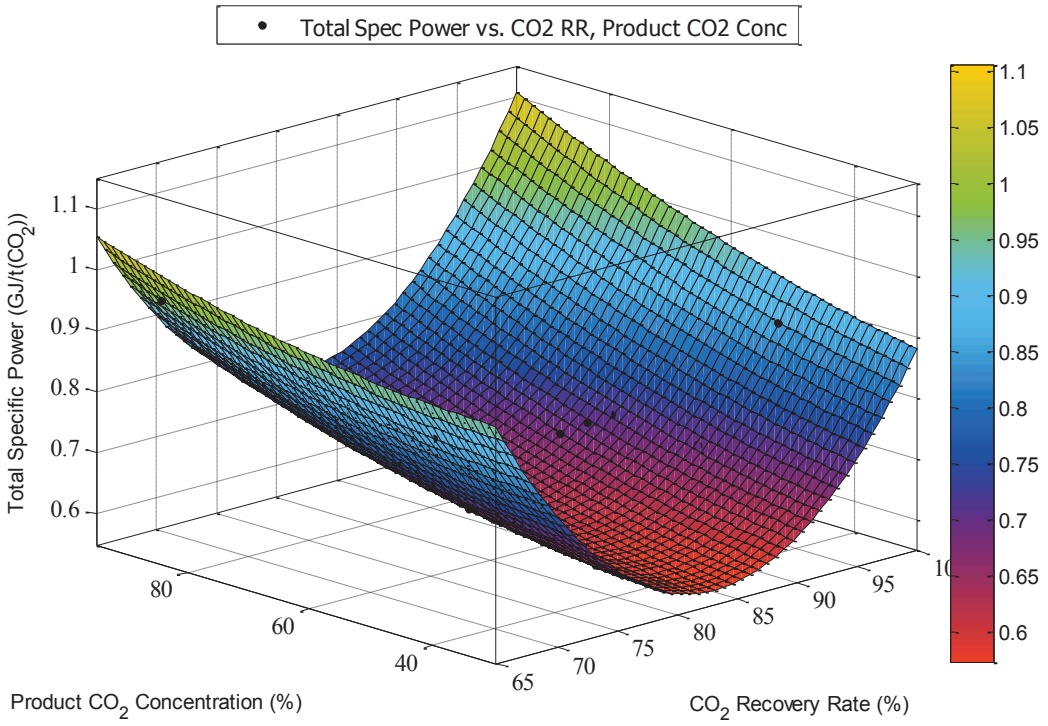

Figure A.6 Case 3 (10 data points) using MATLAB® software with polynomial order x^2 & y^2 plot of 3-D Surface curve fitting of total specific work required (GJ/t(CO_2)) vs product CO_2 concentration (%) vs CO_2 recovery rate (%).

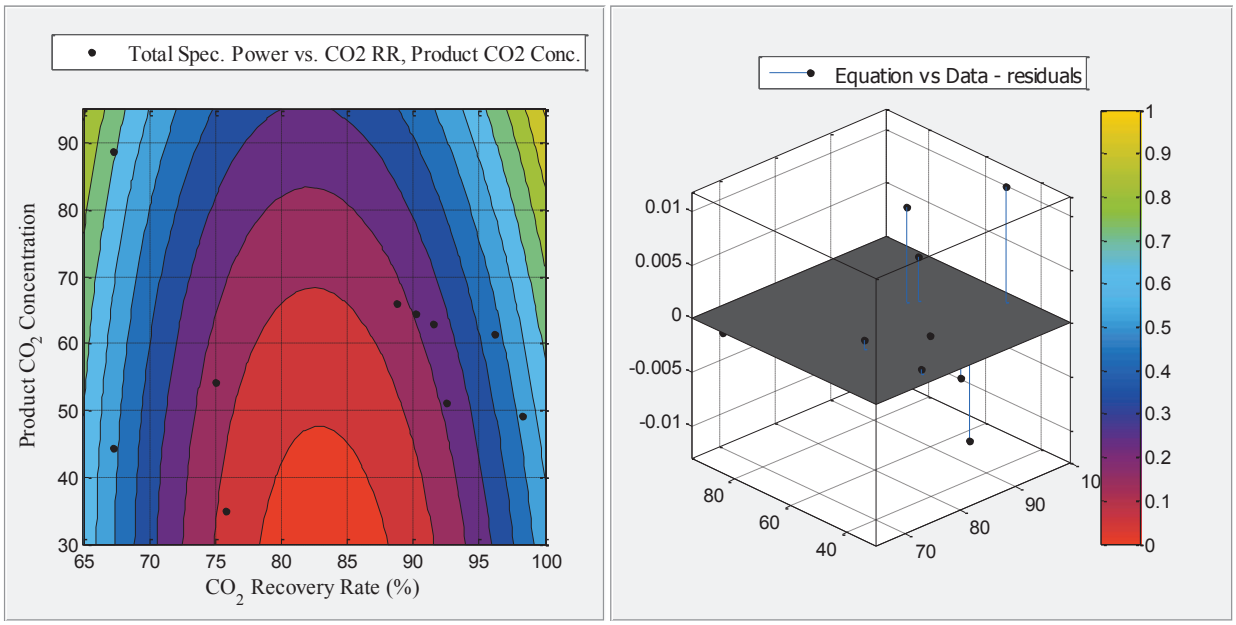

Figure A.7 Case 3 (10 data points) using MATLAB® software with polynomial order x^2 & y^2(a) Contour plot of total specific work required (GJ/t(CO_2)) as a function of product CO_2 concentration (%) and CO_2 recovery rate (%). (b) Residual error plot of the total specific work required (GJ/t(CO_2)).

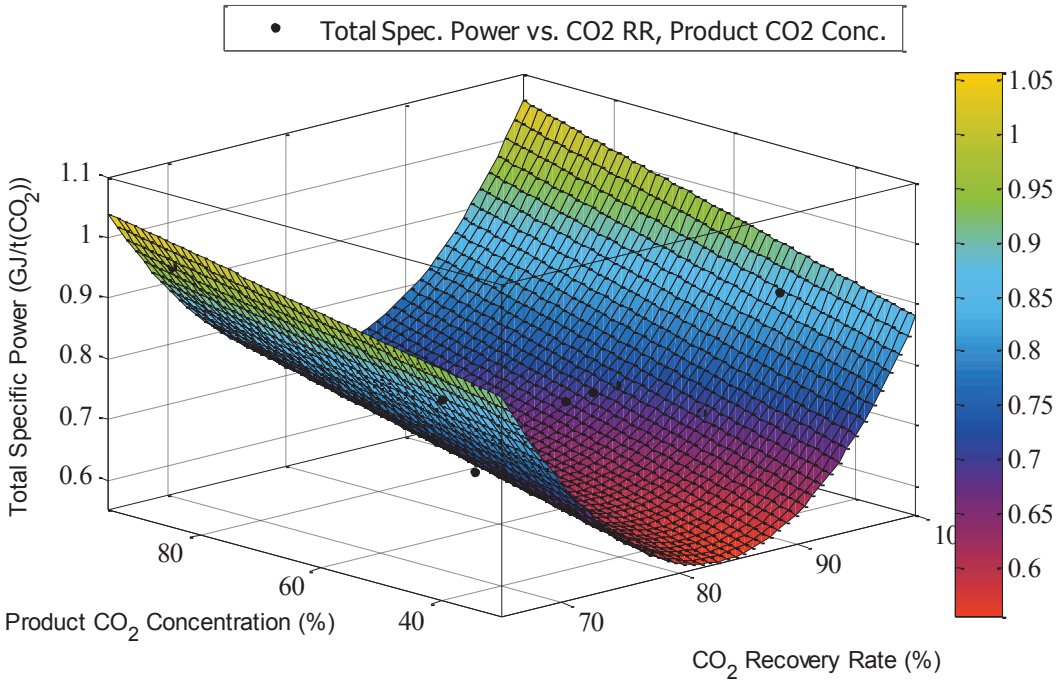

Figure A.8 Case 3 (10 data points) using MATLAB® software with polynomial order x^3 & y^1 plot of 3-D Surface curve fitting of total specific work required (GJ/t(CO_2)) vs product CO_2 concentration (%) vs CO_2 recovery rate (%).

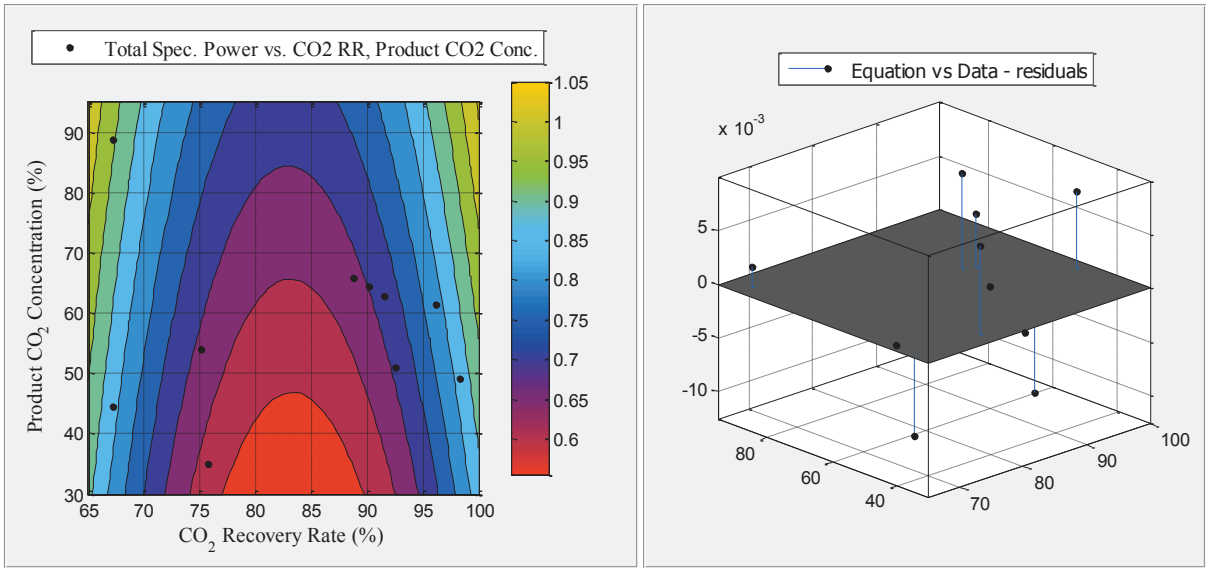

Figure A.9 Case 3 (10 data points) using MATLAB® software with polynomial order x^3 & y^1 (a) Contour plot of total specific work required (GJ/t(CO_2)) as a function of product CO_2 concentration (%) and CO_2 recovery rate (%). (b) Residual error plot of the total specific work required (GJ/t(CO_2)).

A.2 Membrane Process Simulation

Membrane processes throughout this thesis was simulated on Aspen HYSYS® using a membrane module provided by Cuthbertson, Scholes and Kentish (2010). This membrane module was created using Microsoft Visual Basic® to simulate the performance of a membrane in Aspen HYSYS® as well as provide an interface for the user to insert the different design parameters and choose one of the four flow regimes for the membrane process: fully mixed, cross-flow, co-current flow and counter-current flow. The process flow chart and the equations used to simulate each flow regimes is shown in Figure A.11.

Cuthbertson, Scholes and Kentish (2010) compared their model to the literature (Coker, Freeman & Fleming 1998). The results are shown in Figure A.10 and show that the mode values matches the literature values.

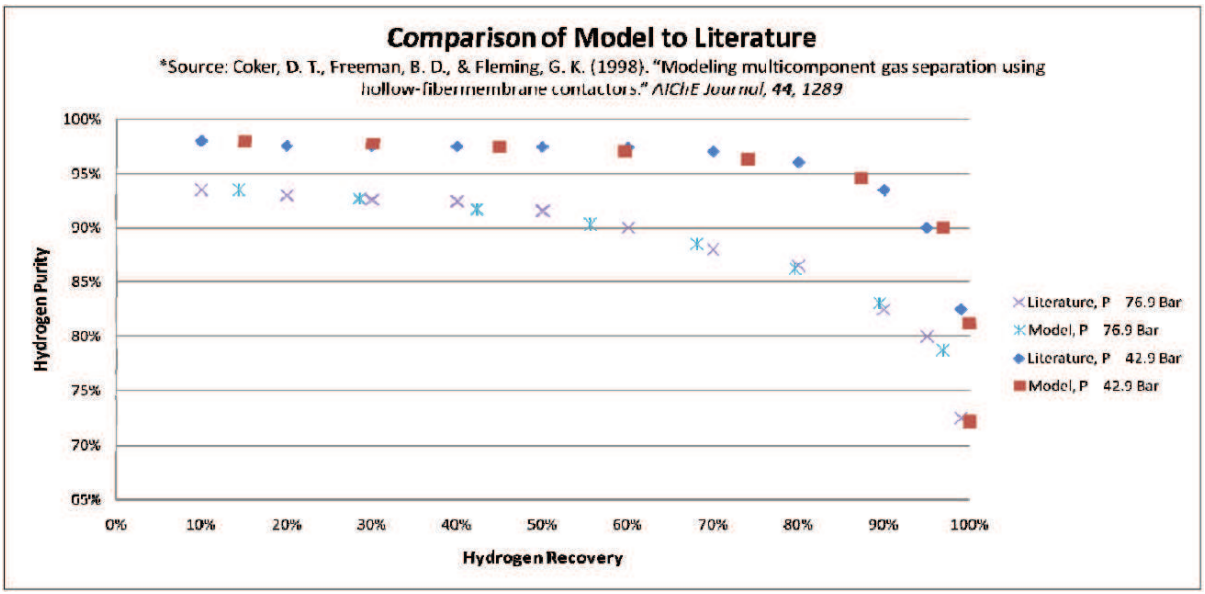

Figure A.10 Graph representing the comparison of Aspen HYSYS® Membrane model vs literature (Cuthbertson, Scholes & Kentish 2010).

Using the membrane model on Aspen HYSYS®, the membrane structural optimisation was performed using MOO using different feed conditions to optimise two objective variables:

i. Maximise CO_2 outlet purity coming out from the membrane system
ii. Minimise the total specific shaft work required from the membrane system.

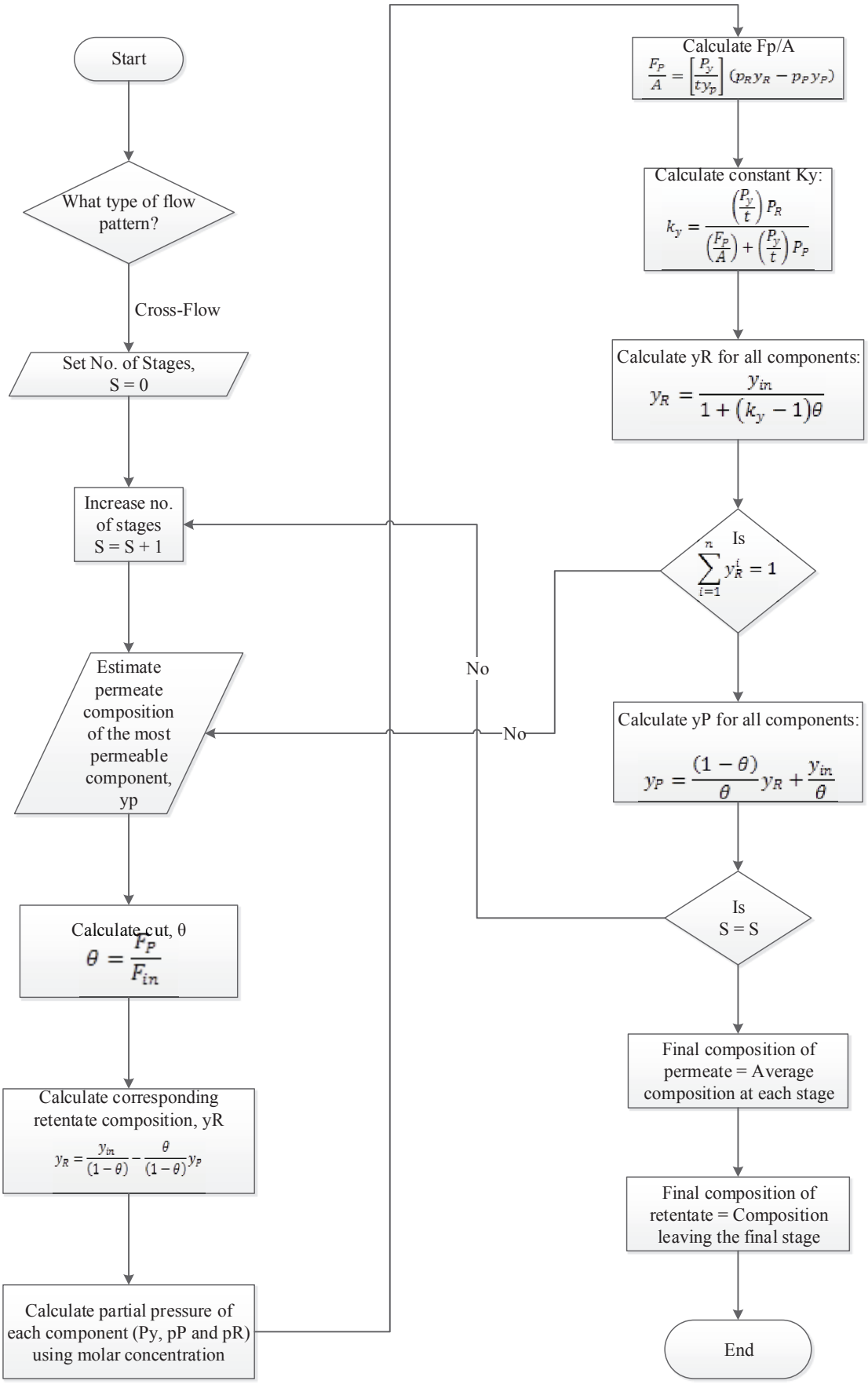

Figure A.11 Process Flow Chart for Membrane Module in Aspen HYSYS®

CO_2 outlet purity and CO_2 recovery rate are the two main parameters that govern the performance of the membrane unit. Therefore, those two parameters needed to be incorporated in the objective variables. The CO_2 outlet purity was selected as the first objective variable and the CO_2 recovered was incorporated in the second objective variable: total specific shaft work, which is the ratio of the total shaft work required by the same to the mass flow rate of the CO_2 recovered. Hence, this allowed the membrane unit to be optimised through the two main parameters and the amount of work required.

Four membrane structures were considered for the membrane process are as follows:

i. Single-stage membrane
ii. Two-stage membrane with the second membrane on the permeate side
iii. Two-stage membrane with the second membrane on the retentate side
iv. Two-stage membrane with an additional two membranes on the permeate side and retentate side of the first membrane respectively with one recycle stream on the permeate side

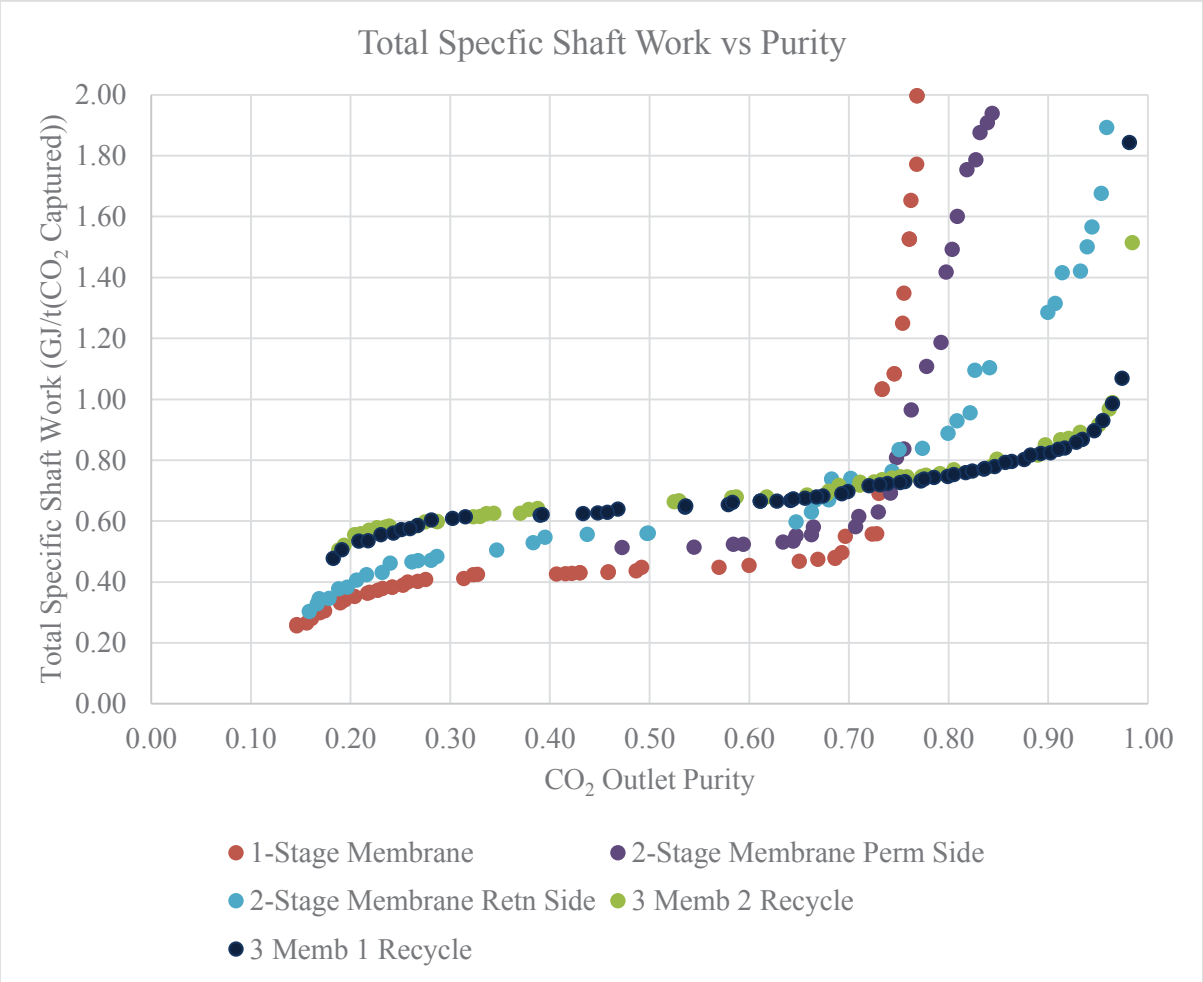

Figure A.12 Pareto Front of membrane structure MOO.

As it can be seen in the Pareto Optimal Front obtained for the membrane structural optimisation in Figure A.12, at CO_2 purity below 75%, the one stage membrane has the best performance and at higher CO_2 outlet purity, the two-stage membrane with an additional two membranes on the permeate side and retentate side of the first membrane respectively with one recycle stream on the permeate side has the best Pareto Front.

Therefore, if only the optimum operating conditions from both of those processes were selected, the optimum Pareto Front would be as shown in Figure A.13

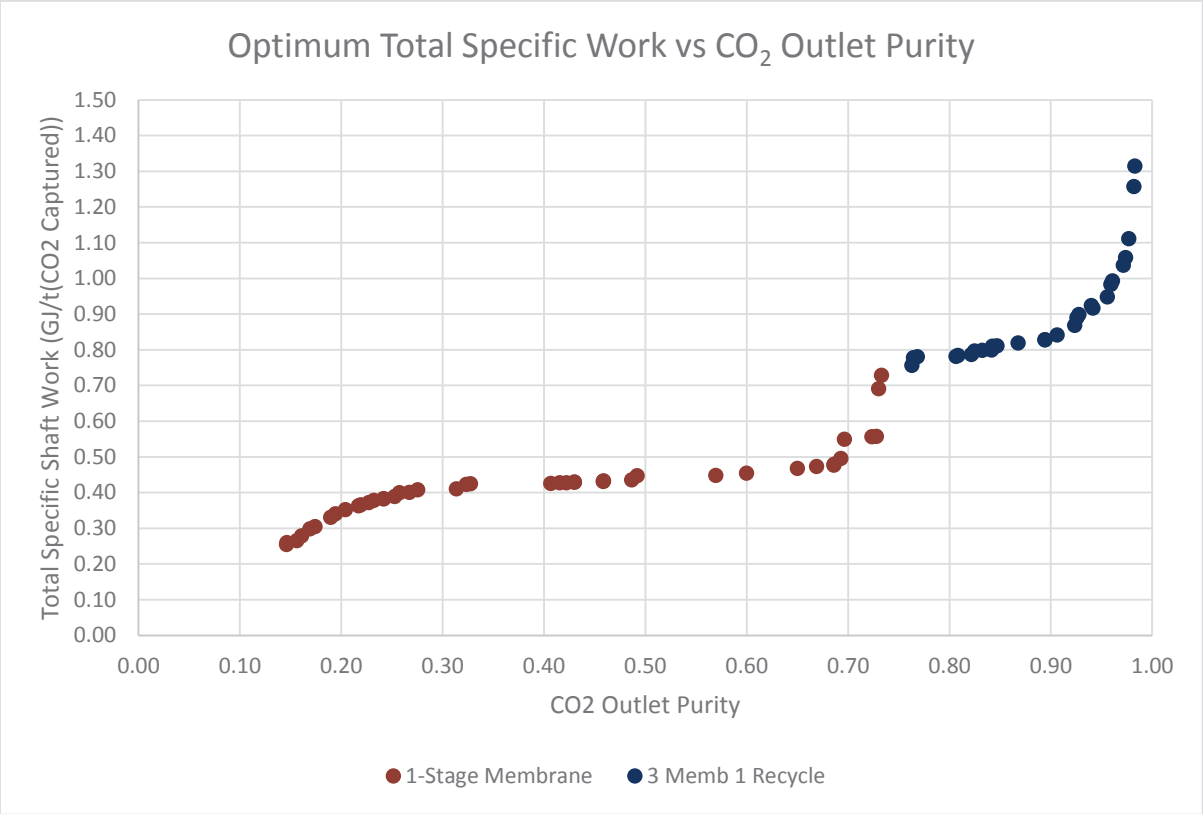

Figure A.13 Optimum Pareto Front of membrane structure MOO.

A.3 Low-Temperature Separation Process Simulations

The final hybrid carbon capture processes in the thesis used mixed ethane/propane refrigerant and propane only refrigerant for the liquefaction and compression of CO_2. The comparison of the performance of liquefaction and compression versus the conventional multi-stage compression was also studied.

Multi-stage compression has been the most common method to compress CO_2 for sequestration. Therefore, they have been extensively studied in the literature, where different models were developed to simulate the process using different software (Pfaff, Oexmann & Kather 2010; Sanpasertparnich et al. 2010; Amrollahi, Ertesvåg & Bolland 2011). In particular, Amrollahi, Ertesvåg and Bolland (2011) used UNISIM software (2008) to model a CO_2 compression cycle and determined the exergetic efficiency of the multi-stage compressors.

In this research case, the configuration of the multi-stage compression can be seen in Figure A.14. The stream is assumed to be the exhaust stream of a post-combustion process which has been purified using a separation process. The stream has a CO_2 molar fraction of 0.80 and enters the compression unit at 1 bar, 38°C. The stream is then compressed to 110 bar in four compressor stages (isentropic efficiency of 80%) with inter-cooling using cooling water. The cooling water is at 25°C and the heat exchangers have a ΔT of 5°C.

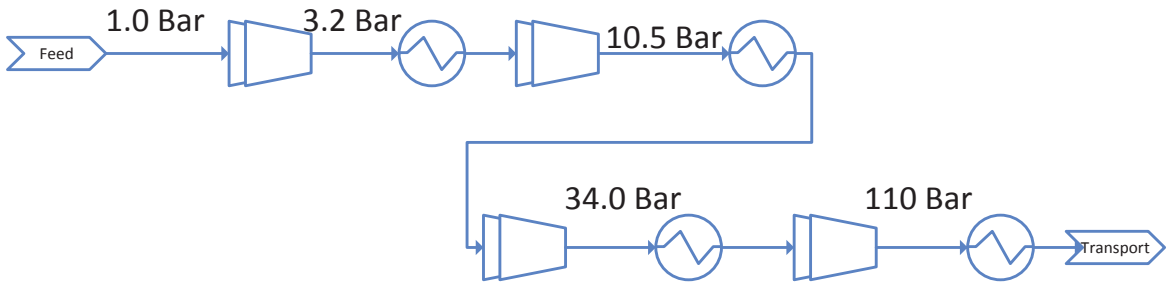

Figure A.14 Schematic diagram of conventional CO_2 multi-stage compression.

CO_2 liquefaction process is less common due to the simplicity of the multi-stage compression process. However, the liquefaction process provides more degrees of freedom such as varying the pressure at which the CO_2 is liquefied and the minimum temperature of the refrigeration system. (Aspelund, Mølnvik & De Koeijer 2006) and Moore and Nored (2008) studied CO_2 liquefaction for ship transport where they varied the liquefaction pressures and cooling system.

In this research, the inlet stream was compressed to 24 bars before being cooled down to around to -40°C, depending on the refrigeration system used. Some additional cooling was achieved by expanding the non-liquefied gas stream. The CO_2 liquid is then pumped to above its critical pressure

to 110 bar and then reheated through heat integration with other process streams as can be seen in Figure A.15.

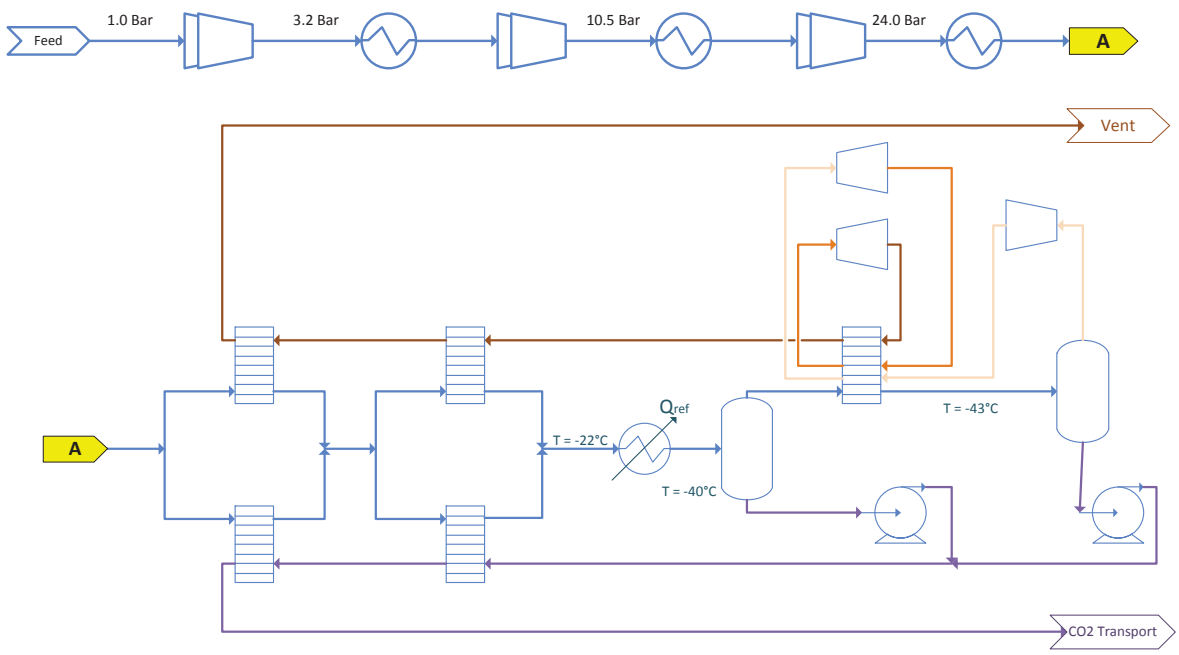

Figure A.15 CO_2 Liquefaction process schematic diagram for propane refrigeration system

In this process, there are two main parameters that determine the purity of CO_2 in the transport stream: the compression pressure and the lowest temperature reached through the refrigeration system. Since the pressure was set to 24 bars, the refrigeration temperature determines the amount CO_2 that is transported for sequestration.

Therefore, the refrigeration system is a major source of work input due to the low temperatures required to liquefy the CO_2. There were three types of refrigeration system in this case: propane refrigeration system, propene refrigeration system and a binary mixed refrigerant propane and ethane refrigeration system. The refrigeration heat exchangers were assumed to have ΔT of 2°C to optimise the CO_2 of the recovery of the process. (The Aspen HYSYS® simulations process flow diagram (PFD) can be found in the Appendix)

- Propane Refrigeration System

Propane refrigerant is commonly used in the natural gas industry to meet the chilling duty required to separate out LPG and as an intermediate refrigerant in LNG processes. A standard propane cascade refrigeration cycle cools the process stream to -40°C followed by residue gas expanders to reduce temperature to -43°C, which is yields a recovery of 84.8% of CO_2 in the feed stream.

There are various configuration of propane refrigeration system available and the three variations of the refrigeration cycles considered in this case were: three-stage refrigeration cycle, four-stage refrigeration cycle and four-stage refrigeration cycle with sub-cooling.

- Propene Refrigeration System

In order to increase the percentage recovery of the CO_2, propene refrigerant was chosen due to its similar attributes to propane. Propene allows the process stream to be chilled to -45°C followed by expanders which reduce the temperature to -48°C and this allowed the recovery to be increased to 87.1%. However, in order to achieve this lower liquefaction temperature, propene needs to be compressed to higher pressures before it is condensed, which increases the compression duty in the refrigeration cycle. Similar configurations to propane refrigeration system were used in this case.

- Mixed Refrigeration System

The mixed refrigerants refrigeration systems are also used in the LNG process industry (Hatcher, Khalilpour & Abbas 2012). In a mixed refrigerant process, the process stream is cooled in stages, where the refrigerant is separated from its liquid and gaseous phases after each stage. The liquid refrigerant is then cooled and flashed across a valve using the Joule-Thompson effect, causing a temperature drop. (Shukri 2004; Hatcher, Khalilpour & Abbas 2012)

In this case study, it was found that 50 mole % of propane and 50 mole % of ethane provided the optimum performance. The lowest temperature reached in the process stream was -45°C (without the need for chilling using the expanders) with a recovery of 84.9%.

The first set of results is the comparison of the propane refrigeration system against the propene refrigeration system. For the propane refrigeration system, both a 3 stage refrigeration system and a 4 stage refrigeration system were studied and similarly for the propene refrigeration system. The minimum work required and the exergy loss rate was calculated and can be seen in Figure A.16. The two refrigeration systems are observed to have very similar results and the two propene refrigeration systems vary significantly in terms of minimum work required. The 3 stage propene refrigeration system has the highest minimum work required, but the 4 stage propene refrigeration system has the lowest minimum work required. Since, the propene refrigeration systems have the lowest exergy lost rate, it was then decided that the 4 stage refrigeration system would be used in the future optimisation of pure refrigeration systems. Therefore, the four stage propene system was further optimised by including sub-cooling in the refrigeration system by making better use of cold stream available in the process.

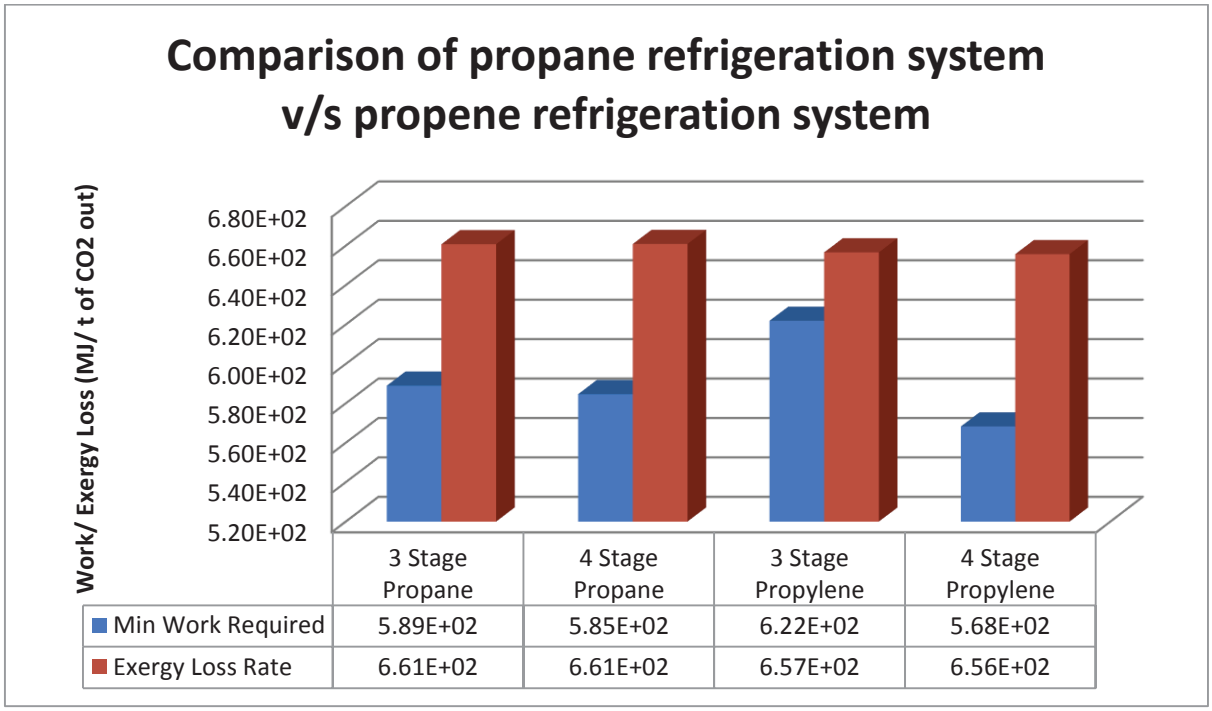

Figure A.16 Comparison of propane refrigeration system v/s propene refrigeration system

This optimised propene refrigeration system with sub-cooling was then compared to the mixed refrigerant case, for liquefaction of CO_2 and the standard four-stage compression of CO_2 and the results can be seen in Figure A.17.

It can be seen that multi-stage compression has the minimum work required as well as the minimum exergy loss rate. However, the minimum work required for the four-stage propene with sub-cooling is only 6.3% more than the minimum work required for the compressor. In terms of exergy loss rate, mixed refrigerant was 9% higher than the compressor exergy loss rate. Therefore, further studies were be made to reduce the energy consumption of the mixed refrigeration process in the hybrid carbon capture processes by applying MOO.

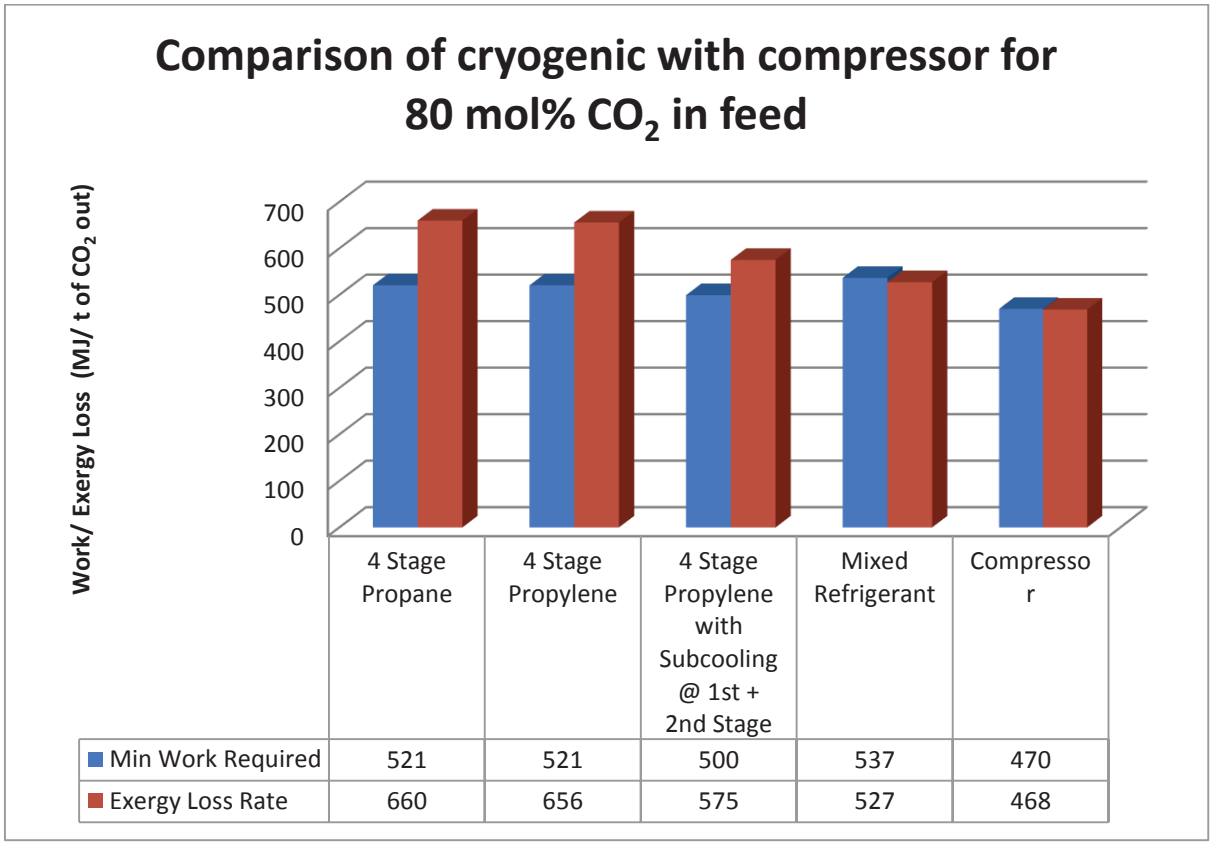

Figure A.17 Comparison of four cryogenic liquefaction of CO_2 v/s compressor of CO_2.

A.4 Cooling Water Calculations

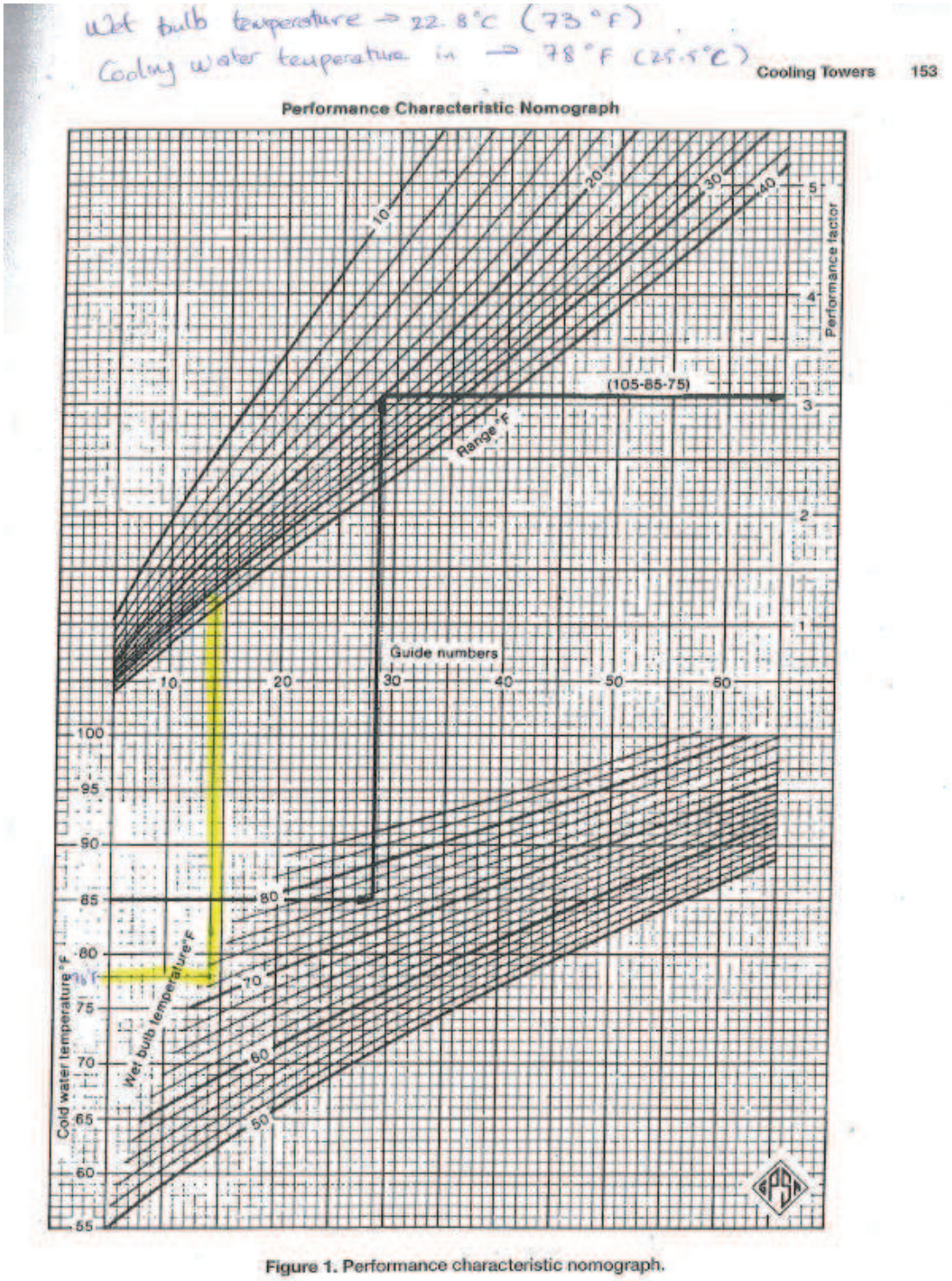

Figure 1. Performance characteristic nomograph.

Figure A.18 GPSA handbook (GPSA 2004) temperature data to determine the cooling water temperature.

B. Simulation Results

B.1 VSA/Low-Temperature Separation Hybrid Carbon Capture MOO Results

Table B.1 Final MOO results that were used to plot the Pareto charts in Chapter 4 (VSA/low-temperature separation hybrid carbon capture) of the thesis.

Decision Variables							Objective Variables	
Refrigerant Ethane Molar Fraction	Refrigerant Molar Flow	Low-Temp Process Stream Outlet Temp.	Multi-Stage Compression Pressure	Membrane Cut	VSA CO_2 Outlet Purity	VSA CO_2 Recovery Rate	Total Work (kW_e)	Recovery Rate
0.41	1.07	-56.66	0.05	1318	0.73	0.75	72180	0.52
0.41	1.07	-56.82	0.05	1318	0.73	0.75	72222	0.53
0.39	1.06	-56.22	0.05	1366	0.74	0.75	72254	0.54
0.41	1.14	-55.68	0.03	1402	0.76	0.75	73004	0.56
0.37	1.12	-55.40	0.09	1405	0.78	0.76	73026	0.60
0.37	1.11	-56.92	0.14	1456	0.79	0.74	73520	0.64
0.39	1.14	-56.42	0.20	1378	0.81	0.75	73794	0.67
0.39	1.14	-56.42	0.22	1570	0.81	0.75	74659	0.69
0.39	1.15	-56.40	0.22	1570	0.81	0.75	74797	0.69
0.37	1.11	-56.72	0.19	2224	0.78	0.74	76572	0.71
0.28	1.18	-53.78	0.35	1723	0.77	0.79	77050	0.75
0.28	1.18	-53.78	0.35	1723	0.77	0.79	77069	0.75
0.22	1.18	-48.12	0.37	3769	0.79	0.77	81158	0.77
0.25	1.17	-53.68	0.27	3355	0.76	0.79	81205	0.78
0.30	1.14	-53.78	0.35	3259	0.77	0.79	81310	0.79
0.30	1.14	-53.78	0.34	3259	0.77	0.79	81434	0.79
0.30	1.14	-53.78	0.35	3259	0.77	0.79	81611	0.79
0.30	1.26	-53.78	0.28	3739	0.77	0.80	83346	0.79
0.28	1.26	-55.24	0.29	2788	0.72	0.82	84149	0.81
0.29	1.15	-52.84	0.36	3751	0.73	0.82	86361	0.82
0.28	1.20	-40.24	0.46	3457	0.71	0.83	89620	0.83
0.27	1.24	-51.76	0.46	3457	0.71	0.83	89924	0.83
0.30	1.25	-56.40	0.28	3079	0.67	0.86	90767	0.85
0.30	1.25	-56.40	0.28	3079	0.67	0.86	90873	0.85
0.26	1.29	-52.88	0.37	3262	0.69	0.87	93259	0.86
0.25	1.29	-53.96	0.35	3619	0.69	0.87	93661	0.86
0.26	1.29	-52.88	0.37	3514	0.69	0.87	94013	0.86
0.26	1.29	-54.16	0.37	3466	0.69	0.87	94224	0.86
0.26	1.29	-52.88	0.37	3466	0.69	0.87	94260	0.87
0.25	1.21	-53.80	0.35	3619	0.67	0.87	94664	0.87
0.35	1.33	-53.70	0.37	3274	0.67	0.87	96755	0.87
0.32	1.22	-52.42	0.35	3811	0.66	0.88	97212	0.88

0.29	1.46	-55.14	0.35	3085	0.67	0.88	97948	0.88
0.29	1.39	-55.14	0.35	3085	0.67	0.89	99551	0.89
0.29	1.46	-55.14	0.35	3085	0.67	0.89	100038	0.89
0.29	1.29	-49.38	0.35	3472	0.66	0.90	101674	0.90
0.35	1.39	-48.72	0.39	2674	0.65	0.91	104249	0.90
0.37	1.39	-48.74	0.39	2770	0.65	0.91	104756	0.90
0.20	1.39	-44.90	0.48	2722	0.65	0.91	106232	0.91
0.23	1.46	-47.50	0.48	2752	0.65	0.91	106676	0.91
0.35	1.39	-48.74	0.48	2674	0.65	0.91	106951	0.91
0.35	1.39	-48.74	0.48	2674	0.65	0.91	107441	0.91
0.29	1.40	-53.84	0.46	2971	0.65	0.91	107557	0.91
0.26	1.49	-44.62	0.41	3424	0.64	0.92	111178	0.92
0.26	1.49	-47.46	0.39	3805	0.64	0.93	113020	0.93
0.35	1.56	-58.44	0.25	3775	0.61	0.93	114760	0.93
0.23	1.26	-42.04	0.39	3904	0.62	0.94	115387	0.93
0.33	1.47	-55.76	0.36	3127	0.61	0.95	117100	0.94
0.33	1.47	-55.76	0.36	3133	0.61	0.95	117398	0.94
0.34	1.57	-52.28	0.35	3898	0.59	0.95	123820	0.95
0.39	1.40	-58.40	0.25	3766	0.61	0.97	125467	0.96
0.25	1.49	-53.72	0.34	3979	0.58	0.97	129005	0.96
0.25	1.49	-53.72	0.34	3979	0.58	0.97	129028	0.96
0.39	1.49	-55.56	0.35	3892	0.58	0.97	130595	0.97
0.27	1.42	-50.74	0.34	3628	0.56	0.98	131511	0.97
0.27	1.42	-50.74	0.34	3628	0.56	0.98	131557	0.97
0.38	1.58	-55.86	0.34	3628	0.56	0.97	133603	0.97
0.41	1.58	-54.68	0.41	2746	0.58	0.98	134162	0.98
0.38	1.58	-55.86	0.34	3628	0.57	0.98	136790	0.98
0.41	1.64	-52.90	0.46	2527	0.57	0.98	137076	0.98
0.49	1.65	-54.20	0.46	2527	0.58	0.98	137407	0.98
0.49	1.65	-52.90	0.46	2527	0.57	0.98	138502	0.98
0.49	1.65	-52.90	0.44	3295	0.57	0.98	141486	0.98
0.33	1.53	-54.36	0.61	2719	0.55	0.99	150002	0.98
0.33	1.53	-54.34	0.61	2719	0.55	0.99	150093	0.98
0.33	1.57	-54.18	0.61	2725	0.55	0.99	150914	0.98
0.33	1.57	-54.20	0.65	2530	0.55	0.99	153123	0.98
0.33	1.57	-54.20	0.65	2530	0.55	0.99	153710	0.98

B.2 Membrane/Low-Temperature Separation Hybrid Carbon Capture MOO Results

This appendix sub-section will display the tables of data used to determine the graphs shown throughout the thesis.

B.2.1 Case I (Mixed Refrigerant) Results

Table B.2 Final MOO results that were used to plot the Pareto charts in Chapter 5 (membrane/low-temperature separation hybrid carbon capture – Case I) of the thesis.

Decision Variables								Objective Variables	
Refrigerant Ethane Molar Fraction	Refrigerant Molar Flow	Low-Temp Process Stream Outlet Temp.	Membrane B Cut	Multi-Stage Compression Pressure	Memb A Feed Pressure	Memb A Permeate Pressure	Memb A Cut	Total Work (MW_e)	Recovery Rate
0.46	1.92	-52.64	0.45	3987	116.51	10.09	0.37	169	1.00
0.65	1.89	-54.63	0.44	3317	110.18	10.09	0.37	164	1.00
0.63	1.64	-54.01	0.45	3629	113.34	10.09	0.37	163	1.00
0.31	1.64	-52.76	0.45	3583	113.34	10.09	0.35	153	1.00
0.29	1.51	-52.99	0.45	3242	110.53	10.18	0.35	147	0.99
0.30	1.52	-54.63	0.45	3704	115.81	10.35	0.33	144	0.99
0.26	2.27	-54.05	0.44	3108	116.16	10.44	0.32	141	0.99
0.28	2.27	-53.97	0.43	3280	110.53	10.09	0.29	132	0.98
0.29	1.44	-54.49	0.45	3465	113.96	10.53	0.29	127	0.98
0.45	1.57	-51.51	0.45	3398	110.88	10.70	0.28	124	0.97
0.32	1.70	-52.60	0.45	2804	127.51	10.53	0.26	118	0.96
0.27	1.52	-54.01	0.44	2828	138.77	10.09	0.24	113	0.95
0.30	1.58	-54.02	0.43	2804	110.18	10.44	0.26	109	0.94
0.27	1.59	-54.01	0.44	2871	112.99	10.26	0.25	106	0.94
0.63	1.63	-54.01	0.45	2941	110.18	10.00	0.23	104	0.91
0.64	1.50	-53.93	0.45	2898	110.26	10.00	0.22	98	0.89
0.25	1.50	-51.68	0.44	2575	113.34	10.00	0.21	92	0.88
0.64	1.53	-54.01	0.45	2769	110.88	10.00	0.20	91	0.86
0.32	1.27	-52.64	0.44	3882	116.60	10.26	0.19	86	0.83
0.46	1.40	-53.85	0.44	2495	111.14	10.18	0.19	82	0.82
0.43	1.46	-51.67	0.35	2554	111.14	10.00	0.18	78	0.79
0.29	1.58	-54.16	0.40	1866	113.26	10.26	0.18	76	0.78
0.26	1.56	-52.76	0.43	2554	112.99	10.00	0.16	72	0.74
0.24	1.63	-50.18	0.35	2597	112.90	10.00	0.16	70	0.72
0.26	1.63	-52.68	0.43	2253	113.08	10.00	0.15	67	0.70
0.26	1.63	-52.68	0.43	2253	113.08	10.18	0.15	67	0.70
0.31	1.02	-53.97	0.43	3231	110.18	10.09	0.14	62	0.68
0.52	1.13	-54.10	0.47	1882	110.88	10.00	0.14	59	0.66
0.31	1.02	-53.97	0.43	1930	116.60	10.26	0.13	55	0.63
0.30	1.02	-51.64	0.44	1930	111.23	10.09	0.13	54	0.63
0.32	1.03	-53.82	0.43	2358	111.23	10.35	0.12	51	0.59

0.27	1.02	-53.81	0.44	1919	110.00	10.09	0.12	49	0.58
0.31	0.84	-52.59	0.38	2828	111.32	10.53	0.11	48	0.56
0.31	0.78	-52.60	0.24	2828	110.62	10.62	0.11	45	0.52
0.34	0.76	-51.28	0.15	2895	110.79	10.09	0.11	45	0.50
0.33	0.80	-53.77	0.33	1573	111.14	10.44	0.11	43	0.49
0.47	0.92	-54.37	0.45	1879	110.70	10.00	0.09	40	0.46
0.31	0.72	-54.80	0.20	3231	111.23	10.26	0.09	39	0.45
0.29	0.70	-51.58	0.34	2210	111.23	11.41	0.09	36	0.42
0.26	0.71	-54.17	0.25	2839	111.32	10.09	0.08	34	0.40
0.31	0.84	-52.60	0.31	2828	110.53	10.26	0.07	34	0.38
0.32	0.72	-54.48	0.31	2199	112.64	10.26	0.07	32	0.37
0.24	0.51	-50.18	0.35	3414	112.90	10.00	0.07	30	0.35
0.31	0.53	-54.18	0.42	2812	111.32	10.53	0.06	28	0.33
0.24	0.58	-50.11	0.15	2726	111.14	10.26	0.07	28	0.31
0.29	0.59	-54.16	0.37	1559	111.06	10.53	0.06	26	0.30
0.31	0.53	-54.18	0.15	2726	111.32	10.26	0.06	26	0.29
0.31	0.59	-53.23	0.38	2118	111.32	10.26	0.05	24	0.26
0.29	0.59	-54.16	0.37	1559	111.06	10.53	0.05	22	0.25
0.27	0.53	-53.86	0.28	2210	111.32	21.44	0.05	21	0.17

B.2.2 Case II (Mixed Refrigerant) Results

Table B.3 Final MOO results that were used to plot the Pareto charts in Chapter 5 (membrane/low-temperature separation hybrid carbon capture – Case II) of the thesis.

Decision Variables							Objective Variables	
Refrigerant Ethane Molar Fraction	Low-Temp Process Stream Outlet Temp.	Membrane B Cut	Multi-Stage Compression Pressure	Memb A Feed Pressure	Memb A Permeate Pressure	Memb A Cut	Total Work (MW)	Recovery Rate
-7.01	-34.44	0.57	3343	111.58	10.26	0.41	199	1.00
-5.44	-34.51	0.57	3978	111.23	10.09	0.39	192	1.00
-10.14	-34.43	0.57	3274	110.62	10.26	0.39	184	1.00
-6.81	-33.82	0.57	3939	110.70	10.26	0.36	177	1.00
-11.31	-33.25	0.57	3352	136.92	10.26	0.34	171	1.00
-5.08	-33.80	0.53	3665	133.05	10.26	0.33	162	1.00
-9.99	-33.82	0.57	3308	112.11	10.26	0.33	157	0.99
-5.44	-34.19	0.57	3123	112.99	10.18	0.32	152	0.99
-3.49	-33.41	0.52	3900	110.18	10.26	0.31	145	0.99
-3.54	-33.41	0.52	3900	111.58	10.00	0.30	141	0.98
-3.88	-34.51	0.53	3274	110.18	10.00	0.31	138	0.98
-10.14	-33.25	0.57	3352	110.18	10.26	0.29	135	0.97
-3.49	-34.68	0.53	3274	114.40	10.09	0.28	128	0.97
-8.21	-34.50	0.53	3665	133.23	10.09	0.26	126	0.96
-3.93	-34.81	0.53	3900	110.79	10.00	0.26	119	0.95
-5.49	-34.51	0.57	3269	110.53	10.18	0.25	119	0.94
-10.14	-34.81	0.53	3900	110.00	10.00	0.24	113	0.93
-8.77	-34.44	0.57	2825	111.76	10.26	0.24	108	0.91
-3.29	-33.80	0.57	3093	111.76	10.09	0.23	106	0.91

-5.05	-34.43	0.55	3040	114.31	10.09	0.22	102	0.90
-3.88	-34.52	0.57	3264	134.46	10.26	0.20	101	0.88
-3.88	-34.81	0.53	3274	111.94	10.09	0.21	95	0.87
-5.05	-34.75	0.53	3274	111.94	10.44	0.20	91	0.85
-5.47	-34.50	0.44	3665	110.70	10.09	0.20	87	0.83
-12.68	-34.98	0.45	3582	111.94	10.09	0.19	82	0.80
-5.05	-34.81	0.53	2917	112.46	10.09	0.17	78	0.78
-3.29	-34.42	0.57	3328	111.94	10.09	0.16	75	0.75
-3.88	-34.53	0.53	3269	114.40	10.26	0.16	73	0.74
-11.51	-34.55	0.57	2942	111.58	10.79	0.16	71	0.72
-6.81	-34.81	0.48	3548	110.70	10.09	0.15	66	0.70
-6.81	-34.81	0.44	3577	110.88	10.00	0.15	65	0.69
-8.43	-34.50	0.45	3274	110.18	10.09	0.15	63	0.68
-3.69	-34.81	0.57	3587	110.00	10.09	0.14	62	0.66
-3.29	-34.82	0.49	3587	110.35	10.09	0.13	59	0.65
-11.31	-33.88	0.57	3035	114.57	10.09	0.13	59	0.63
-12.87	-34.52	0.53	3348	110.18	10.00	0.12	54	0.61
-2.76	-34.51	0.49	3269	111.58	10.00	0.12	51	0.58
-3.98	-34.49	0.53	3274	110.53	10.00	0.11	49	0.55
-3.29	-34.65	0.45	3910	111.58	10.26	0.10	45	0.51
-3.49	-34.49	0.44	3548	111.58	10.18	0.09	41	0.48
-6.62	-34.81	0.45	2957	110.18	10.00	0.09	39	0.46
-3.49	-34.61	0.53	3587	111.58	10.26	0.08	37	0.42
-3.51	-34.52	0.45	3665	110.88	10.09	0.08	35	0.41
-10.53	-34.60	0.53	3607	112.29	10.26	0.08	35	0.40
-9.77	-34.58	0.37	3582	112.29	10.26	0.08	33	0.38
-3.49	-33.81	0.53	3230	110.35	10.00	0.07	30	0.36
-3.49	-34.90	0.49	3582	110.18	11.50	0.06	27	0.31
-3.49	-34.90	0.49	3582	110.18	11.50	0.06	27	0.31
-3.49	-34.90	0.49	3582	110.18	11.50	0.06	27	0.31
-5.44	-34.74	0.40	3020	110.53	10.00	0.05	22	0.25

B.3 Pinch Analysis Results

B.3.1 VSA/Low-Temperature Separation Hybrid Carbon Capture Process Heat Curve Results

Table B.4 Heat curve data used to determine the heat composite curves and grand composite curves in Chapter 4 of the thesis.

Cold Side			Hot Side	
Temp	Heat Flow		Temp	Heat Flow
-49.0	2.19E+07	Start LNG 1	-45.0	2.19E+07
-48.1	2.66E+07		-43.7	2.66E+07
-47.4	3.00E+07		-42.8	3.00E+07
-47.4	3.04E+07		-42.7	3.04E+07

*Continuation from LNG 1

-22.7	9.58E+07		-19.3	9.58E+07
-22.4	9.61E+07		-19.0	9.61E+07
-21.7	9.66E+07		-18.2	9.66E+07
-19.9	9.80E+07		-16.3	9.80E+07

-46.8	3.41E+07		-41.8	3.41E+07		-19.2	9.86E+07		-15.5	9.86E+07
-46.3	3.75E+07		-41.0	3.75E+07		-18.5	9.91E+07		-14.8	9.91E+07
-46.3	3.76E+07		-41.0	3.76E+07		-16.1	1.01E+08		-12.1	1.01E+08
-46.3	3.79E+07		-40.9	3.79E+07		-14.5	1.02E+08		-10.3	1.02E+08
-46.0	4.11E+07		-40.3	4.11E+07		-13.1	1.04E+08		-8.8	1.04E+08
-45.6	4.45E+07		-39.7	4.45E+07		-12.5	1.04E+08		-8.1	1.04E+08
-45.5	4.57E+07		-39.4	4.57E+07		-12.1	1.04E+08		-7.7	1.04E+08
-45.3	4.79E+07		-39.1	4.79E+07		-10.6	1.06E+08		-6.0	1.06E+08
-45.1	5.12E+07		-38.5	5.12E+07		-10.1	1.06E+08		-5.5	1.06E+08
-45.0	5.33E+07		-38.2	5.33E+07		-7.2	1.08E+08		-2.2	1.08E+08
-44.9	5.45E+07		-38.0	5.45E+07		-6.7	1.09E+08		-1.7	1.09E+08
-44.8	5.78E+07		-37.6	5.78E+07		-5.1	1.10E+08		0.1	1.10E+08
-44.7	6.06E+07		-37.2	6.06E+07		-4.3	1.11E+08		1.0	1.11E+08
-44.7	6.08E+07		-37.2	6.08E+07		-3.0	1.12E+08		2.5	1.12E+08
-44.7	6.10E+07		-37.1	6.10E+07		-2.6	1.12E+08		3.0	1.12E+08
-44.7	6.42E+07		-36.7	6.42E+07		-1.5	1.13E+08		4.1	1.13E+08
-44.6	6.74E+07		-36.4	6.74E+07		-1.1	1.14E+08		4.6	1.14E+08
-44.6	6.82E+07		-36.3	6.82E+07		0.6	1.15E+08		6.6	1.15E+08
-44.6	7.06E+07		-36.0	7.06E+07		1.2	1.16E+08		7.2	1.16E+08
-44.7	7.38E+07		-35.7	7.38E+07		2.3	1.17E+08		8.5	1.17E+08
-44.7	7.56E+07		-35.5	7.56E+07		3.8	1.18E+08		10.3	1.18E+08
-44.7	7.70E+07		-35.4	7.70E+07		4.1	1.18E+08		10.6	1.18E+08
-44.8	7.89E+07		-35.2	7.89E+07		6.4	1.20E+08		13.3	1.20E+08
-44.6	7.90E+07		-35.2	7.90E+07		6.7	1.21E+08		13.6	1.21E+08
-44.5	7.91E+07		-35.2	7.91E+07		7.5	1.21E+08		14.5	1.21E+08
-43.1	8.01E+07		-35.1	8.01E+07		8.9	1.23E+08		16.2	1.23E+08
-41.7	8.11E+07		-35.0	8.11E+07		9.7	1.23E+08		17.1	1.23E+08
-39.9	8.25E+07		-34.8	8.25E+07		10.7	1.24E+08		18.4	1.24E+08
-38.7	8.34E+07		-34.8	8.34E+07		11.3	1.25E+08		19.0	1.25E+08
-36.8	8.49E+07		-34.6	8.49E+07		13.7	1.27E+08		21.9	1.27E+08
-35.7	8.57E+07		-33.4	8.57E+07		13.9	1.27E+08		22.0	1.27E+08
-35.5	8.58E+07		-33.3	8.58E+07		15.8	1.29E+08		24.3	1.29E+08
-34.5	8.66E+07		-32.2	8.66E+07		16.0	1.30E+08		24.6	1.30E+08
-32.2	8.83E+07		-29.7	8.83E+07		16.8	1.30E+08		25.6	1.30E+08
-31.3	8.91E+07		-28.7	8.91E+07		17.1	1.31E+08		25.9	1.31E+08
-31.1	8.92E+07		-28.6	8.92E+07		18.3	1.32E+08		27.3	1.32E+08
-28.8	9.09E+07		-26.1	9.09E+07		19.7	1.33E+08		28.9	1.33E+08
-28.7	9.11E+07		-25.9	9.11E+07		20.5	1.34E+08		29.9	1.34E+08
-27.2	9.22E+07		-24.3	9.22E+07		22.3	1.36E+08		32.1	1.36E+08
-26.9	9.25E+07		-23.9	9.25E+07		22.6	1.36E+08		32.5	1.36E+08
-25.6	9.35E+07		-22.5	9.35E+07		24.6	1.38E+08	End	34.9	1.38E+08
						24.6	1.38E+08	LNG 1	35.0	1.38E+08

Cold Side			Hot Side	
Temp	Heat Flow		Temp	Heat Flow
		Start LNG 2		
-53.8	5.99E+06		-50.9	5.99E+06
-53.3	7.36E+06		-50.3	7.36E+06
-53.3	7.45E+06		-50.2	7.45E+06
-53.3	7.58E+06		-50.2	7.58E+06
-53.2	7.83E+06		-50.1	7.83E+06
-52.9	8.75E+06		-49.7	8.75E+06
-52.8	8.92E+06		-49.6	8.92E+06
-52.7	9.19E+06		-49.5	9.19E+06
-52.6	9.49E+06		-49.4	9.49E+06
-52.4	1.02E+07		-49.1	1.02E+07
-52.3	1.04E+07		-49.0	1.04E+07
-52.2	1.08E+07		-48.9	1.08E+07
-52.1	1.11E+07		-48.7	1.11E+07
-51.9	1.17E+07		-48.5	1.17E+07
-51.9	1.19E+07		-48.4	1.19E+07
-51.7	1.24E+07		-48.2	1.24E+07
-51.6	1.27E+07		-48.1	1.27E+07
-51.5	1.32E+07		-47.9	1.32E+07
-51.4	1.35E+07		-47.8	1.35E+07
-51.2	1.40E+07		-47.6	1.40E+07
-51.1	1.43E+07		-47.5	1.43E+07
-51.0	1.48E+07		-47.3	1.48E+07
-50.9	1.50E+07		-47.3	1.50E+07
-50.7	1.56E+07		-47.0	1.56E+07
-50.7	1.58E+07		-47.0	1.58E+07
-50.5	1.65E+07		-46.8	1.65E+07
-50.4	1.67E+07		-46.7	1.67E+07
-50.2	1.73E+07		-46.5	1.73E+07
-50.2	1.73E+07		-46.5	1.73E+07
-50.0	1.82E+07		-46.2	1.82E+07
-49.9	1.83E+07		-46.1	1.83E+07
-49.8	1.88E+07		-46.0	1.88E+07
-49.8	1.88E+07		-46.0	1.88E+07
-49.5	2.00E+07		-45.6	2.00E+07
-49.4	2.01E+07		-45.6	2.01E+07
-49.4	2.03E+07		-45.5	2.03E+07
-49.4	2.04E+07		-45.5	2.04E+07
		End LNG 2		
-49.0	2.19E+07		-45.0	2.19E+07

Cold Side			Hot Side	
Temp	Heat Flow		Temp	Heat Flow
		Start LNG 3		
-55.9	0.00E+00		-53.8	0.00E+00
-55.5	5.68E+05		-53.5	5.68E+05
-55.5	5.99E+05		-53.5	5.99E+05
-55.5	6.34E+05		-53.5	6.34E+05
-55.3	1.14E+06		-53.2	1.14E+06
-55.2	1.20E+06		-53.2	1.20E+06
-55.2	1.25E+06		-53.1	1.25E+06
-54.9	1.72E+06		-52.9	1.72E+06
-54.9	1.79E+06		-52.9	1.79E+06
-54.9	1.85E+06		-52.8	1.85E+06
-54.8	2.31E+06		-52.6	2.31E+06
-54.8	2.39E+06		-52.6	2.39E+06
-54.7	2.45E+06		-52.5	2.45E+06
-54.6	2.90E+06		-52.3	2.90E+06
-54.6	2.99E+06		-52.3	2.99E+06
-54.6	3.05E+06		-52.3	3.05E+06
-54.5	3.50E+06		-52.0	3.50E+06
-54.4	3.59E+06		-52.0	3.59E+06
-54.4	3.64E+06		-52.0	3.64E+06
-54.3	4.11E+06		-51.8	4.11E+06
-54.3	4.19E+06		-51.7	4.19E+06
-54.3	4.23E+06		-51.7	4.23E+06
-54.1	4.73E+06		-51.5	4.73E+06
-54.1	4.79E+06		-51.4	4.79E+06
-54.1	4.81E+06		-51.4	4.81E+06
-54.0	5.36E+06		-51.2	5.36E+06
-53.9	5.39E+06		-51.2	5.39E+06
-53.9	5.40E+06		-51.2	5.40E+06
		End LNG 3		
-53.8	5.99E+06		-50.9	5.99E+06

B.3.2 Membrane/Low-Temperature Separation Hybrid Carbon Capture Process Heat Curve Results – Case I

Table B.5 Heat curve data used to determine the heat composite curves and grand composite curves in Chapter 5 (Case I) of the thesis.

Cold Side			Hot Side	
Temp	Heat Flow		Temp	Heat Flow
-49.6	4.16E+07	Start LNG 1	-41.9	4.16E+07
-48.7	4.65E+07		-40.8	4.65E+07
-48.1	4.97E+07		-40.1	4.97E+07
-47.9	5.09E+07		-39.9	5.09E+07
-47.0	5.51E+07		-39.0	5.51E+07
-46.6	5.76E+07		-38.5	5.76E+07
-46.2	5.94E+07		-38.2	5.94E+07
-45.9	6.12E+07		-37.8	6.12E+07
-45.5	6.35E+07		-37.4	6.35E+07
-45.0	6.59E+07		-36.9	6.59E+07
-44.7	6.76E+07		-36.6	6.76E+07
-44.5	6.85E+07		-36.5	6.85E+07
-44.0	7.17E+07		-35.9	7.17E+07
-43.5	7.45E+07		-35.5	7.45E+07
-43.3	7.57E+07		-35.2	7.57E+07
-42.6	7.97E+07		-34.6	7.97E+07
-42.2	8.23E+07		-34.2	8.23E+07
-42.0	8.34E+07		-34.0	8.34E+07
-42.0	8.37E+07		-34.0	8.37E+07
-41.9	8.44E+07		-33.9	8.44E+07
-41.4	8.77E+07		-33.4	8.77E+07
-41.0	9.01E+07		-33.0	9.01E+07
-40.8	9.16E+07		-32.8	9.16E+07
-40.3	9.55E+07		-32.3	9.55E+07
-40.2	9.62E+07		-32.2	9.62E+07
-39.5	9.70E+07		-32.1	9.70E+07
-37.1	9.96E+07		-31.7	9.96E+07
-35.7	1.01E+08		-31.5	1.01E+08
-34.5	1.02E+08		-31.4	1.02E+08
-34.5	1.02E+08		-31.3	1.02E+08
-33.5	1.04E+08		-31.2	1.04E+08
-33.4	1.04E+08		-31.1	1.04E+08
-32.4	1.05E+08		-30.0	1.05E+08
-29.7	1.08E+08		-27.3	1.08E+08
-28.7	1.09E+08		-26.3	1.09E+08
-27.0	1.11E+08		-24.5	1.11E+08
-26.8	1.11E+08		-24.3	1.11E+08
-25.1	1.13E+08		-22.6	1.13E+08
-24.9	1.13E+08		-22.4	1.13E+08

*Continuation from LNG 1

-14.8	1.25E+08	-11.9	1.25E+08
-14.1	1.25E+08	-11.2	1.25E+08
-13.1	1.27E+08	-10.1	1.27E+08
-11.6	1.28E+08	-8.5	1.28E+08
-11.3	1.29E+08	-8.3	1.29E+08
-11.2	1.29E+08	-8.1	1.29E+08
-8.4	1.32E+08	-5.2	1.32E+08
-7.7	1.33E+08	-4.4	1.33E+08
-7.0	1.34E+08	-3.7	1.34E+08
-5.4	1.36E+08	-1.9	1.36E+08
-3.2	1.38E+08	0.3	1.38E+08
-2.9	1.39E+08	0.7	1.39E+08
-2.4	1.39E+08	1.2	1.39E+08
-1.3	1.41E+08	2.4	1.41E+08
0.5	1.43E+08	4.4	1.43E+08
1.1	1.43E+08	5.0	1.43E+08
3.3	1.46E+08	7.4	1.46E+08
4.7	1.48E+08	8.9	1.48E+08
4.9	1.48E+08	9.2	1.48E+08
5.1	1.49E+08	9.3	1.49E+08
6.0	1.50E+08	10.3	1.50E+08
8.6	1.53E+08	13.2	1.53E+08
8.7	1.53E+08	13.2	1.53E+08
9.5	1.54E+08	14.1	1.54E+08
11.2	1.56E+08	16.0	1.56E+08
11.5	1.57E+08	16.3	1.57E+08
12.2	1.58E+08	17.0	1.58E+08
12.8	1.58E+08	17.7	1.58E+08
13.4	1.59E+08	18.4	1.59E+08
13.7	1.60E+08	18.7	1.60E+08
15.5	1.62E+08	20.7	1.62E+08
16.0	1.63E+08	21.3	1.63E+08
17.7	1.65E+08	23.2	1.65E+08
18.3	1.66E+08	23.9	1.66E+08
18.7	1.66E+08	24.3	1.66E+08
20.5	1.69E+08	26.3	1.69E+08
20.9	1.70E+08	26.7	1.70E+08
21.6	1.71E+08	27.6	1.71E+08
22.5	1.72E+08	28.6	1.72E+08

-21.6	1.17E+08		-19.0	1.17E+08
-20.6	1.18E+08		-17.9	1.18E+08
-20.3	1.18E+08		-17.6	1.18E+08
-19.0	1.20E+08		-16.3	1.20E+08
-18.2	1.21E+08		-15.4	1.21E+08
-15.7	1.23E+08		-12.9	1.23E+08

24.0	1.74E+08		30.2	1.74E+08
24.4	1.75E+08		30.7	1.75E+08
24.5	1.75E+08		30.8	1.75E+08
26.4	1.78E+08		32.9	1.78E+08
26.9	1.79E+08		33.5	1.79E+08
28.3	1.81E+08		35	1.81E+08
29.0	1.82E+08	End LNG 1	37.2	1.82E+08
29.0	1.82E+08		37.2	1.82E+08

Cold Side			Hot Side	
Temp	Heat Flow		Temp	Heat Flow
-53.9	1.97E+07	Start LNG 2	-47.6	1.97E+07
-53.6	2.17E+07		-47.0	2.17E+07
-53.6	2.19E+07		-47.0	2.19E+07
-53.5	2.21E+07		-46.9	2.21E+07
-53.5	2.23E+07		-46.9	2.23E+07
-53.2	2.38E+07		-46.5	2.38E+07
-53.2	2.40E+07		-46.4	2.40E+07
-53.1	2.43E+07		-46.3	2.43E+07
-53.1	2.47E+07		-46.2	2.47E+07
-52.9	2.58E+07		-45.9	2.58E+07
-52.8	2.61E+07		-45.8	2.61E+07
-52.7	2.65E+07		-45.7	2.65E+07
-52.6	2.70E+07		-45.6	2.70E+07
-52.5	2.80E+07		-45.3	2.80E+07
-52.4	2.82E+07		-45.2	2.82E+07
-52.3	2.87E+07		-45.1	2.87E+07
-52.2	2.93E+07		-45.0	2.93E+07
-52.0	3.01E+07		-44.7	3.01E+07
-52.0	3.03E+07		-44.7	3.03E+07
-51.9	3.09E+07		-44.5	3.09E+07
-51.8	3.15E+07		-44.4	3.15E+07
-51.6	3.23E+07		-44.2	3.23E+07
-51.6	3.25E+07		-44.1	3.25E+07
-51.4	3.31E+07		-44.0	3.31E+07
-51.3	3.36E+07		-43.9	3.36E+07
-51.1	3.46E+07		-43.6	3.46E+07
-51.1	3.47E+07		-43.6	3.47E+07
-51.0	3.52E+07		-43.5	3.52E+07
-50.9	3.56E+07		-43.4	3.56E+07
-50.6	3.69E+07		-43.1	3.69E+07
-50.6	3.69E+07		-43.0	3.69E+07
-50.5	3.73E+07		-42.9	3.73E+07

Cold Side			Hot Side	
Temp	Heat Flow		Temp	Heat Flow
-56.7	0.00E+00	Start LNG 3	-53.9	0.00E+00
-56.5	1.83E+06		-53.3	1.83E+06
-56.5	1.97E+06		-53.2	1.97E+06
-56.4	2.13E+06		-53.2	2.13E+06
-56.3	3.68E+06		-52.6	3.68E+06
-56.2	3.85E+06		-52.6	3.85E+06
-56.2	4.15E+06		-52.5	4.15E+06
-56.0	5.57E+06		-52.0	5.57E+06
-56.0	5.74E+06		-52.0	5.74E+06
-56.0	6.15E+06		-51.8	6.15E+06
-55.8	7.48E+06		-51.4	7.48E+06
-55.8	7.65E+06		-51.3	7.65E+06
-55.7	8.12E+06		-51.2	8.12E+06
-55.5	9.43E+06		-50.7	9.43E+06
-55.5	9.57E+06		-50.7	9.57E+06
-55.4	1.01E+07		-50.5	1.01E+07
-55.2	1.14E+07		-50.1	1.14E+07
-55.2	1.15E+07		-50.1	1.15E+07
-55.2	1.20E+07		-49.9	1.20E+07
-54.9	1.34E+07		-49.5	1.34E+07
-54.9	1.35E+07		-49.5	1.35E+07
-54.9	1.39E+07		-49.3	1.39E+07
-54.6	1.55E+07		-48.9	1.55E+07
-54.6	1.55E+07		-48.9	1.55E+07
-54.6	1.59E+07		-48.7	1.59E+07
-54.3	1.75E+07		-48.2	1.75E+07
-54.3	1.76E+07		-48.2	1.76E+07
-54.3	1.78E+07	End LNG 3	-48.2	1.78E+07
-53.9	1.97E+07		-47.6	1.97E+07

-50.5	3.77E+07		-42.9	3.77E+07
-50.1	3.92E+07		-42.5	3.92E+07
-50.1	3.92E+07		-42.5	3.92E+07
-50.1	3.94E+07		-42.4	3.94E+07
-50.0	3.96E+07		-42.4	3.96E+07
		End		
-49.6	4.16E+07	LNG 2	-41.9	4.16E+07

B.3.3 Membrane/Low-Temperature Separation Hybrid Carbon Capture Process Heat Curve Results – Case I

Table B.6 Heat curve data used to determine the heat composite curves and grand composite curves in Chapter 5 (Case II) of the thesis.

Cold Side			Hot Side	
Temp	Heat Flow		Temp	Heat Flow
-29.2	8.46E+07	Start LNG 1	-41.9	4.16E+07
-26.3	8.74E+07		-40.8	4.65E+07
-26.0	8.77E+07		-40.1	4.97E+07
-25.2	8.84E+07		-39.9	5.09E+07
-23.4	9.02E+07		-39.0	5.51E+07
-22.7	9.08E+07		-38.5	5.76E+07
-21.3	9.22E+07		-38.2	5.94E+07
-21.1	9.24E+07		-37.8	6.12E+07
-20.4	9.31E+07		-37.4	6.35E+07
-19.5	9.40E+07		-36.9	6.59E+07
-17.5	9.59E+07		-36.6	6.76E+07
-17.4	9.60E+07		-36.5	6.85E+07
-16.2	9.72E+07		-35.9	7.17E+07
-14.5	9.89E+07		-35.5	7.45E+07
-13.6	9.97E+07		-35.2	7.57E+07
-13.6	9.98E+07		-34.6	7.97E+07
-13.0	1.00E+08		-34.2	8.23E+07
-11.5	1.02E+08		-34.0	8.34E+07
-9.9	1.03E+08		-34.0	8.37E+07
-9.7	1.04E+08		-33.9	8.44E+07
-8.5	1.05E+08		-33.4	8.77E+07
-6.6	1.07E+08		-33.0	9.01E+07
-6.5	1.07E+08		-32.8	9.16E+07
-6.3	1.07E+08		-32.3	9.55E+07
-5.5	1.08E+08		-32.2	9.62E+07
-3.3	1.10E+08		-32.1	9.70E+07
-2.8	1.11E+08		-31.7	9.96E+07
-2.4	1.11E+08		-31.5	1.01E+08
-0.1	1.13E+08		-31.4	1.02E+08
0.1	1.14E+08		-31.3	1.02E+08
0.6	1.14E+08		-31.2	1.04E+08
0.6	1.14E+08		-31.1	1.04E+08
3.1	1.17E+08		-30.0	1.05E+08
3.7	1.17E+08		-27.3	1.08E+08
3.9	1.18E+08		-26.3	1.09E+08
6.2	1.20E+08		-24.5	1.11E+08

*Continuation from LNG 1

6.2	1.20E+08		-11.9	1.25E+08
6.4	1.20E+08		-11.2	1.25E+08
6.8	1.21E+08		-10.1	1.27E+08
7.1	1.21E+08		-8.5	1.28E+08
9.4	1.24E+08		-8.3	1.29E+08
9.9	1.24E+08		-8.1	1.29E+08
10.2	1.24E+08		-5.2	1.32E+08
12.3	1.27E+08		-4.4	1.33E+08
12.4	1.27E+08		-3.7	1.34E+08
13.0	1.28E+08		-1.9	1.36E+08
13.0	1.28E+08		0.3	1.38E+08
13.2	1.28E+08		0.7	1.39E+08
15.4	1.30E+08		1.2	1.39E+08
16.0	1.31E+08		2.4	1.41E+08
16.1	1.31E+08		4.4	1.43E+08
17.8	1.33E+08		5.0	1.43E+08
18.3	1.34E+08		7.4	1.46E+08
18.7	1.34E+08		8.9	1.48E+08
19.2	1.35E+08		9.2	1.48E+08
21.2	1.37E+08		9.3	1.49E+08
21.3	1.37E+08		10.3	1.50E+08
22.4	1.39E+08		13.2	1.53E+08
22.9	1.39E+08		13.2	1.53E+08
23.7	1.40E+08		14.1	1.54E+08
24.0	1.41E+08		16.0	1.56E+08
25.5	1.43E+08		16.3	1.57E+08
26.0	1.43E+08		17.0	1.58E+08
26.7	1.44E+08		17.7	1.58E+08
27.5	1.45E+08		18.4	1.59E+08
28.2	1.46E+08		18.7	1.60E+08
28.7	1.47E+08		20.7	1.62E+08
29.3	1.48E+08		21.3	1.63E+08
30.2	1.49E+08		23.2	1.65E+08
31.8	1.52E+08	End LNG 1	23.9	1.66E+08
18.7	1.66E+08		24.3	1.66E+08

Cold Side			Hot Side	
Temp	Heat Flow		Temp	Heat Flow
-36.4	8.23E+07	Start LNG 2	-23.0	8.23E+07
-34.4	8.23E+07		-23.0	8.23E+07
-34.2	8.24E+07		-22.8	8.24E+07
-34.2	8.24E+07		-22.8	8.24E+07
-33.9	8.25E+07		-22.7	8.25E+07
-33.9	8.25E+07		-22.7	8.25E+07
-33.6	8.26E+07		-22.5	8.26E+07
-33.6	8.26E+07		-22.5	8.26E+07
-33.4	8.27E+07		-22.4	8.27E+07
-33.4	8.27E+07		-22.4	8.27E+07
-33.1	8.28E+07		-22.2	8.28E+07
-33.1	8.28E+07		-22.2	8.28E+07
-32.9	8.30E+07		-22.1	8.30E+07
-32.9	8.30E+07		-22.1	8.30E+07
-32.6	8.31E+07		-21.9	8.31E+07
-32.6	8.31E+07		-21.9	8.31E+07
-32.3	8.32E+07		-21.7	8.32E+07
-32.3	8.32E+07		-21.7	8.32E+07
-32.1	8.33E+07		-21.6	8.33E+07
-32.1	8.33E+07		-21.6	8.33E+07
-31.8	8.34E+07		-21.4	8.34E+07
-31.8	8.34E+07		-21.4	8.34E+07
-31.5	8.36E+07		-21.3	8.36E+07
-31.5	8.36E+07		-21.3	8.36E+07
-31.3	8.37E+07		-21.1	8.37E+07
-31.3	8.37E+07		-21.1	8.37E+07
-31.0	8.38E+07		-21.0	8.38E+07
-31.0	8.38E+07		-21.0	8.38E+07
-30.8	8.39E+07		-20.8	8.39E+07
-30.8	8.39E+07		-20.8	8.39E+07
-30.5	8.40E+07		-20.6	8.40E+07
-30.5	8.40E+07		-20.6	8.40E+07
-30.2	8.41E+07		-20.5	8.41E+07
-30.2	8.41E+07		-20.5	8.41E+07
-30.0	8.43E+07		-20.3	8.43E+07
-30.0	8.43E+07		-20.3	8.43E+07
-29.7	8.44E+07		-20.2	8.44E+07
-29.7	8.44E+07		-20.2	8.44E+07
-29.4	8.45E+07		-20.0	8.45E+07
-29.4	8.45E+07		-20.0	8.45E+07
-29.2	8.46E+07	End LNG 2	-19.9	8.46E+07

Cold Side			Hot Side	
Temp	Heat Flow		Temp	Heat Flow
-36.4	0.00E+00	HX 3	-34.4	0.00E+00
-36.4	4.11E+07		-27.7	4.11E+07
			-23.4	8.20E+07

B.4 Techno-Economic Analysis Detailed Example

This sub-section will show the equations and detailed steps used to obtain the results for the techno-economic analysis for the membrane/low-temperature hybrid carbon capture using propane refrigerant (Case II) at 90% overall CO_2 recovery rate.

B.4.1 Capital Equipment Costs

The first step in the techno-economic analysis was to obtain the capital cost of each equipment since the other costs are a function of the total equipment capital costs.

- **Heat Exchangers**

The heat exchanger cost equation from Sinnott (2009) was used to determine the capital cost and was as follows:

$$\boldsymbol{Cost_{HX} = 24000 + 46 \times A^{1.2}} \qquad \textbf{Eq. B.1}$$

Where, A is the area of the heat exchanger.

The area of the heat exchanger is determined by using the set of heat transfer coefficient shown in Table B.7 and Eq. B.2.

Table B.7 Table of heat transfer coefficients used to determine the heat exchanger area (Sinnott 2009).

Flue gas transfer coefficient	5000	W/m^2.K
Refrigerant transfer coefficient	750	W/m^2.K
Cooling Water transfer coefficient	3430	W/m^2.K
Overall U Flue gas/Water	2034	W/m^2.K
Overall U Flue gas/Refrigerant	652	W/m^2.K
Overall U Refrigerant/Water	615	W/m^2.K

$$\boldsymbol{A = \frac{Q}{k.\Delta T}} \qquad \textbf{Eq. B.2}$$

Where A is the area of the heat exchanger (m^2)

Q is the duty of the heat exchanger (W)

k is the heat transfer coefficient (W/m^2.K)

ΔT is the temperature difference of the heat exchanger (K)

The total heat exchanger equipment cost was calculated by applying Eq. B.1 to all the heat exchangers throughout the process and the breakdown of the cost of each heat exchanger is shown in Table B.8.

Table B.8 Summary of heat exchangers capital cost for Case II membrane/low-temperature hybrid carbon capture at 90% overall CO_2 recovery rate.

Heat Exchanger	Cost (U$ 2009)
Compression Inter-Cooler 1	$36,019
Compression Inter-Cooler 2	$35,241
Compression Inter-Cooler 3	$34,903
Refrigeration Cycle Cooler 4	$265,741
Stream-to-Stream Heat Exchanger 1	$221,015
Stream-to-Stream Heat Exchanger 2	$27,310
Stream-to-Stream Heat Exchanger 3	$933,009

- **Compressors**

The compressors cost were estimated from a correlation (Eq. B.3) developed by (Ho 2007) and used by Harkin (2012).

$$Cost_{compressor} = 800 * p \qquad \textbf{Eq. B.3}$$

Where p is the power requirement of the compressor (kW)

The total compressor capital cost was calculated by applying Eq. B.3 to all the compressors throughout the process as shown in Table B.9.

Table B.9 Summary of compressors capital cost for Case II membrane/low-temperature hybrid carbon capture at 90% overall CO_2 recovery rate.

Compressor	Cost (million A$ 2007)
Pre-Low-Temp Compressor 1	$15.79
Pre-Low-Temp Compressor 2	$15.72
Pre-Low-Temp Compressor 3	$15.27
Refrigeration Compressor 1	$2.14
Refrigeration Compressor 2	$3.75
Vacuum Pump	$21.66
VSA Blower	$3.77

- **Pump**

Due to the high capacity factor required for the CO_2 pump (approximately 700 m^3.kPa/s), the CO_2 pump for the liquefied CO_2 was cost estimated using a scale up from a similar pump installed in a Benfield plant by Furukawa and Bartoo (1997) as shown in Eq. B.4.

$$Cost_{pump} = 259250 \times \frac{Q}{Q_{ref}} \qquad \textbf{Eq. B.4}$$

Where Q is the volumetric flowrate (m^3/s) and

Q_{ref} is the reference volumetric flowrate of 0.372 m^3/s.

Using this equation, the CO_2 pump for our example was estimated to cost U$61 000 (U$ 1997).

- **Separation Vessels**

Separation vessels were required for the knock-out drums in the pre-low-temperature compression train, where water was removed following each inter-stage cooling. The vessels were estimated from Peters, Timmerhaus and West (2002) and shown in Eq. B.5.

$$\boldsymbol{Cost_{Ko} = 73 \times \left(0.091P^{0.849} + 0.83\right) \times W^{0.66}} \quad \textbf{Eq. B.5}$$

Where, P is the pressure (bar) and

W is the weight of the vessel (kg)

In our example, the knock-out drum is at 332.56 kPa and has a weight of 68480 kg and therefore costs U$362 000 (U$ 2003).

- **VSA Vessels**

The VSA vessels were used for the VSA/low-temperature hybrid carbon capture processes. Due to the high vacuum and flowrate required for the vessels, the vessels were estimated using the same method as absorbers columns by Peters, Timmerhaus and West (2002) and shown in Eq. B.6.

$$\boldsymbol{Cost_{vessel} = 3 \times \left(-2244 + 2956D_v + 1241h + 1205D_v^2 + 913D_v h + 20.93h^2 - 42D_v^2 h + 2.4D_v h^2 - 0.5h^3\right)} \quad \textbf{Eq. B.6}$$

- **Total Capital Costs (CAPEX)**

Using the equations shown above, the total equipment costs can be determined by summing all the values and converting all the currency to the same basis, which is A$ 2011. In the example being studied in the appendix, the total equipment cost was estimated to be A$ 109 million.

The CAPEX was then determined by using the parameters shown in Chapter 3 (Table 3.9). The corresponding evaluated costs for the case example are shown in Table B.10.

Table B.10 Breakdown of capital cost components for carbon capture with values for Case II membrane/low-temperature hybrid carbon capture at 90% overall CO_2 recovery rate.

	Capital cost elements	Nominal value	A$ million
A	Process Equipment Cost (PEC)	Sum of all process equipment	109
B	General facilities	30 % PEC	32.7
	Total Equipment Cost (TEC)	A+B	142

C	Instrumentation	15 % TEC	21.
D	Piping	20 % TEC	28.4
E	Electrical	7 % TEC	9.93
F	Total Installed Cost (TIC)	A + B+ C+ D +E	201
G	Start-up costs	8 % TIC	16.1
H	Engineering	5 % TIC	10.1
I	Owners costs	7 % (F + G + H)	15.9
J	Engineering, procurement, construction and owner's cost	F + G + H + I	243
K	Project Contingency	10 % EPCO	24.4
	TOTAL CAPITAL COST (CAPEX)	= J + K	268

B.4.2 Operating Costs

After calculating the CAPEX, the various operating cost parameters were determined using the parameters discussed in Chapter 3 (Table 3.10).

Table B.11 Breakdown of operating cost components for hybrid carbon capture with values for Case II membrane/low-temperature hybrid carbon capture at 90% overall CO_2 recovery rate.

		Operating cost elements	Nominal value	A$ million
Fixed costs	M	Insurance	2% TCC	5.36
	N	Fixed Operating and Maintenance Costs (FOM)	4% TCC + Ins	16.07
	O	Labour Costs		1.97
Variable costs	P	Cooling Costs		1.18
	R	Membrane Replacement Costs	20% Membrane Capital Cost	0.05
		TOTAL OPERATING COST (OPEX)	= Variable Costs + Fixed costs	19.21

B.4.3 Other Costs

Finally, the cost storing the CO_2 and cost of lost power is determined using the parameters shown in Table 3.11 and equations Eq. B.7 and Eq. B.8.

$$\boldsymbol{Cost_{storage} = \dot{m}_{CO_2 Captured} \times k_{storage}} \quad \textbf{Eq. B.7}$$

$$\boldsymbol{Cost_{lost\ power} = E_{capture} \times Cost_{electricity} \times \Phi} \quad \textbf{Eq. B.8}$$

Where, $k_{storage}$ is the cost factor of storage per tonne of CO_2 ($6.03/t ($CO_2$))

$E_{capture}$ is the electricity used to capture the CO_2 (MW)

$Cost_{electricity}$ is the cost price electricity ($40/MWh) and

Φ is the capacity factor of the power plant (7446 hours)

For our example, the corresponding cost of storage is A$ 11.5 million and the cost of lost power is A$ 31.3 million.

B.4.4 Cash Flow

The project is assumed to operate for 25 years with 2 years for commissioning prior to operation and 1 year for decommissioning following operation, totalling 28 years. The CAPEX is distributed in the first two years in a 40:60 ratio. The OPEX, storage cost and loss of revenue (cost of lost power) starts from the first year of operation (Year 3). The summary table for the real value and the present value (using a discount factor of 7%) is shown in Table B.12and Table B.13 respectively.

Table B.12 Summary of techno-economic parameters from real value for Case II membrane/low-temperature hybrid carbon capture at 90% overall CO_2 recovery rate.

Item	Units	Value
Real CAPEX	$m	268
Real OPEX	$m	480
Real Abandonment	$m	67
Real Lost Revenue	$m	781
Real Storage Costs	$m	288
Real Electricity Production	MWh	3.31E+07
Real CO_2 Captured	t CO_2	4.78E+07
Real CO_2 Avoided	t CO_2	2.81E+07

Table B.13 Summary of techno-economic parameters from present value (discount factor 7%) for Case II membrane/low-temperature hybrid carbon capture at 90% overall CO_2 recovery rate.

Item	Units	Value
PV CAPEX	$m	240
PV OPEX	$m	141
PV Abandonment	$m	10
PV Lost Revenue	$m	318
PV Storage Costs	$m	117
PV Electricity Production	MWh	1.35E+07

PV CO_2 Captured	t CO_2	1.95E+07
PV CO_2 Avoided	t CO_2	1.14E+07

From the values of Table B.13, the cost of capture and storage can be determined as shown in

Table B.14 Summary of techno-economic parameters in terms of \$/t(CO_2 captured) and \$/MWh for Case II membrane/low-temperature hybrid carbon capture at 90% overall CO_2 recovery rate.

Item	Units	Value
\$/t CO_2 avoided (Capture)	\$/tCO_2	62.12
\$/t CO_2 captured (Capture)	\$/tCO_2	36.48
\$/t CO_2 avoided (Storage)	\$/tCO_2	10.27
\$/t CO_2 captured (Storage)	\$/tCO_2	6.03
\$/MWh Storage	\$/MWh	8.69
\$/MWh Capture	\$/MWh	52.60
\$/MWh Lost Revenue	\$/MWh	23.58

The differential cost of electricity (DCOE) can be determined from the ratio of PV total costs vs PV electricity Production and the corresponding cost of CO_2 avoidance is DCOE divided by the amount of CO_2 avoided by the hybrid carbon capture process. Finally, the LCOE is the sum of the DCOE and the current cost price of electricity. The values for the example is shown in

Table B.15 DCOE, cost of CO_2 avoidance and LCOE for Case II membrane/low-temperature hybrid carbon capture at 90% overall CO_2 recovery rate.

Item	Units	Value
DCOE	\$/MWh	61.29
Cost of CO_2 avoidance	\$/tCO_2	72.39
LCOE	\$/MWh	101.26

References

Amrollahi, Z, Ertesvåg, IS & Bolland, O 2011, 'Optimized process configurations of post-combustion CO2 capture for natural-gas-fired power plant-Exergy analysis', *International Journal of Greenhouse Gas Control*, vol. 5, no. 6, pp. 1393-405.

Aspelund, A, Mølnvik, MJ & De Koeijer, G 2006, 'Ship Transport of CO2: Technical Solutions and Analysis of Costs, Energy Utilization, Exergy Efficiency and CO2 Emissions', *Chemical Engineering Research and Design*, vol. 84, no. 9, pp. 847-55.

Coker, D, Freeman, B & Fleming, G 1998, 'Modeling multicomponent gas separation using hollow ‐ fiber membrane contactors', *AIChE journal*, vol. 44, no. 6, pp. 1289-302.

Cuthbertson, R, Scholes, CA & Kentish, S 2010, 'Simulation of Membrane Operations with Aspen HYSYS', in *CO2CRC Research Symposium*, Melbourne.

Furukawa, S & Bartoo, R 1997, 'Improved Benfield process for ammonia plants', *Universal Oil Products, Des Plaines, USA*.

GPSA, S 2004, 'Engineering data book', *Gas Processors Suppliers Association*, pp. 16-24.

Harkin, T 2012, 'Multi-Objective Optimisation of CCS using simulation, heat integration and cost estimation', Doctor of Philosophy thesis, Monash University.

Hatcher, P, Khalilpour, R & Abbas, A 2012, 'Optimisation of LNG mixed-refrigerant processes considering operation and design objectives', *Computers and Chemical Engineering*, vol. 41, no. 0, pp. 123-33.

Ho, MT 2007, 'Techno-economic modelling of CO2 capture systems for Australian industrial Sources', Doctor of Philosophy thesis, UNSW.

Moore, JJ & Nored, MG 2008, 'Novel concepts for the compression of large volumes of carbon dioxide', in vol. 7, pp. 645-53.

Peters, MS, Timmerhaus, KD & West, RE 2002, *Plant Design and Economics for Chemical Engineers*.

Pfaff, I, Oexmann, J & Kather, A 2010, 'Optimised integration of post-combustion CO2 capture process in greenfield power plants', *Energy*, vol. 35, no. 10, pp. 4030-41.

Sanpasertparnich, T, Idem, R, Bolea, I, deMontigny, D & Tontiwachwuthikul, P 2010, 'Integration of post-combustion capture and storage into a pulverized coal-fired power plant', *International Journal of Greenhouse Gas Control*, vol. 4, no. 3, pp. 499-510.

Shukri, T 2004, 'LNG technology selection', *Hydrocarbon Engineering*, vol. 9, no. 2, pp. 71-6.

Sinnott, RK 2009, *Chemical engineering design: SI Edition*, Elsevier.

Xiao, G & Webley, P 2013, *VSA Zeolite 13X Experimental Results*.

C. Publications

C.1 Chemeca 2013 Conference Proceedings

Optimisation of a Hybrid CO_2 Purification Process

Jean Christophe Li Yuen Fong[1, 2], Clare Anderson[1, 3], Andrew Hoadley[1, 2]

[1]Cooperative Research Centre for Greenhouse Gas Technologies (CO2CRC)
[2]Department of Chemical Engineering, Monash University, Clayton, VIC 3800
[3]Department of Chemical and Biomolecular Engineering, The University of Melbourne, VIC 3010

ABSTRACT

Multi-stage compression is the normal method to achieve pipeline pressures of 100 bara for the transport of carbon dioxide (CO_2) after capture in a carbon capture and storage (CCS) scheme. An alternative method is to partially compress the gas, liquefy it and then pump the liquid CO_2 to the required pressure. The advantage of this process is that the CO_2 stream can be further purified through liquefaction and this allows separation processes that do not produce a pure CO_2 product such as vacuum swing adsorption (VSA) and membranes to be considered. In this study, the following two cases were analysed:

1) **VSA as the primary separation process followed by a liquefaction process**

2) **VSA as the primary separation process followed by liquefaction and a membrane process**

Cryogenic conditions are required to liquefy the CO_2 and this was achieved by using a mixed refrigerant process comprising ethane and propane.

Multi-objective optimisation was performed on the hybrid systems to determine the minimum power for the maximum CO_2 yield for each case.

Key words: Carbon capture and storage, Cryogenics, Process Optimisation, Multi-objective optimisation

I. INTRODUCTION

A. *Carbon Capture and Storage (CCS)*

Carbon capture and storage (CCS) involves the capture of carbon dioxide (CO_2) gas from within a CO_2 generation process, compressing it into a supercritical fluid and finally sequestrating it. Fossil fuel combustion for energy production is a major source of CO_2 emissions and therefore considered a good opportunity for CCS[1]. The capture of CO_2 can be divided into three main categories: post-combustion capture, pre-combustion capture and oxy-fuel combustion. This research will focus on post-combustion capture and the energy associated with separating and compressing the CO_2 stream.

1) *Separation processes*

In post-combustion capture, CO_2 needs to be separated from the flue gas, which would typically consist of mostly N_2 and CO_2 and some impurities such as oxygen, SO_x, NO_x and water vapour. Leading the carbon capture technologies are: solvent absorption, adsorption and membrane technology. Among those three technologies, solvent absorption is the currently the most prominent due to the fact that it can produce high purity CO_2 streams, which is a major challenge for both adsorption and membrane processes. An established MEA solvent absorption separation system requires approximately 4 GJ_{th}/(t CO_2 recovered) [2]. However, adsorption and membrane technologies are relatively newer technologies and show promising features such as smaller equipment requirement and potentially lower energy requirement compared with solvent absorption. Furthermore, using hybrid technologies, a combination of different capture technologies, also show potential as CO_2 capture technologies and are further discussed in the following Section A.3.

2) *Cryogenic Purification*

Once the CO_2 is separated from the flue gas, the CO_2 gas must be compressed into a supercritical fluid for transport and injection into the storage site. The conventional method to compress the CO_2 would be by using a traditional multi-stage compression. However, this study will look into using cryogenic compression, which partially compresses the CO_2 gas stream and then liquefies the stream by cooling it to cryogenic conditions. Finally, the liquid CO_2 is then pumped to the required pressure. This has the advantage of the lower energy requirement of pumps as opposed to compressors and more importantly, allows the purification of the CO_2 stream by using the difference in condensation temperatures of CO_2 and N_2 gas.

In order to have a high recovery of CO_2 from the cryogenic purification, a refrigeration system that cools to approximately -60°C is required. In this paper, a binary mixture of propane and ethane refrigerant in a mixed refrigeration cycle was used.

3) *Hybrid Processes*

Hybrid systems consist of two or three CO_2 separation technologies combined to separate the CO_2 from the process stream. This allows the different technologies to complement each other to negate the disadvantages of the other. In this study, as shown in Fig 1, the hybrid CO_2 separation process

involves using vacuum swing adsorption (VSA) followed by further purification from cryogenic separation. This allows the low purity yield from the VSA to be purified by the cryogenic process. Additionally, further purification of the waste stream from the cryogenic process is accomplished by a membrane process as seen in Fig 2. In both figures, decision variables used in the optimization are denoted as DV.

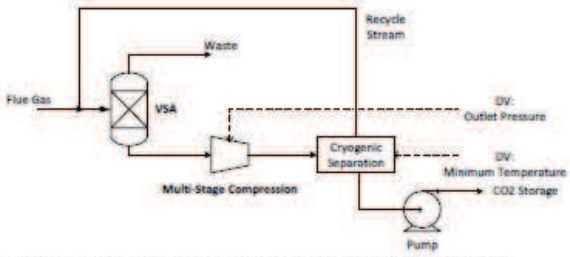

Figure 1. Schematic Diagram of VSA & Cryogenic Process without membranes (Case 1)

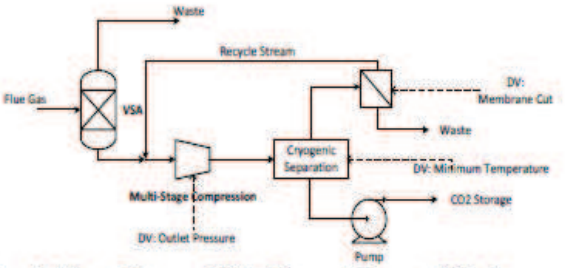

Figure 2. Schematic Diagram of VSA & Cryogenic Process with Membranes (Case 2)

An activated carbon VSA system is assumed to allow any impurities including water to pass through the adsorption bed so that only a binary mixture of CO_2 and N_2 is adsorbed. The values of CO_2 recovery and purity assumed are given in Tab IV. The VSA electrical power requirement was set at 0.62 GJ/(t CO_2 recovered) for each case[3].

The variables that affect the performance of the membrane are the membrane area, permeate outlet pressure and membrane characteristics (selectivity and permeability) which were obtained by taking values of high performance polymer membranes [4]: P_{CO2} = 2000 barrer, α_{CO2N2} = 50. The feed conditions into the membrane module were fixed by the upstream process. The permeate outlet pressure was set to be equal to the VSA outlet to maximize the pressure drop. Finally, the membrane cut, which also determines the area of the membrane, was assumed to be a degree of freedom in the process optimisation.

B. Process optimisation of hybrid processes

Process optimisation is an integral part of any chemical engineering process. Although a process can be optimised for one objective at a time (single objective optimisation, SOO), there are usually multiple objectives that need to be considered simultaneously. This is known as multi-objective optimisation, which refers to finding values of decision variables (DV) which correspond to and provide the optimum of more than one objective [5].

The purpose of using multi-objective optimisation in this paper is that whilst maximising the overall recovery of CO_2 is an obvious objective for a capture system, increasing the recovery usually increases the total work required as well. Therefore, in order to have the best capture system, it is important to determine the minimum power requirement for the maximum CO_2 yield for each case. However, since the two objectives are inversely proportional, there will not be a single best solution, but a series of solutions, called Pareto-optimal solutions and this provides the relationship between the two objectives. The decision variables used in this study can be seen in Fig 1, Fig 2 and in Tab I.

II. MODEL AND SIMULATION FRAMEWORK

In order to optimise the two processes, the processes were configured and simulated on Aspen HYSYS® and the multi-objective optimisation was set up using Microsoft Excel visual basic. This study used the flue gas composition that would typically come from a sub-bituminous black coal 250 MW power station, where the flue gas has been cooled to allow most of the water to be condensed. The flue gas conditions and composition are presented in Tabs I and II.

As mentioned in section I, there were two hybrid cases studied:

Case 1 (Fig 1): Flue gas purification using VSA, followed by a three-stage compression, cryogenic separation with the waste stream being recycled to the feed flue gas. In this case study, there were four design variables which can be seen in Tab I. The objective variables that were optimised were the total shaft work of the whole process (MW) and the overall recovery rate of the process.

TABLE I: FLUE GAS PROCESS FEED COMPOSITION

Material Streams Mole Fraction	
Nitrogen	0.712
CO2	0.112
Oxygen	0.051
SO2	0.002
NO2	0.001
H2O	0.122

TABLE II: FLUE GAS FEED CONDITIONS

Material Streams Conditions		
Vapour Fraction		1.000
Temperature	C	50.3
Pressure	kPa	103.0
Molar flow	kgmole/h	5.78e4
Mass Flow	kg/h	1.67e6

Case 2 (Fig 2): Flue gas purification using VSA, followed by a three-stage compression, cryogenic compression with the waste stream being further purified using a membrane process and the permeate is recycled to the feed flue gas while the retentate is purged. In addition to the four decision variables used in case 1, the membrane cut was also used as a decision variable. The membrane cut is the ratio of the permeate flow to inlet flow (F_P/F_{in}). The objective variables that were optimised were the same as case 1: total shaft work of the whole process (MW) and the overall recovery rate of the process.

In addition to the information given in Tabs I to III, the compressor efficiency for the comparison case was assumed to be 75% and the minimum cooling water approach temperature was assumed to be 40C. Furthermore, the VSA recovery rate and outlet purity values were allowed vary as shown in Tab IV.

TABLE III: TABLE OF DECISION VARIABLES RANGE: CASE 1 AND CASE 2.

Design Variables:		Minimum	Maximum
Ethane Molar Fraction	Case 1	0	0.7
	Case 2	0	0.7
Ref Molar flow (mol/s)	Case 1	0.2	1.4
	Case 2	0.2	1.4
Feed Out Temp(°C)	Case 1	-60	-40
	Case 2	-60	-40
Pressure (kPa)	Case 1	1500	5000
	Case 2	1500	3000
Membrane Cut	Case 1	N/A	N/A
	Case 2	0.2	0.4

TABLE IV: VSA RECOVERY RATE AND OUTLET PURITY VALUES

Recovery Rate (%)	CO_2 Purity in Outlet (%)
75	75
80	70
70	80

III. RESULTS

A. *Pareto Charts*

The Pareto charts for a VSA with recovery rate of 75%, are shown for each design variable as a function of the recovery rate in the following figures.

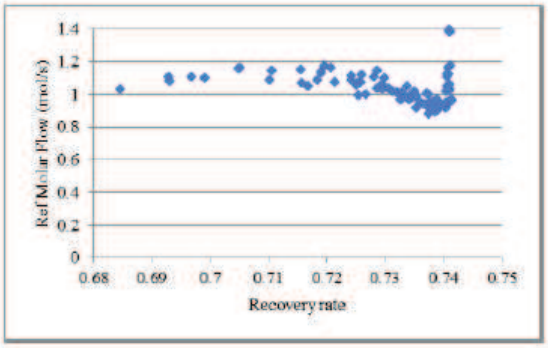

Figure 3. Refrigeration molar flow versus recovery rate - case 1

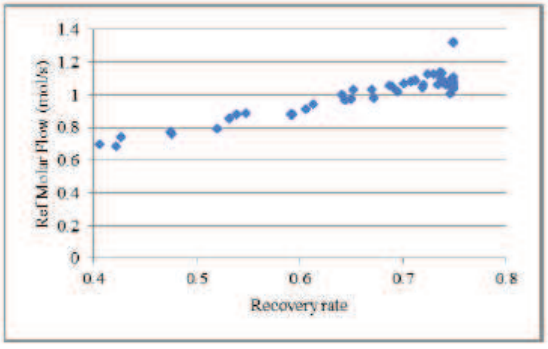

Figure 4. Refrigerant molar flow rate versus recovery rate - case 2

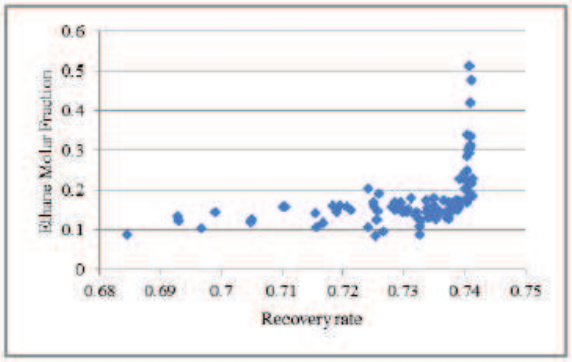

Figure 5. Refrigerant ethane molar fraction versus recovery rate - case 1

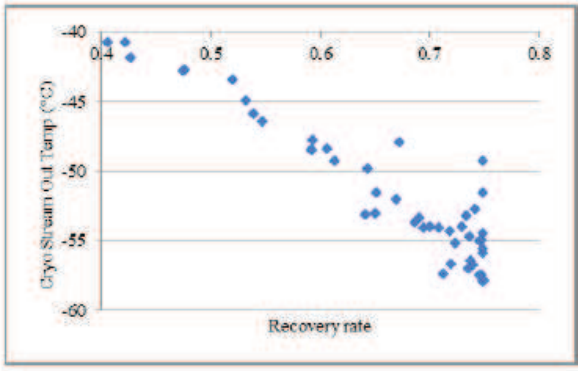

Figure 8. Cryogenic separator temperature versus recovery rate - case 2

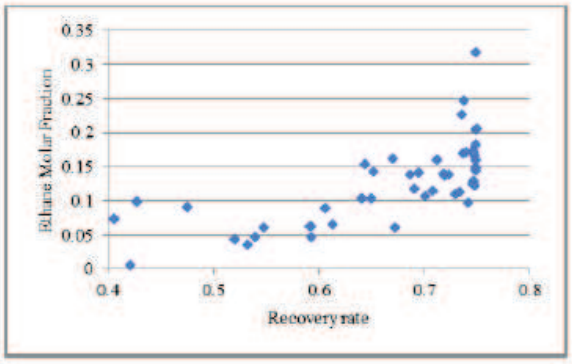

Figure 6. Refrigerant ethane molar fraction versus recovery rate - case 2

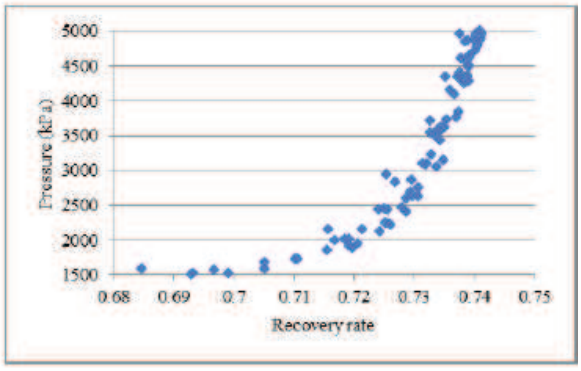

Figure 9. Process stream compression pressure versus recovery rate - case 1

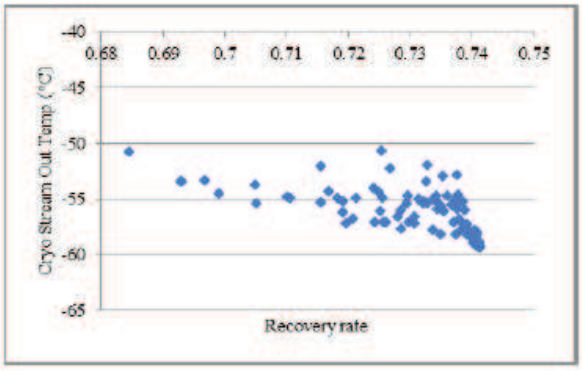

Figure 7. Cryogenic separator temperature versus recovery rate - case 1

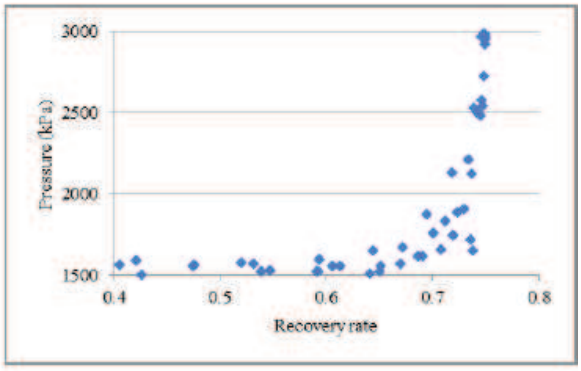

Figure 10. Process stream compression pressure versus recovery rate - case 2

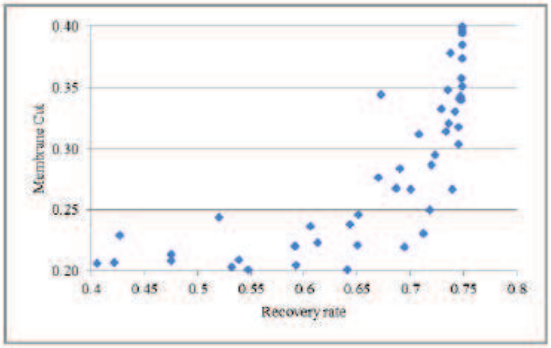

Figure 11. Membrane cut versus recovery rate - case 2

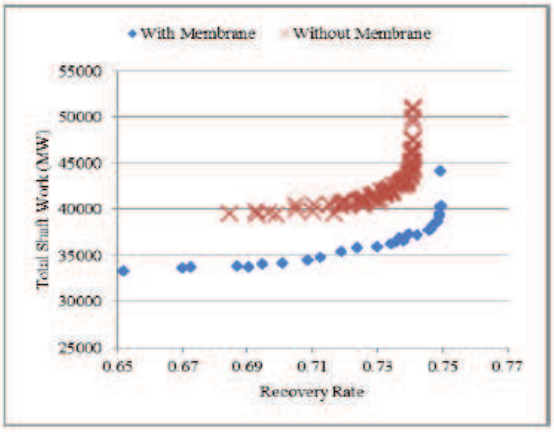

Figure 12. Pareto chart of total shaft work (MW) versus recovery rate for hybrid process for both cases (Recovery rate axis has been truncated at 0.65 for case 2)

B. Influence of Recovery and Purity from VSA unit

As mentioned in section 2, three values of VSA recovery rate and purity (Tab IV) were used in order to study the influence of the VSA performance on the overall recovery rate and total shaft work required. The Pareto charts for each VSA value can be seen in Figs 13 and 14 for case 1 and Figs 15 and 16 for case 2.

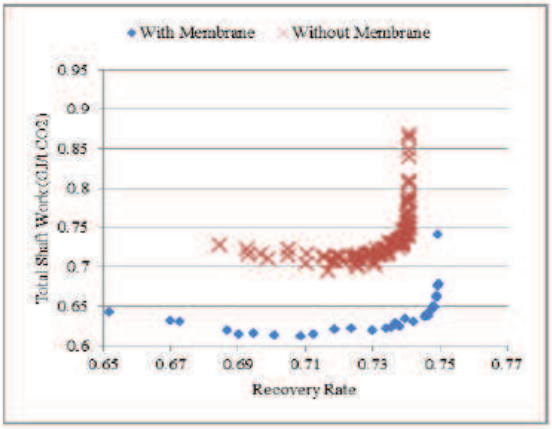

Figure 13. Pareto chart of specific total shaft work (GJ/t CO2) versus recovery rate for hybrid process for both cases (Recovery rate axis has been truncated at 0.65 for case 2)

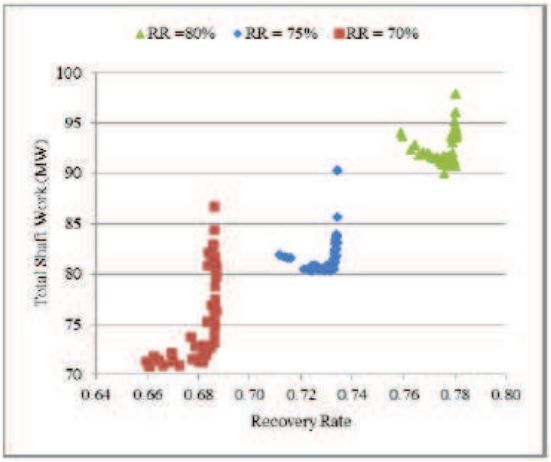

Figure 14. Graph of total shaft work (MW) versus recovery rate sensitivity analysis of different VSA recovery rate and VSA purity outlet for case 1 (Recovery Rate = 80%, Purity = 70%; Recovery Rate = 75%, Purity = 75%; Recovery Rate = 70%, Purity = 80%)

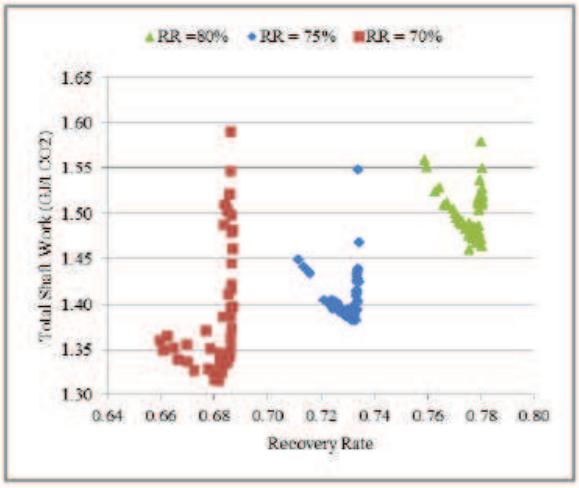

Figure 15. Graph of total specific shaft work (GJ/t CO2) versus recovery rate sensitivity analysis of different VSA recovery rate and VSA purity outlet for case 1(Recovery Rate = 80%, Purity = 70%; Recovery Rate = 75%, Purity = 75%; Recovery Rate = 70%, Purity = 80%)

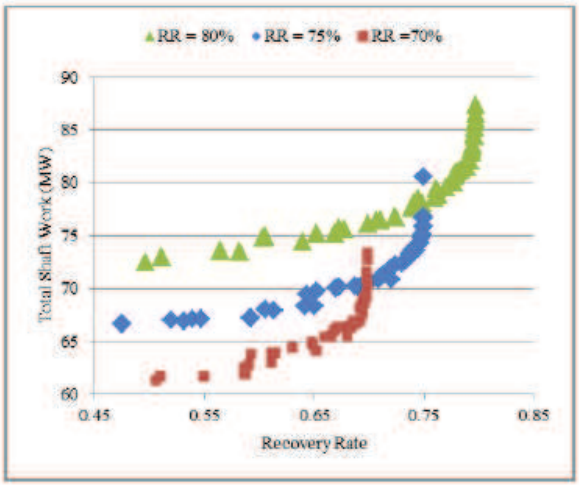

Figure 16. Graph of total shaft work (MW) versus recovery rate sensitivity analysis of different VSA recovery rate and VSA purity outlet for case 2 (Recovery Rate = 80%, Purity = 70%; Recovery Rate = 75%, Purity = 75%; Recovery Rate = 70%, Purity = 80%) (Recovery rate axis has been truncated at 0.45 for case 2)

IV. DISCUSSION

A. *Pareto Charts*

The Pareto Charts for the refrigerant flow rate versus recovery rate and refrigerant ethane molar fraction for both cases (Figs 3-6) show that those two variables do not have a significant effect at low recovery rates. However at high recovery rates, both the refrigerant flow rate and refrigerant ethane molar fraction increase exponentially. This can be explained from the temperature and pressure Pareto charts.

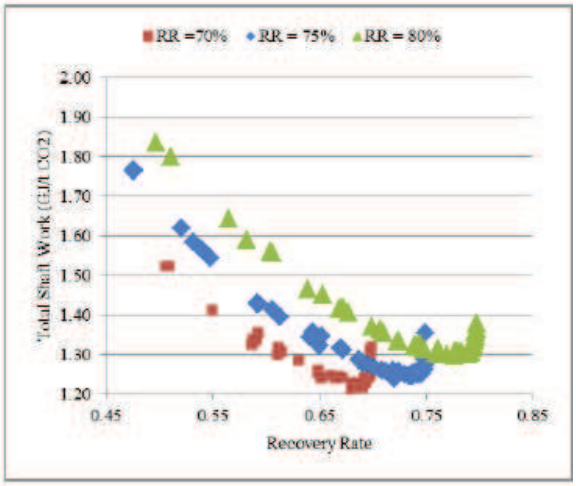

Figure 17. Graph of total specific shaft work (GJ/t CO2) versus recovery rate sensitivity analysis of different VSA recovery rate and VSA purity outlet for case 2(Recovery Rate = 80%, Purity = 70%; Recovery Rate = 75%, Purity = 75%; Recovery Rate = 70%, Purity = 80%) (Recovery rate axis has been truncated at 0.45 for case 2)

From the temperature versus recovery rate Pareto chart, Fig 7 and Fig 8, it can be observed that the points tend to clutter at the lowest temperature, but do not go below -59.2°C (case 1) and -57.2°C (case 2). This is due to the fact that at lower temperatures, more CO_2 can be liquefied and separated at the cryogenic section but the minimum temperature is limited by the constraint imposed to prevent CO_2 freeze out by not operating below this temperature, which is also a function of pressure. Therefore, higher pressures would be preferable to lower the CO_2 freeze out temperature. This is observed in the pressure versus recovery rate Pareto chart, Fig 9 and Fig 10, which show that the pressure has an exponential relationship with the recovery rate.

Figs 12 and 13 compare the total work required (MW) and total specific work required (GJ/t CO_2) respectively for both case 1 and case 2. It can be seen that case 2, which includes a membrane, has a wider lower range of recovery rate than case 1. This is due to the additional waste stream which exits from the membrane unit which also loses CO_2 and thus reduces the recovery rate. Furthermore, it can be observed that when the recovery rate is approximately 73% and lower, case 2 requires less shaft work and specific shaft work than case 1. This can be explained by the fact that the membrane process is effectively using the high pressure stream coming out of the cryogenic process to further purify the stream.

B. *VSA Recovery Rate*

Section 3.3 compares the total shaft work and total specific shaft work versus recovery rate Pareto charts with varying VSA recovery rate values for both case 1 and case 2. Fig 14 and Fig 15 show the influence of VSA performance for case 1, and Fig 16 and Fig 17, which show the sensitivity analysis for case 2. It can be observed that with the range of the decision variables provided, the VSA recovery rate distinctively dictates the overall recovery rate. Also, as expected, as the VSA recovery rate increases, the total work required increases. However, for case 2, the graphs overlap each other which allow a higher flexibility for each of the VSA recovery rate cases.

Furthermore, for the total specific work required for both cases, Fig 15 and Fig 17, it can be seen that there is minimum value for each VSA recovery rates values. Therefore, there is a theoretical minimum value that can be achieved for the overall recovery rate that is represented by the dotted lines. This can be useful when comparing different VSA capture systems performances.

CONCLUSIONS

In conclusion, it can be observed that the cryogenic separator temperature and pressure are the decision variables that affect the two cases the most. Furthermore, the lowest temperature is limited by the freeze out temperature, which is a function of the pressure of the stream exiting the compression unit. Due to this limiting factor, the other decision variables increase rapidly at high recovery rates.

The VSA recovery rate sets the maximum overall recovery rate possible by the system for case 1 but has a less prominent influence on the overall recovery rate in case 2 due to the additional waste stream in the membrane operation.

Although each case has a Pareto chart for the total work versus recovery rate, there was an optimum operating point for the minimum amount of specific work required.

To compare the performance of the VSA/cryogenic system, the values can be compared to an established MEA solvent absorption separation system, which requires approximately 4 GJ_{th}/(t CO_2 recovered) [2] (1.3 GJ_e/(t CO_2 recovered)) with a recovery rate of approximately 90%. Since the solvent absorption has a high recovery rate, the optimum point for the minimum specific work required for VSA system with an 80% recovery rate was chosen. Therefore, the VSA/Cryogenic system with membrane purification with a 75.9% overall recovery rate was selected. Although the absorption system has a significantly higher recovery rate at 90%, the hybrid system has slightly a slightly lower specific work requirement.

Currently there is active research into the optimization of activated carbon adsorption systems, which hold potential for reducing the work below the value of 0.62 GJ/(t CO_2 recovered) assumed in this study. Furthermore, due to the small equipment sizes of the hybrid system, a full economic analysis should be performed to determine whether the hybrid process is competitive with the cost of a solvent absorption process.

ACKNOWLEDGEMENT

The author would like to thank the Australian Government for funding this CO2CRC program through the CRC program as well as all the CO2CRC partners for their support.

REFERENCES

1. "Carbon dioxide capture and storage: Special report of the intergovernmental panel on climate change". 2005: Cambridge University Press.
2. B. Belaissaoui, et al., "Hybrid membrane cryogenic process for post-combustion co2 capture". Journal of Membrane Science. (0), 2012.
3. J. Zhang, P.A. Webley, and P. Xiao, "Effect of process parameters on power requirements of vacuum swing adsorption technology for co2 capture from flue gas". Energy Conversion and Management. **49**(2): p. 346-356, 2008.
4. B.T. Low, et al., "A parametric study of the impact of membrane materials and process operating conditions on carbon capture from humidified flue gas". Journal of Membrane Science. **431**(0): p. 139-155, 2013.
5. G.P. Rangaiah, "Multi-ojective optimization. Techniques and applications in chemical engineering". Advances in process systems engineering. 2009 Vol. 1. World Scientific Publishing Co. Pte. Ltd.

C.2 PRES 2014 Conference Proceedings (Chemical Engineering Transactions)

CHEMICAL ENGINEERING TRANSACTIONS
VOL. 39, 2014
A publication of AIDIC
The Italian Association of Chemical Engineering
www.aidic.it/cet
Guest Editors: Petar Sabev Varbanov, Jiří Jaromír Klemeš, Peng Yen Liew, Jun Yow Yong

ISBN 978-88-95608-30-3; **ISSN** 2283-9216

Multi-Objective Optimisation of Hybrid CO_2 Capture Processes using Exergy Analysis

Jean C. Li Yuen Fong[a,b], Clare Anderson[a,c], Barry Hooper[a], Gongkui Xiao[a], Paul Webley[a,c], Andrew Hoadley*[a,b]

[a]Cooperative Research Centre for Greenhouse Gas Technologies (CO2CRC)
[b]Department of Chemical Engineering, Monash University, Clayton, VIC 3800
[c]Department of Chemical Engineering and Biomolecular Engineering, The University of Melbourne, VIC 3010
andrew.hoadley@monash.edu

Carbon dioxide (CO_2) purification is an essential step in the carbon capture and storage (CCS) process. The leading technology consists of a solvent absorption carbon capture process followed by a multi-stage CO_2 gas compression into supercritical state for sequestration. This study considers a hybrid system of vacuum swing adsorption (VSA), membranes and cryogenic separation. Replacing the multi-stage gas compression with the cryogenic separation has two main advantages: firstly, it further purifies the CO_2 stream, which is valuable for both VSA and membrane processes since both processes struggle to achieve high purity product. Secondly, it produces liquid CO_2 that can be pumped to the supercritical state, which is required for transport and sequestration. Due to the higher degree of freedom available in hybrid processes, a new methodology using multi-objective optimisation combined with exergy analysis was used to optimise the process. This allowed different decision variables to be considered and studied to find the range of optimum operating conditions for each capture processes. It was determined that the refrigerant flow rate, multi-stage compression and process stream minimum temperature had the biggest impact on the recovery rate. Furthermore, it was observed that the total specific shaft work had a linear relationship with the specific exergy loss rate.

1. Introduction

The negative effects of greenhouse gases (GHG) in the atmosphere have been widely reported. The IPCC fifth assessment report increased the scientific certainty that changes in the anthropogenic CO_2 concentrations and atmospheric temperature are related (Edenhofer and Seyboth, 2013). Therefore, reduction of CO_2 from major sources such as fossil fuel power generation is critical. Among a portfolio of technologies required to mitigate those emissions, integration of Carbon Dioxide Capture and Storage (CCS) into coal fired power stations is a technology that can significantly reduce the carbon emissions from stationary sources. Post-combustion CCS involves the separation and capture of the CO_2 from the flue gas generated by the power plants, compressing the separated CO_2 into a supercritical fluid and then storing it in geological structures such as deep saline formations.

In order to implement CCS, equipment needs to be installed to capture and compress the carbon dioxide. Heat and electrical energy are required to operate the equipment, which reduces the efficiency of the power plant. The main CO_2 capture methods involve: solvent absorption, adsorption, membranes, cryogenic separation and hybrid processes. (Pires et al., 2011), each of these technologies has different advantages and disadvantages. For example, solvent absorption can achieve the high CO_2 purity and recovery rate by having a high solvent loading, however this comes at a high recovery heat energy required to regenerate the solvent. Furthermore, high solvent loading also requires larger equipment. On the other hand, vacuum swing adsorption (VSA) and membrane processes, on principal, require smaller equipment sizes due to their separation mechanisms. However, both of these processes draw a large amount of electrical energy. It is possible that by combining two or more capture processes, the advantages and disadvantage of each process can complement each other to have a better overall

performance. Several studies have investigated different configurations of hybrid process; Scholes et al. (2013) n, Belaissaoui et al. (2012). In the former hybrid which involved a solvent membrane system, the hybrid performed better in terms of both energy consumption and CAPEX than the membrane process but could not match the base MEA solvent absorption. Similarly, in the second study involving membranes and cryogenic separation, the hybrid process improved the energy efficiency of the individual capture processes, but still underperformed when compared to an MEA process. While energy analysis has been predominantly used to assess the performance of a process, exergy analysis has also been used (Hagi et al., 2013).

This work aims to optimise the integration of post-combustion hybrid carbon capture with exergy performance and CO_2 recovery rate as the two main performance indicators. In order to do so, a combination of simulation and multi-objective optimisation is used.

2. Methodology and Framework

The post-combustion flue gas properties were based on a 300 MW sub-bituminous coal-fired power station. The flue gas was then assumed to have been pre-treated to remove the impurities and water, to result in a stream composed of a binary mixture of CO_2 and N_2 as shown in Table 1.

The hybrid capture process investigated in this study was a combination of Vacuum Swing Adsorption (VSA), cryogenics and membrane, as shown in Figure 1. All simulations were performed using the Aspen HYSYS® software package, version 8.4, using the Peng-Robinson fluid package throughout the whole capture process plant. The VSA electrical power requirement, which uses the VSA CO_2 recovery rate and CO_2 outlet purity as the input variable was used according to the following mathematical model represented in equations 1-3 (Xiao and Webley, 2013).

$$\text{Blower Power} = 2.06 - 5.37E\text{-}02x + 1.08E\text{-}02y + 3.58E\text{-}04x^2 - 1.05E\text{-}04xy \quad (1)$$

$$\text{Vacuum Pump Power} = 4.55 - 1.21E\text{-}01x + 2.66E\text{-}02y + 8.18E\text{-}04x^2 - 2.61E\text{-}04xy \quad (2)$$

$$\text{Total power} = \text{Blower Power} + \text{Vacuum Pump Power} \quad (3)$$

Where x is the CO_2 recovery rate and y is the CO_2 outlet purity

The CO_2 outlet stream from the VSA was partially compressed in a three-stage compression with inter-cooling using cooling water. In order to achieve cryogenic temperatures in the cryogenic separation, a mixed ethane/propane refrigeration system was used. The membrane process was a module based on mass transfer equations, specifically developed for applications in carbon capture simulations.

There are a number of key operating conditions, known as decision variables, in those capture processes that can be varied to observe the impact that the capture processes have on the two objectives (exergy loss rate and overall CO_2 recovery rate of the hybrid process). Therefore, MOO would be a useful tool to take into consideration those decision variables as it provides a range of solutions, called the 'Pareto-Optimal' solutions. Using this range of solutions, the user can make the final selection by either looking at the impact the decision variables have on the optimised solution or by performing further analysis on the optimised solutions.

In this MOO, seven decision variables were allowed to be varied including: refrigerant ethane molar fraction, refrigerant molar flow, cryogenic process stream outlet temperature, multi-stage compression pressure and the membrane cut. Table 2 shows the range of values that those decision variables were allowed to vary for the hybrid capture process.

Table 1: Post-combustion flue gas properties based on a 300 MW sub-bituminous coal fired power station after pre-treatment

Feed Conditions		
Vapour Fraction		1.00
Temperature	(°C)	50.3
Pressure	(kPa)	103
Molar Flow	(kmol/h)	5.78e4
Mass Flow	(kg/h)	1.67e6
Composition	(mol frac)	
CO2		0.64
N_2		0.36

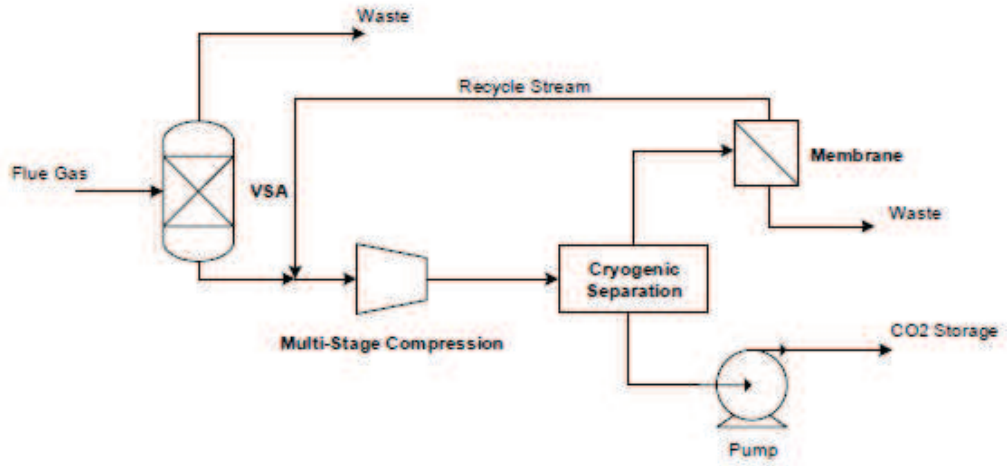

Figure 1: Schematic diagram of VSA, cryogenics and membrane hybrid carbon capture process

Table 2: Table of decision variable range for MOO of the hybrid process

Decision Variable		Minimum	Maximum
Refrigerant Ethane Molar Fraction		0	0.4
Refrigerant Molar Flow	(mol/s)	0.2	1.7
Cryogenic Process Stream Outlet Temperature	(°C)	-60	-30
Multi-Stage Compression Pressure	(kPa)	500	4000
VSA CO_2 Recovery Rate	%	95	98
VSA CO_2 Outlet Purity	%	62	65

All other process unit conditions were operated using default HYSYS parameters where applicable. The compression stage for both the multi-stage compression and refrigerant compression had an efficiency of 75%, with inter-stage coolers using cooling water with an approach temperature of 40°C and a pressure drop of 40kPa. The heat exchangers in the cryogenic separation were plate-fin heat exchangers with a pressure drop of 50kPa on both the process side and refrigerant side.

3. Results

3.1 Decision Variables Pareto Charts

The Pareto charts of the first four decision variables are shown in Figure 2.

3.2 Objective Variables Pareto Charts

The Pareto charts of the objective variables are shown in Figure 3(a).

From the objective variables Pareto charts, it could be observed that with increasing recovery rate, there was an increase in exergy loss rate. Therefore, in order to better understand the exergy loss rate with respect to the amount of CO_2 being captured by hybrid capture process, a new graph of specific exergy loss rate v/s recovery rate was generated (Figure 3(b)), where specific exergy loss rate is the exergy loss rate per mass of CO_2 being recovered by the process.

3.3 Additional Results

In addition to the decision variables and objective variables, other key process performance variable were also recorded while performing the MOO. Two of those variables can be seen in Figure 5(a) and 5(b), which were the 'total shaft work required' and the 'total specific shaft work required'. This enabled a relationship between the exergy loss rate and the total shaft work required to be examined from the Figure 6. Finally, the third variable that was monitored was the exergy coefficient of performance (COP), which is the ratio of exergy going out and exergy going in and can be seen in Figure 7.

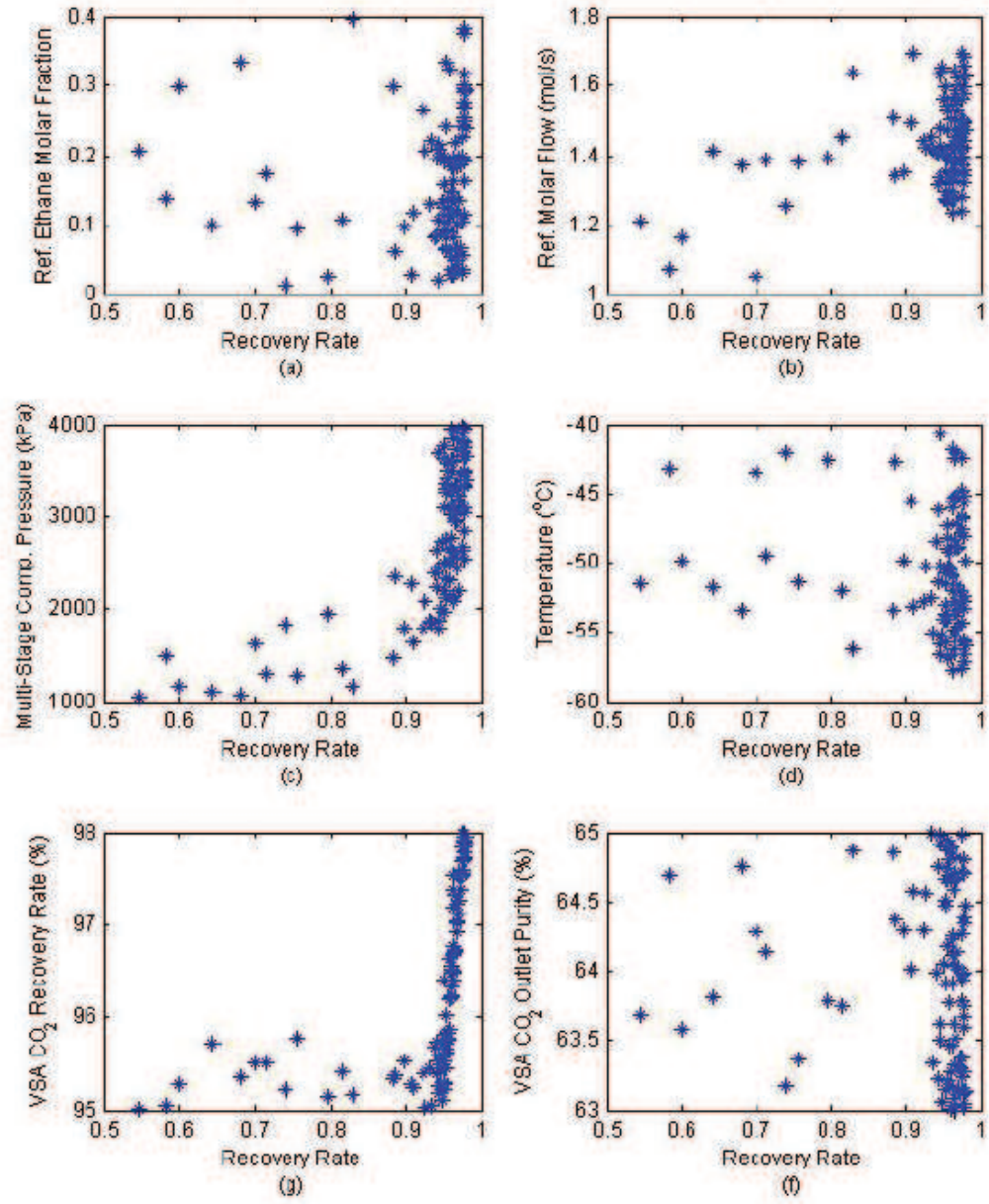

Figure 2(a) Graph of ethane molar fraction versus recovery rate Pareto Chart; 2(b) Graph of refrigerant molar flow (mol/s) versus recovery rate Pareto Chart; 2(c) Graph of multi-stage compression pressure (kPa) versus recovery rate Pareto Chart; 2(d) Graph of process stream minimum temperature (°C) versus recovery rate Pareto Chart; 2(e) Graph of VSA CO_2 Recovery Rate versus recovery rate Pareto Chart; 2(f) Graph of VSA CO_2 outlet purity versus recovery rate Pareto Chart.

4. Discussion

It can be seen from Figure 2 that most decision variables seem to have a scattered effect over the recovery rate except for two main decision variables; multi-stage compression pressure and the VSA CO_2 recovery rate. The higher compression pressure increases the partial pressure of CO_2 and therefore facilitates the separation of CO_2 from nitrogen. Also important is the pressure of the stream, which lowers the CO_2 freeze out temperature, which effectively allows the stream to be cooled to the lowest temperature possible before forming solid CO_2. Finally, the VSA CO_2 recovery rate dictates the overall recovery rate since the CO_2 lost in the waste stream from the VSA cannot be recovered.

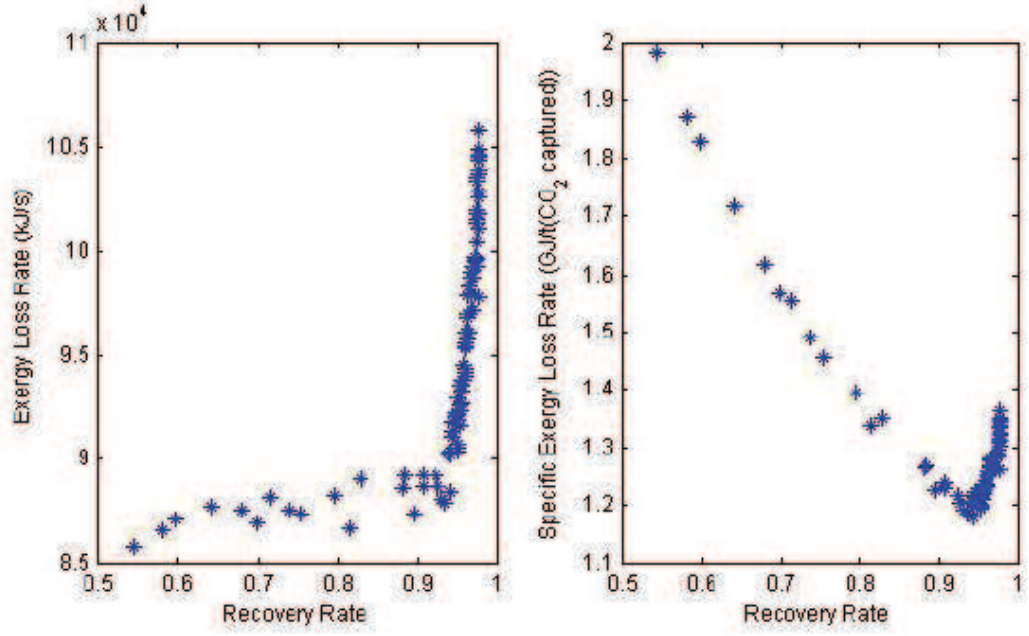

Figure 3(a): Graph of objective variables exergy loss rate (kJ/s) versus recovery rate; 2(b): Graph of specific exergy loss rate (kJ/s) versus recovery rate.

As expected from Figure 3(a), the exergy loss rate increased with increasing recovery rate. That can be explained by the increase in exergy required in the compressors in the multi-stage compression of the process strea. Figure 3(b) shows that the rate of exergy loss is lower than the rate of CO_2 being captured and thus the specific exergy loss rate decreases with increasing CO_2 being captured. Interestingly Figure 3(b) shows that the specific exergy loss rate has a minimum point at a recovery rate of approximately 95% and total specific exergy loss rate of around 1.6 GJ/t (CO_2 recovered).

Figure 4(a) and 4(b) yielded results that were similar to Figure 3(a) and Figure 3(b), which means that the total shaft work required and exergy loss rate have a linear relationship. This was further proven in Figure 5, where the total specific exergy loss rate and total specific shaft work required showed a linear graph. This relationship can be explained by the fact that most of the exergy input is from the shaft work in the compressors.

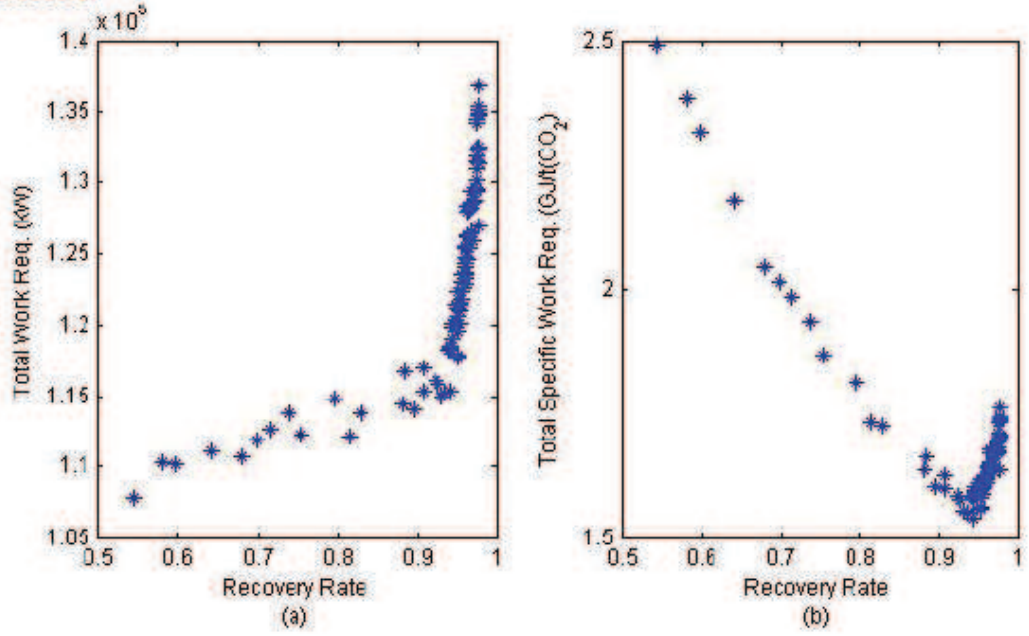

Figure 4(a): Graph of total shaft work required (kW) versus recovery rate. (b): Graph of specific shaft work required (kJ/t (CO_2)) versus recovery rate.

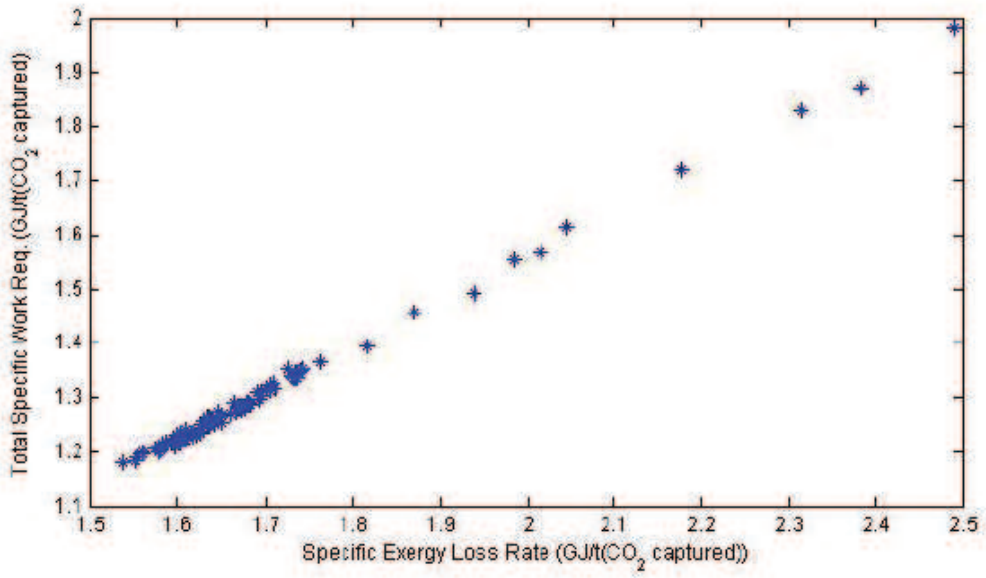

Figure 5: Graph of total specific shaft work required (kJ/t (CO2)) v/s specific exergy loss rate (MJ/t(CO2))

5. Conclusion

An overall exergy analysis of a hybrid carbon capture system has been performed while optimising the process using MOO. This allowed different key decision variables to be varied to understand the effect that they have on the overall recovery rate and exergy loss rate.It was determined that the multi-stage compression and the VSA recover rate had the biggest impact on the overall recovery rate.

Furthermore, it was observed that the total specific shaft work had a linear relationship with the specific exergy loss rate. This would be due to the fact that the compressors account for the majority of the exergy going into the system as well as the total shaft work. However, this can be further investigated by selecting an optimum point on the Pareto chart in Figure 3(b) and performing an advanced exergy analysis on each individual processes to breakdown the exergy loss rate. Finally, an exergy analysis should be performed on a solvent absorption capture process, where the exergetic requirement would come from both compressors and heat energy, and the results could then be compared to this hybrid process.

Acknowledgement

The author would like to thank the Australian Government for funding this CO2CRC program through the CRC program as well as all the CO2CRC partners for their support.

References

BELAISSAOUI, B., LE MOULLEC, Y., WILLSON, D. & FAVRE, E. 2012. Hybrid membrane cryogenic process for post-combustion CO2 capture. *Journal of Membrane Science*.

EDENHOFER, O. & SEYBOTH, K. 2013. Intergovernmental Panel on Climate Change (IPCC). *In:* SHOGREN, J. F. (ed.) *Encyclopedia of Energy, Natural Resource, and Environmental Economics*. Waltham: Elsevier.

HAGI, H., NEMER, M., LE MOULLEC, Y. & BOUALLOU, C. 2013. Assessment of the flue gas recycle strategies on oxy-coal power plants using an exergy-based methodology. *Chemical Engineering Transactions,* 35, 343-348.

PIRES, J. C. M., MARTINS, F. G., ALVIM-FERRAZ, M. C. M. & SIMÕES, M. 2011. Recent developments on carbon capture and storage: An overview. *Chemical Engineering Research and Design,* 89, 1446-1460.

SCHOLES, C. A., ANDERSON, C. J., CUTHBERTSON, R., STEVENS, G. W. & KENTISH, S. E. 2013. Simulations of Membrane Gas Separation: Chemical Solvent Absorption Hybrid Plants for Pre- and Post-Combustion Carbon Capture. *Separation Science and Technology (Philadelphia),* 48, 1954-1962.

XIAO, G. & WEBLEY, P. 2013. *RE: VSA Zeolite 13X Experimental Results.*

C.3 Journal of Cleaner Production

ARTICLE IN PRESS

Journal of Cleaner Production xxx (2015) 1–11

Contents lists available at ScienceDirect

Journal of Cleaner Production

journal homepage: www.elsevier.com/locate/jclepro

Multi-objective optimisation of a hybrid vacuum swing adsorption and low-temperature post-combustion CO_2 capture

Jean Christophe Li Yuen Fong [a, b, *], Clare J. Anderson [c], Gongkui Xiao [d], Paul A. Webley [a, c], Andrew F.A. Hoadley [a, b, **]

[a] Cooperative Research Centre for Greenhouse Gas Technologies (CO_2CRC), Australia
[b] Department of Chemical Engineering, Monash University, Clayton, VIC 3800, Australia
[c] Department of Chemical Engineering and Biomolecular Engineering, The University of Melbourne, VIC 3010, Australia
[d] School of Mechanical and Chemical Engineering, The University of Western Australia, WA 6009, Australia

ARTICLE INFO

Article history:
Received 24 December 2014
Received in revised form
3 August 2015
Accepted 8 August 2015
Available online xxx

Keywords:
Hybrid carbon capture
Process integration
Coal-fired power station
Membranes
Cryogenics
Adsorbents
Solvents

ABSTRACT

In practice, carbon capture processes in CCS (Carbon Capture and Storage) consist of two main units: the carbon dioxide (CO_2) capture plant and the CO_2 compression unit. This study considered a hybrid capture system that combined both the capture and the compression units. In doing so, the conventional multi-stage CO_2 compression unit was replaced with a low-temperature carbon capture separation and pressurising step. The advantages of replacing the compression unit are two-folds: firstly, the low-temperature separation unit can further purify the CO_2 stream and secondly, it produces liquid CO_2 that can be pumped to the supercritical state required for transportation and sequestration. In order to take advantage of the extra CO_2 purification of the low-temperature separation unit, a vacuum swing adsorption (VSA) was used as the initial CO_2 recovery stage. A hybrid process has a higher degree of freedom available and therefore a Multi-Objective Optimisation (MOO) technique in combination with heat integration was used to optimise the total shaft work and the overall CO_2 recovery rate of the capture process. The MOO provided a range of optimal solutions where the total shaft work increased with the total CO_2 being recovered by the hybrid process. However, a minimum optimum was determined for the total specific shaft work required at an overall recovery rate of 88.9%, which required 1.40 GJ/(t CO_2 captured).

1. Introduction

According to the IPCC report (Metz, 2005), one of the primary causes of global warming is the greenhouse gas emission that has been increasing from the start of the industrial era since the mid-18th century. The energy sector is a large contributor to the increasing carbon dioxide emissions, which is mainly attributed to the dependence of electricity production through existing coal-fired power stations. While a transition towards more sustainable sources of energy such as solar, wind and biomass energy is necessary, CCS has been seen as the technology to reduce CO_2 emissions in the short-term and provide more time to the energy sector to transition into an array of sustainable energy sources (Stocker et al., 2013). Retro-fitting CCS to existing coal-fired power plant can reduce the carbon emission of the power plant, but it also reduces the overall efficiency of the power plant (Wennersten et al., 2014).

Following in this section is a description of the main CO_2 capture processes and the hybrid process which will combine the individual processes. Section 2 describes the methodology and framework used to integrate and optimise the hybrid processes. Section 3 gives the results of the multi-objective optimisation (MOO) followed by discussion and conclusions in Sections 4 and 5, respectively.

1.1. Carbon Capture and Storage (CCS)

Among the different capture technologies, solvent absorption has been considered to be the benchmark among the post-combustion carbon capture technologies. However, there are other technologies that have also shown potential to be energy and

* Corresponding author. Department of Chemical Engineering, Monash University, Clayton, VIC 3800, Australia.
** Corresponding author. Cooperative Research Centre for Greenhouse Gas Technologies (CO_2CRC), Australia.

http://dx.doi.org/10.1016/j.jclepro.2015.08.033
0959-6526/

Please cite this article in press as: Li Yuen Fong, J.C., et al., Multi-objective optimisation of a hybrid vacuum swing adsorption and low-temperature post-combustion CO_2 capture, Journal of Cleaner Production (2015), http://dx.doi.org/10.1016/j.jclepro.2015.08.033

cost competitive such as: adsorption, membranes and low-temperature separation (also referred to as "cryogenics" in the literature) (Aaron and Tsouris, 2005; Sreenivasulu et al., 2015). Each of those technologies has their respective advantages and disadvantages (Huisingh et al., 2015).

1.2. Solvent absorption

Solvent absorption is currently the most prominent capture process due to the fact that it is the most advanced technology since it has been extensively used for CO_2 removal in the natural gas processing industry (Rufford et al., 2012). A schematic diagram of the absorption process is shown in Fig. 1 and can be divided into two main steps: the absorption step, where lean solvent is contacted with the flue gas stream to capture the CO_2 in the absorption column, and the desorption step that occurs in the stripping column, where the solvent is either heated or the pressure is reduced to desorb the CO_2 from the solvent, yielding a high purity stream of CO_2 and regenerating the solvent which is recycled back to the absorption column. Solvents involving chemical reactions are usually regenerated by heating in a reboiler, which utilises a significant proportion of the steam generated by the power station (Harkin et al., 2010).

Chemical absorption is generally used in the post-combustion capture but still has some challenges such as scaling-up issues, solvent degradation, high reboiler duty and environmental impacts. Research is on-going into amine-based solvents such as MEA (mono ethanolamine), ammonia and potassium-carbonate based solvents (Smith et al., 2009).

1.3. Membranes

A membrane process consists of a membrane, which is a specially developed material that allows the selective permeation of a gas through it (permeate stream). The selectivity of each membrane depends on the nature of the material and the way it has been developed and also the pressure difference driving force that allows the gas to flow through the membrane. Therefore, high pressure streams are preferred when using membrane separation processes. Membranes have been used for air separation, gas dehydration and CO_2 removal from synthesis gas for hydrogen production (Bernardo et al., 2009). However, membranes in large scale CO_2 capture such as in CCS has not yet been implemented due to the fact that it is a relatively new technology which has not been tested on a sufficiently large scale, nor does it produce the high purity CO_2 stream that is easily achieved by solvent absorption (Favre, 2011; Khalilpour et al., 2014). Fig. 2 shows a simple membrane process schematic diagram, where the flue gas needs to be compressed prior to being supplied to the membrane unit to provide the necessary driving force required for the gas separation. However, the pressure difference can also be generated by applying a vacuum pressure to the retentate side of the membrane. Merkel et al. (2010) showed that this configuration can reduce the compressor work requirement by approximately 55%.

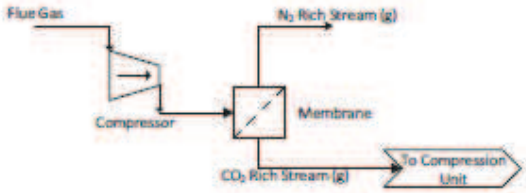

Fig. 2. Schematic diagram of the membrane process.

1.4. Adsorption

In adsorption processes, molecules adhere to the porous surface of a solid either by physical and/or chemical forces. The schematic adsorption separation process is shown in Fig. 3 and typically consists of three steps:

i) The adsorption step, where a film of the adsorbate (CO_2) is formed on the surface of the adsorbent (molecular sieves or activated carbon)
ii) A purging step, where the other gases are purged from the vessel
iii) A desorption step, where the CO_2 is desorbed from the adsorbent by pressure swing operation (PSA) or temperature swing operation (TSA). PSA has proved to be a more attractive operation than TSA due to the fact that TSA requires longer operating time to heat the adsorbents for regeneration leading to larger sorbent inventory.

Adsorption processes have very similar performance to membranes and have also been used for air separation, gas dehydration and CO_2 removal from synthesis gas for hydrogen production (Sircar, 1979). Zhang and Webley (2008) stated that pressure/vacuum swing adsorption technology has been frequently investigated for the carbon capture process due to its relative simplicity and low energy requirements. However, one disadvantage of adsorption is that the gaseous feed needs to be treated before passing it through the adsorber and like the membrane process, the adsorption process also does not readily yield a high purity CO_2 stream such as occurs with the solvent absorption regeneration process.

There are many CO_2 selective adsorbents, such as Activated Carbon and Zeolite 13X that have been developed and have shown some promising results in the CO_2 separation due to the small equipment required and the good CO_2 selectivity (Xiao et al., 2008; Webley, 2014).

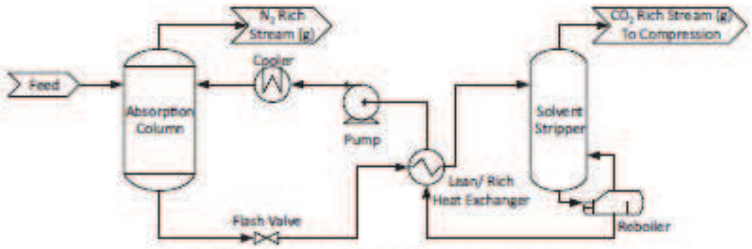

Fig. 1. Schematic diagram of the solvent absorption process.

Please cite this article in press as: Li Yuen Fong, J.C., et al., Multi-objective optimisation of a hybrid vacuum swing adsorption and low-temperature post-combustion CO_2 capture, Journal of Cleaner Production (2015), http://dx.doi.org/10.1016/j.jclepro.2015.08.033

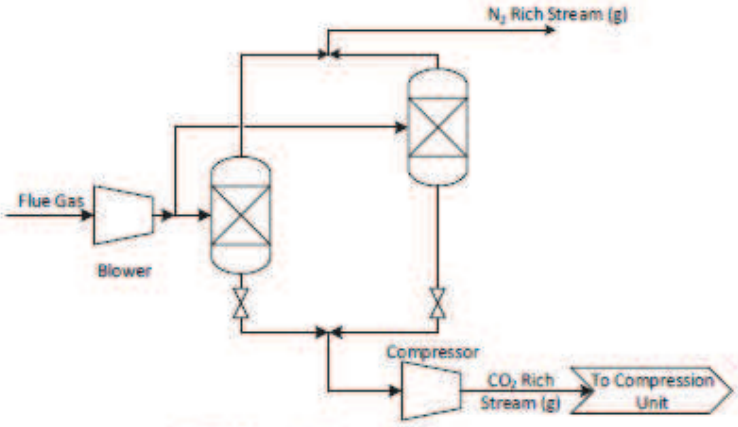

Fig. 3. Schematic diagram of the adsorption process.

1.5. Low-temperature separation

Low-temperature separation of CO_2 from post-combustion flue gas is achieved by cooling followed by vapour–liquid phase separation (Berstad et al., 2013). A representation of low-temperature separation is shown in Fig. 4, where the flue gas is compressed to an intermediate pressure, to facilitate the liquefaction of CO_2 in the chiller. The liquid CO_2 is separated from the N_2 rich flue gas which can be pumped to an appropriate pressure for transportation and sequestration.

The main advantage of low-temperature separation is that it yields liquid CO_2 that can more readily be pumped to a supercritical state relative to gaseous CO_2 that would require a separate compression train. Berstad et al. (2013) reported that low-temperature separation shows promising results for feed gas with a high CO_2 composition, such as oxy-fuel combustion. Therefore, for post-combustion carbon capture, low-temperature processes can be used as part of a two-step hybrid capture process as shown in Fig. 5, where an initial recovery step would increase the concentration of CO_2 in the flue gas while trying to limit the amount of CO_2 lost in the waste gas. The second step would then be a purification step, which would further purify the CO_2 stream to the required sequestration concentration. The low-temperature separation would be ideal as the purification step as it performs better at high CO_2 concentration feed gas and would also eliminate the necessity of a compression train after the capture process.

1.6. Carbon Capture and Storage hybrid processes

In this study, hybrid systems involved a combination of two carbon capture technologies that have been integrated to attempt to compliment the advantages of each process with the aim to reduce the energy penalty and consequently, the cost of carbon capture. As shown in Fig. 5, the stages in this hybrid process are:

i. The CO_2 recovery stage which discharges nitrogen to the atmosphere with as low a CO_2 concentration as possible.
ii. The CO_2 purification stage that would purify the CO_2 stream to a level required for storage.

The different configurations of the two-step hybrid process are shown in Fig. 6. The potential of each hybrid process has been assessed based on the requirements of high CO_2 recovery rate (horizontal rows) for the initial CO_2 recovery stage and high CO_2 purity (columns) for the secondary stage. The '✗' in the table reflects combinations that do not show potential and '✓' represent options with potential. The justification for those assessments is given in Sections 1.7 to 1.10.

1.7. Solvent absorption process in a hybrid process

Solvent absorption (Fig. 1) has been the leading carbon capture technology as a stand alone carbon capture process, due in part to

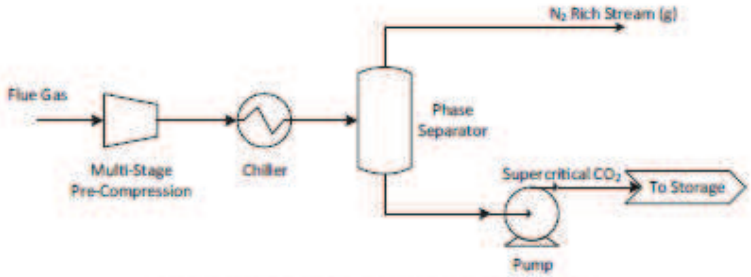

Fig. 4. Schematic diagram of the low-temperature capture process.

Please cite this article in press as: Li Yuen Fong, J.C., et al., Multi-objective optimisation of a hybrid vacuum swing adsorption and low-temperature post-combustion CO_2 capture, Journal of Cleaner Production (2015), http://dx.doi.org/10.1016/j.jclepro.2015.08.033

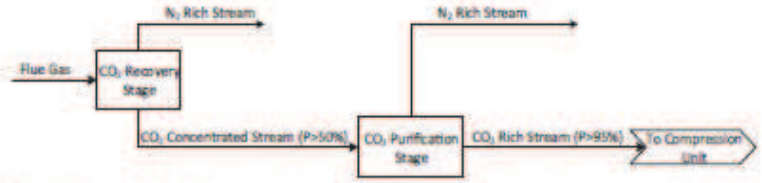

Fig. 5. Schematic diagram of a hybrid capture process consisting of two capture processes: recovery stage and purification stage.

the ability to obtain high recovery rates and simultaneously high purity required for carbon sequestration. The main drawback of solvent absorption is the high reboiler duty required to regenerate the solvent in the stripper column when recovering a large amount of CO_2. Hence, when considering the solvent absorption process in a hybrid process, the main aim would be to reduce the reboiler duty. There exists active research into new molecules that have a lower specific reboiler duty (i.e. MJ/ton CO_2), but this is not the subject of this study.

Since the amount of solvent is dependent on the CO_2 concentration, one way to reduce the amount of solvent required for absorption is to increase the concentration of CO_2 in the flue gas as this would improve the absorption kinetics (Rochedo and Szklo, 2013). Hence, solvent absorption would be more appropriate as a purification stage, where the feed gas to the solvent absorption process would have been CO_2 enriched from the recovery stage.

Scholes et al. (2013a)[3] considered a hybrid system consisting of membrane as a CO_2 recovery stage, followed by a solvent absorption process for both post-combustion and pre-combustion carbon capture. This study showed that the hybrid systems had a higher energy demand for both processes, but would also reduce the solvent absorber height and diameter, which would lead to a reduction in capital cost for this piece of equipment.

It should be noted that some studies have been performed using a hybrid process of solvent absorption and membrane that uses a chemical solvent to increase the performance of the membrane (Zhou et al., 2010)[1]. However, this may be considered as an enhanced membrane process rather than a true integration of two different capture technologies.

1.8. Low-temperature capture process in a hybrid process

The main energy requirement for low-temperature capture processes (Fig. 4) is attributed to the shaft work of the compression of the feed gas prior to the chilling and the compression train required for the refrigeration system. Hence, if implemented as the recovery stage, the low-temperature separation would have a high electric power requirement, as it would have involved compressing the large amount of N_2 in the feed gas compression stage.

CO_2 Recovery \ CO_2 Purity	Absorption	Low-Temp	Adsorption	Membrane
Absorption		×	×	×[1]
Low-Temp	×		×	×
Adsorption	✓[2]	✓		✓
Membrane	✓[3]	✓[4]	×	

Fig. 6. Matrix of two-process hybrid systems with assessment of potential for making a hybrid process which gives high CO_2 recovery and purity. Literature references are given in numbers.

Furthermore, at low CO_2 concentration and thus low CO_2 partial pressure, a lower temperature would be required to recover the CO_2 resulting in a higher refrigeration duty.

Therefore, the low-temperature capture process performs better as a CO_2 purification stage, when dealing with a smaller feed gas flowrate and higher concentration of CO_2. The common concentration of CO_2 preferable for low-temperature separation ranges from 15% to 60% (Belaissaoui et al., 2012a) and is dependent on the pressure of the flue gas (Berstad et al., 2013). More importantly, since the low-temperature vapour–liquid separation produces liquid CO_2 ready to be pumped to a supercritical state for transportation, it is best for the low-temperature separation process to be used as a purification stage.

1.9. Adsorption process in a hybrid process

Adsorption process (Fig. 3) has shown potential as a stand-alone carbon capture process but has had some challenges meeting the high purity of CO_2 required (>95%) for carbon storage and high CO_2 recovery at the same time (Zhang et al., 2008). In order to obtain high purity in a Vacuum Swing Adsorption (VSA) process, deep vacuum levels are required to desorb the CO_2 molecules from the adsorbents. This property makes adsorption inefficient as a purification stage but more appropriate for the CO_2 recovery stage, where the VSA process can recover the CO_2 from the flue gas to an intermediate CO_2 concentration that can then go through a CO_2 purification stage.

1.10. Membrane process in a hybrid process

Finally, membrane separation processes (Fig. 2) provide more flexibility in a hybrid system, partly due to the balance between permeability and selectivity that usually dictates the performance of a membrane (Favre, 2011), as is shown in Fig. 7. In order to use membranes as a CO_2 recovery step, a high permeability of CO_2 should be prioritised as it will allow more CO_2 through the membrane. On the other hand, when using membranes as a CO_2 purification step, a high selectivity of CO_2/N_2 should be given priority to obtain a high purity CO_2 outlet stream.

Belaissaoui et al. (2012a)[4] and Scholes et al. (2013b)[4] studied the potential application of using membranes as the CO_2 recovery stage with low-temperature separation as the purification stage. Belaissaoui et al. (2012a) reported that this hybrid system showed great potential, especially in the low-temperature separation and pressurisation of the CO_2, where the power requirement was less than a traditional six-stage intercooled compressor by approximately 10%. Scholes et al. (2013b) reported that the hybrid process were cost competitive with state of the art MEA solvent technology for CO_2 capture from a brown coal-fired power station.

The results obtained by Belaissaoui et al. (2012a) and Scholes et al. (2013b) show that hybrid processes can be competitive with

Please cite this article in press as: Li Yuen Fong, J.C., et al., Multi-objective optimisation of a hybrid vacuum swing adsorption and low-temperature post-combustion CO_2 capture, Journal of Cleaner Production (2015), http://dx.doi.org/10.1016/j.jclepro.2015.08.033

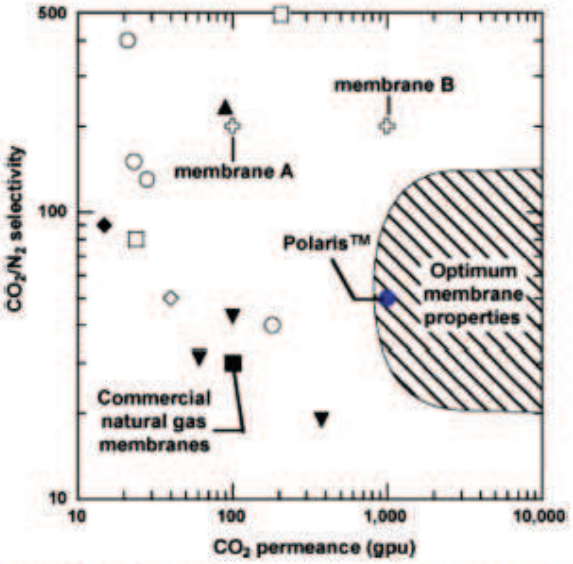

Fig. 7. CO_2/N_2 selectivity and CO_2 permeance trade-off plot comparing the performance of different membranes reported in the literature. The shaded area represents the region of optimum membrane properties for the separation of CO_2 from flue gas as a single-technology. (Merkel et al., 2010).

the CCS benchmark process but require further studies to optimise and evaluate other hybrid configurations.

1.11. Process integration and optimisation in CCS

In order to optimise the hybrid process when retrofitting it to a coal-fired power station, chemical process design and integration need to be performed. Process integration can be done in two main steps: structural optimisation and parameter optimisation (Smith, 2005). Structural optimisation synthesises alternative structures of the process such as choosing the right hybrid process configuration by using the properties of each capture process to determine which process would be the best as the recovery and/or purification stage, as represented in the matrix in Fig. 1. Parameter optimisation changes the operating conditions of the process to improve the performance of the process. Heat integration (pinch analysis) provides a systematic method of parameter optimisation to maximise the process efficiency in terms of heat source and heat sinks available in the process. Pinch analysis also determines the minimum energy target required for the process to run in the ideal situation (Linhoff and Senior, 1983).

Processes that require heat sources or sinks, such as solvent absorption and low-temperature separation benefit most from the pinch analysis technique. Harkin et al. (2009) performed a heat and process integration analysis of a brown coal-fired power station with a solvent absorption carbon capture process, with a focus on the pinch analysis. Their study showed that heat integration was a highly valuable technique since the energy penalty was reduced by approximately 15% with effective heat integration. Capture processes that require mainly electrical power, such as membrane processes, would not provide significant improvement through pinch analysis. Therefore, parameter optimisation can be done by systematically varying process operating conditions and monitoring their effects on the performance of the overall process as performed by (Belaissaoui et al., 2012b). Scholes et al. (2013a) also performed a parameter optimisation on a hybrid membrane/solvent absorption carbon capture process by systematically varying parameters such as membrane driving force and the membrane selectivity to study their effects on the CAPEX. Xiao et al. (2008) used both structural and parameter optimisation to integrate a VSA carbon capture process with Zeolite 13X as the adsorbent. Structural optimisation was performed by studying a 9-step cycle versus a 12-step cycle and parameter optimisation was performed by varying several key variables whilst monitoring the VSA power performance.

Another method of parameter optimisation is Multi-Objective Optimisation (MOO) technique, which finds the values of operating conditions, known as decision variables, which provide the optimum of more than one objective (Rangaiah, 2009). The advantage of using MOO is that it generates a set of optimal solution known as Pareto-optimal solutions. These are a range of solutions that are all non-dominated, i.e. each solution is the best solution specific to the objective at hand. A non-dominated sorting genetic algorithm is used for the generation of the Pareto optimal solutions. This is a well-developed method which produces solutions with a Pareto curve that is well dispersed (Bhutani et al., 2006). Therefore, it provides a number of solutions that the designer can select from.

Furthermore, MOO can be combined with other process analyses such as Life Cycle Analysis (Theodosiou et al., 2014), techno-economic analysis (Harkin et al., 2012a) and heat integration (Harkin et al., 2012b). Heat integration has been used in academia as well as industry since Linhoff and Senior (1983) identified pinch analysis as a systematic way to improve the thermodynamic efficiency of a process. Since then, heat integration has been heavily studied (Klemeš et al., 2013) with recent developments studying total site heat integration (Liew et al., 2014). In this study, heat integration was used in combination with MOO to improve the heat exchange between the process stream and the refrigeration system.

2. Methodology and framework

The aim of this paper is to optimise the retrofitting of a hybrid carbon capture system to a coal-fired power plant station. The power plant used in this study was a 300 MW sub-bituminous black coal-fired power plant that has a base CO_2 emission of 1.01 t/MWh. The flue gas was considered to be pre-treated and the impurities such as the SO_x and NO_x removed, resulting in a binary mixture of nitrogen and carbon dioxide, the properties of the flue gas is shown in Table 1. The hybrid carbon capture plant was integrated with the coal-fired power plant as shown in Fig. 8. A VSA process using Zeolite 13X was used as the CO_2 recovery stage, followed by low-temperature separation as the CO_2 purification stage. The vacuum pump used in the VSA, saturates the CO_2 rich product stream exiting the VSA process with water. Therefore a TSA adsorption was used as a dehydration process to reduce the water concentration to below 5 ppm to prevent the formation of ice in the low-temperature separation unit. Although not shown in the

Table 1
Post-combustion flue gas properties based on a 300 MW sub-bituminous coal-fired power station after pre-treatment.

Feed conditions	Units	Value
Vapour fraction	–	1.00
Temperature	(°C)	50
Pressure	(kPa)	103
Molar flow	(kmol/h)	57,800
Mass flow	(kg/h)	1,670,000
Composition	**(mol frac)**	
CO_2	–	0.1141
N_2	–	0.8859

Please cite this article in press as: Li Yuen Fong, J.C., et al., Multi-objective optimisation of a hybrid vacuum swing adsorption and low-temperature post-combustion CO_2 capture, Journal of Cleaner Production (2015), http://dx.doi.org/10.1016/j.jclepro.2015.08.033

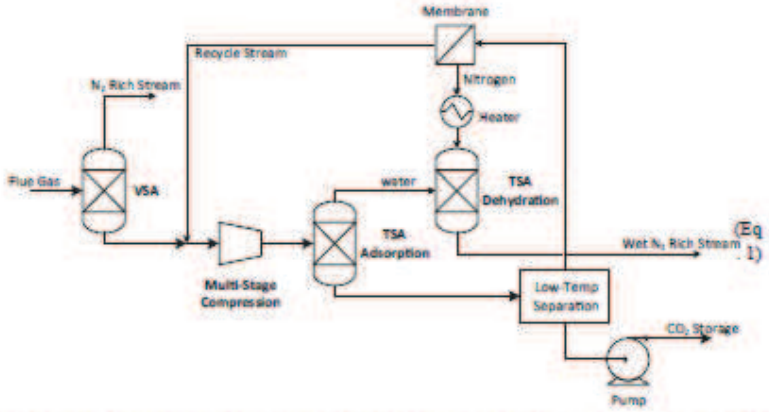

Fig. 8. Schematic diagram of hybrid carbon capture process using VSA as CO_2 recovery stage and low-temperature separation as CO_2 purification stage.

schematic diagram, some water was removed in the inter-stage cooling in the multi-stage compression. Finally, a membrane process was used to recover the CO_2 from the low-temperature separation unit gaseous waste stream.

In order to determine the optimum operating conditions for each operation in the capture unit, multi-objective optimisation was used to optimise two objective variables:

1. maximising the overall CO_2 recovery rate of the capture process
2. minimising the total shaft work required for the capture process

There were 7 decision variables that were used to optimise the objective variables, which are further discussed in the next section and a table of the decision variables is found in Table 2. All process simulations were performed on Aspen HYSYS® using the Peng-Robinson Package and Microsoft Excel® and Microsoft VBA® was used as the MOO interface (Rangaiah, 2009).

2.1. Adsorption

A Vacuum Swing Adsorption (VSA) process with Zeolite 13X as the adsorbent was used as the CO_2 recovery stage. In order to simulate the performance of a the VSA carbon capture process on Aspen HYSYS®, the results obtained from a 3-bed VSA cycle from Aspen Adsim® was used (Xiao and Webley, 2013).The results were then regressed to obtain the blower power (Eq. (1)) and vacuum pump power (Eq. (2)) with two input variables: VSA CO_2 recovery rate and VSA CO_2 outlet purity. The total VSA power requirement was the summation of the blower power and vacuum pump power (Equation (3)), where x is the CO_2 recovery rate in % mass fraction and y is the CO_2 outlet purity in % mass fraction. The different VSA CO_2 recovery rate and VSA CO_2 outlet purity were obtained by varying the vacuum pressure (4.4–4.5 kPa) and the CO_2 concentration (1.3%–1.7%) in the N_2 rich waste stream.

$$\text{Blower Power}\left(\text{GJ/tCO}_2\right) = 2.06 - \left(5.37\times10^{-2}\right)x + \left(1.08\times10^{-2}\right)y + \left(3.58\times10^{-4}\right)x^2 - \left(1.05\times10^{-4}\right)x\cdot y \quad (1)$$

$$\text{Vacuum Pump Power}\left(\text{GJ/tCO}_2\right) = 4.55 - \left(1.21\times10^{-1}\right)x + \left(2.66\times10^{-2}\right)y + \left(8.18\times10^{-4}\right)x^2 - \left(2.61\times10^{-4}\right)x\cdot y \quad (2)$$

$$\text{Total VSA power} = \text{Blower Power} + \text{Vacuum Pump Power} \quad (3)$$

Since the VSA CO_2 recovery rate and VSA CO_2 outlet purity were the two variables that dictate the power requirement of the VSA process, they were the two decision variables that were used in the MOO to obtain the optimum performance of the VSA.

2.2. Low-temperature separation

There are two important processes in the low-temperature separation carbon capture unit: the pre-compression unit and the refrigeration cycle required to obtain the low-temperature. The compression unit used in this study is a three-stage compression unit with inter-stage cooling. The CO_2-rich stream exiting the VSA capture unit is saturated with water; therefore, after each inter-stage cooling, the condensed water is removed by using a phase separator to reduce the work load of the temperature swing adsorption (TSA). A TSA is necessary to reduce the water

Table 2
Table of decision variable range for MOO and optimum operating conditions of hybrid process.

Decision variable		Minimum	Maximum
VSA CO_2 recovery rate	%	90.3	98.5
VSA CO_2 outlet purity	%	61.9	65.0
Refrigerant ethane molar fraction		0.004	0.700
Refrigerant molar flow	(mol/s)	0.67	2.0
Low-temp process stream outlet temp.	(°C)	-60.5	-40.0
Multi-stage compression pressure	(kPa)	930	4000
Membrane cut		0.05	0.75

Please cite this article in press as: Li Yuen Fong, J.C., et al., Multi-objective optimisation of a hybrid vacuum swing adsorption and low-temperature post-combustion CO_2 capture, Journal of Cleaner Production (2015), http://dx.doi.org/10.1016/j.jclepro.2015.08.033

composition of the stream to below 5 ppm to avoid any formation of ice. As it can be seen from Fig. 8, the TSA desorption stage and re-pressurisation was performed by using the pressurised nitrogen stream from the membrane retentate stream and heating it to the required temperature.

While the CO_2 and N_2 need to be at very low temperatures, in the range of −40 °C to −60 °C, in order to separate the liquefied CO_2 from the gaseous N_2, the final CO_2 stream is transported at environmental temperatures and the waste nitrogen-rich gas needs to be at room temperature before passing through the membrane. Therefore, a heat exchanger network was used to recover the energy from the cold streams prior to CO_2 transportation and before passing through the membrane, respectively.

In order to achieve the low temperatures, a mixed ethane-propane refrigerant refrigeration cycle was used with two-stage compression. A mixed ethane-propane refrigerant was used over a propane-only refrigerant system as preliminary work showed that the mixed refrigerant reduced the total shaft work in the compression train, which was a result of a better stream composite curve in the heat integration.

This low-temperature separation unit provides a lot of flexibility to the hybrid process since it has a high degree of freedom throughout the unit. Therefore, the following four decision variables were used to optimise this unit:

i. Pre-compression pressure.
ii. Temperature of the CO_2 process stream.
iii. Refrigerant molar flowrate.
iv. Refrigerant ethane-propane composition.

An important task in the low-temperature separation is to ensure that the CO_2 is not allowed to form solids at the low temperature. The temperature at which CO_2 forms solids, known as the CO_2 freeze out temperature, which is a property of the CO_2-rich process stream, is determined using Aspen HYSYS®. Therefore, a constraint was embedded in the MOO to reject any process simulation when the CO_2-rich process stream temperature is lower than its CO_2 freeze out temperature.

2.3. Membrane

A membrane unit was attached to the gaseous waste stream of the low-temperature separation unit to capture the CO_2 that was not recovered in the low temperature unit. Since the stream was at a high pressure, this membrane unit would further purify the gaseous stream without requiring further work.

A high performance polymer membrane (Low et al., 2013) was used with a permeance of CO_2 (PCO2) of 1000 GPU and selectivity of CO_2 versus N_2 ($\alpha_{CO2/N2}$) of 50. The permeate stream was recycled back to the feed of the pre-compression stage, therefore the permeate stream pressure was set to match the pre-compression stage feed stream. The feed stream of the membrane was determined by the performance of the low-temperature separation unit, and no extra work was required to operate the membrane. There was only one decision variable used to optimise the membrane unit: the membrane cut, i.e., the ratio of the permeate flow to inlet flow (F_p/F_{in}), which is effectively determined by the membrane area.

A summary of the decision variables, including their range included in the MOO, is shown in Table 2.

2.4. Modelling parameters

In order to run the simulations on Aspen HYSYS®, process parameters such as compressor efficiency and cooling water temperature needed to be constant throughout all the processes. Those process parameters are shown in Table 3.

A minimum ΔT in heat exchangers of 2 °C was used in the plate-fin heat exchangers to improve the heat transfer efficiency between the refrigerant stream and process stream. High thermal efficiency is important at the low operating temperature range required to liquefy the CO_2 in the process stream in order to reduce the work load of the refrigeration system.

3. Results

The Pareto Optimal Front is the solution obtained from the last generation of the Genetic Algorithm of the non-dominated solution set. The results shown are for a MOO using 75 individuals with 50 generations. The Pareto charts of the objective variables are shown in Fig. 9(a).

From the objective variables Pareto charts, it is observed that with increasing recovery rate, there was an increase in total shaft work required. Therefore, in order to better understand the total work required with respect to the amount of CO_2 being captured by hybrid capture process, a new graph, using the Pareto-Optimal solutions, of total specific shaft work as a function of recovery rate was produced (Fig. 9(b)). The total specific shaft work required is the rate of total shaft work required per mass of CO_2 being recovered by the process.

From Fig. 9(b), it is observed that there is an optimum minimum specific work required at an overall recovery rate of 88.9% and requires a total specific shaft work of 1.40 GJ/(t CO_2 captured). The operating conditions of the decision variables are shown in Table 4.

4. Discussion

4.1. Decision variables Pareto charts

MOO is a very useful tool to also understand how the decision variables affect the each objective individually. The Pareto charts of the decision variables for the different carbon capture stages are shown in Fig. 10, **11** and **12** as a function of objective 1: Maximum CO_2 Recovery.

Fig. 10 shows the two decision variables that were varied to change the power requirement of the VSA CO_2 recovery process. As was expected, higher CO_2 recovery rate from the VSA was required to obtain higher overall CO_2 recovery rate from the hybrid system since the waste stream from the VSA was not being recovered. On the other hand, the VSA CO_2 outlet purity does not seem to have a significant impact on the overall recovery rate of the hybrid system.

Fig. 11 displays the four decision variables that determined the performance of the low-temperature separation. As expected, the pre-compression pressure Pareto chart in Fig. 11(c) shows that a higher pressure is required to obtain higher recovery rates since higher compression pressures increase the partial pressure of CO_2 and therefore facilitates the separation of CO_2 from nitrogen. Also important is that a higher pressure of the stream lowers the CO_2 freeze out temperature and effectively allows the stream to be cooled to the lowest temperature possible before forming solid CO_2. The decision variables in Fig. 11 (a), (b) and (d) effectively

Table 3
Table of process modelling parameters used throughout process simulations.

Process parameters		Minimum
Isentropic compressor efficiency	%	80
Cooling water temperature	°C	30
Minimum ΔT in heat exchangers	°C	2
Minimum CO_2 purity in CO_2 capture stream	%	95

Please cite this article in press as: Li Yuen Fong, J.C., et al., Multi-objective optimisation of a hybrid vacuum swing adsorption and low-temperature post-combustion CO_2 capture, Journal of Cleaner Production (2015), http://dx.doi.org/10.1016/j.jclepro.2015.08.033

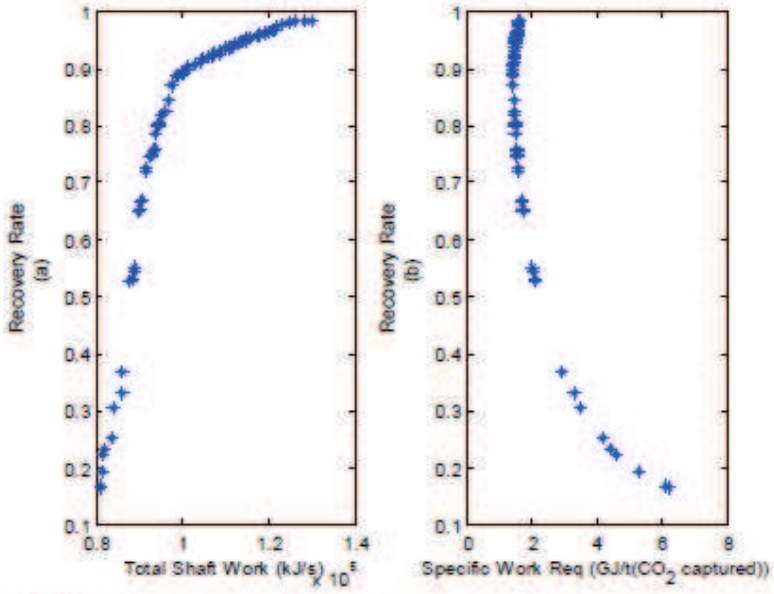

Fig. 9. (a): Recovery rate as a function of objective variables total shaft work required (kJ/s); (b): Recovery rate as a function of specific shaft work (kJ/s).

Table 4
Table of decision variable range for MOO and optimum operating conditions of hybrid process.

Decision variable	Units	Minimum	Maximum	Optimum
VSA CO_2 recovery rate	%	90.3	88.5	90.4
VSA CO_2 outlet purity	%	61.9	65.0	64.5
Refrigerant ethane molar fraction	–	0.004	0.700	0.3525
Refrigerant molar flow	(mol/s)	0.67	2.0	1.4
Low-temp process stream outlet temp.	(°C)	−60.5	−40.0	−57.2
Multi-stage compression pressure	(kPa)	930	4000	1786
Membrane cut	–	0.05	0.75	0.41

determined the power requirement of the refrigeration system. The three parameters: the ethane molar fraction, the minimum temperature achieved by the process stream and the refrigerant molar flowrate show a linear relationship with the objective variable, which is explained by the higher duty required to cool the higher amount of CO_2.

The final decision variable, the membrane cut of the membrane process is shown in Fig. 12. It can be seen that in order to achieve

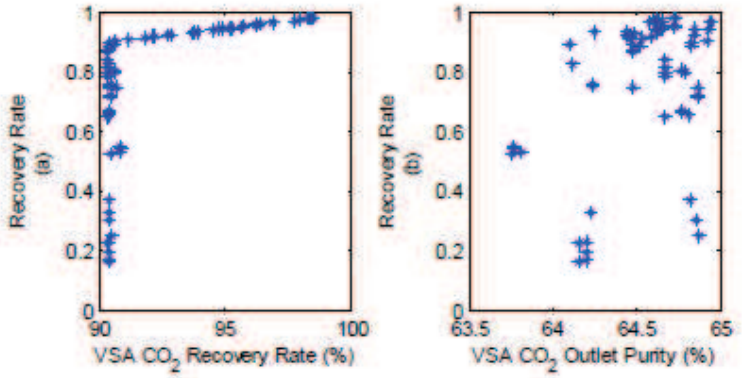

Fig. 10. Pareto chart of the two decision variables for the VSA capture process versus the overall hybrid process CO_2 recovery rate. (a) CO_2 recovery rate of the VSA process (%); (b) CO_2 outlet purity of the VSA process (%).

Please cite this article in press as: Li Yuen Fong, J.C., et al., Multi-objective optimisation of a hybrid vacuum swing adsorption and low-temperature post-combustion CO_2 capture, Journal of Cleaner Production (2015), http://dx.doi.org/10.1016/j.jclepro.2015.08.033

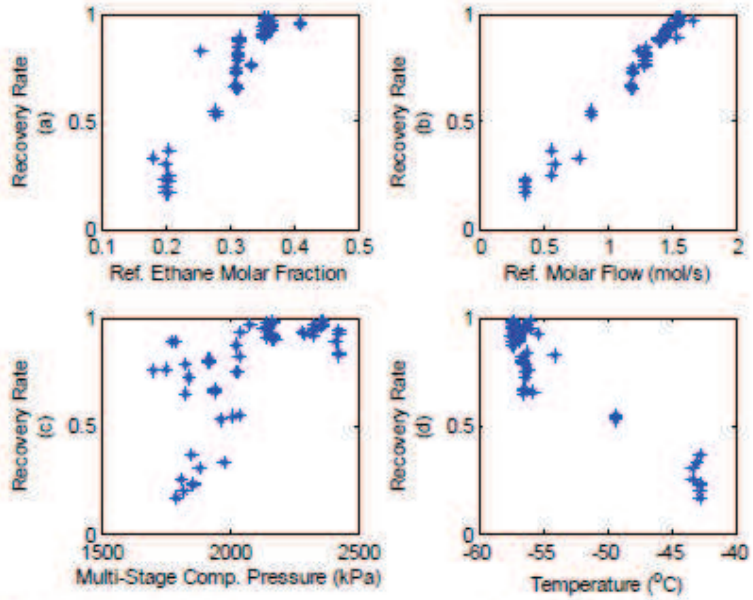

Fig. 11. Pareto chart of the four decision variables governing the low-temperature capture process versus the overall hybrid process CO_2 recovery rate. (a) Refrigerant ethane molar fraction (b) Refrigerant molar flow (mol/s); (c)Multi-stage compression pressure (kPa); (d) Process stream minimum temperature (°C).

the higher overall CO_2 recovery rate, a higher membrane cut value is required to allow more CO_2 to be recycled back into the system and hence, less CO_2 to be lost in the retentate stream. However, at lower recovery rate, no gas is allowed to permeate through the membrane. This is to reduce the amount of CO_2 being recycled, which leads to a reduced loading in the low-temperature separation.

4.2. Objective variables Pareto charts and optimum specific work required

This optimum operating condition of minimum specific work of 1.40 GJ/(t CO_2 captured) and overall recovery rate of 88.9% obtained

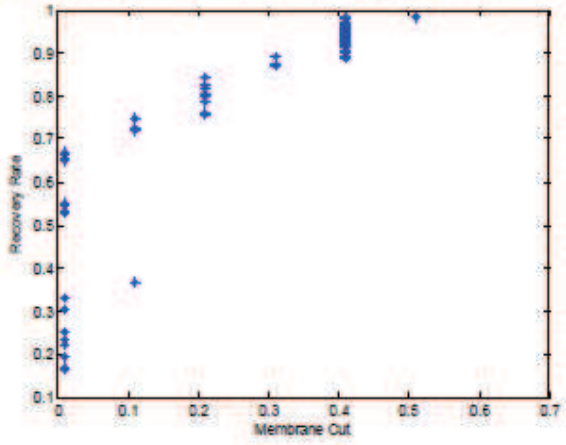

Fig. 12. Pareto chart of the overall hybrid process CO_2 recovery rate as a function of the decision variable (membrane cut) governing the membrane capture process.

in Section 3 can be used to further analyse the performance of the hybrid process. The heat composite curve of the heat integrated low-temperature separation was generated and shown in Fig. 13 and the work requirement of each component was analysed and displayed in Fig. 14.

The stream composite curve in Fig. 13 shows that the pinch point occurs at the lowest temperature and since the refrigeration system is included in this composite curve, no extra cooling duty is required. A near pinch also occurs at just below −40 °C, where the CO_2 just starts to condense. This is seen most clearly in the Grand Composite Curve in Fig. 13, where the extent of process to process heat exchange is about 4×10^7 kJ/h.

The power requirement of the hybrid carbon capture process was analysed at the optimum operating conditions. There are four consumers of power throughout the process: The VSA process, pre-compression prior to the low-temperature separation, the refrigeration compression train required in the refrigeration system and the pump that pressurises the pure liquid CO_2 to supercritical state. The pump requirement is negligible throughout the process (<0.1%); therefore Fig. 14 shows the division of the shaft work required by the three other processes. The low-temperature separation unit, which comprises of both the pre-compression and refrigeration cycle compression, requires a total of 59% of the total shaft work requirement, which corresponds to 98,800 kJ/s. The VSA process, which consists of the blower to compress the flue gas prior to entering the VSA and the vacuum pump required to go to vacuum pressure for the desorption stage, requires 41% of the total shaft work.

The two main power consumers are the pre-compression train and the VSA power requirement. The pre-compression train cannot be further optimised other than the decision variables that have been allocated. The second main power consumer is the VSA process and in order to improve the power requirement, further improvement to the VSA process would be required such as better adsorbents or different VSA configurations.

Please cite this article in press as: Li Yuen Fong, J.C., et al., Multi-objective optimisation of a hybrid vacuum swing adsorption and low-temperature post-combustion CO_2 capture, Journal of Cleaner Production (2015), http://dx.doi.org/10.1016/j.jclepro.2015.08.033

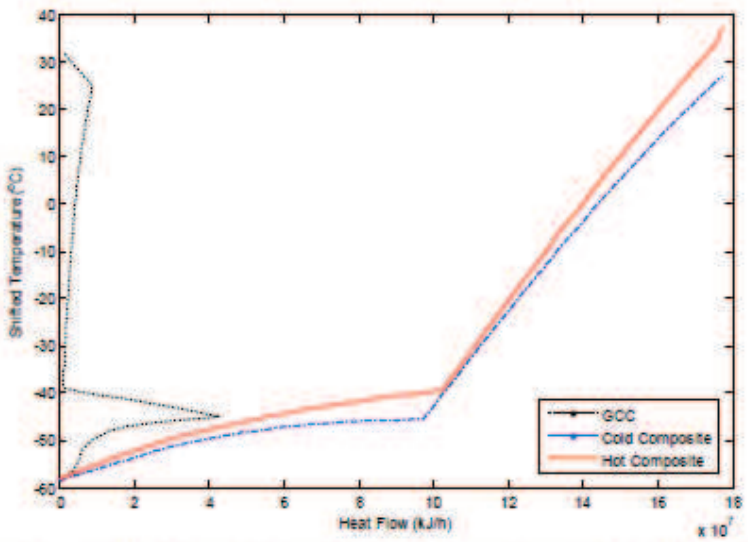

Fig. 13. Stream composite curve and the grand composite curve shows that the pinch temperature occurs at the cold end of the heat exchangers.

5. Conclusion

The VSA/Low-temperature separation hybrid carbon capture process shows that it can achieve a high CO_2 recovery rate and high CO_2 purity required for carbon sequestration, while also performing well in terms of the energy consumption. The MOO technique was used to obtain a range of overall CO_2 recovery rates and the corresponding minimum amount of shaft work required to operate the hybrid capture process along with the corresponding operating decision variables. The total specific shaft work required by the hybrid capture process (GJ/t (CO_2 captured)) was obtained by dividing the total shaft work required (MW) by the corresponding amount of CO_2 being recovered for capture (kg/s). This resulted in an optimum minimum specific shaft work of 1.40$_e$ GJ/(t CO_2 captured) when 88.9% of the CO_2 is being recovered by the hybrid process (with CO_2 purity of 98.2%).

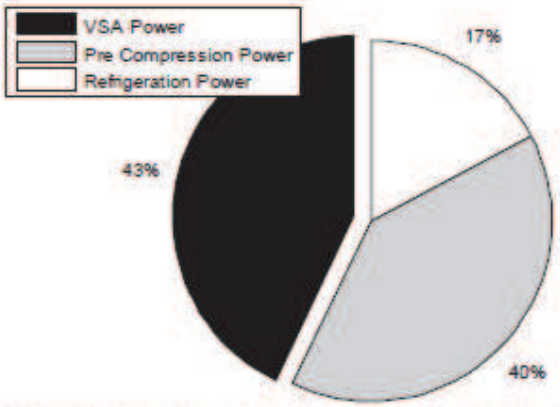

Fig. 14. Pie chart of total shaft work required for the hybrid capture process. The low-temperature separation process comprises of the pre-compression and refrigeration power requirement. The VSA total power requirement consists of both the blower prior to entering the VSA and the vacuum pump required to provide vacuum pressures.

It is to be noted that a comparable established MEA solvent absorption separation system with a multi-stage compression system requires 4 GJ$_{th}$/(t CO_2 recovered) (Belaissaoui et al., 2012a) that converts to approximately 1.3 GJ$_e$/(t CO_2 recovered). Therefore, in order for the hybrid process to match the MEA solvent absorption separation system, the VSA process would have to reduce its energy requirement by 17% while still having the same CO_2 recovery rate and CO_2 outlet purity. The energy requirements of the hybrid system have shown great potential to be competitive with solvent absorption capture processes. Therefore, further work needs to be performed to reduce energy requirements and to evaluate the economic performance of the hybrid process.

Acknowledgements

The author would like to thank the Australian Government for funding this CO_2CRC program through the CRC program as well as all the CO_2CRC partners for their support.

Appendix A. Supplementary data

Supplementary data related to this article can be found at http://dx.doi.org/10.1016/j.jclepro.2015.08.033.

References

Aaron, D., Tsouris, C., 2005. Separation of CO_2 from flue gas: a review. Sep. Sci. Technol. 40, 321–348.
Belaissaoui, B., Le Moullec, Y., Willson, D., Favre, E., 2012a. Hybrid membrane cryogenic process for post-combustion CO_2 capture. J. Membr. Sci. 415–416, 424–434.
Belaissaoui, B., Willson, D., Favre, E., 2012b. Membrane gas separations and post-combustion carbon dioxide capture: parametric sensitivity and process integration strategies. Chem. Eng. J. 211–212, 122–132.
Bernardo, P., Drioli, E., Golemme, G., 2009. Membrane Gas separation: a review/state of the art. Ind. Eng. Chem. Res. 48, 4638–4663.
Berstad, D., Anantharaman, R., Neksâ, P., 2013. Low-temperature CO_2 capture technologies – applications and potential. Int. J. Refrig. 36, 1403–1416.
Bhutani, N., Ray, A.K., Rangaiah, G., 2006. Modeling, simulation, and multi-objective optimization of an industrial hydrocracking unit. Ind. Eng. Chem. Res. 45, 1354–1372.

Please cite this article in press as: Li Yuen Fong, J.C., et al., Multi-objective optimisation of a hybrid vacuum swing adsorption and low-temperature post-combustion CO_2 capture, Journal of Cleaner Production (2015), http://dx.doi.org/10.1016/j.jclepro.2015.08.033

Favre, E., 2011. Membrane processes and postcombustion carbon dioxide capture: challenges and prospects. Chem. Eng. J. 171, 782–793.
Harkin, T., Hoadley, A., Hooper, B., 2009. Process integration analysis of a brown coal-fired power station with CO_2 capture and storage and lignite drying. Energy Procedia 1, 3817–3825.
Harkin, T., Hoadley, A., Hooper, B., 2010. Reducing the energy penalty of CO_2 capture and compression using pinch analysis. J. Clean. Prod. 18, 857–866.
Harkin, T., Hoadley, A., Hooper, B., 2012a. Optimisation of power stations with carbon capture plants – the trade-off between costs and net power. J. Clean. Prod. 34, 98–109.
Harkin, T., Hoadley, A., Hooper, B., 2012b. Using multi-objective optimisation in the design of CO_2 capture systems for retrofit to coal power stations. Energy 41, 228–235.
Huisingh, D., Zhang, Z., Moore, J.C., Qiao, Q., Li, Q., 2015. Recent advances in carbon emissions reduction: policies, technologies, monitoring, assessment and modeling. J. Clean. Prod. 103.
Khalilpour, R., Mumford, K., Zhai, H., Abbas, A., Stevens, G., Rubin, E.S., 2014. Membrane-based carbon capture from flue gas: a review. J. Clean. Prod. 103, 286–300.
Klemeš, J.J., Varbanov, P.S., Kravanja, Z., 2013. Recent developments in process integration. Chem. Eng. Res. Des. 91, 2037–2053.
Liew, P.Y., Wan Alwi, S.R., Lim, J.S., Varbanov, P.S., Klemeš, J.J., Abdul Manan, Z., 2014. Total site heat integration incorporating the water sensible heat. J. Clean. Prod. 77, 94–104.
Linhoff, B., Senior, P.R., 1983. Energy Targets Clarify Scope for Better Heat Integration. Process Engineering, London, p. 64.
Low, B.T., Zhao, L., Merkel, T.C., Weber, M., Stolten, D., 2013. A parametric study of the impact of membrane materials and process operating conditions on carbon capture from humidified flue gas. J. Membr. Sci. 431, 139–155.
Merkel, T.C., Lin, H., Wei, X., Baker, R., 2010. Power plant post-combustion carbon dioxide capture: an opportunity for membranes. J. Membr. Sci. 359, 126–139.
Metz, B., 2005. IPCC Special Report on Carbon Dioxide Capture and Storage. Cambridge University Press for the Intergovernmental Panel on Climate Change.
Rangaiah, G.P., 2009. Multi-ojective Optimization. Techniques and Applications in Chemical Engineering. World Scientific Publishing Co. Pte. Ltd., Singapore.
Rochedo, P.R.R., Szklo, A., 2013. Designing learning curves for carbon capture based on chemical absorption according to the minimum work of separation. Appl. Energy 108, 383–391.
Rufford, T.E., Smart, S., Watson, G.C.Y., Graham, B.F., Boxall, J., Diniz da Costa, J.C., May, E.F., 2012. The removal of CO_2 and N_2 from natural gas: a review of conventional and emerging process technologies. J. Petroleum Sci. Eng. 94–95, 123–154.
Scholes, C.A., Anderson, C.J., Cuthbertson, R., Stevens, G.W., Kentish, S.E., 2013a. Simulations of membrane gas separation: chemical solvent absorption hybrid plants for pre- and post-combustion carbon capture. Sep. Sci. Technol. Phila. 48, 1954–1962.
Scholes, C.A., Ho, M.T., Wiley, D.E., Stevens, G.W., Kentish, S.E., 2013b. Cost competitive membrane—cryogenic post-combustion carbon capture. Int. J. Greenh. Gas Control 17, 341–348.
Sircar, S., 1979. Separation of Multicomponent Gas Mixtures, in: Patent, U.S. (Ed.). Air Products and Chemicals, Inc., Allentown, Pa, p. 13.
Smith, K., Ghosh, U., Khan, A., Simioni, M., Endo, K., Zhao, X., Kentish, S., Qader, A., Hooper, B., Stevens, G., 2009. Recent developments in solvent absorption technologies at the CO2CRC in Australia. Energy Procedia 1, 1549–1555.
Smith, R., 2005. Chemical Process Design and Integration. Hoboken, NJ. John Wiley & Sons, Hoboken, NJ.
Sreenivasulu, B., Gayatri, D.V., Sreedhar, I., Raghavan, K.V., 2015. A journey into the process and engineering aspects of carbon capture technologies. Renew. Sustain. Energy Rev. 41, 1324–1350.
Stocker, T., Qin, D., Plattner, G., Tignor, M., Allen, S., Boschung, J., Nauels, A., Xia, Y., Bex, V., Midgley, P., 2013. IPCC, 2013: Climate Change 2013: the Physical Science Basis. Contribution of Working Group I to the Fifth Assessment Report of the Intergovernmental Panel on Climate Change. Cambridge University Press, Cambridge.
Theodosiou, G., Stylos, N., Koroneos, C., 2014. Integration of the environmental management aspect in the optimization of the design and planning of energy systems. J. Clean. Prod. 106.
Webley, P.A., 2014. Adsorption technology for CO_2 separation and capture: a perspective. Adsorption 20, 225–231.
Wennersten, R., Sun, Q., Li, H., 2014. The future potential for carbon capture and storage in climate change mitigation – an overview from perspectives of technology, economy and risk. J. Clean. Prod. 103.
Xiao, G., Webley, P., 2013. VSA Zeolite 13X Experimental Results.
Xiao, P., Zhang, J., Webley, P., Li, G., Singh, R., Todd, R., 2008. Capture of CO_2 from flue gas streams with zeolite 13X by vacuum-pressure swing adsorption. Adsorption 14, 575–582.
Zhang, J., Webley, P.A., 2008. Cycle development and design for CO_2 capture from flue gas by vacuum swing adsorption. Environ. Sci. Technol. 42, 563–569.
Zhang, J., Webley, P.A., Xiao, P., 2008. Effect of process parameters on power requirements of vacuum swing adsorption technology for CO_2 capture from flue gas. Energy Convers. Manag. 49, 346–356.
Zhou, S.J., Meyer, H., Bikson, B., Ding, Y., 2010. Hybrid Membrane Absorption Process for Post Combustion CO_2 Capture, San Antonio, TX.

Please cite this article in press as: Li Yuen Fong, J.C., et al., Multi-objective optimisation of a hybrid vacuum swing adsorption and low-temperature post-combustion CO_2 capture, Journal of Cleaner Production (2015), http://dx.doi.org/10.1016/j.jclepro.2015.08.033

C.4 APCChe 2014 Conference Proceedings

Paper no. 3126421

APCChE 2015 Congress incorporating Chemeca 2015
27 Sept – 01 Oct 2015, Melbourne, Victoria

Optimisation of a hybrid multi-stage membrane and low-temperature carbon dioxide purification process

Jean Christophe Li Yuen Fong[1, 2] and Andrew Hoadley[1, 2*]

[1] *Department of Chemical Engineering, Monash University, Clayton, VIC 3800*
[2] *Cooperative Research Centre for Greenhouse Gas Technologies (CO2CRC), Australia*

[*] *Corresponding author. Email:* [redacted]

Abstract: Carbon capture and storage (CCS) is one of the technologies required to reduce the greenhouse gas emissions to limit the atmospheric concentration of CO_2 to less than 450ppm. However, CCS is energy intensive. The aim of this study is to reduce the energy requirement of CCS by using a hybrid process that combines both the purification and compression stages. The hybrid system is made of a membrane process followed by a low-temperature CO_2 separation and pressurisation. The effect of the low-temperature separation process was investigated by using two different refrigeration cycles in the low-temperature carbon capture unit. The first configuration used a mixed ethane-propane refrigerant that yielded a minimum temperature of -60°C. The second configuration used a propane refrigerant with a minimum temperature of -35°C. Using Multi-Objective Optimisation (MOO), it was determined that the mixed ethane-propane refrigerant hybrid system yielded better performance. Under the optimised conditions a total specific work of around 1.2 GJ_e/t (CO_2 captured) can be achieved, which is competitive with the commercial solvent systems.

Keywords: Carbon capture, Cryogenics, Hybrid Process, Membrane, Multi-objective optimisation, Process Optimisation.

1 Introduction

The global concern on climate change due to greenhouse gas emissions is increasing. According to the studies performed by the International Panel for Climate Change (IPCC)[1], the atmospheric content of carbon dioxide will keep increasing unless a combination of technologies is implemented to reduce the anthropogenic carbon emissions. Post-combustion and pre-combustion carbon capture and storage (CCS) for coal-based electricity generation is seen as one of the technologies that will assist with the transition to a low-carbon emission economy. This paper will focus on the integration and optimisation of post-combustion carbon capture processes (**Figure 1**) in a coal-fired power station with the aim of reducing the energy required to retrofit the CCS process.

Figure 1: Membrane and Low-Temperature Hybrid Carbon Capture Schematic Diagram

1.1 Carbon Capture Technologies

In post-combustion capture, CO_2 needs to be separated from the flue gas, which would typically consist of mostly N_2 and CO_2 and some impurities such as O_2, SO_x, NO_x and water vapour. There are four leading post-combustion carbon capture technologies [2, 3]: solvent absorption, adsorption, membranes and low-temperature separation (known as cryogenic separation in some of the literature). Among those technologies, solvent absorption is currently the most prominent capture

process in both post-combustion and pre-combustion, since it has been extensively used in the natural gas processing industry[4]. However, each of the carbon capture technologies has their advantages and disadvantages and by combining different carbon capture technologies, it may be possible to find a combination which negates the disadvantages of the other[5]. The combination of two or more capture technologies is known as hybrid carbon capture, which as depicted in Figure 2 has two main stages:

i. The CO_2 recovery stage which discharges nitrogen to the atmosphere with as low a CO_2 concentration as possible.
ii. The CO_2 purification stage that would purify the CO_2 stream to a level required for storage.

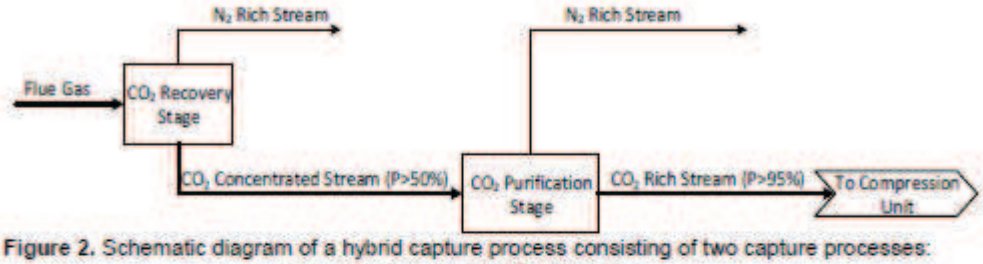

Figure 2. Schematic diagram of a hybrid capture process consisting of two capture processes: recovery stage and purification stage.

As shown in **Figure 3**, the hybrid CO_2 separation process involves a single-stage membrane unit as the CO_2 recovery stage, and a low-temperature separation, as the CO_2 purification stage. Due to the high degree of freedom to integrate and optimise the hybrid process, a multi-objective optimisation technique was used to determine the optimum operating condition of the process.

1.2 Process Integration and Optimisation of Hybrid Carbon Capture Processes

Process optimisation is an integral part of any chemical engineering process. Although a process can be optimised for one objective at a time (single objective optimisation, SOO), there are usually multiple objectives that need to be considered simultaneously. This is known as multi-objective optimisation, which refers to finding values of decision variables (DV) which correspond to and provide the optimum of more than one objective [6].

The purpose of using multi-objective optimisation in this paper is that whilst maximising the overall recovery of CO_2 is an obvious objective for a capture system, increasing the recovery usually increases the total work required as well. Therefore, in order to have the best capture system, it is important to determine the minimum power requirement for the maximum CO_2 yield for each case. However, since the two objectives conflict with each other, there will not be a single best solution, but a series of solutions, called Pareto-optimal solutions and this provides the relationship between the two objectives. The decision variables used in this study can be seen in Fig 1, Fig 2 and in Tab I.

2 Methodology and Simulation Framework

2.1 General Framework

The post-combustion flue gas properties were based on a 300 MW sub-bituminous coal-fired power station. The flue gas was then assumed to have been pre-treated to remove the impurities and water by including the energy cost for this pre-treatment step in the calculations. The feed gas composition and conditions are shown in **Table 1** and **Table 2**, respectively.

Table 1: Post-combustion flue gas conditions based on a 300 MW sub-bituminous coal fired power station after pre-treatment

Feed Conditions	Units	Value
Vapour Fraction	-	1.00
Temperature	(°C)	50
Pressure	(kPa)	103
Molar Flow	(kmol/h)	5.78×10^4
Mass Flow	(kg/h)	1.67×10^6

Table 2: Post-combustion flue gas composition based on a 300 MW sub-bituminous coal fired power station after pre-treatment

Composition	Units	Value
CO_2	(mol frac)	0.14
N_2	(mol frac)	0.86

All other process unit conditions were operated using industry accepted parameters. The compression stage for both the multi-stage compression and refrigerant compression had an isentropic efficiency of 80 %, with inter-stage coolers using cooling water with an approach temperature of 30 °C and a pressure drop of 40 kPa. The heat exchangers in the cryogenic separation were plate-fin heat exchangers with a pressure drop of 50 kPa on both the process side and the refrigerant side.

2.2 Membrane and Low-Temperature Hybrid Carbon Capture Unit

The hybrid capture process investigated in this study was a combination of membrane and low-temperature carbon capture units as shown in **Figure 3** and **Figure 4**. Heat integration was performed on the low-temperature separation unit to reduce the cold duty of the refrigeration system and obtain outlet streams at approximately 25°C. All simulations were performed using the Aspen HYSYS® software package, version 8.4, using the Peng-Robinson fluid package for the phase equilibria.

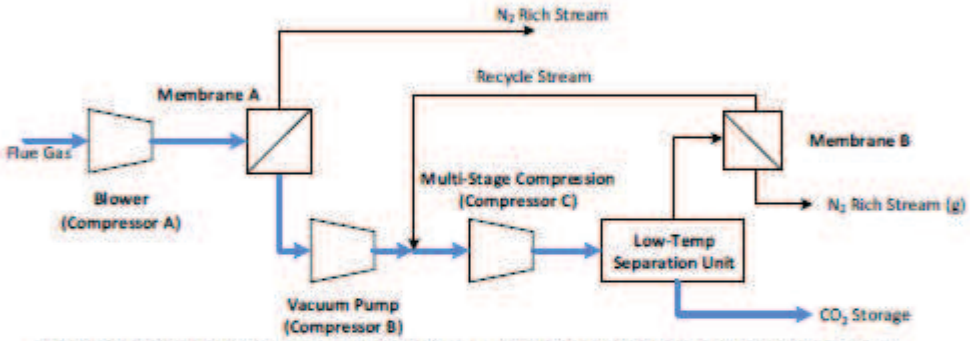

Figure 3: Membrane and Low-Temperature Hybrid Carbon Capture Schematic Diagram

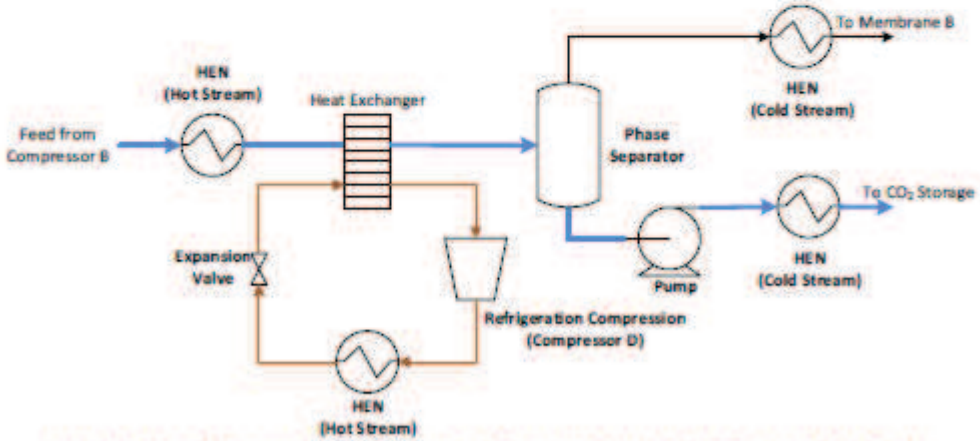

Figure 4: Low-Temperature Unit Schematic Diagram (HEN – Heat Exchanger Network)

The membrane process was an Aspen HYSYS® module based on mass transfer equations, specifically developed for applications in carbon capture simulations[7]. A high performance polymer membrane[8] was used with a permeability of CO_2 (P_{CO2}) of 2000 barrer and selectivity of CO_2 versus N_2 ($\alpha_{CO2/N2}$) of 50. The permeate stream from Membrane A is then sent to the low-temperature separation carbon capture unit.

There are two important processes in the low-temperature separation carbon capture unit: the pre-compression unit and the refrigeration cycle required to chill the process gas to the separation temperature. The pre-compression unit used in this study is a three-stage compression unit with inter-stage cooling. Two refrigeration cycle systems were studied:

Case I – Mixed ethane/propane refrigerant system (minimum temperature of -60°C).
Case II – Propane refrigerant system (minimum temperature of -40°C)

Furthermore, a membrane unit (Membrane B) was attached to the gaseous waste stream of the low-temperature separation unit to capture the CO_2 that was not recovered in the low-temperature unit. Since the stream was at a high pressure, this membrane unit would further purify the gaseous stream without requiring any additional work[9].
The streams exiting the low-temperature separation unit are typically in the temperatures below 0°C. Therefore, in order to recover the cold duty available in those streams, a heat exchanger network was used to recover the energy from the cold streams.

2.3 Process Integration and Optimisation

Due to the high degree of freedom available in the integration of the hybrid carbon capture process, multi-objective optimisation (MOO)[6] was used to determine the optimum operating conditions of each stage of the hybrid carbon capture process. There are a number of key operating variables, known as decision variables, for each capture process that can be varied to optimise the overall performance of the hybrid carbon capture system. For both refrigeration options, two objective variables were simultaneously optimised to determine the performance of the hybrid system: overall CO_2 recovery rate of the hybrid system and total work required for the hybrid process. The range of each decision variables are shown in **Table 3**.

3 Results

3.1 Optimisation Pareto Charts

The Pareto charts of the objective variables are shown in **Figure 5**.
From the objective variables Pareto charts, it could be observed that with increasing recovery rate, there was an increase in total work required. Therefore, in order to better understand the total work required with respect to the amount of CO_2 being captured by the hybrid process, a new graph using the Pareto-Optimal solutions, of total specific work required (GJ/t(CO_2 recovered)) versus recovery rate was generated (**Figure 6**).

Table 3: Table of range of decision variables for Case I and Case II.

		Case I - Mixed Refrigerant		Case II - Propane Refrigerant	
	Units	Min	Max	Min	Max
Membrane A Cut	-	0.1	0.8	0.1	0.9
Membrane A Feed Pressure	(kPa)	115	200	120	200
Membrane A Permeate Pressure	(kPa)	20	100	10	100
Refrigerant Molar Flow	(mol/s)	1.2	3	*N/A*	*N/A*
Refrigerant Ethane Molar Fraction	-	0.2	0.8	*N/A*	*N/A*
Heat Exchanger Network Intermediate Temperature	(°C)	*N/A*	*N/A*	-15	5
Low-Temp. Process Stream Outlet Temp.	(°C)	-60	-40	-35	-25
Multi-Stage Compression Pressure	(kPa)	1250	3000	2000	4500
Membrane B Cut	-	0.05	0.8	0.25	0.9

The Pareto Optimal Front is the solution obtained from the last generation of the Genetic Algorithm of the non-dominated solution set. The results shown are for a MOO using 50 individuals with 50 generations. The Pareto

charts of the four decision variables with the highest impact on the objective variables are shown in **Figure 7** plotted against the objective 1: Maximum CO_2 Recovery.

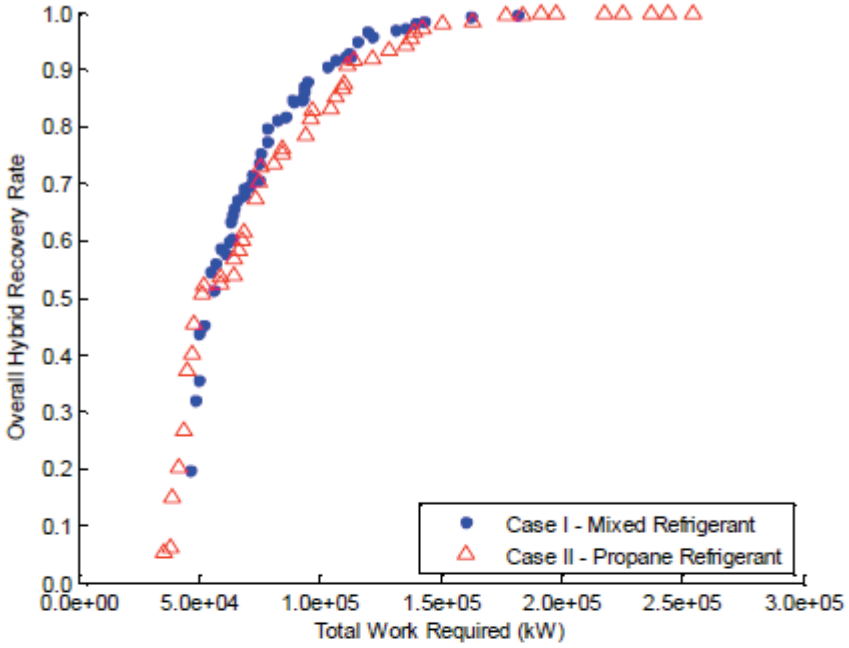

Figure 5: Overall recovery rate of hybrid system as a function of total work required (kW) for two hybrid processes

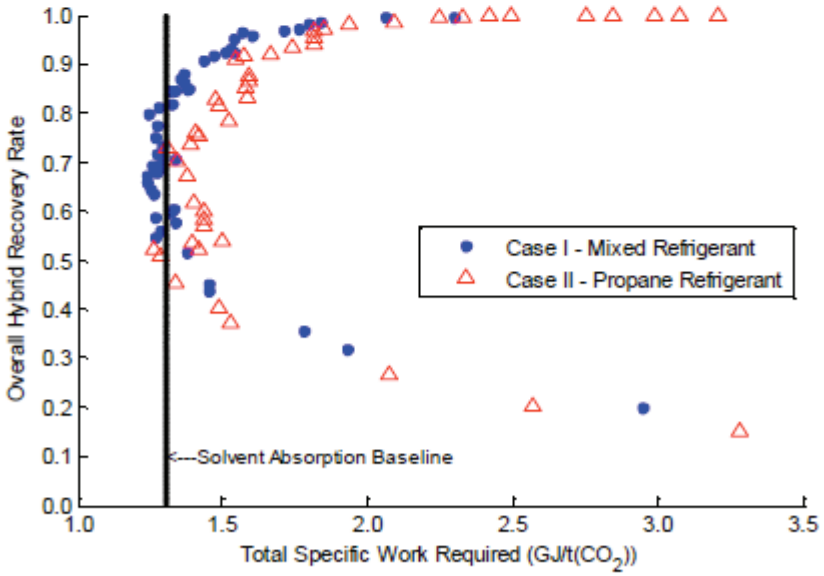

Figure 6: Overall recovery rate of hybrid system as a function of total specific work required (GJ/t(CO_2)) for two hybrid processes

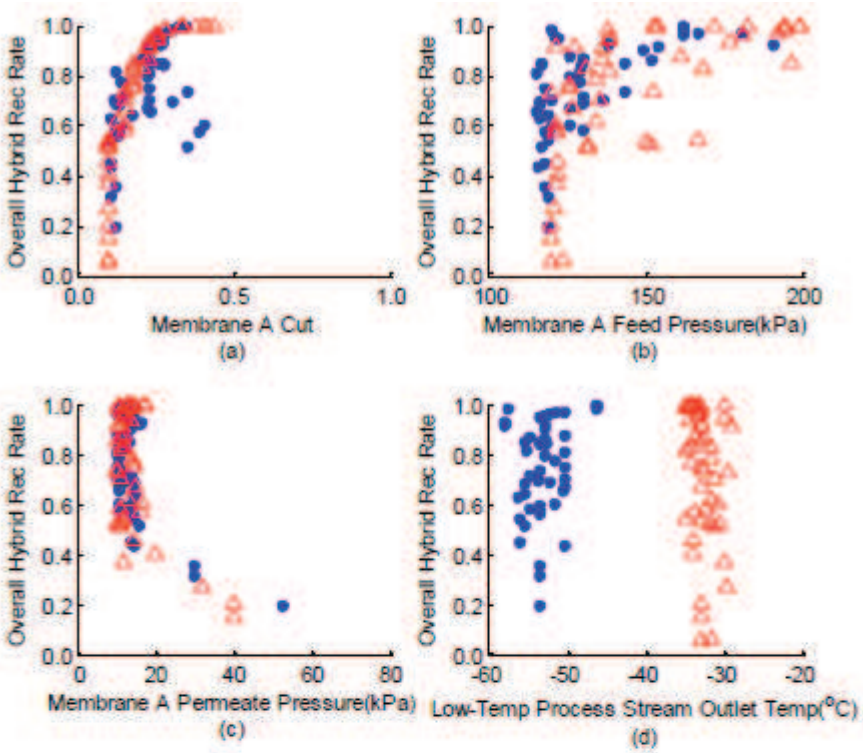

Figure 7: Pareto chart of the four main decision variables versus the CO_2 recovery rate (a) Membrane A Cut (b) Membrane A Feed Pressure; (c) Membrane A Permeate Pressure (kPa); (d) Process stream minimum temperature (°C)

3.2 Additional Results

In addition to the decision variables and objective variables, other key process performance variables were also recorded while performing the MOO. Three of those variables can be seen in **Figure 8**.

4 Discussion

The objective Pareto chart for Case 1, represented by the blue circles in **Figure 5**, shows that an increase in total work is required to increase the overall CO_2 recovery rate of the hybrid process. This increase in total work is reflected in the decision variables Pareto chart in **Figure 7**, where the feed pressure of Membrane A (**Figure 7(b)**) increases with increasing recovery rate and the permeate stream pressure of Membrane A (**Figure 7(c)**) decreases with increasing recovery rate. Increase in feed pressure and decrease in pressure below atmospheric pressure for the permeate stream represents an increase in power requirement for the blower and vacuum pump respectively.

The total work required per mass of CO_2 captured provides a better baseline to compare the hybrid carbon capture process with other established carbon capture technology, which is shown in **Figure 6**; the total specific work required has a quadratic relationship with the overall recovery rate of the hybrid system. This quadratic relationship has an optimum minimum total specific work of 1.24 GJ_e/t (CO_2 captured) required with an overall recovery rate of 79.7%.

The Pareto charts for Case II show a similar trend to the objective variables and decision variables Pareto charts of Case I; the total work required increases with increasing recovery rate, which results in a quadratic relationship between the total specific work required and the overall recovery rate of the hybrid system. The optimum minimum for Case II occurs at a total specific work of 1.26 GJ_e/t (CO_2 captured) required with an overall recovery rate of 52.3%. Furthermore, in order to obtain a recovery rate of 80%, approximately 1.5 GJ_e/t (CO_2 captured) is required.

This difference in optimum performance between the two cases can be seen in Section 3.2, where the Pareto Charts of the three main components that require work are shown in **Figure 8**. **Figure 8(a)**

shows that the work requirements for Membrane A in both cases are similar. This mirrors the results obtained in **Figure 7(b)** and **Figure 7(c)**, where the feed pressure and permeate pressure of Membrane A for both cases are comparable.

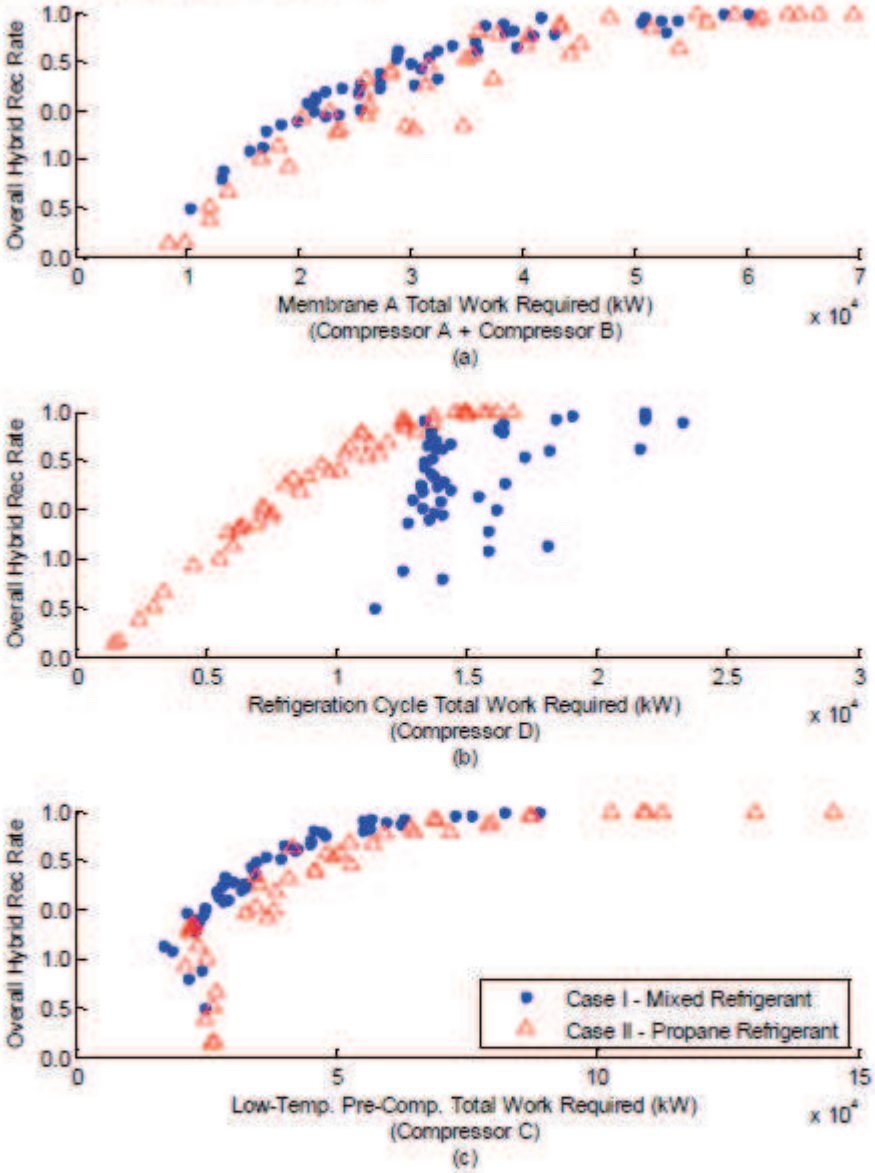

Figure 8: Pareto chart of the three main components requiring work versus the CO_2 recovery rate (a) Total Work Required for Membrane A unit (Compressor A + B); (b) Refrigeration Cycle Compressors (Compressor D); (c) Low-Temperature Pre-Compression (Compressor C)

Figure 8(b) represents the total work required in the compression train of the refrigeration cycles for each case. As expected, the propane refrigerant refrigeration cycle (Case II), requires less work than the mixed refrigerant refrigeration cycle (Case I). This is due to the lower temperatures obtained by the propane refrigerant, which require lower pressure ratios in comparison to the mixed refrigerant, where higher pressure ratios are required to achieve the colder temperatures. However, it can also be observed that the difference in work requirement is greater at lower recovery rates than higher recovery rates.

Figure 8(c) shows the total work required for the pre-compression of the feed stream entering the low-temperature separation. It can be observed that both cases have the same trend, whoever, at recovery rates greater than 60%, the mixed refrigerant hybrid system requires less work. This can be explained from the fact that the mixed refrigerant hybrid system has lower temperatures in the low-temperature unit. The lower temperature allows the CO_2 to be liquefied at lower pressure, therefore requiring less work in the pre-compression train.

The difference in work requirement for the refrigeration unit and pre-compression unit explains the difference in optimum operating conditions of each case, where at lower recovery rates the propane refrigerant performs better due to the higher temperatures and similar pre-compression work requirement. On the other hand, at higher recovery rate, the mixed refrigerant has a better performance since to the colder temperatures results in a lower pre-compression work requirement. This shows that the membrane/low-temperature hybrid system provides a high degree of flexibility to distribute the CO_2 separation work load between both capture processes.

5 Conclusions

As it can be seen in **Figure 3**, MEA solvent absorption separation system with a multi-stage compression system requires 4 GJ_{th}/(t CO_2 recovered) [10] that converts to approximately 1.3 GJ_e/(t CO_2 recovered). Both Case I and Case II considered have an optimum minimum specific work required of approximately 1.25 GJ_e/(t CO_2 recovered) with an overall recovery rate of 79.7% and 52% respectively. Both cases provide a highly competitive option to the commercial MEA solvent absorption separation system on an energy requirement basis. Furthermore, membrane processes and low-temperature separation require smaller equipment and simpler process operating conditions. The choice of which of the two systems should be employed would probably be based on other factors, such as relative ease of operation or capital cost.

Acknowledgements

The author would like to thank the Australian Government for funding this CO2CRC program through the CRC program as well as all the CO2CRC partners for their support.

References

1. Stocker, T., et al., (2013), *IPCC, 2013: Climate Change 2013: The Physical Science Basis. Contribution of Working Group I to the Fifth Assessment Report of the Intergovernmental Panel on Climate Change*. Cambridge: Cambridge University Press.
2. Sreenivasulu, B., et al., (2015), *A journey into the process and engineering aspects of carbon capture technologies*. Renewable and Sustainable Energy Reviews. **41**(0): p. 1324-1350.
3. Pires, J.C.M., et al., (2011), *Recent developments on carbon capture and storage: An overview*. Chemical Engineering Research and Design. **89**(9): p. 1446-1460.
4. Smith, K., et al., (2009), *Recent developments in solvent absorption technologies at the CO2CRC in Australia*. Energy Procedia. **1**(1): p. 1549-1555.
5. Scholes, C.A., et al., (2013), *Cost competitive membrane—cryogenic post-combustion carbon capture*. International Journal of Greenhouse Gas Control. **17**(0): p. 341-348.
6. Rangaiah, G.P., (2009), *Multi-Ojective Optimization. Techniques and Applications in Chemical Engineering*. Advances in Process Systems Engineering. Vol. 1, Singapore: World Scientific Publishing Co. Pte. Ltd.
7. Scholes, C.A., et al., (2013), *Simulations of Membrane Gas Separation: Chemical Solvent Absorption Hybrid Plants for Pre- and Post-Combustion Carbon Capture*. Separation Science and Technology (Philadelphia). **48**(13): p. 1954-1962.
8. Low, B.T., et al., (2013), *A parametric study of the impact of membrane materials and process operating conditions on carbon capture from humidified flue gas*. Journal of Membrane Science. **431**(0): p. 139-155.
9. Li Yuen Fong, J.C., Anderson, C J and Hoadley, A F, (2013), *Optimisation of a Hybrid CO_2 Purification Process*, in *Chemeca 2013*: Brisbane.
10. Belaissaoui, B., et al., (2012), *Hybrid membrane cryogenic process for post-combustion CO2 capture*. Journal of Membrane Science. (0).

Presenting author biography

Chris Li graduated from Monash University in Bachelor in Engineering (Chemical Engineering) in 2011. He is a postgraduate student at Monash University, currently undertaking his PhD candidature. His research focuses mainly on hybrid carbon capture systems, which is conducted between the

Department of Chemical Engineering in Monash University and Cooperative Research Centre for Greenhouse Gas Technologies (CO2CRC).